Technical Report Documentation Page

1. Report No. FHWA/TX-11/0-6005-4	2. Government Accession No.	3. Recipient's Catalog No.
4. Title and Subtitle Developing a Testing Device for Total Pavements Acceptance: Third-Year Report		5. Report Date December 2011; Revised May 2012, Published August 2012 6. Performing Organization Code
7. Author(s) Kenneth H. Stokoe, II, Jung-Su Lee, Boo H. Nam, Mike Lewis, Richard Hayes (CTR); Thomas Scullion and Wenting Liu (TTI)		8. Performing Organization Report No. 0-6005-4
9. Performing Organization Name and Address Center for Transportation Research The University of Texas at Austin 1616 Guadalupe St, Suite 4.202 Austin, TX 78701 Texas Transportation Institute Texas A&M University System 3135 TAMU College Station, Texas 77843-3135		10. Work Unit No. (TRAIS) 11. Contract or Grant No. 0-6005
12. Sponsoring Agency Name and Address Texas Department of Transportation Research and Technology Implementation Office P.O. Box 5080 Austin, TX 78763-5080		13. Type of Report and Period Covered Technical Report September 2008–August 2011 14. Sponsoring Agency Code

15. Supplementary Notes
Project performed in cooperation with the Texas Department of Transportation and the Federal Highway Administration.

16. Abstract

During the third year of Project 0-6005, significant progress was made towards building the Total Pavement Acceptance Device (TPAD). The TPAD will be a multi-function pavement evaluating device that will be used to profile continuously along pavements at speeds in the range of 3 to 7 mph. The test functions will include those associated with Rolling Dynamics Deflectometer (RDD), ground penetrating radar (GPR), Distance Measurement Instrument (DMI), and high-precision differential GPS, and surface temperature measurements, as well as digital video imaging of the pavement and right-of-way conditions. The TPAD mobile platform and dedicated hauling equipment, a tractor and trailer system, were delivered to CTR in late fall 2010. Acceptance testing for the TPAD mobile platform was initiated in winter 2010 and continued through summer 2011. Acceptance testing involved evaluating (1) the speed control, (2) the static load control, (3) the dynamic load control, (4) the portable load calibration system, and (5) the DMI. Some improvements were identified that were completed by the manufacturer. Progress was also made in developing (1) improved rolling sensors and associated data analysis methods commensurate with the target testing speeds and (2) a second-generation integrated data acquisition and display system that records all test functions on the same time and distance baselines.

17. Key Words Continuous Deflection Profiling, Testing Speed, GPR and GPS Measurements, Video Imaging, Single Moving Platform	18. Distribution Statement No restrictions. This document is available to the public through the National Technical Information Service, Springfield, Virginia 22161; www.ntis.gov.

19. Security Classif. (of report) Unclassified	20. Security Classif. (of this page) Unclassified	21. No. of pages 176	22. Price

Form DOT F 1700.7 (8-72) Reproduction of completed page authorized

DEVELOPING A TESTING DEVICE FOR TOTAL PAVEMENTS ACCEPTANCE: THIRD-YEAR REPORT

CTR
Kenneth H. Stokoe, II,
Jung-Su Lee
Boo H. Nam
Mike Lewis
Richard Hayes

TTI
Thomas Scullion
Wenting Liu

CTR Technical Report:	0-6005-4
Report Date:	December 2011; Revised May 2012
Project:	0-6005
Project Title:	Developing a Testing Device for Total Pavements Acceptance
Sponsoring Agency:	Texas Department of Transportation
Performing Agency:	Center for Transportation Research at The University of Texas at Austin and Texas Transportation Institute

Project performed in cooperation with the Texas Department of Transportation and the Federal Highway Administration.

Center for Transportation Research
The University of Texas at Austin
1616 Guadalupe, Suite 4.202
Austin, TX 78701

Texas Transportation Institute
Texas A&M University System
3135 TAMU
College Station, Texas 77843-3135

www.utexas.edu/research/ctr

Copyright (c) 2012
Center for Transportation Research
The University of Texas at Austin

All rights reserved
Printed in the United States of America

Disclaimers

Author's Disclaimer: The contents of this report reflect the views of the authors, who are responsible for the facts and the accuracy of the data presented herein. The contents do not necessarily reflect the official view or policies of the Federal Highway Administration or the Texas Department of Transportation (TxDOT). This report does not constitute a standard, specification, or regulation.

Patent Disclaimer: There was no invention or discovery conceived or first actually reduced to practice in the course of or under this contract, including any art, method, process, machine manufacture, design or composition of matter, or any new useful improvement thereof, or any variety of plant, which is or may be patentable under the patent laws of the United States of America or any foreign country.

Engineering Disclaimer

NOT INTENDED FOR CONSTRUCTION, BIDDING, OR PERMIT PURPOSES.

Project Engineer: Kenneth H. Stokoe, II
Professional Engineer License State and Number: Texas No. 49095
P. E. Designation: Research Supervisor

Acknowledgments

The research team wishes to express its sincere gratitude to TxDOT for supporting this research project. The interaction and support from the Research Monitoring Committee—Mr. Joe Leidy, Mr. Ed Oshinski, Dr. Dar Hao Chen, and Dr. German Claros—has been very important to the progress of the project. The UT Staff—Mr. Cecil Hoffpauir, Mr. Curtis Mullins, and Dr. Farn-Yuh Menq—helped significantly in the field tests with the UT RDD used in developing improved rolling sensors and an improved data analysis software, as well as evaluating new data collection hardware. We owe much to Industrial Vehicles Incorporated (IVI) for developing the prototype IVI RDD that was used in Year 1. The generosity of Mr. Jay Bird, Mr. Elmo Christensen, and Mr. Mike Grady of IVI in sharing their ideas and the prototype vehicle and prototype rolling sensors with us, at no cost to the project, in Year 2 is appreciated. Further, the willingness of IVI to loan the hydraulic system associated with Rolling Sensor #2 for prototype testing in Year 3 and for the constant interaction and strong support between IVI and CTR and TTI during acceptance testing are greatly appreciated. Finally, we are grateful to Mr. Don Ramsey and the personnel of the TxDOT Flight Services Facility for their kindness in allowing us to continue to use a pavement testbed at their facility during Year 3 of the project.

Table of Contents

Chapter 1. Introduction **1**
1.1 Project Objectives and Overview 1
1.2 Outline of Progress during Year 3 1

Chapter 2. Delivery of TPAD Mobile Platform and Dedicated Hauling Equipment and Acceptance Testing **3**
2.1 Introduction 3
2.2 Delivery of the TPAD Mobile Platform 3
2.3 Delivery of the Tractor and Trailer (Dedicated Hauling Equipment) 3
2.4 Acceptance Testing of TPAD Mobile Platform 4
2.4.1 TPAD Speed Control 4
2.4.2 TPAD Static Load Control 8
2.4.3 Calibration of Portable TPAD Load Calibration System 9
2.4.4 TPAD Dynamic Sinusoidal Loading 11
2.4.5 Distance Measurement Instrument, DMI 14
2.5 Summary 14

Chapter 3. Improvements to the RDD Portion of the TPAD **19**
3.1 Introduction 19
3.2 Assembly and Installation of Speed-Improved Rolling Sensors 19
3.3 Testing of Speed-Improved Rolling Sensors with the TPAD 23
3.3.1 Combined CTR and TTI Testing 23
3.3.2 CTR TPAD Testing 28
3.3.3 Stationary Deflection Measurements with the TPAD 34
3.3.4 Justification for 3-mph Testing Speed of Current Rolling Sensor and Array 35
3.4 Modifications Made to Frame Used to Position Rolling Sensor #2 38
3.4.1 Replacement of Two-Coil Isolators with Three-Coil Isolators 38
3.4.2 Trial of Rigid Trailing-Arm Installation 38
3.4.3 Removal of Hydraulic Lift Cylinder and Addition of Air Accumulator 40
3.5 Noise Measurements with Towing Frame at PRC 42
3.6 “Design” of New Hold-Down and Lifting System 49
3.7 Summary 49

Chapter 4. Improvements to the TTI Data Acquisition and Processing Systems **51**
4.1 Overview 51
4.2 Rolling Deflection Field Testing Activities 52
4.3 Updates to the Data Acquisition Software 55
4.4 RDD Field Data Analysis Software Development 58

Chapter 5. Summary of Year 3 Activities **67**

References **69**

Appendix A: Noise-Level Measurements with Towing Frame at PRC **71**

Appendix B: TPAD Measurements at TxDOT FSF **107**

List of Figures

Figure 2.1: Photograph of the TPAD Mobile Platform and Dedicated Hauling Equipment at UT's Pickle Research Center 4
Figure 2.2: Speed Control Testing of the TPAD Mobile Platform at Pickle Research Center in December 2010 5
Figure 2.3: Speed Calculated Every 100 ft along a 500-ft Stretch of PRC Asphalt Road for Different Speed Settings 6
Figure 2.4: Comparison between Speed Settings and Average Calculated Speed (at PRC) 6
Figure 2.5: Speed Calculated Every 100 ft along a 500-ft Stretch of Jointed Concrete Pavement at TxDOT FSF for Different Speed Settings 7
Figure 2.6: Comparison between Speed Setting and Average Calculated Speed at TxDOT FSF, ABIA after Software Modifications 7
Figure 2.7: TPAD Loading Rollers Sitting on the Truck Scales during Static-Load Acceptance Testing at TxDOT FSF, ABI on December 09, 2010 8
Figure 2.8: Comparison between Static-Load Settings and Static Loads Measured with Truck Scales at TxDOT FSF, ABIA during Second Week of December 2010 9
Figure 2.9: Calibration of TPAD Load Calibration System at Ferguson Structural Engineering Laboratory at Pickle Research Center 10
Figure 2.10: Calibration Curve between TPAD Load Calibration System and the UT Reference Load Cell 11
Figure 2.11: (a) Installation of TPAD Load Calibration system under the TPAD and (b) TPAD Loading Rollers Sitting on TPAD Load Calibration Fixture; Testing Conducted during Second Week of December 2011 12
Figure 2.12: TPAD Dynamic Load Readings from the Independent TPAD Load Calibration System and the TPAD Computer for Load Settings at Different Operating Frequencies 14
Figure 2.13: 1-Sec Time Domain Signals of TPAD Dynamic Load from the Independent TPAD Load Calibration System and the TPAD Computer for Load Peak-to-Peak Settings at Different Operating Frequencies 17
Figure 3.1: (a) One 9-in. Diameter Wheel with the Bearing Set, and (b) Cart Body with Three, 9-in. Diameter Wheels 20
Figure 3.2: Speed-Improved Rolling Sensors before Installation on the TPAD 21
Figure 3.3: Speed-Improved Rolling Sensors Installed in Position under the TPAD 22
Figure 3.4: Photograph of the TPAD on Dedicated Hauling Equipment at TxDOT FSF, ABIA 23
Figure 3.5: Testing Path E Used in TPAD Performance Testing at TxDOT FSF, ABIA 24
Figure 3.6: Photograph of the TPAD at Starting Point of Path E, TxDOT FSF 24
Figure 3.7: Continuous Deflection Profile at 0.5 mph Using Speed-Improved Rolling Sensors and TPAD along Path E at TxDOT FSF (CTR and TTI Combined Testing) 25

Figure 3.8: Continuous Deflection Profiles at 0.5 and 1 mph Using Speed-Improved Rolling Sensors and TPAD along Path E at TxDOT FSF (CTR and TTI Combined Testing)..... 26
Figure 3.9: Continuous Deflection Profiles at 0.5 and 2mph Using Speed-Improved Rolling Sensors and TPAD along Path E at TxDOT FSF (CTR and TTI Combined Testing)..... 26
Figure 3.10: Continuous Deflection Profiles at 0.5 and 3mph Using Speed-Improved Rolling Sensors and TPAD along Path E at TxDOT FSF (CTR and TTI Combined Testing)..... 27
Figure 3.11: Continuous Deflection Profiles at 0.5 and 4mph Using Speed-Improved Rolling Sensors and TPAD along Path E at TxDOT FSF (CTR and TTI Combined Testing)..... 27
Figure 3.12: Continuous Deflection Profile at 0.5mph Using Speed-Improved Rolling Sensors and TPAD along Path E at TxDOT FSF (CTR Testing)..... 28
Figure 3.13: Continuous Deflection Profiles at 0.5 and 1 mph Using Speed-Improved Rolling Sensors and TPAD along Path E at TxDOT FSF (CTR Testing)..... 29
Figure 3.14: Continuous Deflection Profiles at 0.5 and 2 mph Using Speed-Improved Rolling Sensors and TPAD along Path E at TxDOT FSF (CTR Testing)..... 29
Figure 3.15: Continuous Deflection Profiles at 0.5 and 3 mph Using Speed-Improved Rolling Sensors and TPAD along Path E at TxDOT FSF (CTR Testing)..... 30
Figure 3.16: Continuous Deflection Profiles at 0.5 and 4 mph Using Speed-Improved Rolling Sensors and TPAD along Path E at TxDOT FSF (CTR Testing)..... 30
Figure 3.17: Noise Induced Deflection Profile at 0.5 mph Using Speed-Improved Rolling Sensors and TPAD along Path E at TxDOT FSF 31
Figure 3.18: Noise Induced Deflection Profile at 1 mph Using Speed-Improved Rolling Sensors and TPAD along Path E at TxDOT FSF 32
Figure 3.19: Noise Induced Deflection Profile at 2 mph Using Speed-Improved Rolling Sensors and TPAD along Path E at TxDOT FSF 32
Figure 3.20: Noise Induced Deflection Profile at 3 mph Using Speed-Improved Rolling Sensors and TPAD along Path E at TxDOT FSF 33
Figure 3.21: Noise Induced Deflection Profile at 4 mph Using Speed-Improved Rolling Sensors and TPAD along Path E at TxDOT FSF 33
Figure 3.22: Increases of Noise Level and Rolling Deflection with Increasing Testing Speeds 34
Figure 3.23: Comparison between Stationary and Rolling (Continuous) Dynamic Deflection Measurements on Two, 8-in. Thick Slabs at TxDOT FSF 35
Figure 3.24: Similar Continuous Deflection Profiles at 1 and 3 mph with First Generation TPAD along Path E at TxDOT FSF (CTR Testing)..... 36
Figure 3.25: Sensor #1 Output in the Time and Frequency Domains on an 8-in. Thick Slab in the Mid-Slab Region at TxDOT FSF Collected at 1 mph 37
Figure 3.26: Sensor #1 Output in the Time and Frequency Domains on an 8-in. Thick Slab in the Mid-Slab Region at TxDOT FSF Collected at 2 mph 37

Figure 3.27: Sensor #1 Output in the Time and Frequency Domains on an 8-in. Thick Slab in the Mid-Slab Region at TxDOT FSF Collected at 3 mph 38
Figure 3.28: Trailing Arms Installed to Sensor #2 39
Figure 3.29: Time and Frequency Domain Signals of Sensor #2 with and without Trailing Arms Collected in the Mid-Slab Region with Stationary Measurements 40
Figure 3.30: Hydraulic Lift Cylinder before Disconnection and Dead Weight and Air Accumulator Added to the White Location Frame for Sensor #2 41
Figure 3.31: Comparison of Continuous RDD Deflection Profiles for Testing at 1 mph with and without the Hydraulic Lift Cylinder for Sensor #2 41
Figure 3.32: Comparison of Continuous RDD Deflection Profiles for Testing at 3 mph with and without the Hydraulic Lift Cylinder for Sensor #2 42
Figure 3.33: Speed-Improved Rolling Sensor, Computer, DAQ and Battery Installed on an Independent Towing Frame at the Former Texas Accelerated Pavement Test Site 43
Figure 3.34: Four Configurations of the Speed-Improved Rolling Sensor Installed in the Independent Towing Frame 44
Figure 3.35: Rolling Noise Levels at Three Different Testing Speeds around Three Possible RDD Operating Frequencies (f_o) Measured with Rolling Sensor Configuration SA 45
Figure 3.36: Rolling Noise Levels at Three Different Testing Speeds around Three Possible RDD Operating Frequencies (f_o) Measured with Rolling Sensor Configuration SB 46
Figure 3.37: Rolling Noise Levels at Three Different Testing Speeds around Three Possible RDD Operating Frequencies (f_o) Measured with Rolling Sensor Configuration SC 47
Figure 3.38: Rolling Noise Levels at Three Different Testing Speeds around Three Possible RDD Operating Frequencies (f_o) Measured with Rolling Sensor Configuration SD 48
Figure 4.1: First Test in September 2010 53
Figure 4.2: Mounted Data Acquisition computer and control box in the classic RDD 53
Figure 4.3: All the components that are installed to the old RDD vehicle 54
Figure 4.4: Inside the Control box 54
Figure 4.5: First time RDD geophones are installed in TPAD at TXDOT terminal of Austin 55
Figure 4.6: Main Menu in Updated TPAD Data Acquisition Program 55
Figure 4.7: Main Input Screen for Controlling Data Collection Rates 57
Figure 4.8: Entering Equipment Calibration Information (GPR Calibration Factors) 57
Figure 4.9: Entering Geophone Information in Updated Data Acquisition Software 58
Figure 4.10: The field RDD Data Processing Software Main Interface (Toolbar Buttons) 59
Figure 4.11: Set Up Menu for the Geophone Processing System 62
Figure 4.12: Raw Geophone Data 63

Figure 4.13: Power Density Spectra Data for One of the Data Sets (Peak being at 30 Hz) 63
Figure 4.14: Display of both Raw and Filtered Geophone Data, with Peaks Defined 64
Figure 4.15: Typical Final Deflection Data Set from TxDOT Terminal 64
Figure 4.16: Dynamic Load Profile from Test Run 65
Figure 4.17: Static (Hold-Down) Load Profile for Test Run 65

Appendix Figures

Figure A.1: SA with 20 lb Hold-Down Weight at 1 mph 71
Figure A.2: SA with 40 lb Hold-Down Weight at 1 mph 72
Figure A.3: SA with 90 lb Hold-Down Weight at 1 mph 73
Figure A.4: SA with 20 lb Hold-Down Weight at 3 mph 74
Figure A.5: SA with 40 lb Hold-Down Weight at 3 mph 75
Figure A.6: SA with 90 lb Hold-Down Weight at 3 mph 76
Figure A.7: SA with 20 lb Hold-Down Weight at 5 mph 77
Figure A.8: SA with 40 lb Hold-Down Weight at 5 mph 78
Figure A.9: SA with 90 lb Hold-Down Weight at 5 mph 79
Figure A.10: SB with 20 lb Hold-Down Weight at 1 mph 80
Figure A.11: SB with 40 lb Hold-Down Weight at 1 mph 81
Figure A.12: SB with 90 lb Hold-Down Weight at 1 mph 82
Figure A.13: SB with 20 lb Hold-Down Weight at 3 mph 83
Figure A.14: SB with 40 lb Hold-Down Weight at 3 mph 84
Figure A.15: SB with 90 lb Hold-Down Weight at 3 mph 85
Figure A.16: SB with 20 lb Hold-Down Weight at 5 mph 86
Figure A.17: SB with 40 lb Hold-Down Weight at 5 mph 87
Figure A.18: SB with 90 lb Hold-Down Weight at 5 mph 88
Figure A.19: SC with 20 lb Hold-Down Weight at 1mph 89
Figure A.20: SC with 40 lb Hold-Down Weight at 1mph 90
Figure A.21: SC with 90 lb Hold-Down Weight at 1mph 91
Figure A.22: SC with 20 lb Hold-Down Weight at 3 mph 92
Figure A.23: SC with 40 lb Hold-Down Weight at 3 mph 93
Figure A.24: SC with 90 lb Hold-Down Weight at 3 mph 94
Figure A.25: SC with 20 lb Hold-Down Weight at 5 mph 95
Figure A.26: SC with 40 lb Hold-Down Weight at 5 mph 96
Figure A.27: SC with 90 lb Hold-Down Weight at 5 mph 97
Figure A.28: SD with 20 lb Hold-Down Weight at 1 mph 98
Figure A.29: SD with 40 lb Hold-Down Weight at 1 mph 99
Figure A.30: SD with 90 lb Hold-Down Weight at 1 mph 100
Figure A.31: SD with 20 lb Hold-Down Weight at 3 mph 101

Figure A.32: SD with 40 lb Hold-Down Weight at 3 mph 102
Figure A.33: SD with 90 lb Hold-Down Weight at 3 mph 103
Figure A.34: SD with 20 lb Hold-Down Weight at 5 mph 104
Figure A.35: SD with 40 lb Hold-Down Weight at 5 mph 105
Figure A.36: SD with 90 lb Hold-Down Weight at 5 mph 106
Figure B.1: Processed Static Force Signal with 0.5 mph 110
Figure B.2: Processed Peak-to-Peak Dynamic Force Signal with 0.5 mph 110
Figure B.3: Time Domain Signal of Raw Data for Combined Static and Dynamic Forces with 0.5 mph along Whole Testbed Length 111
Figure B.4: Frequency Domain Signal (Linear Scale) of Raw Data for Combined Static and Dynamic Forces with 0.5 mph along Whole Testbed Length 111
Figure B.5: Frequency Domain Signal (Decibel Scale) of Raw Data for Combined Static and Dynamic Forces with 0.5 mph along Whole Testbed Length 111
Figure B.6: Time Domain Signal of Raw Data for Combined Static and Dynamic Forces with 0.5 mph along 16-in. Thick Slab Section 112
Figure B.7: Frequency Domain Signal (Linear Scale) of Raw Data for Combined Static and Dynamic Forces with 0.5 mph along 16-in. Thick Slab Section 112
Figure B.8: Frequency Domain Signal (Decibel Scale) of Raw Data for Combined Static and Dynamic Forces with 0.5 mph along 16-in. Thick Slab Section 112
Figure B.9: Time Domain Signal of Raw Data for Combined Static and Dynamic Forces with 0.5 mph along 8- and 10-in. Thick Slab Section 113
Figure B.10: Frequency Domain Signal (Linear Scale) of Raw Data for Combined Static and Dynamic Forces with 0.5 mph along 8- and 10-in. Thick Slab Section 113
Figure B.11: Frequency Domain Signal (Decibel Scale) of Raw Data for Combined Static and Dynamic Forces with 0.5 mph along 8- and 10-in. Thick Slab Section 113
Figure B.12: Processed Rolling Sensor #1 Signal with 0.5 mph 114
Figure B.13: Time Domain Signal of Raw Data for Rolling Sensor #1 with 0.5 mph along Whole Testbed Length 114
Figure B.14: Frequency Domain Signal (Linear Scale) of Raw Data for Rolling Sensor #1 with 0.5 mph along Whole Testbed Length 114
Figure B.15: Frequency Domain Signal (Decibel Scale) of Raw Data for Rolling Sensor #1 with 0.5 mph along Whole Testbed Length 115
Figure B.16: Time Domain Signal of Raw Data for Rolling Sensor #1 with 0.5 mph along 16-in. Thick Slab Section 115
Figure B.17: Frequency Domain Signal (Linear Scale) of Raw Data for Rolling Sensor #1 with 0.5 mph along 16-in. Thick Slab Section 115
Figure B.18: Frequency Domain Signal (Decibel Scale) of Raw Data for Rolling Sensor #1 with 0.5 mph along 16-in. Thick Slab Section 116
Figure B.19: Time Domain Signal of Raw Data for Rolling Sensor #1 with 0.5 mph along 8- and 10-in. Thick Slab Section 116

Figure B.20: Frequency Domain Signal (Linear Scale) of Raw Data for Rolling Sensor #1 with 0.5 mph along 8- and 10-in. Thick Slab Section 116
Figure B.21: Frequency Domain Signal (Decibel Scale) of Raw Data for Rolling Sensor #1 with 0.5 mph along 8- and 10-in. Thick Slab Section 117
Figure B.22: Processed DMI Signal with 0.5 mph 117
Figure B.23: Time Domain Signal of Raw Data for DMI with 0.5 mph along Whole Testbed Length..... 117
Figure B.24: Time Domain Signal of Raw Data for DMI with 0.5 mph along 16-in. Thick Slab Section 118
Figure B.25: Time Domain Signal of Raw Data for DMI with 0.5 mph along 8- and 10-in. Thick Slab Section 118
Figure B.26: Processed Static Force Signal with 1.0 mph..... 119
Figure B.27: Processed Peak-to-Peak Dynamic Force Signal with 1.0 mph..... 119
Figure B.28: Time Domain Signal of Raw Data for Combined Static and Dynamic Forces with 1.0 mph on Whole Testbed Length..... 120
Figure B.29: Frequency Domain Signal (Linear Scale) of Raw Data for Combined Static and Dynamic Forces with 1.0 mph along Whole Testbed Length..... 120
Figure B.30: Frequency Domain Signal (Decibel Scale) of Raw Data for Combined Static and Dynamic Forces with 1.0 mph along Whole Testbed Length..... 120
Figure B.31: Time Domain Signal of Raw Data for Combined Static and Dynamic Forces with 1.0 mph along 16-in. Thick Slab Section..... 121
Figure B.32: Frequency Domain Signal (Linear Scale) of Raw Data for Combined Static and Dynamic Forces with 1.0 mph along 16-in. Thick Slab Section 121
Figure B.33: Frequency Domain Signal (Decibel Scale) of Raw Data for Combined Static and Dynamic Forces with 1.0 mph along 16-in. Thick Slab Section 121
Figure B.34: Time Domain Signal of Raw Data for Combined Static and Dynamic Forces with 1.0 mph along 8- and 10-in. Thick Slab Section 122
Figure B.35: Frequency Domain Signal (Linear Scale) of Raw Data for Combined Static and Dynamic Forces with 1.0 mph along 8- and 10-in. Thick Slab Section 122
Figure B.36: Frequency Domain Signal (Decibel Scale) of Raw Data for Combined Static and Dynamic Forces with 1.0 mph along 8- and 10-in. Thick Slab Section 122
Figure B.37: Processed Rolling Sensor #1 Signal with 1.0 mph 123
Figure B.38: Time Domain Signal of Raw Data for Rolling Sensor #1 with 1.0 mph along Whole Testbed Length 123
Figure B.39: Frequency Domain Signal (Linear Scale) of Raw Data for Combined Static and Dynamic Forces with 1.0 mph along Whole Testbed Length..... 123
Figure B.40: Frequency Domain Signal (Decibel Scale) of Raw Data for Rolling Sensor #1 with 1.0 mph along Whole Testbed Length..... 124
Figure B.41: Time Domain Signal of Raw Data for Rolling Sensor #1 with 1.0 mph along 16-in. Thick Slab Section..... 124
Figure B.42: Frequency Domain Signal (Linear Scale) of Raw Data for Rolling Sensor #1 with 1.0 mph along 16-in. Thick Slab Section..... 124

Figure B.43: Frequency Domain Signal (Decibel Scale) of Raw Data for Rolling Sensor #1 with 1.0 mph along 16-in. Thick Slab Section 125
Figure B.44: Time Domain Signal of Raw Data for Rolling Sensor #1 with 1.0 mph along 8- and 10-in. Thick Slab Section 125
Figure B.45: Frequency Domain Signal (Linear Scale) of Raw Data for Rolling Sensor #1 with 1.0 mph along 8- and 10-in. Thick Slab Section 125
Figure B.46: Frequency Domain Signal (Decibel Scale) of Raw Data for Rolling Sensor #1 with 1.0 mph along 8- and 10-in. Thick Slab Section 126
Figure B.47: Processed DMI Signal with 1.0 mph 126
Figure B.48: Time Domain Signal of Raw Data for DMI with 1.0 mph along Whole Testbed Length 126
Figure B.49: Time Domain Signal of Raw Data for DMI with 1.0 mph along 16-in. Thick Slab Section 127
Figure B.50: Time Domain Signal of Raw Data for DMI with 1.0 mph along 8- and 10-in. Thick Slab Section 127
Figure B.51: Processed Static Force Signal with 2.0 mph 128
Figure B.52: Processed Pak-to-Peak Dynamic Force Signal with 2.0 mph 128
Figure B.53: Time Domain Signal of Raw Data for Combined Static and Dynamic Forces with 2.0 mph on Whole Testbed Length 129
Figure B.54: Frequency Domain Signal (Linear Scale) of Raw Data for Combined Static and Dynamic Forces with 2.0 mph along Whole Testbed Length 129
Figure B.55: Frequency Domain Signal (Decibel Scale) of Raw Data for Combined Static and Dynamic Forces with 2.0 mph along Whole Testbed Length 129
Figure B.56: Time Domain Signal of Raw Data for Combined Static and Dynamic Forces with 2.0 mph along 16-in. Thick Slab Section 130
Figure B.57: Frequency Domain Signal (Linear Scale) of Raw Data for Combined Static and Dynamic Forces with 2.0 mph along 16-in. Thick Slab Section 130
Figure B.58: Frequency Domain Signal (Decibel Scale) of Raw Data for Combined Static and Dynamic Forces with 2.0 mph along 16-in. Thick Slab Section 130
Figure B.59: Time Domain Signal of Raw Data for Combined Static and Dynamic Forces with 2.0 mph along 8- and 10-in. Thick Slab Section 131
Figure B.60: Frequency Domain Signal (Linear Scale) of Raw Data for Combined Static and Dynamic Forces with 2.0 mph along 8- and 10-in. Thick Slab Section 131
Figure B.61: Frequency Domain Signal (Decibel Scale) of Raw Data for Combined Static and Dynamic Forces with 2.0 mph along 8- and 10-in. Thick Slab Section 131
Figure B.62: Processed Rolling Sensor #1 Signal with 2.0 mph 132
Figure B.63: Time Domain Signal of Raw Data for Rolling Sensor #1 with 2.0 mph along Whole Testbed Length 132
Figure B.64: Frequency Domain Signal (Linear Scale) of Raw Data for Combined Static and Dynamic Forces with 2.0 mph along Whole Testbed Length 133
Figure B.65: Frequency Domain Signal (Decibel Scale) of Raw Data for Rolling Sensor #1 with 2.0 mph along Whole Testbed Length 133

Figure B.66: Time Domain Signal of Raw Data for Rolling Sensor #1 with 2.0 mph along 16-in. Thick Slab Section 133
Figure B.67: Frequency Domain Signal (Linear Scale) of Raw Data for Rolling Sensor #1 with 2.0 mph along 16-in. Thick Slab Section 134
Figure B.68: Frequency Domain Signal (Decibel Scale) of Raw Data for Rolling Sensor #1 with 2.0 mph along 16-in. Thick Slab Section 134
Figure B.69: Time Domain Signal of Raw Data for Rolling Sensor #1 with 2.0 mph along 8- and 10-in. Thick Slab Section 134
Figure B.70: Frequency Domain Signal (Linear Scale) of Raw Data for Rolling Sensor #1 with 2.0 mph along 8- and 10-in. Thick Slab Section 135
Figure B.71: Frequency Domain Signal (Decibel Scale) of Raw Data for Rolling Sensor #1 with 2.0 mph along 8- and 10-in. Thick Slab Section 135
Figure B.72: Processed DMI Signal with 2.0 mph 136
Figure B.73: Time Domain Signal of Raw Data for DMI with 2.0 mph along Whole Testbed Length 136
Figure B.74: Time Domain Signal of Raw Data for DMI with 2.0 mph along 16-in. Thick Slab Section 136
Figure B.75: Time Domain Signal of Raw Data for DMI with 2.0 mph along 8- and 10-in. Thick Slab Section 137
Figure B.76: Processed Static Force Signal with 3.0 mph 138
Figure B.77: Processed Pak-to-Peak Dynamic Force Signal with 3.0 mph 138
Figure B.78: Time Domain Signal of Raw Data for Combined Static and Dynamic Forces with 3.0 mph on Whole Testbed Length 139
Figure B.79: Frequency Domain Signal (Linear Scale) of Raw Data for Combined Static and Dynamic Forces with 3.0 mph along Whole Testbed Length 139
Figure B.80: Frequency Domain Signal (Decibel Scale) of Raw Data for Combined Static and Dynamic Forces with 3.0 mph along Whole Testbed Length 139
Figure B.81: Time Domain Signal of Raw Data for Combined Static and Dynamic Forces with 3.0 mph along 16-in. Thick Slab Section 140
Figure B.82: Frequency Domain Signal (Linear Scale) of Raw Data for Combined Static and Dynamic Forces with 3.0 mph along 16-in. Thick Slab Section 140
Figure B.83: Frequency Domain Signal (Decibel Scale) of Raw Data for Combined Static and Dynamic Forces with 3.0 mph along 16-in. Thick Slab Section 140
Figure B.84: Time Domain Signal of Raw Data for Combined Static and Dynamic Forces with 3.0 mph along 8- and 10-in. Thick Slab Section 141
Figure B.85: Frequency Domain Signal (Linear Scale) of Raw Data for Combined Static and Dynamic Forces with 3.0 mph along 8- and 10-in. Thick Slab Section 141
Figure B.86: Frequency Domain Signal (Decibel Scale) of Raw Data for Combined Static and Dynamic Forces with 3.0 mph along 8- and 10-in. Thick Slab Section 141
Figure B.87: Processed Rolling Sensor #1 Signal with 3.0 mph 142
Figure B.88: Time Domain Signal of Raw Data for Rolling Sensor #1 with 3.0 mph along Whole Testbed Length 142

Figure B.89: Frequency Domain Signal (Linear Scale) of Raw Data for Combined Static and Dynamic Forces with 3.0 mph along Whole Testbed Length 142
Figure B.90: Frequency Domain Signal (Decibel Scale) of Raw Data for Rolling Sensor #1 with 3.0 mph along Whole Testbed Length 143
Figure B.91: Time Domain Signal of Raw Data for Rolling Sensor #1 with 3.0 mph along 16-in. Thick Slab Section 143
Figure B.92: Frequency Domain Signal (Linear Scale) of Raw Data for Rolling Sensor #1 with 3.0 mph along 16-in. Thick Slab Section 143
Figure B.93: Frequency Domain Signal (Decibel Scale) of Raw Data for Rolling Sensor #1 with 3.0 mph along 16-in. Thick Slab Section 144
Figure B.94: Time Domain Signal of Raw Data for Rolling Sensor #1 with 3.0 mph along 8- and 10-in. Thick Slab Section 144
Figure B.95: Frequency Domain Signal (Linear Scale) of Raw Data for Rolling Sensor #1 with 3.0 mph along 8- and 10-in. Thick Slab Section 144
Figure B.96: Frequency Domain Signal (Decibel Scale) of Raw Data for Rolling Sensor #1 with 3.0 mph along 8- and 10-in. Thick Slab Section 145
Figure B.97: Processed DMI Signal with 3.0 mph 145
Figure B.98: Time Domain Signal of Raw Data for DMI with 3.0 mph along Whole Testbed Length 145
Figure B.99: Time Domain Signal of Raw Data for DMI with 3.0 mph along 16-in. Thick Slab Section 146
Figure B.100: Time Domain Signal of Raw Data for DMI with 3.0 mph along 8- and 10-in. Thick Slab Section 146
Figure B.101: Processed Static Force Signal with 4.0 mph 147
Figure B.102: Processed Pak-to-Peak Dynamic Force Signal with 4.0 mph 147
Figure B.103: Time Domain Signal of Raw Data for Combined Static and Dynamic Forces with 4.0 mph on Whole Testbed Length 148
Figure B.104: Frequency Domain Signal (Linear Scale) of Raw Data for Combined Static and Dynamic Forces with 4.0 mph along Whole Testbed Length 148
Figure B.105: Frequency Domain Signal (Decibel Scale) of Raw Data for Combined Static and Dynamic Forces with 4.0 mph along Whole Testbed Length 148
Figure B.106: Time Domain Signal of Raw Data for Combined Static and Dynamic Forces with 4.0 mph along 16-in. Thick Slab Section 149
Figure B.107: Frequency Domain Signal (Linear Scale) of Raw Data for Combined Static and Dynamic Forces with 4.0 mph along 16-in. Thick Slab Section 149
Figure B.108: Frequency Domain Signal (Decibel Scale) of Raw Data for Combined Static and Dynamic Forces with 4.0 mph along 16-in. Thick Slab Section 149
Figure B.109: Time Domain Signal of Raw Data for Combined Static and Dynamic Forces with 4.0 mph along 8- and 10-in. Thick Slab Section 150
Figure B.110: Frequency Domain Signal (Linear Scale) of Raw Data for Combined Static and Dynamic Forces with 4.0 mph along 8- and 10-in. Thick Slab Section 150

Figure B.111: Frequency Domain Signal (Decibel Scale) of Raw Data for Combined Static and Dynamic Forces with 4.0 mph along 8- and 10-in. Thick Slab Section 150
Figure B.112: Processed Rolling Sensor #1 Signal with 4.0 mph 151
Figure B.113: Time Domain Signal of Raw Data for Rolling Sensor #1 with 4.0 mph along Whole Testbed Length 151
Figure B.114: Frequency Domain Signal (Linear Scale) of Raw Data for Combined Static and Dynamic Forces with 4.0 mph along Whole Testbed Length 151
Figure B.115: Frequency Domain Signal (Decibel Scale) of Raw Data for Rolling Sensor #1 with 4.0 mph along Whole Testbed Length 152
Figure B.116: Time Domain Signal of Raw Data for Rolling Sensor #1 with 4.0 mph along 16-in. Thick Slab Section 152
Figure B.117: Frequency Domain Signal (Linear Scale) of Raw Data for Rolling Sensor #1 with 4.0 mph along 16-in. Thick Slab Section 152
Figure B.118: Frequency Domain Signal (Decibel Scale) of Raw Data for Rolling Sensor #1 with 4.0 mph along 16-in. Thick Slab Section 153
Figure B.119: Time Domain Signal of Raw Data for Rolling Sensor #1 with 4.0 mph along 8- and 10-in. Thick Slab Section 153
Figure B.120: Frequency Domain Signal (Linear Scale) of Raw Data for Rolling Sensor #1 with 4.0 mph along 8- and 10-in. Thick Slab Section 153
Figure B.121: Frequency Domain Signal (Decibel Scale) of Raw Data for Rolling Sensor #1 with 4.0 mph along 8- and 10-in. Thick Slab Section 154
Figure B.122: Processed DMI Signal with 4.0 mph 154
Figure B.123: Time Domain Signal of Raw Data for DMI with 4.0 mph along Whole Testbed Length 154
Figure B.124: Time Domain Signal of Raw Data for DMI with 4.0 mph along 16-in. Thick Slab Section 155
Figure B.125: Time Domain Signal of Raw Data for DMI with 4.0 mph along 8- and 10-in. Thick Slab Section 155

List of Tables

Table 4.1: Options in RDD Data Collection Software 56
Table 4.2: Pull Down Menu Options in the Field RDD Processing Software..... 60

Chapter 1. Introduction

1.1 Project Objectives and Overview

The primary objective of Project 0-6005 is to develop the Total Pavement Acceptance Device (TPAD), which is a new nondestructive testing device that will be used to continuously assess pavement structural conditions. The TPAD will be a multi-function device that includes the capacities of the Rolling Dynamic Deflectometer (RDD), Ground Penetrating Radar (GPR), Distance Measurement Instrument (DMI), and high-precision differential GPS measurements. In addition, pavement surface temperature measurements and digital video imaging of the pavement will be included.

This 4-year project began in September 2008. The third-year efforts are discussed in this report. The project is a joint effort between the Center for Transportation Research (CTR) at the University of Texas (UT) and the Texas Transportation Institute (TTI) at Texas A&M University. CTR researchers, working with researchers at UT's Center for Electromechanics (CEM), are responsible for developing all aspects dealing with the RDD portion of the TPAD. This work includes developing (1) the specifications, construction, and purchase of the TPAD mobile platform and transportation equipment, (2) improvements to the RDD rolling sensors, and (3) improvements to the RDD data analysis procedure. Researchers at TTI are responsible for developing TPAD data acquisition analysis and processing systems, including GPR, DMI, GPS, temperature, and video imaging.

1.2 Outline of Progress during Year 3

In Year 2, the TPAD mobile platform and transportation (haul) equipment were developed. During that period, bids on all pieces of equipment were accepted.

During Year 3, the TPAD mobile platform and transportation equipment were delivered to the Pickle Research Center (PRC) at UT and acceptance testing was initially performed on one of the asphalt roads at PRC. Subsequently, acceptance testing was performed using the jointed concrete pavements testbed at the Texas Department of Transportation (TxDOT) Flight Services Facility (FSF). Acceptance testing included (1) the speed control, (2) the static load control, (3) the dynamic load control, (4) the portable load calibration system, and (5) DMI. During the acceptance testing, some improvements were identified in the static and dynamic load measurements and in the speed control. The manufacturer completed improvements in these TPAD loading and control functions.

.

Simultaneously, developments to the speed-improved rolling sensors were performed and the performance of the improved rolling sensors was evaluated. Based on the performance of these rolling sensors, the target testing speed for the TPAD was adjusted to 3 to 7 mph. Delivery of the TPAD mobile platform and dedicated hauling equipment and the acceptance testing of the TPAD mobile platform are described in Chapter 2. Improvements to the RDD portion of the TPAD (Speed-Improved Rolling Sensors) to achieve the target testing speed are presented in Chapter 3. Justification for the 3-mph testing speed of the rolling sensors is also discussed in Chapter 3. In Chapter 4, improvements to the Data Acquisition (DAQ) system developed by TTI are presented.

Chapter 2. Delivery of TPAD Mobile Platform and Dedicated Hauling Equipment and Acceptance Testing

2.1 Introduction

The TPAD mobile platform and associated dedicated hauling equipment, a tractor and trailer system, were delivered to UT's PRC in late fall 2010. Acceptance testing for the TPAD mobile platform was subsequently performed at PRC and at the TxDOT FSF at Austin Bergstrom International Airport (ABIA) in spring 2011. The acceptance testing involved evaluating (1) the speed control, (2) the static load control, (3) the dynamic load control, (4) the portable load calibration system, and (5) the DMI.

2.2 Delivery of the TPAD Mobile Platform

During the first week of October 2010, personnel from CTR and TTI visited Industrial Vehicles International, Inc. (IVI) in Tulsa, Oklahoma, to check the progress of the construction of the TPAD Mobile Platform. The TTI data acquisition and GPR systems were delivered to IVI for testing fitting on the Mobile Platform at that time. The TPAD mobile platform was delivered to PRC at UT during the third week of November 2010. Specifications for the TPAD are documented in the Second-Year Progress Report (Stokoe et al., 2011).

2.3 Delivery of the Tractor and Trailer (Dedicated Hauling Equipment)

The tractor and trailer should be able to transport the TPAD mobile platform to and from each project location and store and support minor maintenance equipment required for normal TPAD operations. The tractor can tow the trailer and load across a broad spectrum of pavement/terrain conditions, and has the capacity to haul and store the TPAD support equipment. The trailer should have a minimum load angle and the capacity to transport the TPAD mobile platform and supporting equipment. The tractor and trailer were delivered to PRC at UT on December 3, 2010. The TPAD mobile platform and transportation equipment are shown in Figure 2.1. Specifications for the tractor and trailer are documented in the Second-Year Progress Report (Stokoe et al., 2011).

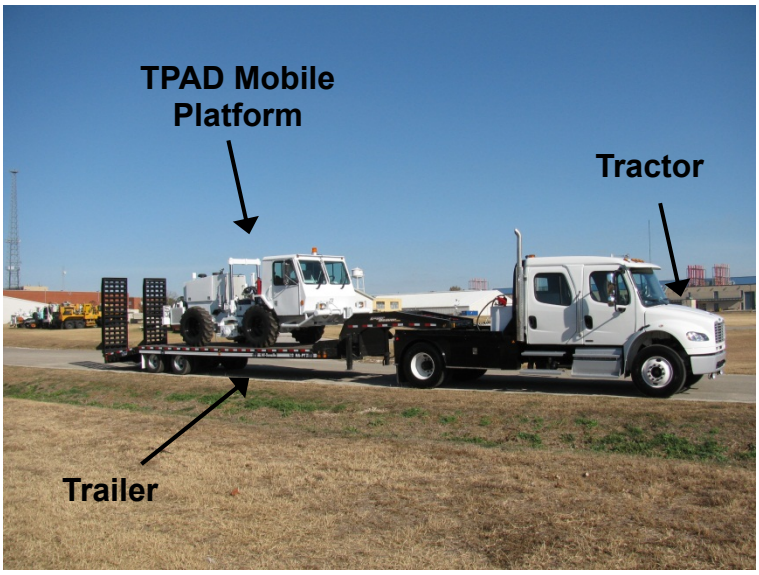

Figure 2.1: Photograph of the TPAD Mobile Platform and Dedicated Hauling Equipment at UT's Pickle Research Center

2.4 Acceptance Testing of TPAD Mobile Platform

Acceptance testing of the TPAD mobile platform began during the second week of December 2010 at PRC. Acceptance testing continued at the TxDOT FSF at various times over the next several months along with addressing various modifications to software and hardware issues as documented below.

2.4.1 TPAD Speed Control

In the specifications for the vehicle portion of the TPAD, the mobile platform should be able to provide electric-servo-speed control over a range of 1 to 10 mph, with the capability of controlling within +/- 0.2 mph. Prior to going to the FSF testbed, the first trial of the speed control was performed along a 500-ft long asphalt pavement at PRC on December 8, 2010. Photographs during the testing are shown in Figure 2.2. The marker cones were placed on the ground every 100 ft and the time was measured when the TPAD passed each cone to calculate the speed. The calculated speed was then compared with the speed set in the computer program used to control the TPAD

The speed calculated every 100 ft with different speed settings (ranging from 1 to 5 mph) is presented in Figure 2.3 and comparisons between the speed setting and the average calculated speed are shown in Figure 2.4. As seen in Figures 2.3 and 2.4, the speed control is less accurate as the TPAD speed increases. At speeds of 3, 4 and 5 mph, differences between speed setting and calculated speed exceed the required specification of +/- 0.2 mph. It was found that the software in the TPAD computer program needed to be modified. IVI undertook the modifications on the same day as the TPAD speed control testing was performed.

(a)

(b)

Figure 2.2: Speed Control Testing of the TPAD Mobile Platform at Pickle Research Center in December 2010

After modifications to the computer software, the speed-control check was again performed at FSF one day after the TPAD speed control testing at PRC. The testing procedure was the same as followed at PRC. Marker cones were placed on the pavement at 100-ft intervals and the time when the TPAD passed the location of each cone was measured and recorded.

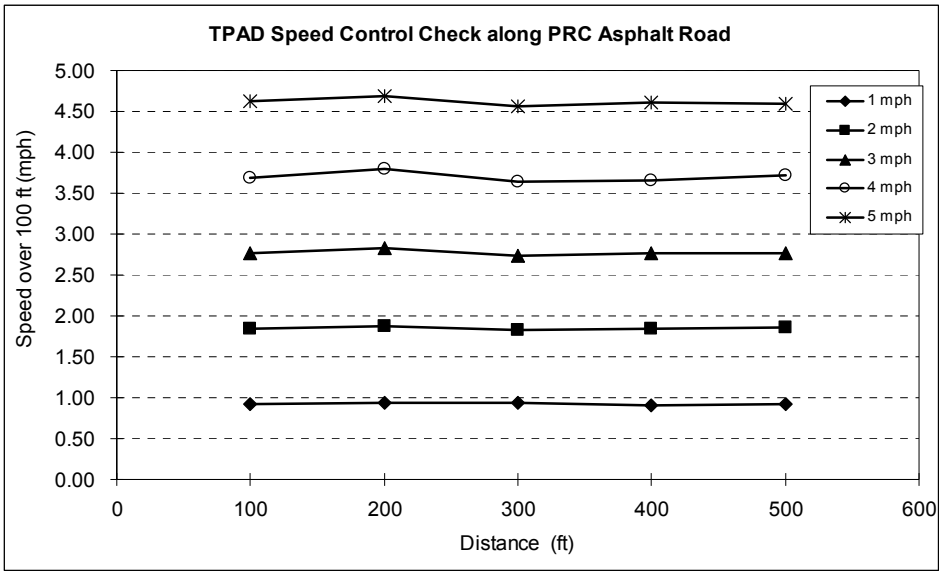

Figure 2.3: Speed Calculated Every 100 ft along a 500-ft Stretch of PRC Asphalt Road for Different Speed Settings

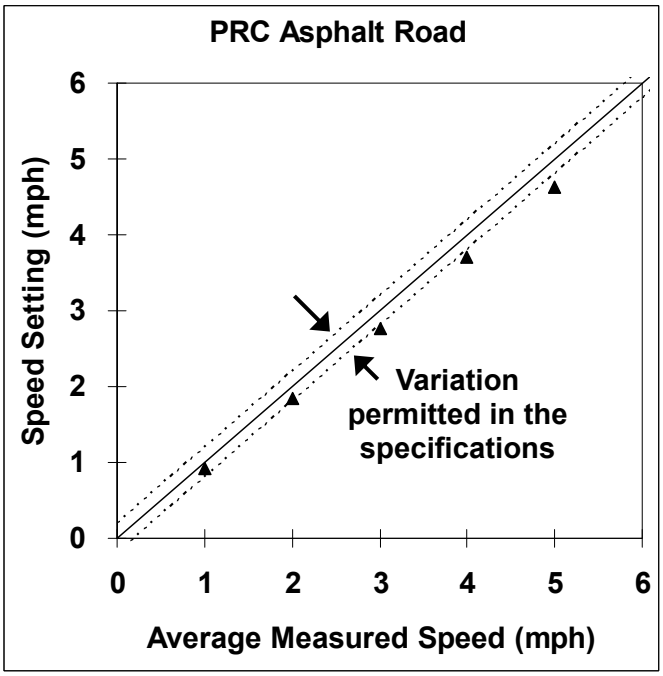

Figure 2.4: Comparison between Speed Settings and Average Calculated Speed (at PRC)

The speed was calculated every 100 ft for different speeds (1 to 5 mph) and then the average calculated speed in each trial was compared with the speed setting. The results are shown in Figures 2.5 and 2.6. The acceptance testing for the TPAD speed control performed after software modifications found that the speed setting was more accurate than that found in the original testing at PRC. The difference between the set speed and average calculated speed (real speed) was much less than the specifications (+/-0.02 mph vs. +/-0.2 mph).

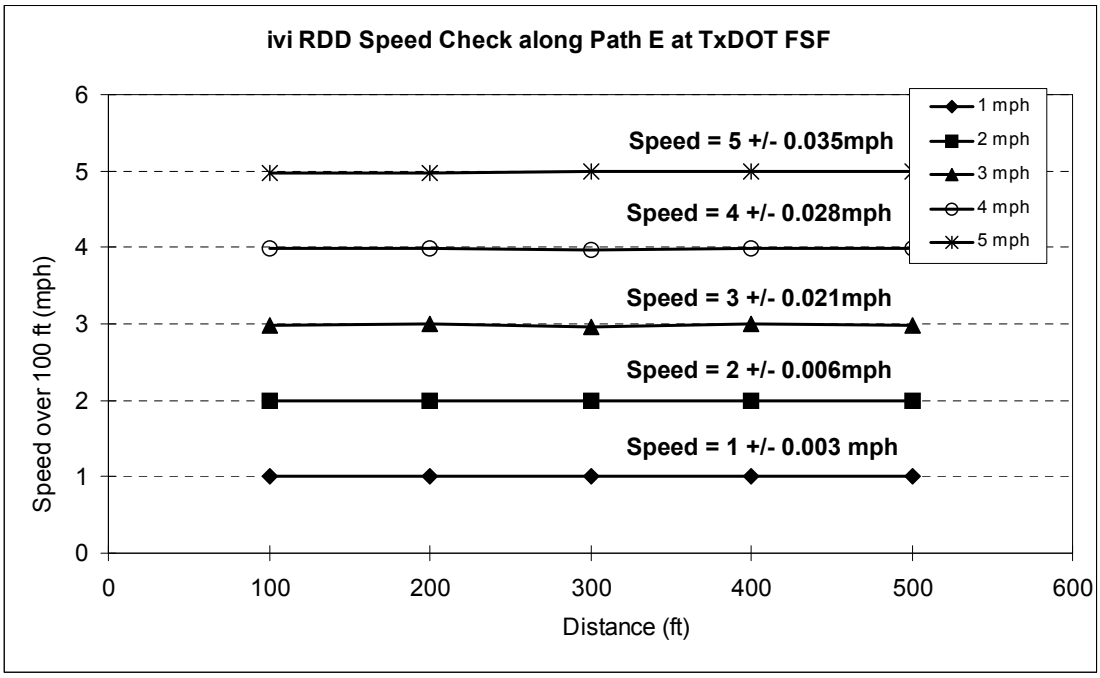

Figure 2.5: Speed Calculated Every 100 ft along a 500-ft Stretch of Jointed Concrete Pavement at TxDOT FSF for Different Speed Settings

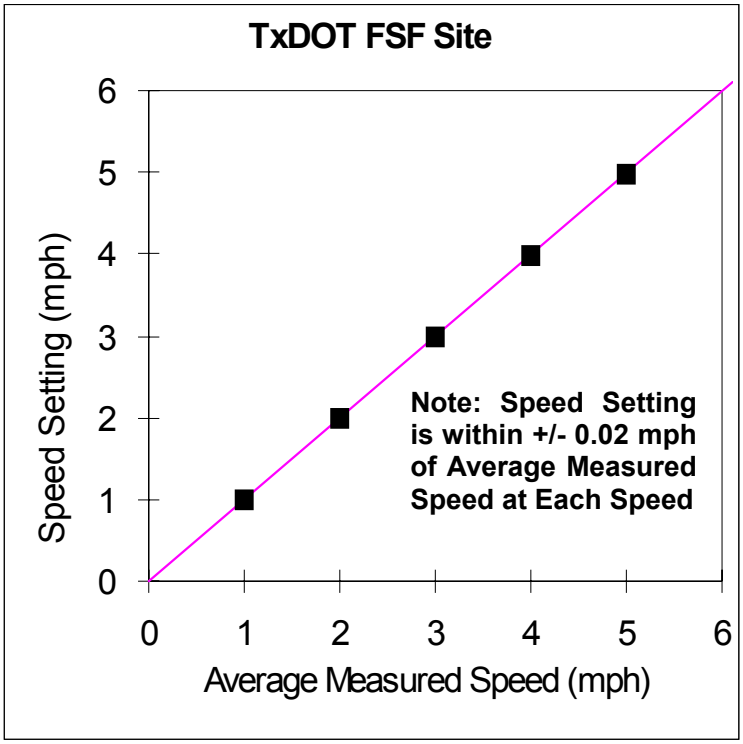

Figure 2.6: Comparison between Speed Setting and Average Calculated Speed at TxDOT FSF, ABIA after Software Modifications

2.4.2 TPAD Static Load Control

The acceptance testing of the TPAD static load control was performed on the 8-in. thick slab at the TxDOT FSF. Truck scales from CEM were used for this testing. To check the static load applied by the loading rollers, two truck scales were placed under the TPAD. The TPAD loading roller was then moved so that each was located directly over a truck scale. After setting the input static load level, truck scales were read after the scale display stabilized. The input static loads and the truck scale readings were compared. A photograph of the TPAD loading rollers sitting on the truck scales is shown in Figure 2.7.

The acceptance testing for static loading was conducted over a 4000-lb to 12000-lb range, in increments of 1000 lb. The comparison between the static load settings and static loads measured with the truck scales is shown in Figure 2.8. According to the specifications for the TPAD static-load control, the difference should be within 300 lb. The average difference for all measurements between the setting and measured static loads is 248 lb, which is less than 300 lb. However, the differences were bigger than 300 lb in the case of load levels of 8000, 9000, and 10000 lbs. It was found that computer software modifications needed to be made to meet the original specifications. IVI engineers returned to Tulsa, OK to improve the software. In June, 2011, IVI personnel and a consultant software engineer came to PRC and made modifications to the TPAD computer program.

It should be noted that the TPAD load calibration system was not used to evaluate the static load during acceptance testing. This system will, however, be used in the future.

Figure 2.7: TPAD Loading Rollers Sitting on the Truck Scales during Static-Load Acceptance Testing at TxDOT FSF, ABI on December 09, 2010

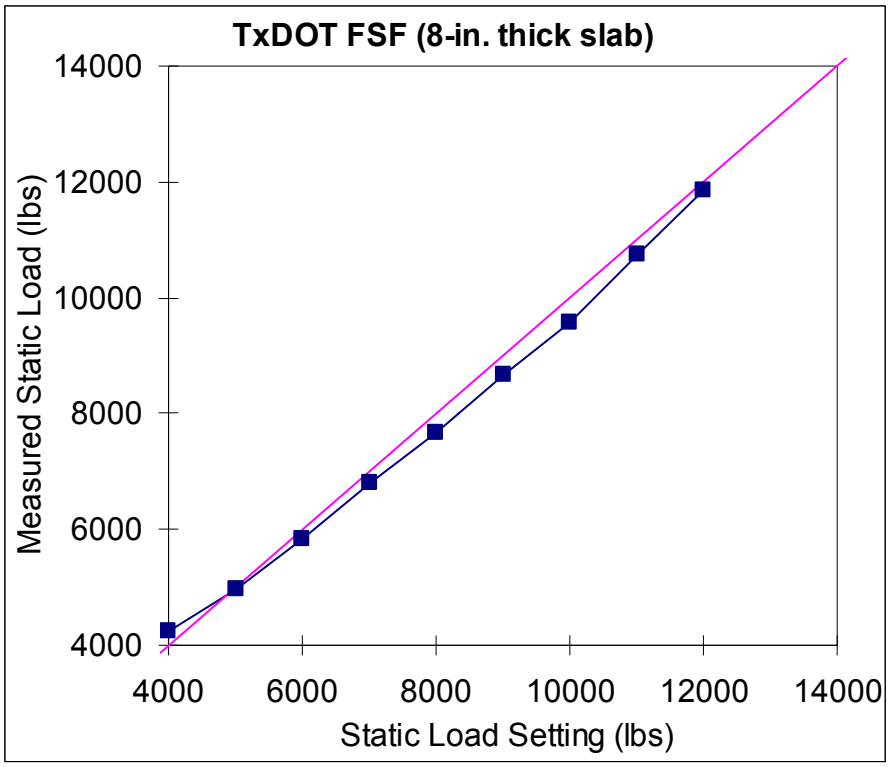

Figure 2.8: Comparison between Static-Load Settings and Static Loads Measured with Truck Scales at TxDOT FSF, ABIA during Second Week of December 2010

2.4.3 Calibration of Portable TPAD Load Calibration System

For the calibration of the TPAD dynamic loading functions, equipment was specially designed and fabricated which is called the TPAD load calibration system. The TPAD load calibration system consists of a steel frame that houses four load cells used to measure the load level generated by the TPAD. Although it can be taken to the field, the system weighs about 400 lbs so special handling equipment is required.

Before using the calibration system to evaluate the TPAD dynamic load control, the system itself had to be calibrated to verify the calibrations given by IVI. Calibration of this system was performed at Ferguson Laboratory at PRC with a 25-kip reference loadcell from UT. The reference UT load cell was also thoroughly calibrated. Photographs taken during the calibrations are presented in Figure 2.9.

The calibration was performed from 0 lb to 22000 lb in increments of about 1000 lb. The results are shown in Figure 2.10. As shown in Figure 2.10, the TPAD load calibration system matched well with the reference load cell (UT load cell).

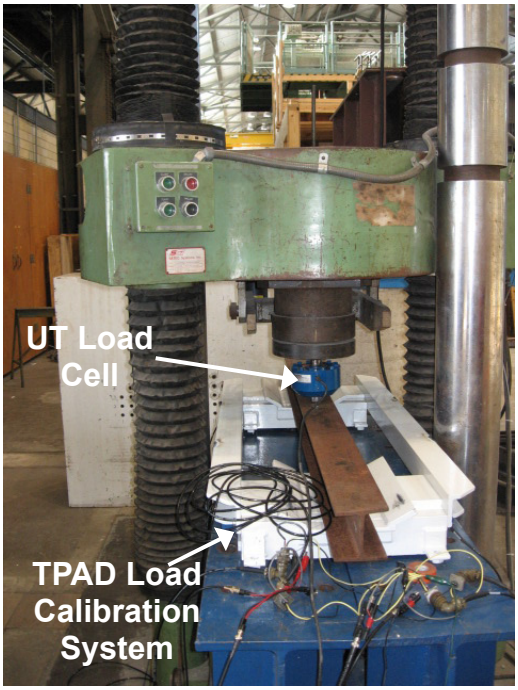

(a)

(b)

Figure 2.9: Calibration of TPAD Load Calibration System at Ferguson Structural Engineering Laboratory at Pickle Research Center

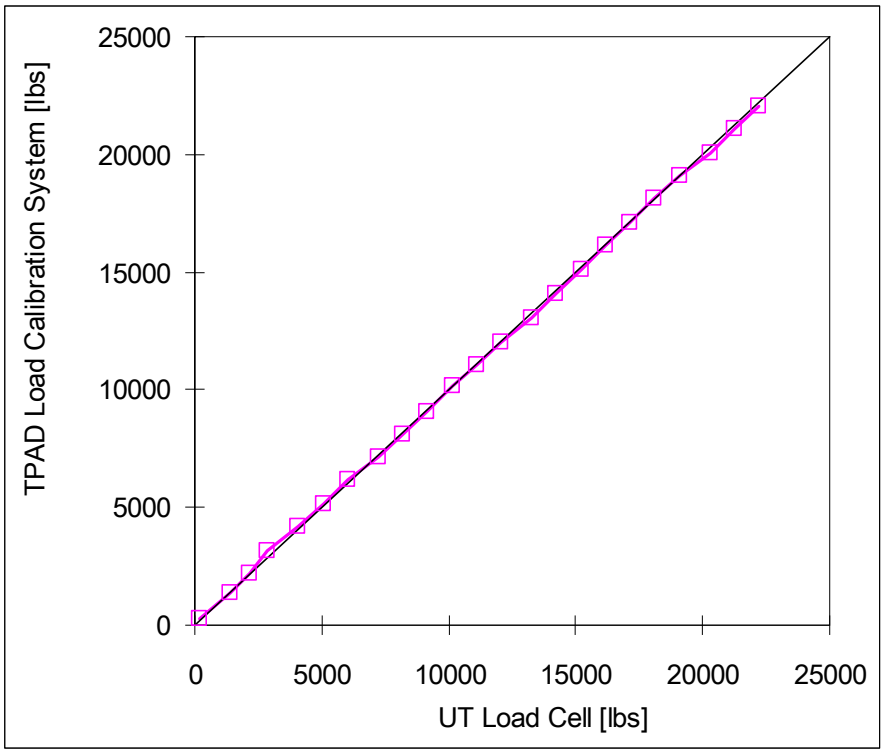

Figure 2.10: Calibration Curve between TPAD Load Calibration System and the UT Reference Load Cell

2.4.4 TPAD Dynamic Sinusoidal Loading

Once the TPAD Load Calibration System was calibrated, acceptance testing of the TPAD dynamic sinusoidal loads applied by the loading rollers was performed. This testing was performed on the 16-in. thick slab at TxDOT FSF using the load calibration system. A 16-in. thick slab was selected as the test slab because of the known small deflections of these slabs at the FSF. To measure the TPAD generated loading functions, the TPAD load calibration system was located under the TPAD and then the loading rollers were lowered onto the calibration system. Figure 2.11 shows installation of the calibration fixture under the TPAD (Figure 2.11 (a)) and TPAD loading rollers placed on the calibration system (Figure 2.11 (b)).

(a) Installation of Load Calibration System under the TPAD

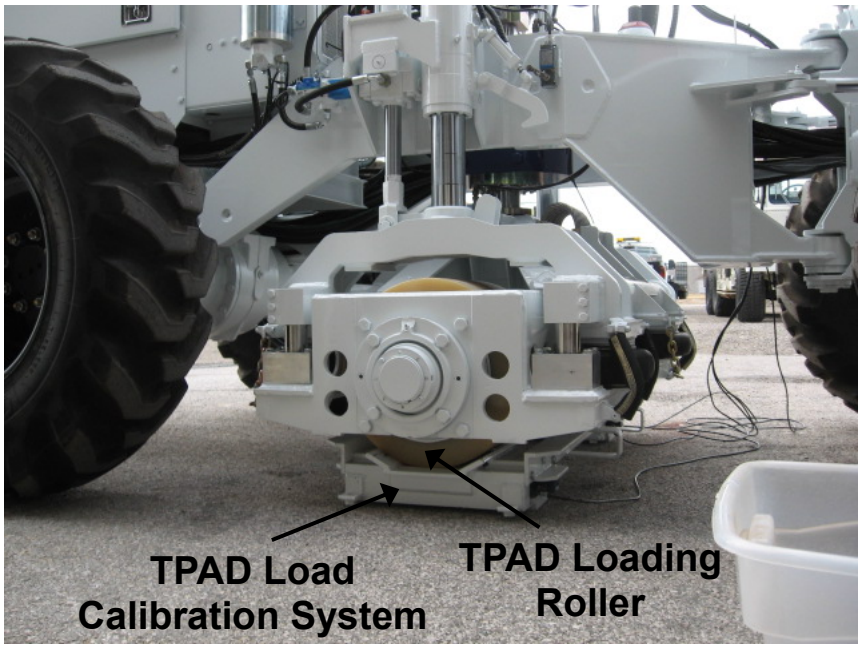

(b)

Figure 2.11: (a) Installation of TPAD Load Calibration system under the TPAD and (b) TPAD Loading Rollers Sitting on TPAD Load Calibration Fixture; Testing Conducted during Second Week of December 2011

The acceptance testing for the TPAD dynamic sinusoidal loading was conducted with dynamic peak-to-peak load settings from 6000 lb to 10000 lb with increments of 2000 lb and at operating frequencies (f_0) of 20, 25, 30, 35, and 40 Hz. The output of the load calibration system

and the TPAD computer for each setting were recorded and compared. As required in the specifications for the TPAD dynamic force measurement, the output from the TPAD computer was calculated using accelerometers on the TPAD loading mass and loading roller frame and the dynamic load levels for the calibration system were measured from the steady-state portion of a 5-second time window. The results for the TPAD dynamic load evaluations are shown in Figure 2.12. In Figure 2.12, significant differences between the load settings on the TPAD computer and the dynamic loads measured with the independent TPAD load calibration system at all operating frequencies exist. IVI personnel attributed these differences in the TPAD dynamic load settings and measured peak-to-peak dynamic loads to the TPAD software. This was addressed in June 2011 but not successfully resolved. Work on the software continued through the summer 2011 and September 2011.

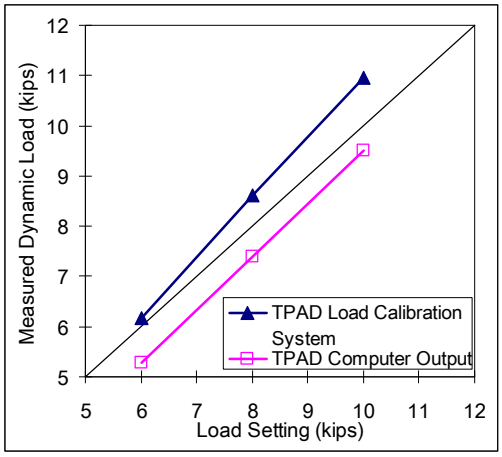

(a) Operating Frequency of 20 Hz

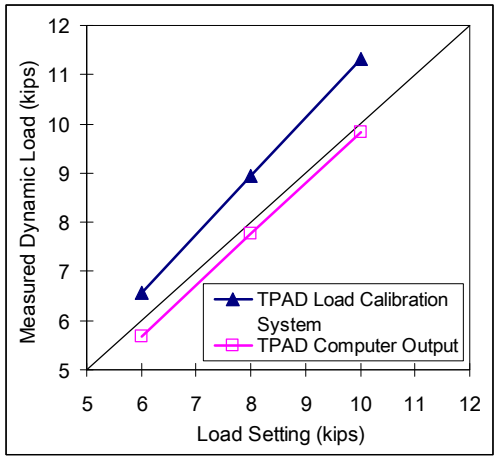

(b) Operating Frequency of 25 Hz

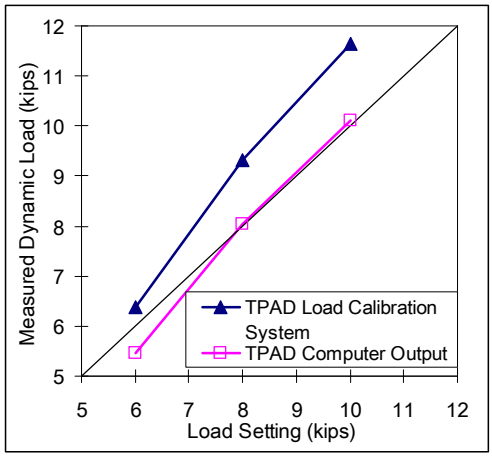

(c) Operating Frequency of 30 Hz

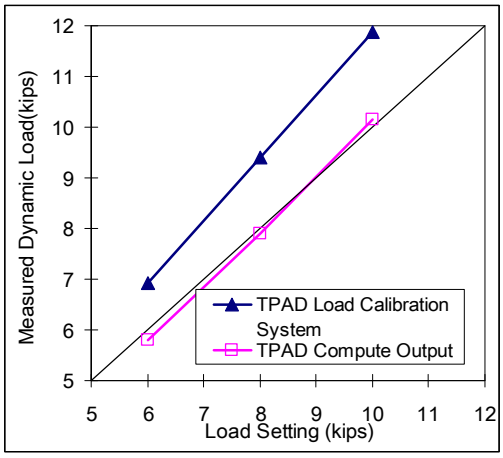

(d) Operating Frequency of 35 Hz

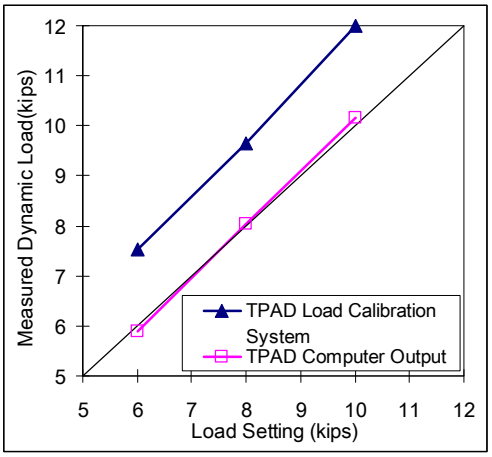

(e) Operating Frequency of 40 Hz

Figure 2.12: TPAD Dynamic Load Readings from the Independent TPAD Load Calibration System and the TPAD Computer for Load Settings at Different Operating Frequencies

The time domain signal of the TPAD computer output and TPAD load calibration system in 1-sec time windows are shown in Figures 2.13. For time domain signals at operating frequencies of 20, 25, and 30 Hz, the TPAD load calibration system shows complex waveforms. In addition, the TPAD computer output also exhibits loading variations while a constant sinusoidal force was applied to the pavement. Based on the variations in peak amplitudes from the computer output and complex waveforms monitored by the load calibration system, IVI personnel continued to improve the TPAD software.

2.4.5 Distance Measurement Instrument, DMI

The distance measurement was not evaluated directly during the initial acceptance testing. It was, however, indirectly evaluated because it is part of the speed control that worked properly after the software modifications discussed in Section 2.4.1.

During the initial testing with the combined TPAD and TTI data acquisition (DAQ) system in December 2010, it was discovered that an incompatibility existed when connecting the TTI DAQ to the TPAD which caused the DMI to malfunction. As a result, a second DMI was added by IVI for the TTI DAQ system which was used on subsequent tests in 2011.

2.5 Summary

In this chapter, deliveries of the TPAD mobile platform and associated transportation equipment are presented. Results of acceptance tests of the TPAD mobile platform which were performed during the second week of December 2010 are presented and discussed.

Through the acceptance testing, it was confirmed that the speed control of the TPAD was acceptable. However, the static load control and dynamic sinusoidal loading functioning of the TPAD do not fulfill the specifications. It was determined that the software in the TPAD program needed to be modified. After the modification of the software, the TPAD loading functions were re-tested and continued improvements were required. The final testing is scheduled for spring 2012.

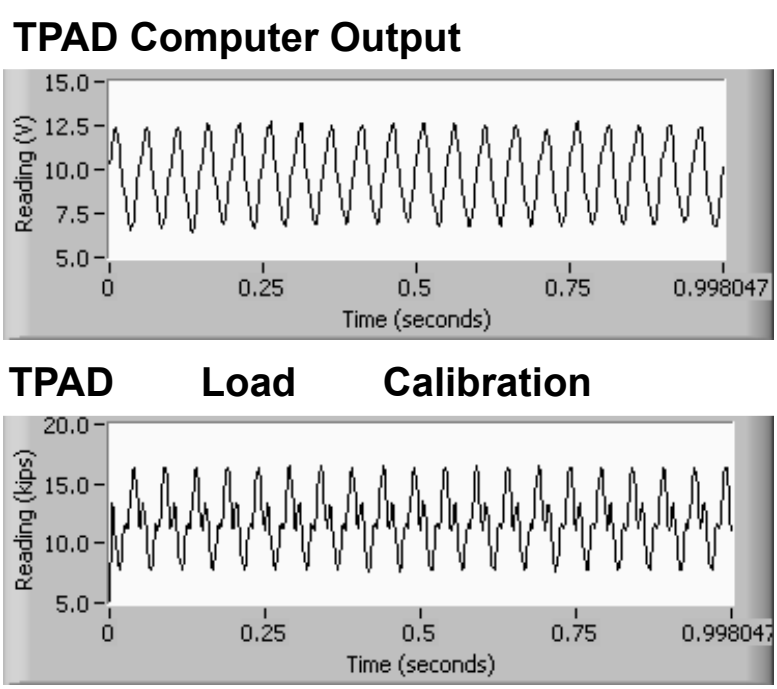

(a) Operating Frequency of 20 Hz

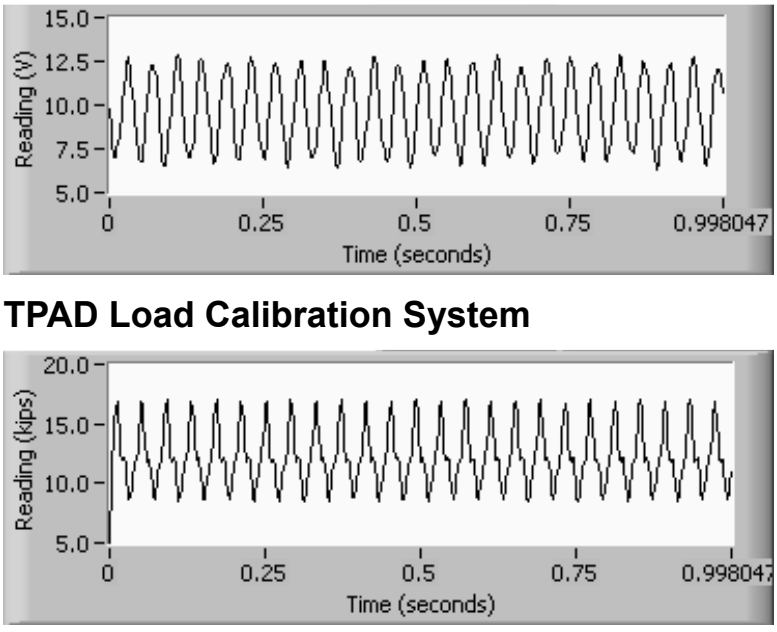

(b) Operating Frequency of 25 Hz

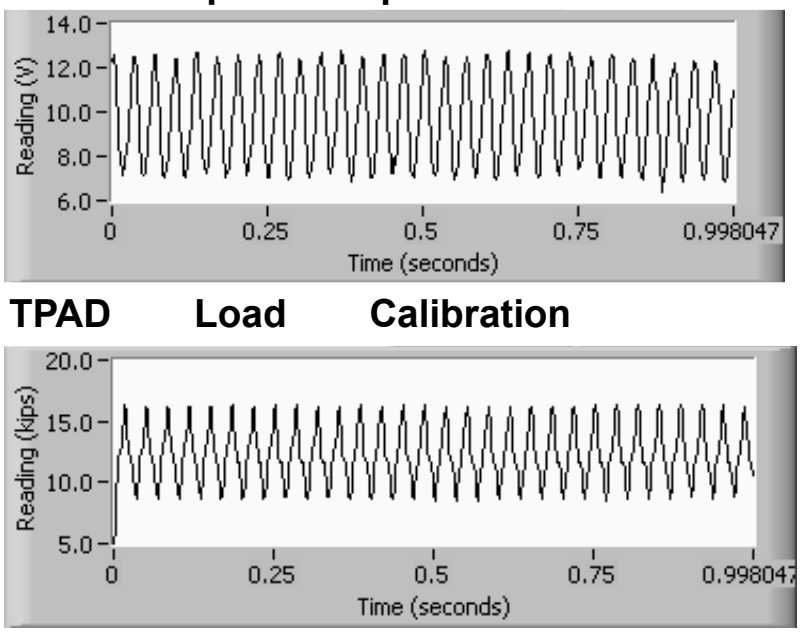

(c) Operating Frequency of 30 Hz

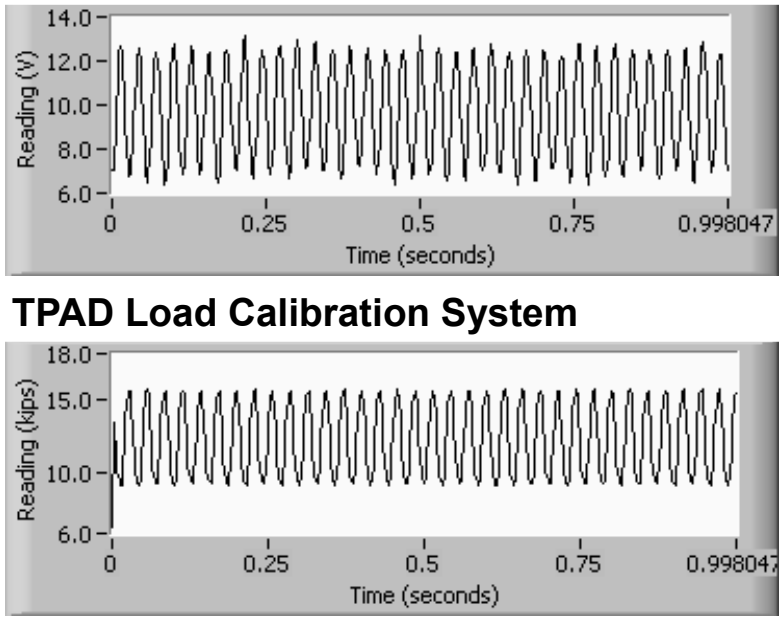

(d) Operating Frequency of 35 Hz

TPAD Computer Output

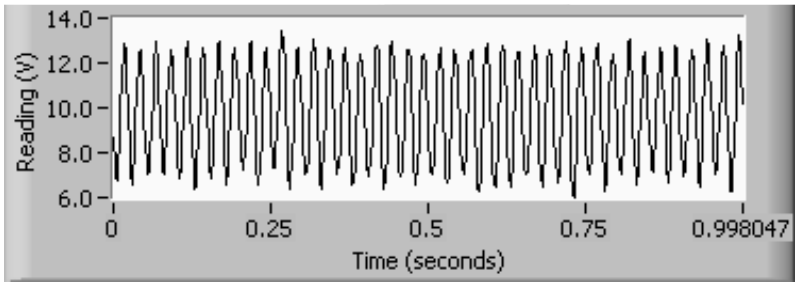

TPAD Load Calibration System

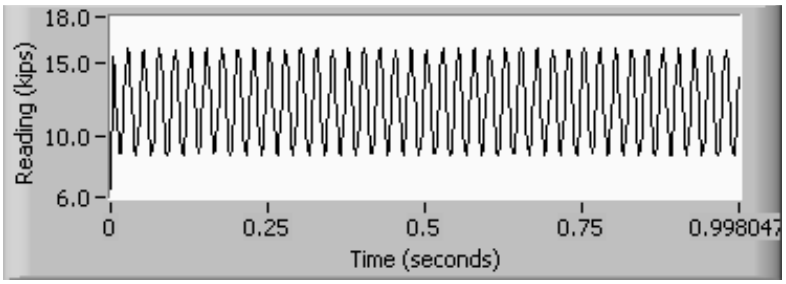

(e) Operating Frequency of 40 Hz

Figure 2.13: 1-Sec Time Domain Signals of TPAD Dynamic Load from the Independent TPAD Load Calibration System and the TPAD Computer for Load Peak-to-Peak Settings at Different Operating Frequencies

Chapter 3. Improvements to the RDD Portion of the TPAD

3.1 Introduction

As discussed in Chapter 2, the TPAD mobile platform and TPAD dedicated hauling equipment were delivered and acceptance testing was performed during Year 3. The need for some improvements and modifications were uncovered during the acceptance testing and these modifications, mainly on the TPAD computer software, were made to improve the TPAD performance.

As discussed in Sections 3.2, 3.3, and 3.4, two speed-improved rolling sensors were assembled and installed on the TPAD using hardware loaned to the project by IVI. During initial testing with the rolling sensors, it was found that sensor #1, located mid-way between the two loading rollers, can be used up to a testing speed of 3 mph. On the other hand, sensor #2 showed lateral oscillations in the direction of travel when crossing joints or cracks at testing speeds of 2 or 3 mph. Modifications to the IVI positioning mechanism of sensor #2 were made and additional tests were conducted. The modifications were somewhat helpful but were not completely successful in preventing the lateral movements of sensor #2.

Originally, four different sets of rolling wheels for the speed-improved rolling sensor were designed. Only one set of wheels has been used in the preliminary TPAD testing. The performance of all four sets of wheels was evaluated on an asphalt pavement at PRC in terms of the level of rolling noise by the different wheels. This testing and the results are presented in Section 3.5. An independent towing frame built by CEM personnel was used for measuring the noise;three hold-down weights (20, 40, and 90 lb) and three approximate speeds were evaluated (about 1, 3, and 5 mph) in this study.

Finally, a new concept for the TPAD hold-down and lifting system was proposed to replace the current IVI sensor positioning system. This work is scheduled to be implemented and evaluated in fall 2011.

3.2 Assembly and Installation of Speed-Improved Rolling Sensors

The speed-improved rolling sensors were developed to reduce rolling noise, improve tracking of pavement deflections, and improve signal fidelity as specified in the second-year Progress Report. The roller body parts that were prepared during the second year were assembled during the third year and installed on the TPAD. One wheel with the bearing set is shown in Figure 3.1 (a) and the cart body assembled with three wheels is shown in Figure 3.1 (b). All three wheels are 9 in. in diameter.

(a)

(b)

Figure 3.1: (a) One 9-in. Diameter Wheel with the Bearing Set, and (b) Cart Body with Three, 9-in. Diameter Wheels

As a beginning point, two speed-improved rolling sensors were installed under the TPAD. One sensor was installed mid-way between the two loading rollers of the TPAD. This rolling sensor is designated as sensor #1. The second rolling sensor, designated as sensor #2, was installed about 25 inches in front of sensor #1. The distance of 25 in. represents the horizontal distance between the measurement points on the pavement. Because of space limitations around the TPAD loading rollers, each rolling sensor has 9-in. diameter wheels; the single wheel on one side is 2-in. wide and the other two wheels on the opposite side of the cart are each 1 inch wide. These three wheels are shown on the cart in Figure 3.1(b). Figures 3.2 (a) and (b) show sensors #1 and #2 before they are installed under the TPAD. The white frames in Figure 3.2 were constructed by IVI and were loaned to the project. Photographs of sensors #1 and #2 installed under the TPAD are shown in Figure 3.3.

(a) Sensor #1

(b) Sensor #2

Figure 3.2: Speed-Improved Rolling Sensors before Installation on the TPAD

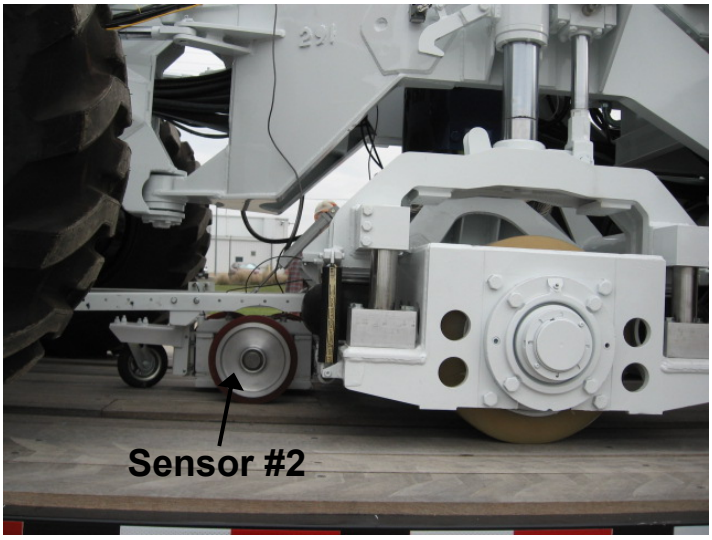

(a) Sensor #2 in the Lowered Position with TPAD on the Trailer

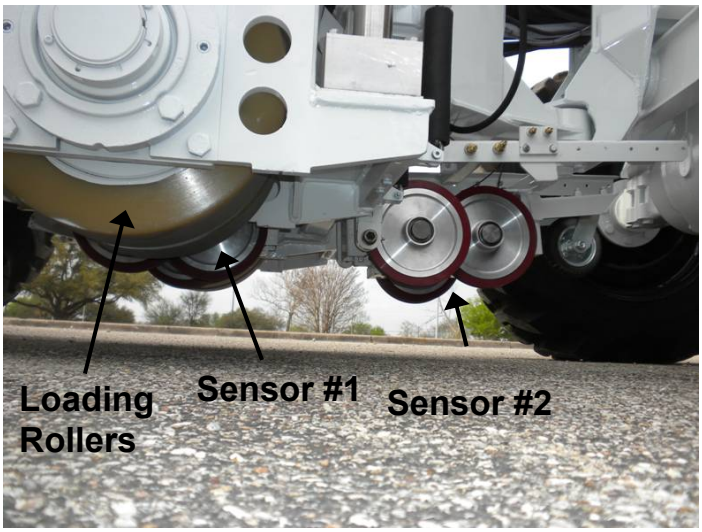

(b) Sensors #1 and #2 in the Up-Position during Re-Location
of the TPAD for Testing Along the Pavement

Figure 3.3: Speed-Improved Rolling Sensors Installed in Position under the TPAD

3.3 Testing of Speed-Improved Rolling Sensors with the TPAD

In this section, deflection results from testing performed at the TxDOT FSF with speed-improved rolling sensors on the TPAD are presented. The first testing of the speed-improved sensors was conducted as a combined effort between CTR and TTI in March 2011. After this initial combined effort, several additional sets of tests were performed by CTR and CEM personnel. These tests were directed at modifications to sensor #2 to improve its performance. As part of testing, it was confirmed that sensor #1 was performing well up to a testing speed of 3 mph.

3.3.1 Combined CTR and TTI Testing

In March 2011, personnel from CTR and TTI performed TPAD testing at the TxDOT FSF. During this testing, both CTR and TTI data acquisition (DAQ) systems were used. In this chapter, only the data collected with the CTR DAQ are presented. The results of all TTI testing are presented in Chapter 4. This testing was conducted to check the performance of the speed-improved rolling sensors and the consistency of both the CTR and TTI DAQ systems. Figure 3.4 shows a photograph of the TPAD on dedicated hauling equipment during delivery to the TxDOT FSF.

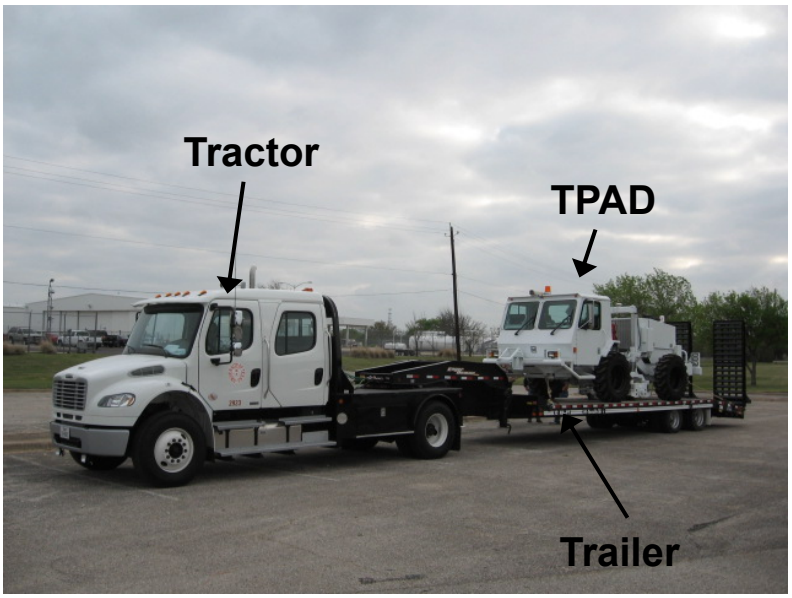

Figure 3.4: Photograph of the TPAD on Dedicated Hauling Equipment at TxDOT FSF, ABIA

Testing Path E at the TxDOT FSF was used as the testing path for the TPAD project. Testing Path E is shown in the aerial photograph of the TxDOT FSF in Figure 3.5.This testing path has been used with the "Classic" RDD in a preliminary study. The TPAD at the starting point of Path E is shown in Figure 3.6. In a preliminary study on the effect of pavement temperature using the classic Rolling Dynamic Deflectometer (RDD), it was shown that the deflection at joints significantly decreased and mid-slab deflections slightly increased as the pavement surface temperature increased (joint deflection dropped from 38 mils/10kips at 91 F to 12 mils/10 kips at 128 F; Stokoe et al., 2010). To avoid the effect of temperature on the rolling dynamic deflections, testing was always performed before noon (spring to summer) when

pavement temperature was low (from 65 to 85 F). The pavement surface temperature was monitored during testing.

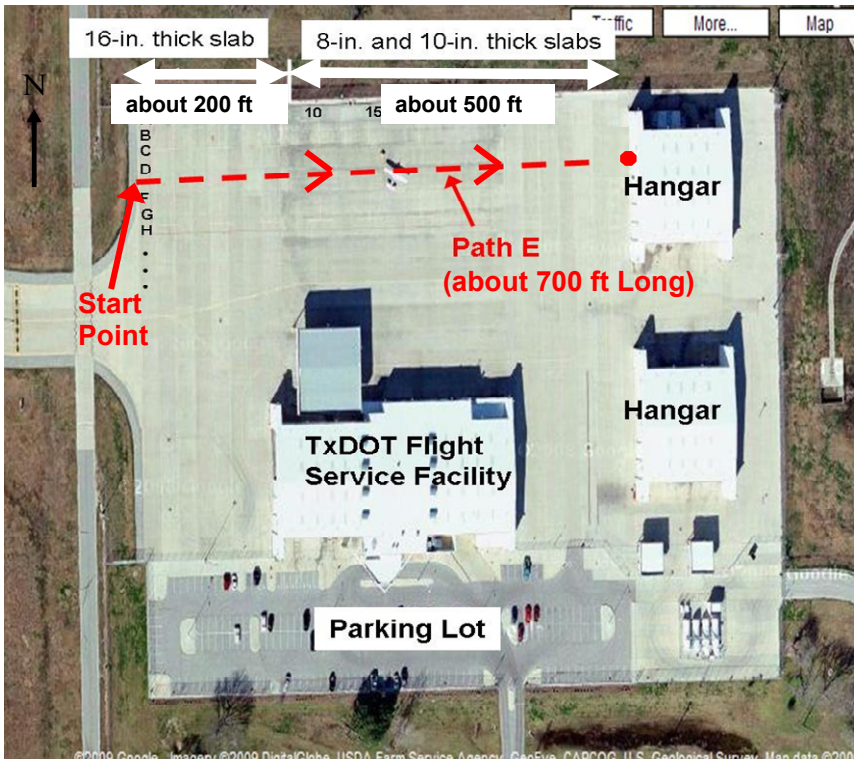

Figure 3.5: Testing Path E Used in TPAD Performance Testing at TxDOT FSF, ABIA

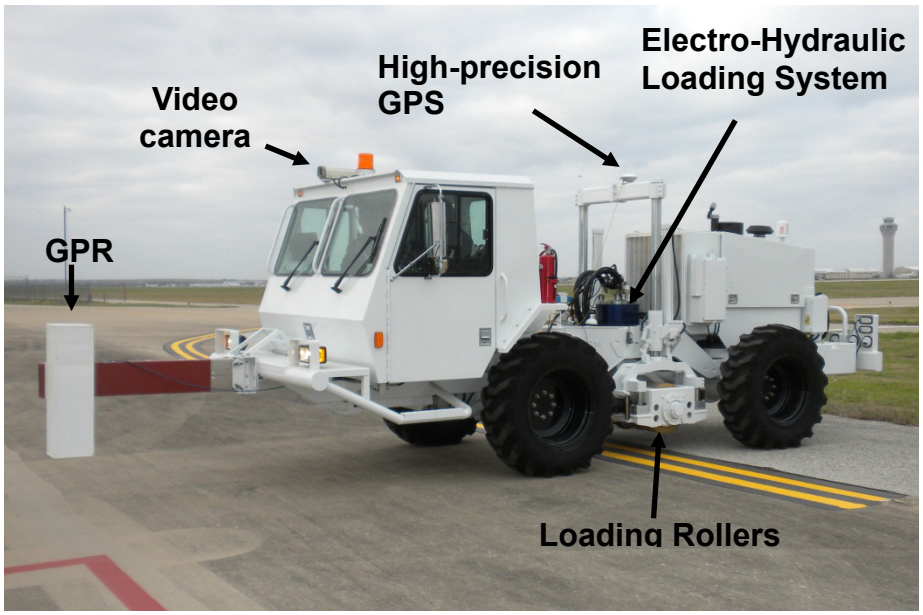

Figure 3.6: Photograph of the TPAD at Starting Point of Path E, TxDOT FSF

Continuous profiling along Path E using the speed-improved rolling sensors was performed at average testing speeds of 0.5, 1, 2, 3, and 4 mph. The rate of sampling the rolling

sensor outputs was 512 Hz for 0.5 and 1 mph and was proportionally increased at faster speeds (1024 Hz at 2 mph, 1536 Hz at 3 mph, etc.). The deflection profiles collected with sensor #1 at testing speeds of 0.5, 1, 2, 3, and 4 mph are shown in Figures 3.7, 3.8, 3.9, 3.10, and 3.11, respectively. In the figures, a testing speed of 0.5 mph is used as the reference. It is well known that the rolling noise level generally increases as the testing speed increases. By comparing Figures 3.7, 3.8 and 3.9, it can be seen that 0.5, 1 and 2 mph show quite similar results, with the main difference due to rolling noise increasing with increasing speed. The comparison shown in Figure 3.10 of deflections measured at speeds of 0.5 and 3 mph also exhibited reasonably matched results, except for the joints on the 16-in. thick slabs and a few other joints.

During the combined TPAD testing, it was found that sensor #2 oscillated laterally at high speeds when crossing joints and the sensor-array positioning system that is used to position sensor #2 needed to be modified to prevent or at least minimize, sensor #2 from oscillating back and forth.

Figure 3.11 shows significant differences in the pavement deflections between measurements at 0.5 and 4 mph. These differences are because of the high level of rolling noise generated at 4 mph. The rolling noise level is always higher at joints than mid-slab areas but the general pattern of high joint deflections and lower mid-slab deflections is still shown in the deflection profile at 4 mph.

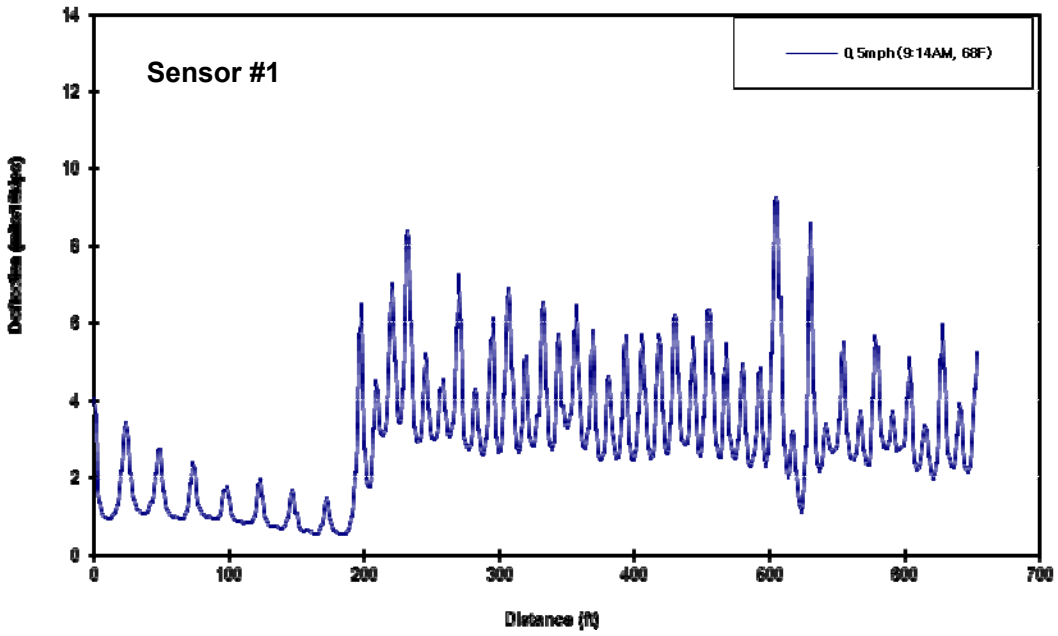

Figure 3.7: Continuous Deflection Profile at 0.5 mph Using Speed-Improved Rolling Sensors and TPAD along Path E at TxDOT FSF (CTR and TTI Combined Testing)

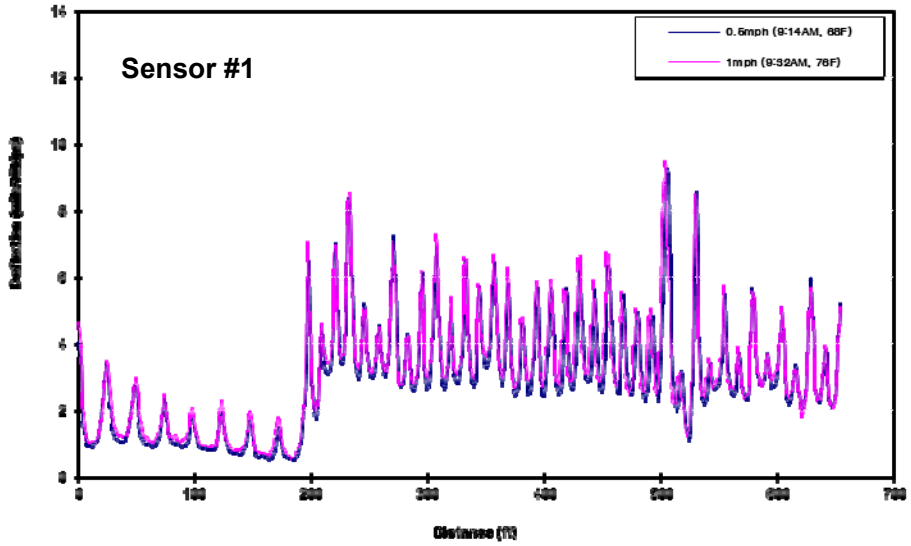

Figure 3.8: Continuous Deflection Profiles at 0.5 and 1 mph Using Speed-Improved Rolling Sensors and TPAD along Path E at TxDOT FSF (CTR and TTI Combined Testing)

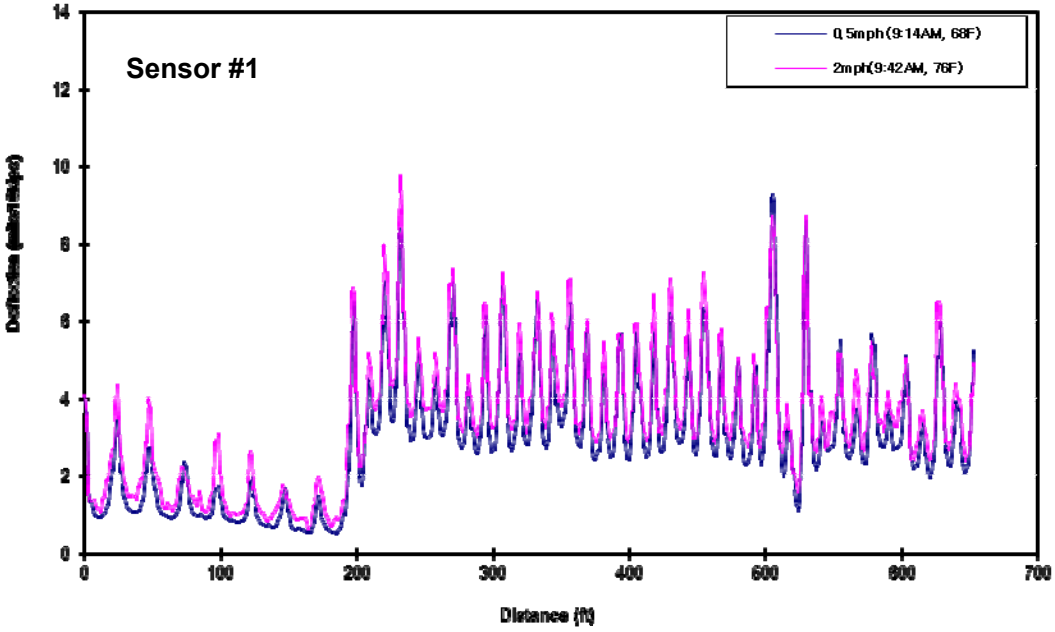

Figure 3.9: Continuous Deflection Profiles at 0.5 and 2mph Using Speed-Improved Rolling Sensors and TPAD along Path E at TxDOT FSF (CTR and TTI Combined Testing)

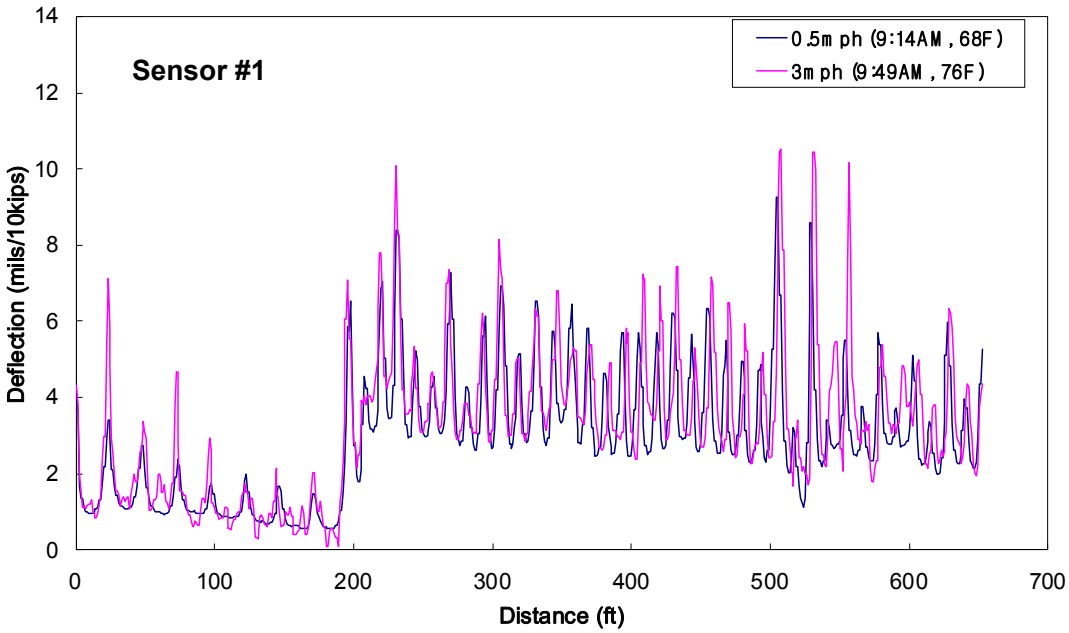

Figure 3.10: Continuous Deflection Profiles at 0.5 and 3mph Using Speed-Improved Rolling Sensors and TPAD along Path E at TxDOT FSF (CTR and TTI Combined Testing)

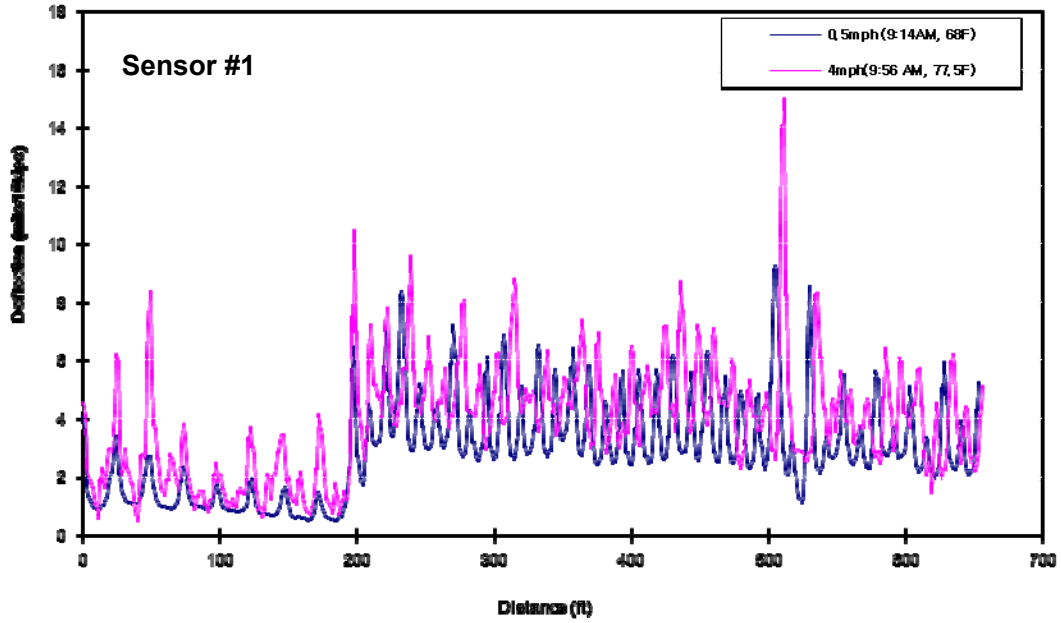

Figure 3.11: Continuous Deflection Profiles at 0.5 and 4mph Using Speed-Improved Rolling Sensors and TPAD along Path E at TxDOT FSF (CTR and TTI Combined Testing)

3.3.2 CTR TPAD Testing

In April 2011, CTR personnel performed additional TPAD testing at the TxDOT FSF. Testing at that time included measurements of (1) continuous pavement deflections, (2) continuous noise-level deflections, and (3) stationary deflection measurements. Continuous deflection measurements involved testing speeds of 0.5, 1, 2, 3, and 4 mph and were performed along Path E. The continuous deflection profiles for 0.5, 1, 2, 3, and 4 mph collected with sensor #1 are shown in Figures 3.12, 3.13, 3.14, 3.15, and 3.16, respectively. In this section, sensor #1 results are presented because sensor #2 still oscillated back and forth at the higher testing speeds. It was observed that all deflection profiles collected up to 3 mph showed quite similar results on 8- and 10-in. thick slabs. However, the deflection profile measured at 4 mph still showed reasonable agreement with the other results. On 16-in. thick slabs, it seemed that the higher differences were due to the high levels of rolling noise at joints.

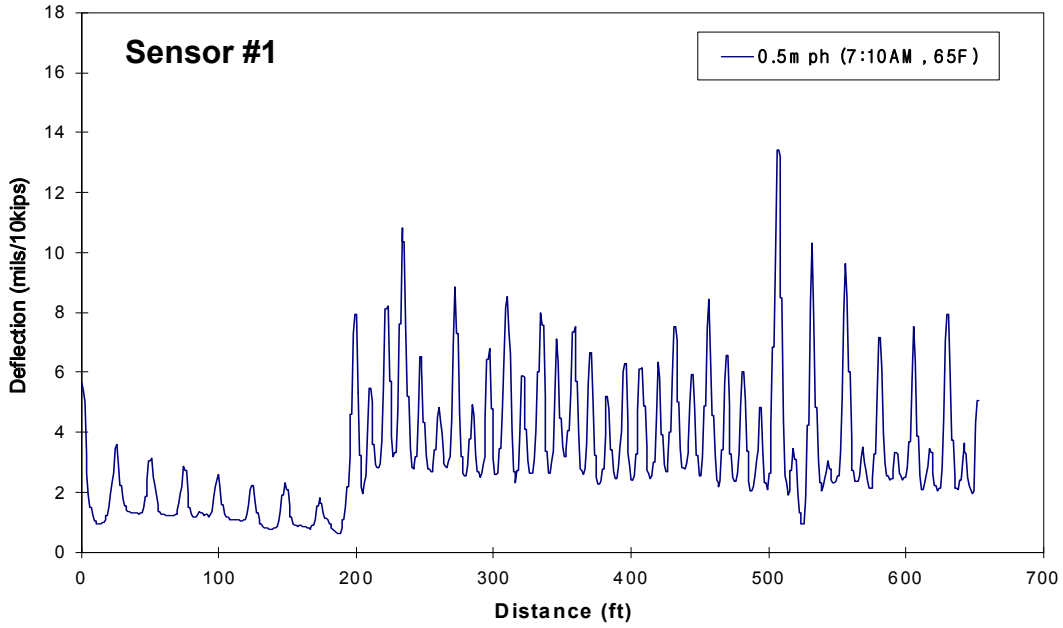

Figure 3.12: Continuous Deflection Profile at 0.5mph Using Speed-Improved Rolling Sensors and TPAD along Path E at TxDOT FSF (CTR Testing)

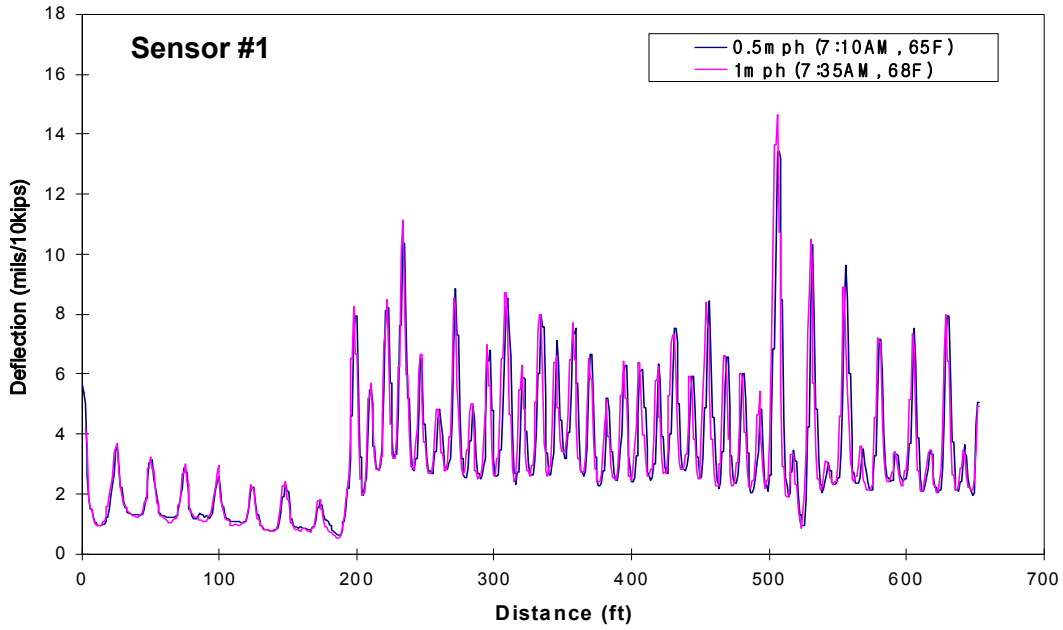

Figure 3.13: Continuous Deflection Profiles at 0.5 and 1 mph Using Speed-Improved Rolling Sensors and TPAD along Path E at TxDOT FSF (CTR Testing)

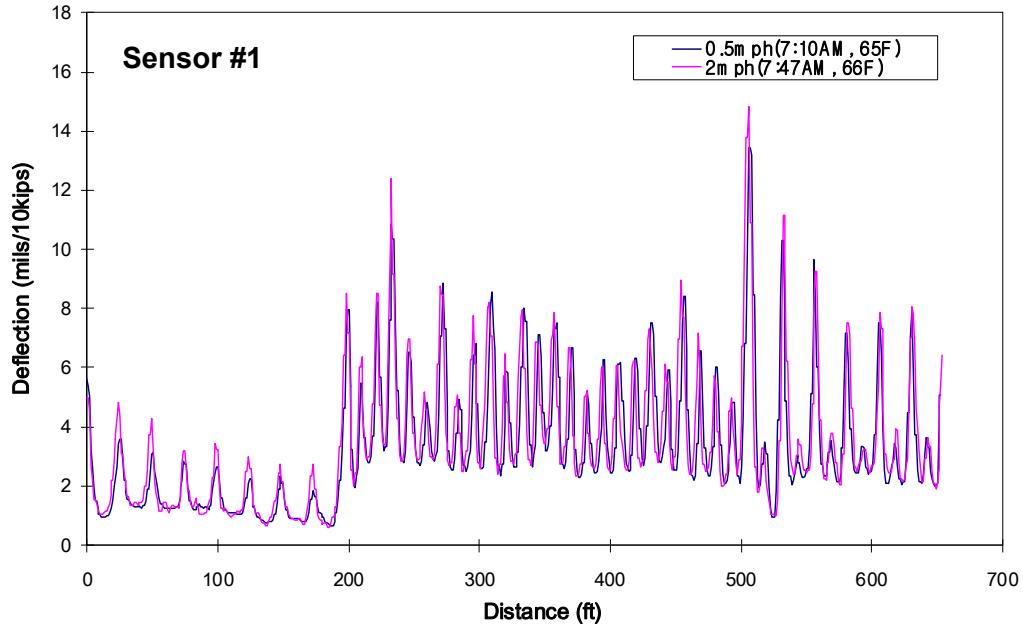

Figure 3.14: Continuous Deflection Profiles at 0.5 and 2 mph Using Speed-Improved Rolling Sensors and TPAD along Path E at TxDOT FSF (CTR Testing)

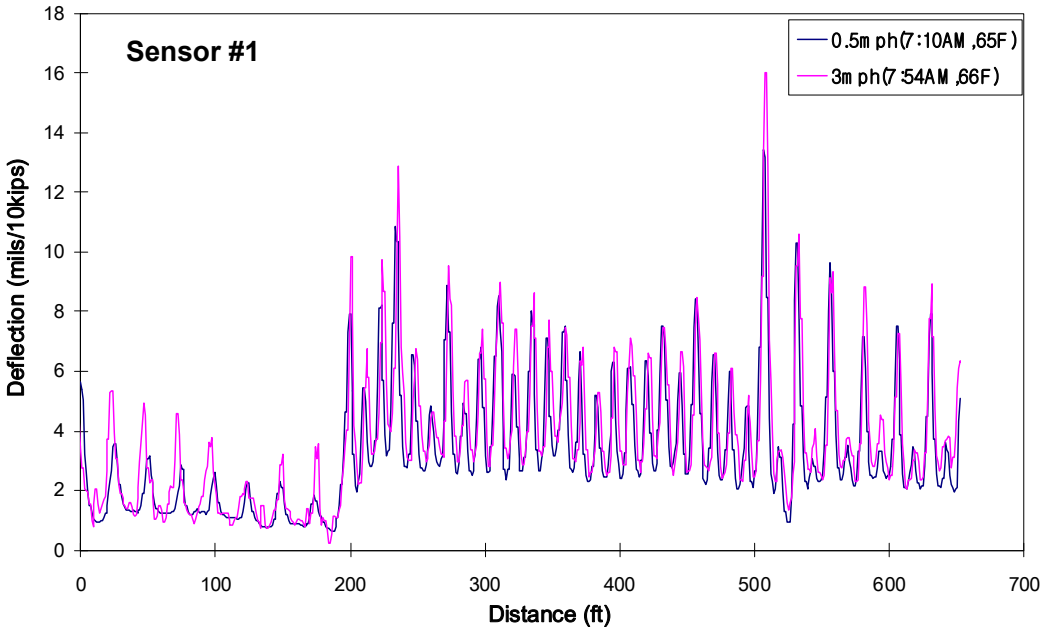

Figure 3.15: Continuous Deflection Profiles at 0.5 and 3 mph Using Speed-Improved Rolling Sensors and TPAD along Path E at TxDOT FSF (CTR Testing)

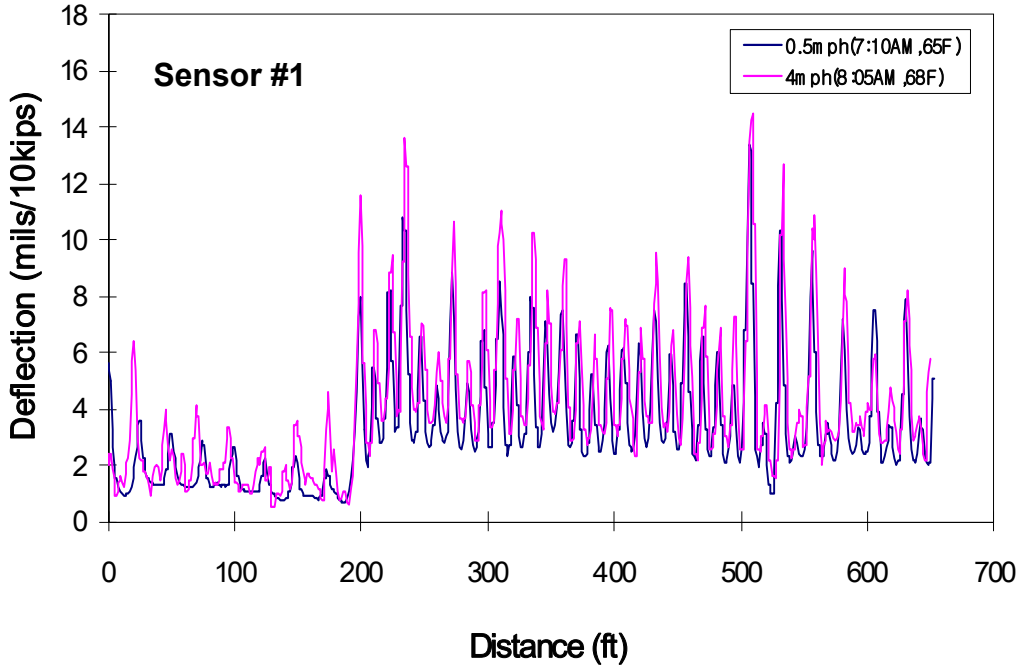

Figure 3.16: Continuous Deflection Profiles at 0.5 and 4 mph Using Speed-Improved Rolling Sensors and TPAD along Path E at TxDOT FSF (CTR Testing)

Continuous rolling noise measurements using the speed-improved rolling sensors with the TPAD were also performed along the Path E. The noise induced measurements were performed with the loading rollers statically loading the pavement but not vibrating (no dynamic loading). Therefore, the rolling sensor recorded only rolling noise which is mainly caused by pavement roughness and cracks/joints. To calculate the noise induced-deflections, the raw data recorded with the rolling sensors were passed through the notch-pass filter, which passed only the bandwidth of frequencies depending on the filter settling time and the sampling frequency. This process is the same process followed when collecting pavement deflections. In this application, the filter bandwidth around 30 Hz, the current TPAD operating frequency, was used. The resultant noise induced deflections represent the values that are so close to the operating frequency that the notch-pass filter cannot remove them from the dynamic loading induced deflections.

Noise-induced deflections at testing speeds of 0.5, 1, 2, 3, and 4 mph are shown in Figures 3.17, 3.18, 3.19, 3.20, and 3.21, respectively. In these figures, the approximately 700-ft long test section (Path E) is divided into two parts. The first part is the first 200-ft long section consisting of 16-in. thick slabs and the other part is the 500-ft section consisting of 10- and 8- in. thick slabs. The average noise-level and standard deviations have been calculated for the 16-in. thick slabs (first part) and the 10- and 8-in. thick slabs (second part) separately. As illustrated in Figures 3.17 through 3.21, the noise level increases as testing speed increases and joints can cause much higher noise levels than mid-slab areas at the same testing speed. In addition, as mentioned earlier, wider joint spacings in the 16-in. thick slabs tended to cause the highest noise level along Path E, resulting in a higher average noise level. Even with the testing speed of 0.5 mph, joints in the 16-in. thick slabs showed quite high noise levels. These higher noise levels at joints in the 16-in. thick slabs contributed to the higher differences between 0.5 mph measurements and faster speeds at joints in these slabs.

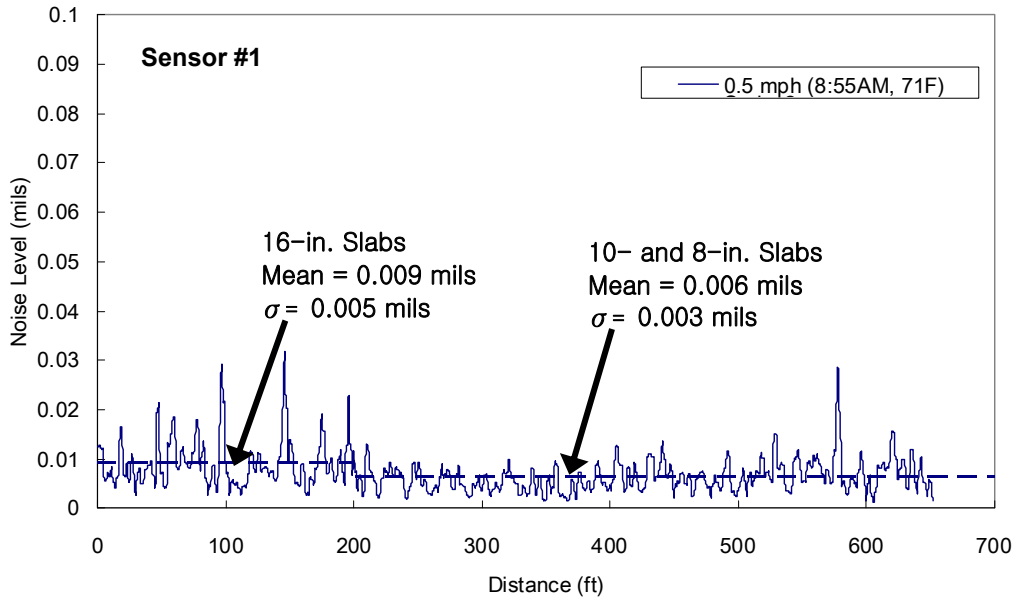

Figure 3.17: Noise Induced Deflection Profile at 0.5 mph Using Speed-Improved Rolling Sensors and TPAD along Path E at TxDOT FSF

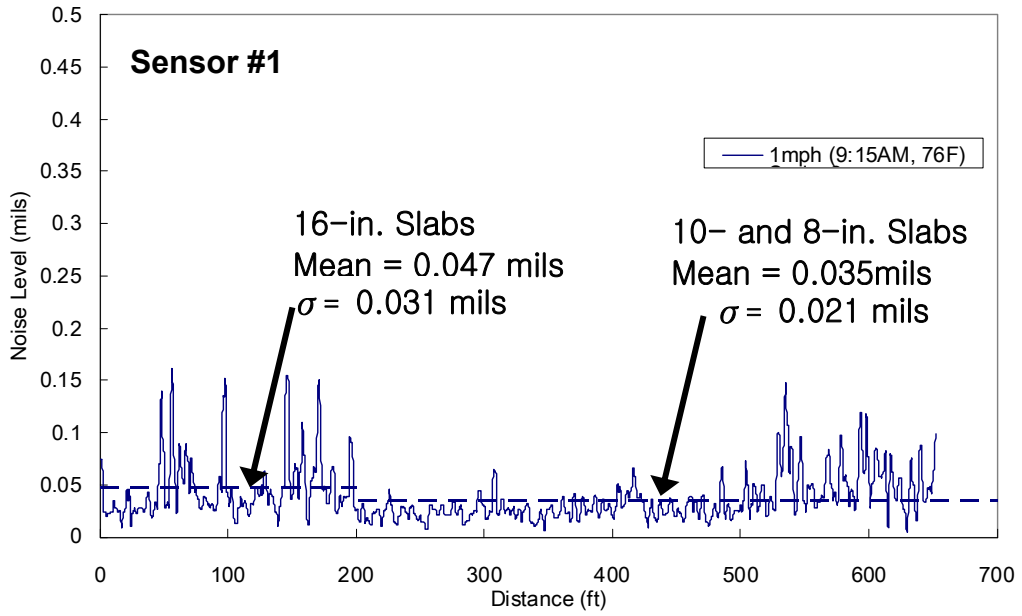

Figure 3.18: Noise Induced Deflection Profile at 1 mph Using Speed-Improved Rolling Sensors and TPAD along Path E at TxDOT FSF

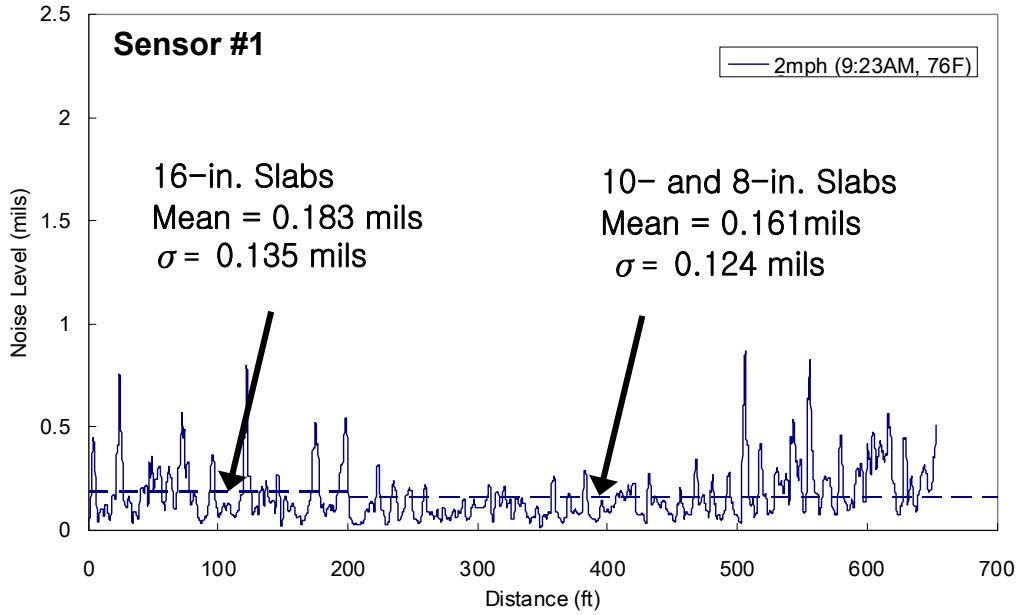

Figure 3.19: Noise Induced Deflection Profile at 2 mph Using Speed-Improved Rolling Sensors and TPAD along Path E at TxDOT FSF

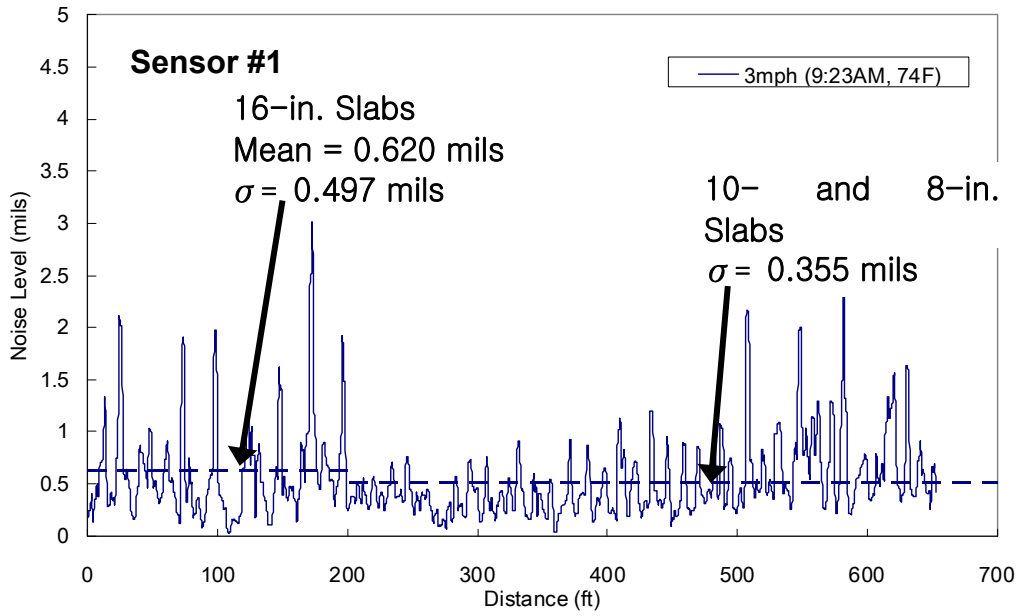

Figure 3.20: Noise Induced Deflection Profile at 3 mph Using Speed-Improved Rolling Sensors and TPAD along Path E at TxDOT FSF

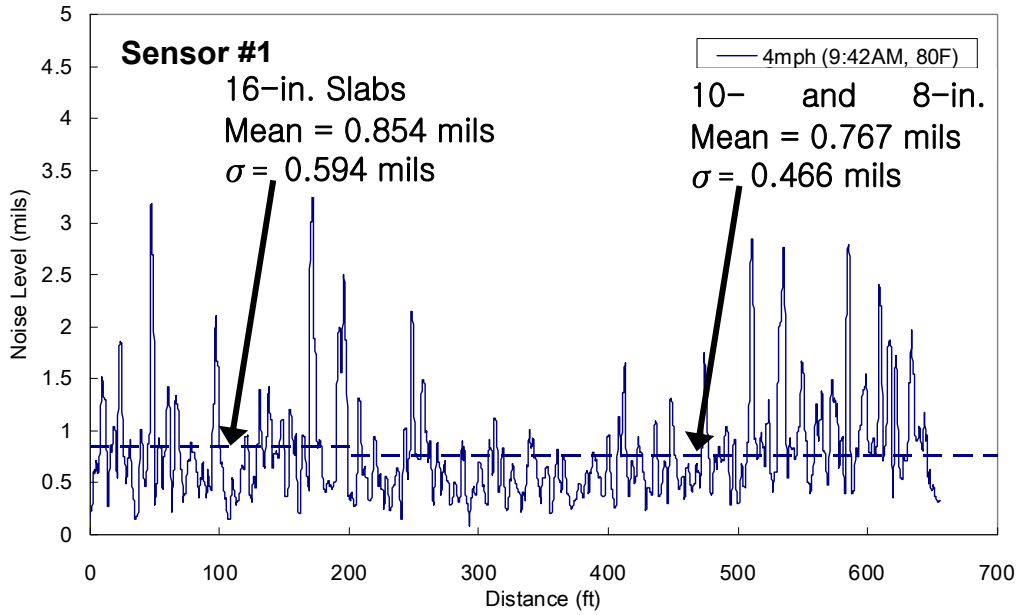

Figure 3.21: Noise Induced Deflection Profile at 4 mph Using Speed-Improved Rolling Sensors and TPAD along Path E at TxDOT FSF

Increases in the average rolling noise level with respect to the testing speeds are shown in Figure 3.22. The approximate mid-slab deflections are also shown in the figure. The approximate mid-slab deflections were determined using Figure 3.12 through 3.16 and were estimated using "by eye" fitting. The deflections and noise level for 16-in. and 10- and 8-in. thick slabs are shown separately. It is interesting to note that mid-slab deflections slightly increase as

the testing speed increases but not as much as the noise level increases. This difference is because the average noise level shown in Figures 3.17 through 3.21 contains the noise caused by the joints while the mid-slab deflections measured while rolling more closely approximate the pure mid-slab deflections. Therefore, it can be reasonably concluded that the increase in the noise level occurred at joints with high testing speeds. It is also interesting to note that the ratio of the approximate mid-slab deflection to average noise level on the 10- and 8- in. thick slabs is 500, 86, 20, 6, and 4 at testing speeds of 0.5, 1.0, 2.0, 3.0 and 4.0 mph, respectively. On the 16-in. thick slabs, this rate is 110, 21, 7, 2, and 1.5 at testing speeds of 0.5, 1.0, 2.0, 3.0, and 4.0 mph, respectively. Hence, this ratio is at least six at 3 mph on 10- and 8-in. thick slabs.

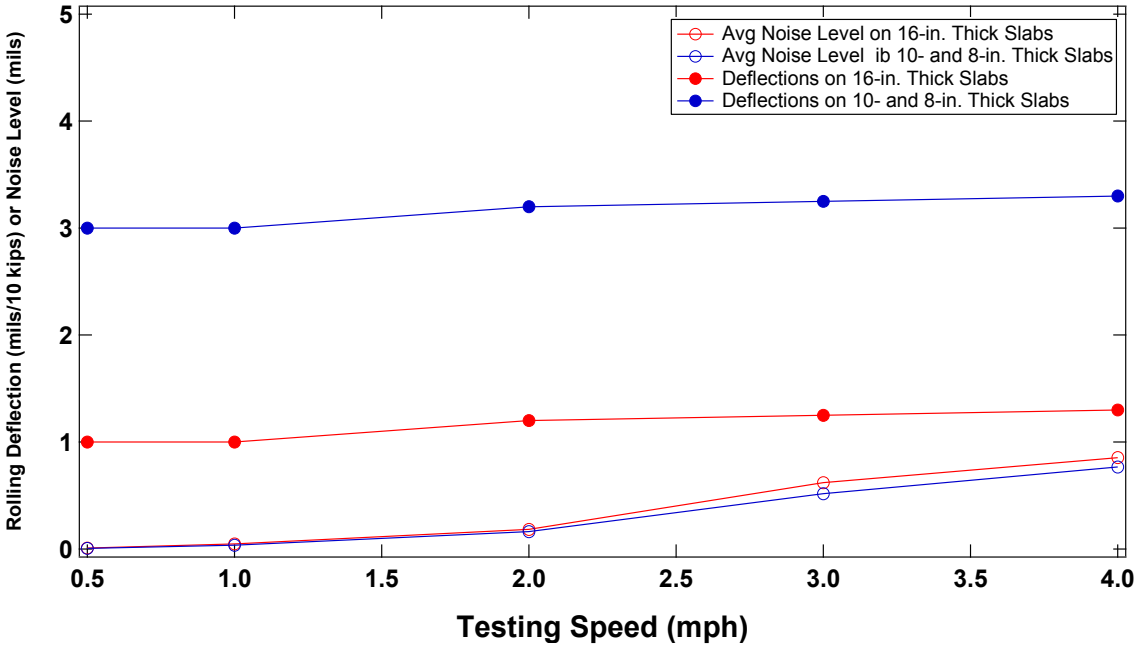

Figure 3.22: Increases of Noise Level and Rolling Deflection with Increasing Testing Speeds

3.3.3 Stationary Deflection Measurements with the TPAD

Stationary deflection measurements with the TPAD were performed at several locations on two, 8-in. thick slabs. These measurements were conducted to determine the dynamic response of the slabs as well as to make a comparison between the rolling (continuous) dynamic deflections with the stationary dynamic deflections. The comparison between the rolling and stationary deflections measured with the TPAD is shown in Figure 3.23. In the figure, the deflection profile collected at 0.5 mph is expanded from Figure 3.12 (at distances of 15 to 645 ft) for the comparison. It is important to note that the stationary measurements are almost the same as the rolling dynamic deflections in the mid-slab areas but are higher than the dynamic deflections around the joints. The higher joint deflections under stationary loading occur because they are not averaged over some horizontal distance. For example, at 0.5 mph the continuous measurements are averaged over 1.5 ft.

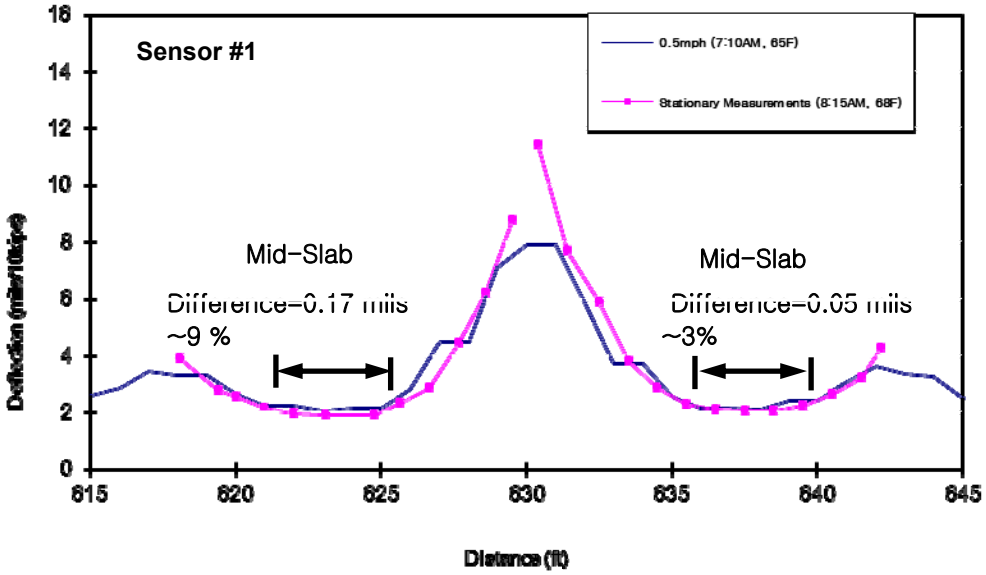

Figure 3.23: Comparison between Stationary and Rolling (Continuous) Dynamic Deflection Measurements on Two, 8-in. Thick Slabs at TxDOT FSF

3.3.4 Justification for 3-mph Testing Speed of Current Rolling Sensor and Array

Initially, the current system used to hold the TPAD rolling sensors in position was made by IVI. This sensor frame system is scheduled for possible redesigning in fall 2011. In addition, only one design of the speed-improved rolling sensor has been used; that is, a cart with 9-in. diameter wheels with one, 2-in. wide wheel and two, 1-in. wide wheels. The deflection profile collected at 1 and 3 mph in July 2011 with sensor #1 along Path E at the TxDOT FSF is shown in Figure 3.24. In this figure, it can be seen that the deflection profiles are quite similar, with the deflections at 3 mph containing more noise. With these results and many other similar tests and with the concurrence of the TxDOT oversight committee, it seems reasonable to assume that the first-generation TPAD can be used at testing speeds up to 3 mph. A re-designed sensor positioning frame and other rolling sensor cart configurations may allow for further increases to the data collection speed.

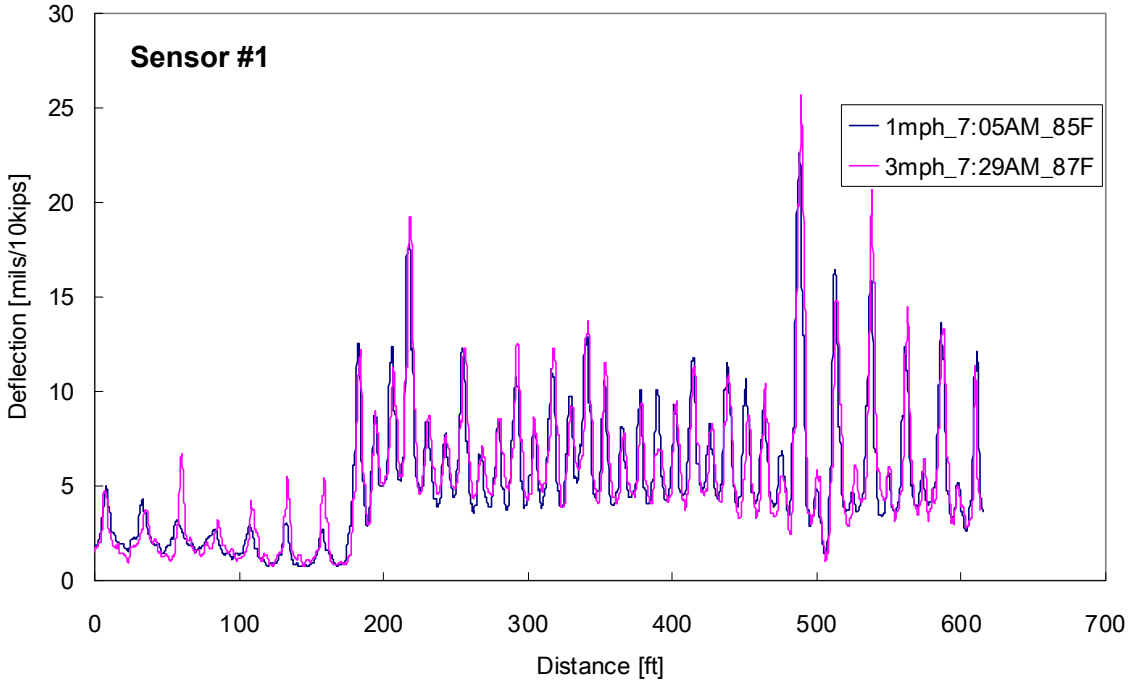

Figure 3.24: Similar Continuous Deflection Profiles at 1 and 3 mph with First Generation TPAD along Path E at TxDOT FSF (CTR Testing)

In the RDD data processing procedure, the RDD signal is defined as the signal induced by applying the RDD loading function at the single operating frequency of 30 Hz. Therefore, any signals outside of the operating frequency are regarded as rolling noise. However, rolling noise can exist in the operating frequency. It is desirable to have higher signal-to-noise ratios (SNR) for more accurate pavement deflection measurements. The SNR is defined as shown in Equation 3.1:

$$SNR = 20\log_{10}\left(\frac{V_{RDD,30\,Hz}}{V_{20-40\,Hz}}\right) \tag{3.1}$$

where

$V_{RDD,30Hz}$ = voltage measured at the RDD operating frequency (30 Hz),
$V_{20\text{-}40Hz}$ = average voltage measured in the frequency band between 20 and 40 Hz (excluding the amplitude at 30 Hz).

Time and frequency domain signals from sensor #1 measurements in the mid-slab region of an 8-in. thick slab at testing speeds of 1, 2, and 3 mph are shown in Figures 3.25, 3.26, and 3.27, respectively. The time domain signal is over a 1-sec time window and the frequency domain signal is a fast Fourier transform of the 1-sec time domain signal. The SNRs are also shown in the figures. As expected the SNR decreases as the testing speed increases. However, as illustrated in the figures, the lowest SNR of sensor #1 is 20 dB at 3 mph, meaning that the signal is 10 times higher than rolling noise. It can be concluded that the first generation TPAD is working reasonably well at a testing speed of 3 mph on this pavement.

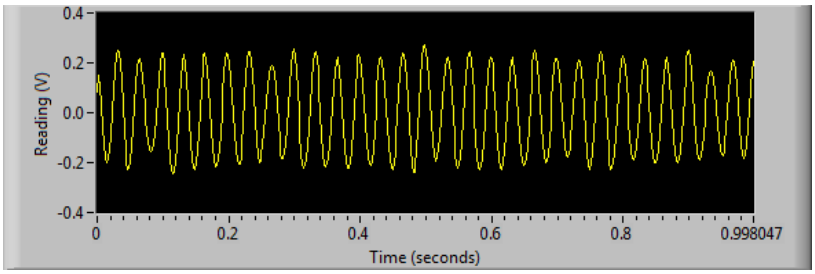

(a)Time Domain Signal (over 1-sec Time Window)

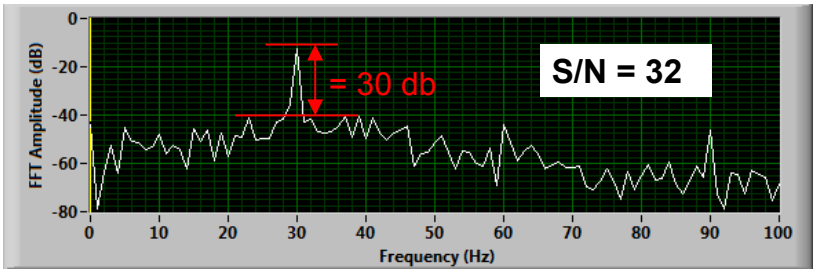

(b)Frequency Domain Signal (Fast Fourier Transform of Time Domain Signal)

Figure 3.25: Sensor #1 Output in the Time and Frequency Domains on an 8-in. Thick Slab in the Mid-Slab Region at TxDOT FSF Collected at 1 mph

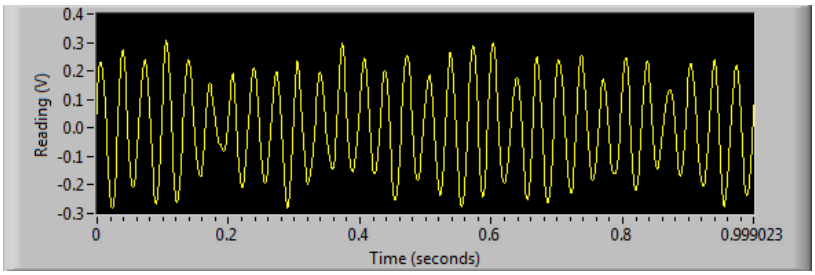

(a)Time Domain Signal (over 1-sec Time Window)

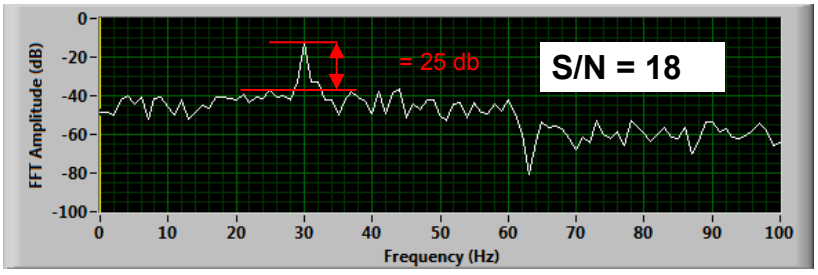

(b)Frequency Domain Signal (Fast Fourier Transform of Time Domain Signal)

Figure 3.26: Sensor #1 Output in the Time and Frequency Domains on an 8-in. Thick Slab in the Mid-Slab Region at TxDOT FSF Collected at 2 mph

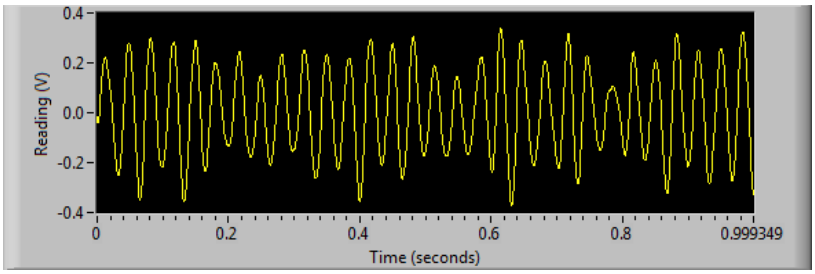

(a)Time Domain Signal (over 1-sec Time Window)

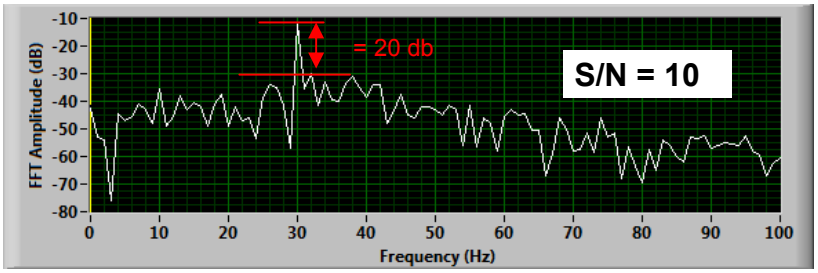

(b)Frequency Domain Signal (Fast Fourier Transform of Time Domain Signal)

Figure 3.27: Sensor #1 Output in the Time and Frequency Domains on an 8-in. Thick Slab in the Mid-Slab Region at TxDOT FSF Collected at 3 mph

3.4 Modifications Made to Frame Used to Position Rolling Sensor #2

As mentioned earlier, it was found that sensor #2 oscillated back and forth when crossing joints at higher testing speeds. In this section, modifications which have been made to the rolling towing frame used to position sensor #2 are presented.

3.4.1 Replacement of Two-Coil Isolators with Three-Coil Isolators

Four, two-coil isolators that had been used to keep sensor #2 in position while rolling were replaced with three-coil isolators to provide more stability against sensor #2 oscillating at high TPAD testing speeds when crossing joints. It was found that the three-coil isolators were stiffer and could provide a little more stability but not enough to prevent the sensor #2 oscillations.

3.4.2 Trial of Rigid Trailing-Arm Installation

With the three-coil isolators in position, the oscillations of sensor #2 during RDD testing were still observed. Therefore, two rigid trailing arms were installed and tested. A photograph of the trailing-arm installation to sensor #2 is shown in Figure 3.28. It was obvious that trailing arms give more stability against back and forth oscillations. However, it was suspected that the vibration of the white TPAD support frames for sensor #2 could be transmitted to the sensor through the trailing arms. To measure more accurate pavement responses induced by the loading rollers, it is desirable to isolate more completely the rolling sensors from the ambient vibrations of the TPAD rolling platform and the vibrations induced by the sinusoidal loading.

The output signals from sensor #2 in a mid-slab area with and without the trailing arms were recorded with the TPAD not moving. Since the measurements were performed with the

TPAD stationary, the frequency-domain signal should have only the component at the operating frequency and no components at other frequencies (from rolling noise). The time and frequency domain signals with and without the trailing arms are shown in Figure 3.29. As seen in the figure, the signal without trailing arms shows a clean sinusoidal response in the time-domain and the Fast Fourier Transform (FFT) of this time domain signal (frequency domain signal) exhibits a clear 30-Hz frequency component and essentially no components at other frequencies (see Figure 3.29 (a)). On the other hand, the sensor signal when trailing arms are in place shows no clean sinusoidal response in the time domain. The FFT of this signal exhibits the highest component at 30 Hz but also shows components at other frequencies, meaning that some other vibrations were transmitted to the sensor (Figure 3.29 (b)). Based on these tests, it was concluded that the addition of rigid trailing arms to sensor #2 was detrimental to the signal response and they should not be used.

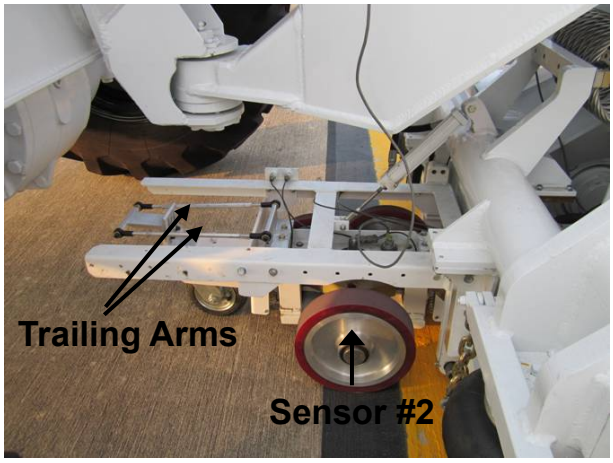

Figure 3.28: Trailing Arms Installed to Sensor #2

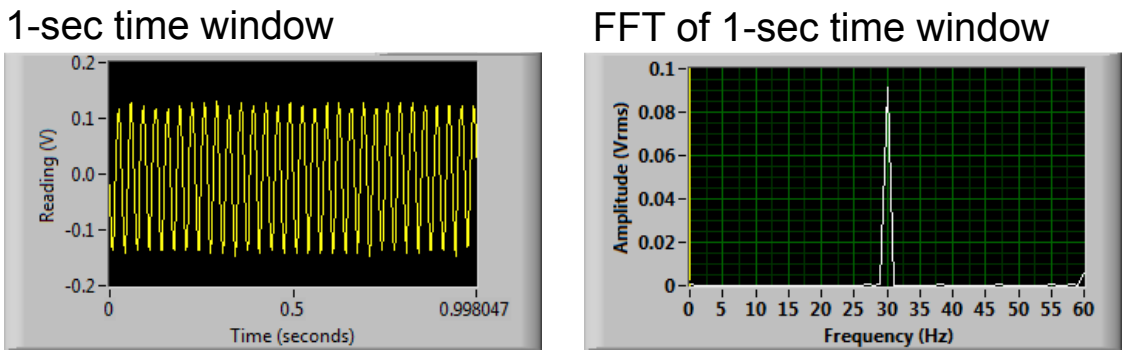

(a)Without Trailing Arms (Operating Frequency = 30 Hz)

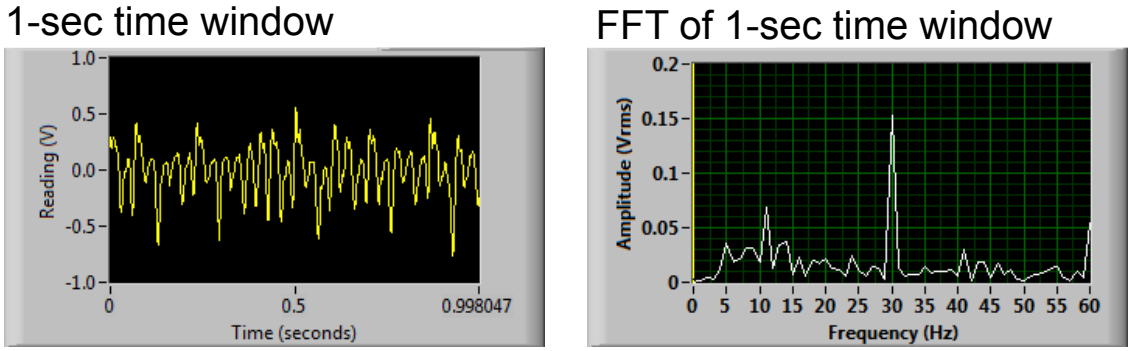

(b)With Trailing Arms (Operating Frequency = 30 Hz)

Figure 3.29: Time and Frequency Domain Signals of Sensor #2 with and without Trailing Arms Collected in the Mid-Slab Region with Stationary Measurements

3.4.3 Removal of Hydraulic Lift Cylinder and Addition of Air Accumulator

Transmission of vibrations to sensor #2 through a hydraulic cylinder, which is attached to the loading frame of the loading rollers, was suspected. The hydraulic cylinder was used to raise and lower rolling sensor #2. Testing was conducted along Path E at FSF. During testing, a dead weight and an air accumulator were added to reduce the end movements of the sensor positioning frame and provide more reliable regulation of the hold-down air pressure. Again, these trials were made on sensor #2. Figure 3.30 shows (1) the hydraulic lift cylinder before disconnection and (2) the dead weight and air accumulator installed on the white positioning frame for sensor #2.

The TPAD moved to the starting point of Path E and then the loading rollers and rolling sensors were lowered to the pavement. Testing was conducted after the hydraulic lift cylinder was disconnected. The continuous deflection profiles collected with the connected and disconnected hydraulic cylinder at 1 and 3 mph are shown in Figures 3.31 and 3.32, respectively. In Figure 3.31, no significant difference is found with testing speed of 1 mph. In Figure 3.32, contrary to our expectations, the results with the hydraulic cylinder disconnected showed the noisier deflection profile. It was concluded that disconnecting the hydraulic cylinder had a negative effect on the pavement deflection measurements at the 3 mph testing speed.

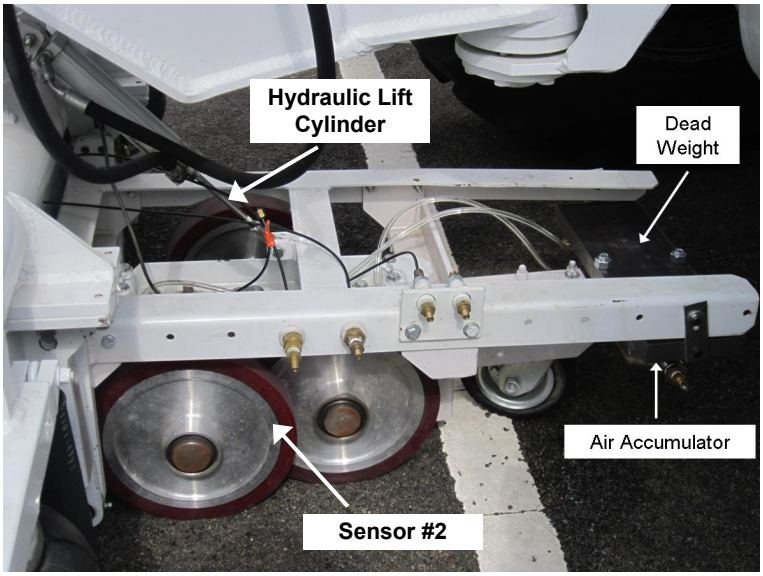

Figure 3.30: Hydraulic Lift Cylinder before Disconnection and Dead Weight and Air Accumulator Added to the White Location Frame for Sensor #2

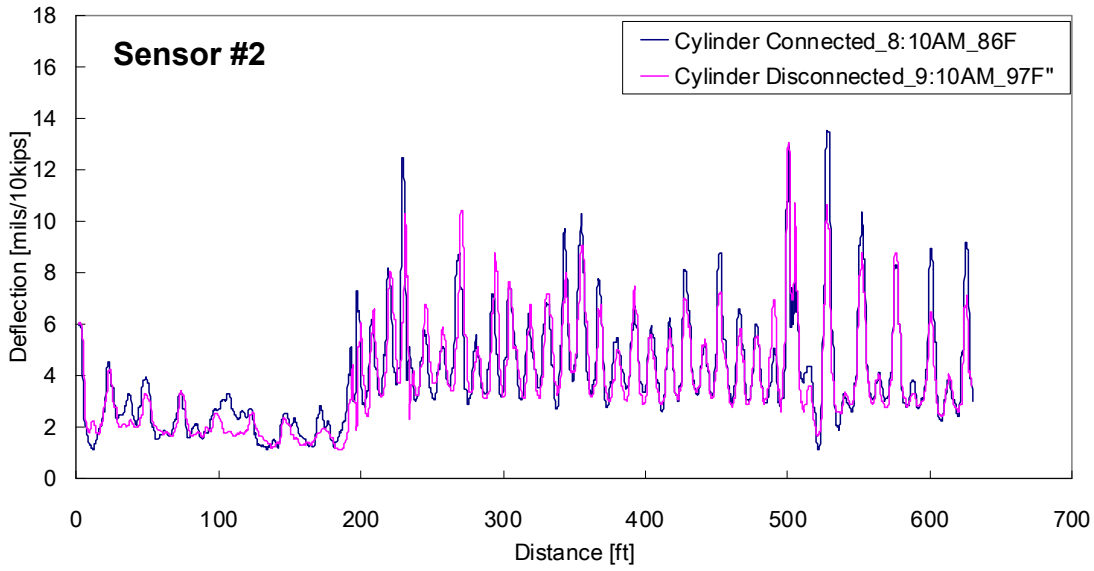

Figure 3.31: Comparison of Continuous RDD Deflection Profiles for Testing at 1 mph with and without the Hydraulic Lift Cylinder for Sensor #2

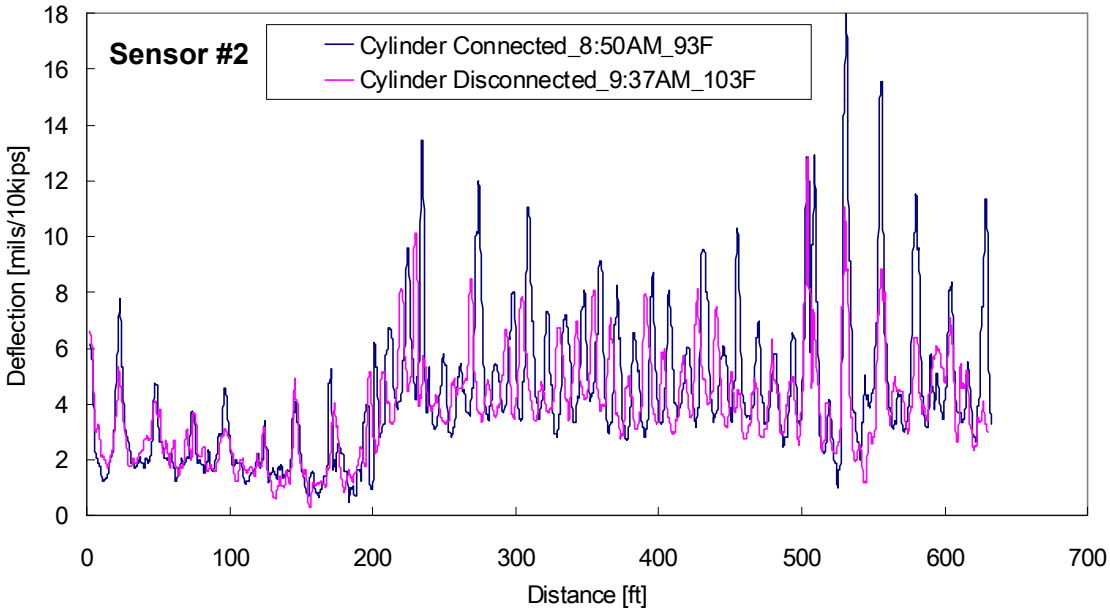

Figure 3.32: Comparison of Continuous RDD Deflection Profiles for Testing at 3 mph with and without the Hydraulic Lift Cylinder for Sensor #2

3.5 Noise Measurements with Towing Frame at PRC

As mentioned in Section 3.3.4, the rolling sensor that was used in all of the initial testing had one, 9-in. diameter wheel with a 2-in. wide tread and two, 9-in. diameter wheels with 1-in. wide treads as shown in Figure 3.1(b). This size and configuration of wheels is among four proposed configurations of the speed-improved rolling sensors. In addition, a hold-down weight of 40 lb was the only hold-down weight initially used. Therefore, all four configurations of speed-improved rolling sensors with several different hold-down weights needed to be tested.
The testing location for studying the rolling sensors was the former Texas accelerated pavement test site at PRC. This site is an asphalt pavement and is shown in Figure 3.33. One version of the speed-improved rolling sensor, computer, DAQ system, and battery for the computer installed on a towing frame used in studying the performance of the different rolling sensor configurations are also shown in Figure 3.33.

Parameters which could affect the sensor performance were investigated during these tests. The parameters are (1) diameter of wheels, (2) width of treads, (3) hold-down weight, and (4) testing speed. As specified in the Second-Year Progress Report (Stokoe et al., 2011), CEM designed four configurations of the speed-improved rolling sensors. For convenience, they are designated as follows:

SA: 9-in. diameter wheels; two, 1-in. wide treads and one, 2-in. wide tread,

SB: 9-in. diameter wheels; two, 2-in. wide treads and one, 4-in. wide tread,

SC: 12-in. diameter wheels; two, 1-in. wide treads and one, 2-in. wide tread, and

SD: 12-in. diameter wheels; two, 2-in. wide treads and one, 4-in. wide tread.

Photographs of the four configurations of the speed-improved rolling sensors installed in the towing frame are shown in Figure 3.34.

The initial IVI design of the weight in the hold-down mechanism used a 40-lb weight. For this testing, three different hold-down weights were constructed: (1) 20 lb, (2) 40 lb, and (3) 90 lb. Testing speeds were assumed that "slow walking" was about 1 mph, "fast walking" was about 3 mph, and "slow running" was about 5 mph. At each testing speed, the time for travelling the fixed path was measured to keep the right testing speed in each trial.

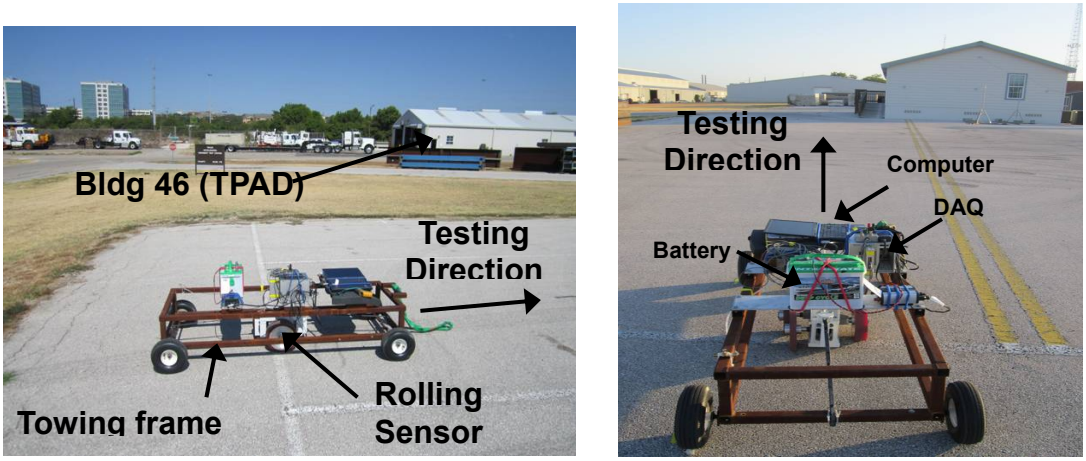

(a) *(b)*

Figure 3.33: Speed-Improved Rolling Sensor, Computer, DAQ and Battery Installed on an Independent Towing Frame at the Former Texas Accelerated Pavement Test Site

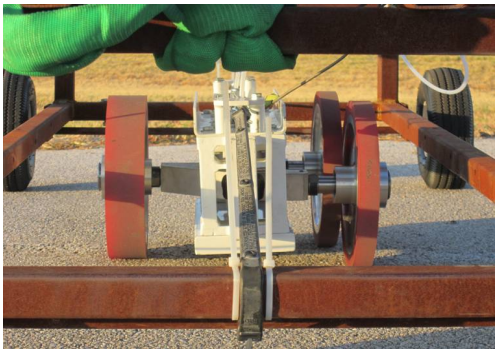

(a) SA: 9-in. Diameter Wheels; *Two, 1-in.and One, 2-in. Wide Treads*

(b) SB: 9-in. Diameter Wheels; *Two, 2-in.and One, 4-in. Wide Treads*

(c) SC: 12-in. Diameter Wheels; *Two, 1-in.and One, 2-in. Wide Treads*

(d) SD: 12-in. Diameter Wheels; *Two, 2-in.and One, 4-in. Wide Treads*

Figure 3.34: Four Configurations of the Speed-Improved Rolling Sensor Installed in the Independent Towing Frame

In this study, each sensor was installed in the independent towing frame borrowed from UT and then, the cart was pulled along the 90-ft long testing path on the asphalt pavement. Noise levels were recorded for each set of tests. The results of the noise-level measurements at the three testing speeds are shown in Figures 3.35, 3.36, 3.37, and 3.38. Noise levels in three possible RDD operating frequency ranges were investigated for each testing speed. These RDD operating frequency ranges are (1) 30 Hz, (2) 40 Hz, and (3) 50 Hz. The three frequency ranges were considered because of a possible use of different operating frequencies (f_o) for the TPAD. Figures 3.35 through 3.38 show the mean and plus and minus one standard deviation of the noise level for the sensors. Raw data of the noise measurements are attached in Appendix A.

As speed increases, noise level increases as expected. It is interesting to note that as speed changes from 3 to 5 mph, noise level approximately doubles. In addition, noise level decreases as the measurement frequency increases. In general, the configurations with the rolling cart having larger diameter wheels (SC and SD) and the heaviest hold-down weight (90 lb) performed better than the smaller diameter wheels (SA and SB) and the lighter hold-down weights. Rolling noise-level differences between the narrow and wide treads were mixed but generally showed about the same results.

As of the date of this report, the noise measurements with the independent towing frame were performed on asphalt pavement at PRC. Evaluation of the noise level on jointed concrete pavement is scheduled to be performed at the TxDOT FSF in fall 2011.

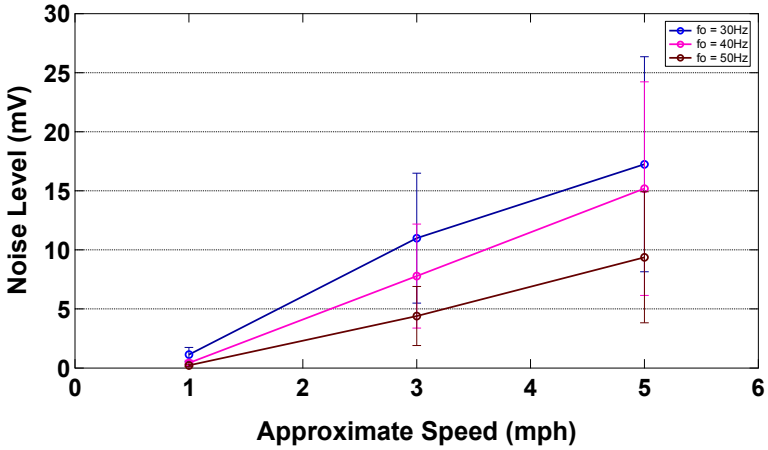

(a) Rolling Sensor Configuration SA with 20-lb Hold-Down Weight

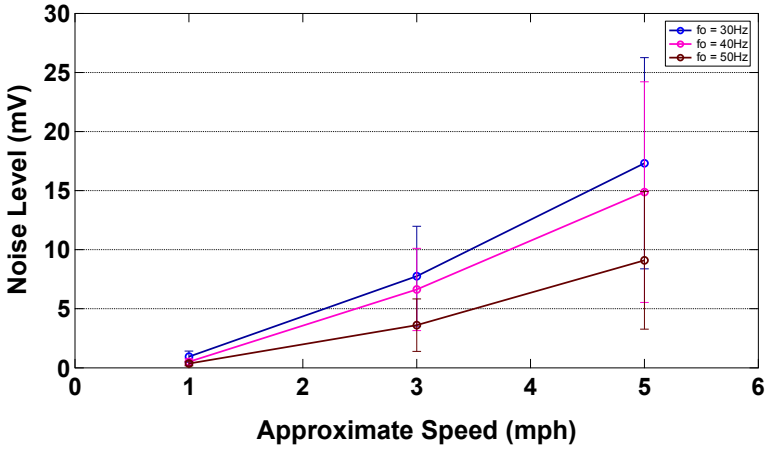

(b) Rolling Sensor Configuration SA with 40-lb Hold-Down Weight

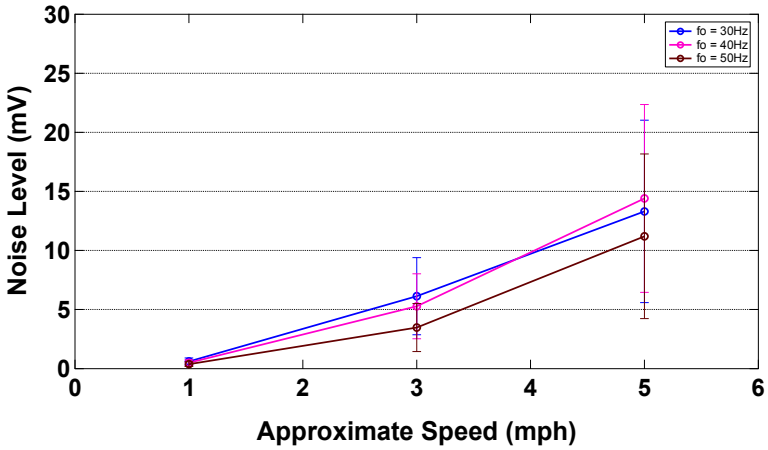

(c) Rolling Sensor Configuration SA with 90-lb Hold-Down Weight

Figure 3.35: Rolling Noise Levels at Three Different Testing Speeds around Three Possible RDD Operating Frequencies (f_o) Measured with Rolling Sensor Configuration SA

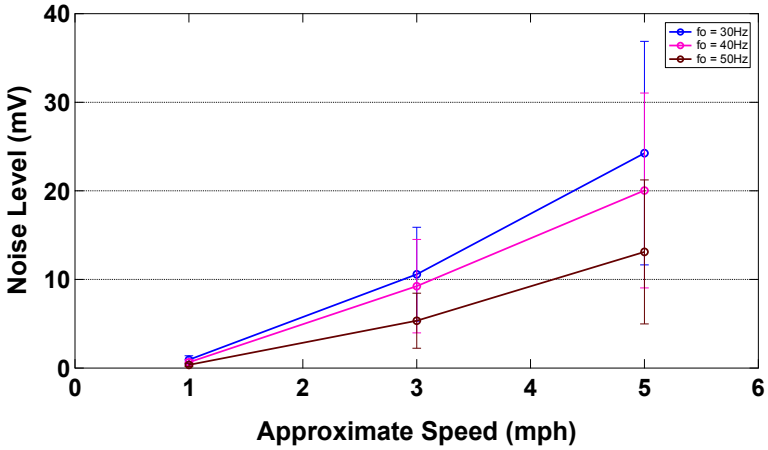

(a) Rolling Sensor Configuration SB with 20-lb Hold-Down Weight

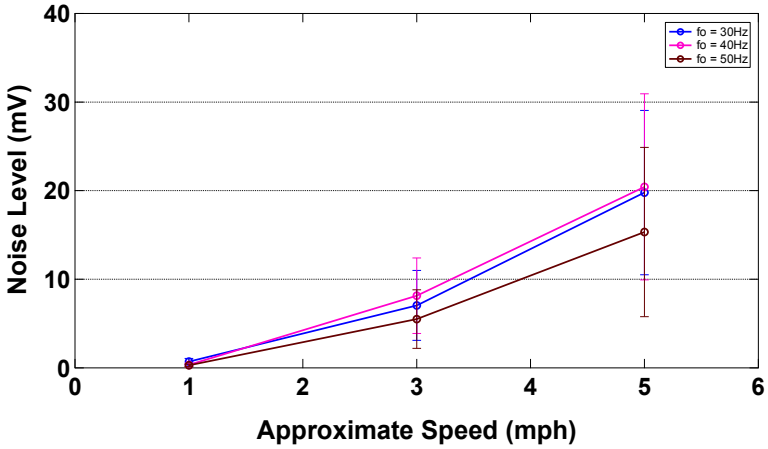

(b) Rolling Sensor Configuration SB with 40-lb Hold-Down Weight

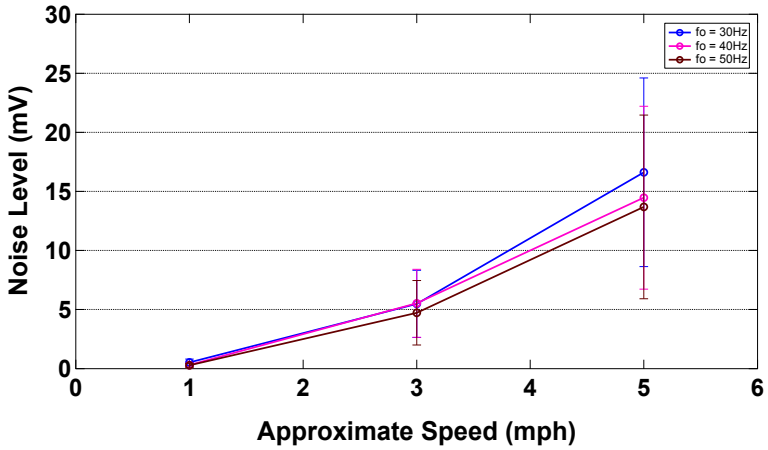

(c) Rolling Sensor Configuration SB with 90-lb Hold-Down Weight

Figure 3.36: Rolling Noise Levels at Three Different Testing Speeds around Three Possible RDD Operating Frequencies (f_o) Measured with Rolling Sensor Configuration SB

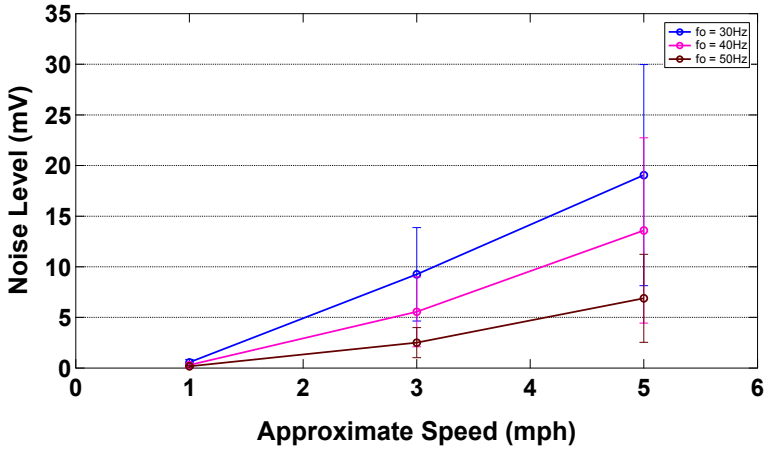

(a) Rolling Sensor Configuration SC with 20-lb Hold-Down Weight

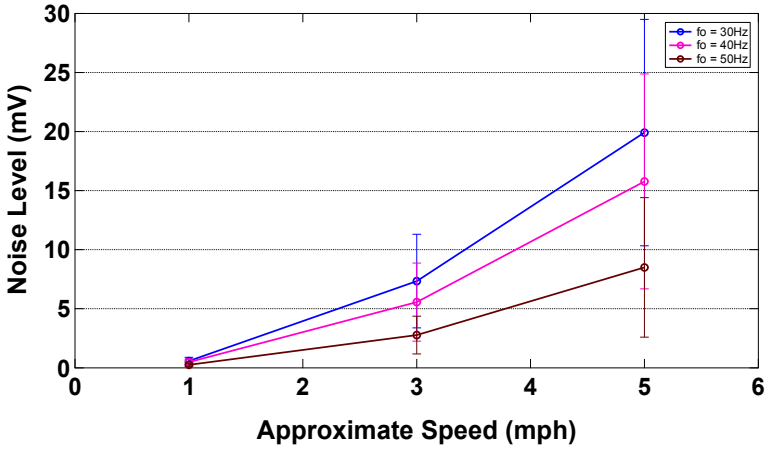

(b) Rolling Sensor Configuration SC with 40-lb Hold-Down Weight

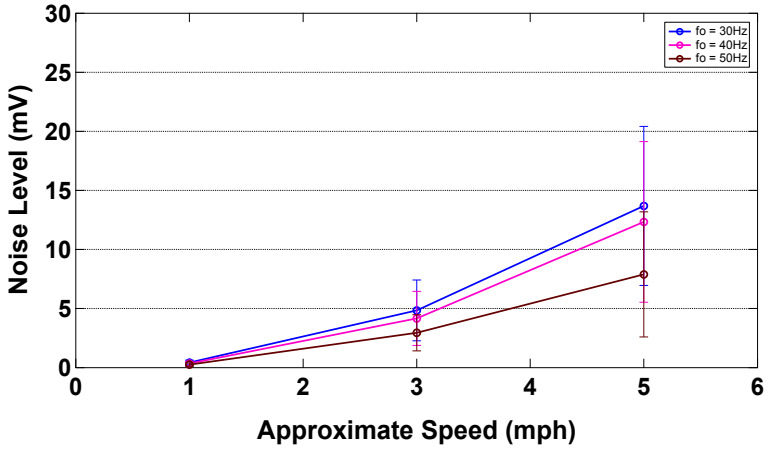

(c) Rolling Sensor Configuration SC with 90-lb Hold-Down Weight

Figure 3.37: Rolling Noise Levels at Three Different Testing Speeds around Three Possible RDD Operating Frequencies (f_o) Measured with Rolling Sensor Configuration SC

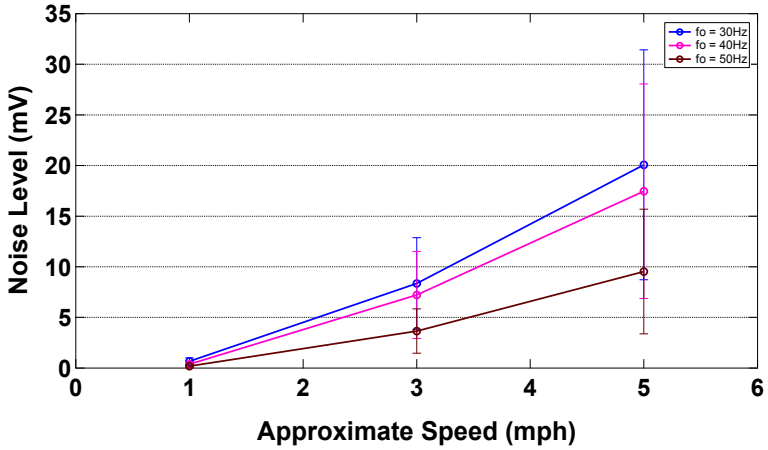

(a) Rolling Sensor Configuration SD with 20-lb Hold-Down Weight

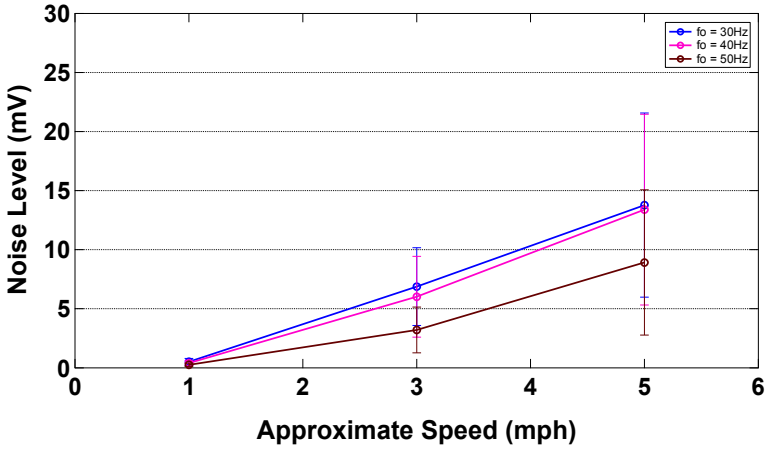

(b) Rolling Sensor Configuration SD with 40-lb Hold-Down Weight

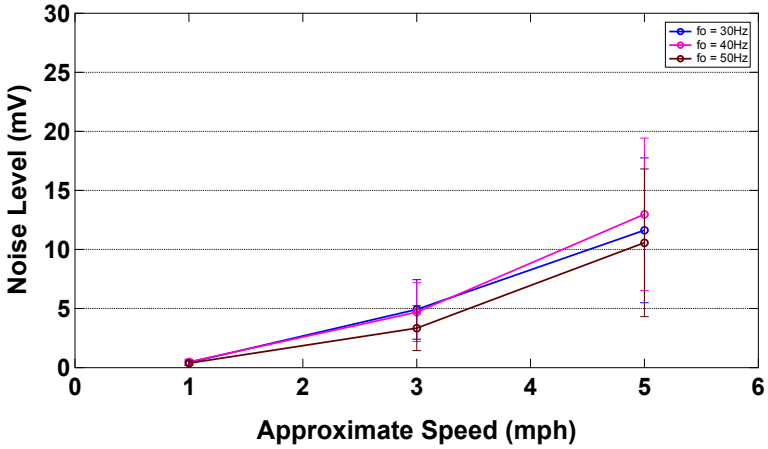

(c) Rolling Sensor Configuration SD with 90-lb Hold-Down Weight

Figure 3.38: Rolling Noise Levels at Three Different Testing Speeds around Three Possible RDD Operating Frequencies (f_o) Measured with Rolling Sensor Configuration SD

3.6 “Design” of New Hold-Down and Lifting System

A new design of the TPAD hold-down and lifting system for the rolling sensors has been proposed to replace the current IVI-designed system. The new towing and lifting frame on the TPAD will be used to tow three rolling sensors and will be integrated with the automation that raises and lowers the rolling sensors when they are not in use. The design of this TPAD towing frame and raising/lowering system is scheduled to be completed in October 2011.

3.7 Summary

The speed-improved rolling sensors were designed and assembled during the second year of TxDOT project 0-6005. They were installed in the TPAD and the first-generation RDD portion of the TPAD was tested at a testbed at TxDOT FSF (Path E, see Figure 3.5). Through several series of tests, it was shown that sensor #1 can be used up to a testing speed of 3 mph. However, it was found that sensor #2 oscillated laterally when crossing joints and cracks at the higher testing speeds. Modifications were made to the sensor #2 towing frame, including replacement of the two-coil isolator with three-coil isolators, installation of rigid trailing arms, removal of the lift cylinder, and adding an air accumulator. These trials were helpful understanding the performance but they were not completely successful; work is continuing in fall 2011 to improve the performance of the sensor #2 assembly.

Rolling noise measurements with four configurations of the speed-improved rolling sensor were performed with an independent towing frame on the asphalt pavement at PRC. It was concluded that larger diameter wheels and heavier hold-down weights showed the lowest noise levels. Narrow and wide treads exhibited about the same noise levels. The rolling noise level at the sinusoidal operating frequency was also studied on the asphalt pavement at PRC. Noise level measurements around 30, 40, and 50 Hz were evaluated. Only minor differences existed between 30 and 40 Hz. However, at 50 Hz and a testing speed of 3 mph, the noise level was substantially decreased (about half the noise level at 30 Hz). Even though this improvement occurred, the operating frequency of 30 Hz was selected because: (1) the inertial effect of the pavement is less and (2) 30 Hz is a predominant frequency in the FWD test.Testing will continue on jointed concrete pavement at the TxDOT FSF in fall 2011.

Chapter 4. Improvements to the TTI Data Acquisition and Processing Systems

4.1 Overview

At the end of the second year of project 0-6005, TTI researchers competed the first phase of the TPAD data acquisition system development, and the prototype software was tested in the office with the simulator software system. The TPAD data acquisition software was also field tested with the old UT Austin RDD system on March of 2010.

In the third year of TPAD project, the main task was, in coordination with IVI and UT Austin, to install the TTI data acquisition system into the new TPAD vehicle. Tests were then conducted to verify the whole system and to debug the hardware and software. In addition TTI developed RDD data analysis software for instant analysis of the raw deflection data immediately after completing the field test. In summary the following tasks were undertaken in the third year of this project:

- Coordinate with IVI to integrate the RDD data collection with the TTI data acquisition system and install all necessary components of the data acquisition and data collection peripherals.
- Coordinate with UT Austin to field test the new IVI hardware
- Conduct testing with UT Austin at the TxDOT FSF with their new geophone sensor design at different speeds.
- Continue to test and debug the RDD data acquisition software
- Code a new RDD data analysis post-processing software for analyzing the RDD data immediately after data acquisition,
- Verify the RDD data acquisition system at the TTI Riverside campus test site.
- Build the electronics control box for integrating all the electronic components into one box for simplifying the system installation.

TTI was also involved with the following field testing activities:

- Sept. 20~21, 2010: First test of the new TTI data acquisition system in the old "classic" RDD system. In addition to the existing geophones, TTI installed a 1 GHz air coupled GPR antenna, an industrial grade digital camera, and an infrared sensor and DMI encoder. The panel-mounted industrial computer was also used to collect data.
- Oct. 5~7, 2010: TTI visited IVI in Tulsa, Oklahoma to discuss the installation of the TTI data acquisition hardware into the TPAD.
- Dec. 9~10, 2010: first test of the rolling deflectometer on the TPAD, however no geophones were installed, so this test was made to evaluate the TPAD static and dynamic load signals during calibration.
- March 15~18, 2011: TPAD rolling deflectometer testing with the new geophone setup system at the TxDOT FSF, Austin.

- June 22~23, 2011: the new TPAD was shipped to the TTI Riverside campus for testing. Two sections of concrete pavement were successfully tested.
- Sept. 1, 2011: We conducted rolling deflection tests at TXDOT's FSF terminal at speeds of 1, 3, and 4 mile/hour.

From the field testing we concluded the following:

- During the Dec. 9~10, 2010 session, it was determined that the original encoder for the distance measurement could not be shared between the TTI and IVI data acquisition systems. As a temporary measure, a second encoder was added for the TTI data acquisition system. However on March 15~18, 2011 a new single encoder system was installed and tested; it was found to work very well and the distance data can be shared between the TTI and IVI data acquisition systems.
- During the initial RDD tests on Dec. 9~10, 2010, we noticed that the GPR signal had a high frequency noise. In the past, this type of noise has been found to be related to the quality of the power supply system. On June 22~23, 2011, TTI purchased and tested a new power supply and the GPR signal was found to be clean without significant noise.
- In the rolling deflectometer testing conducted on Dec. 9~10, 2010, it was found that the load signal was not stable. The data was shown to IVI and they solved the problem.

4.2 Rolling Deflection Field Testing Activities

The first tests of the complete "TPAD" integrated system with the TTI data acquisition system was conducted in Sept of 2010 with the classic RDD; this is shown in Figure 4.1. The TTI data acquisition system was installed as shown in Figure 4.2.

Figure 4.1: First Test in September 2010

Figure 4.2: Mounted Data Acquisition computer and control box in the classic RDD

This was a pilot test of the integrated system. All of the components installed are shown in Figure 4.3; Figure 4.4 shows the inside of the control box.

Figure 4.3: All the components that are installed to the old RDD vehicle

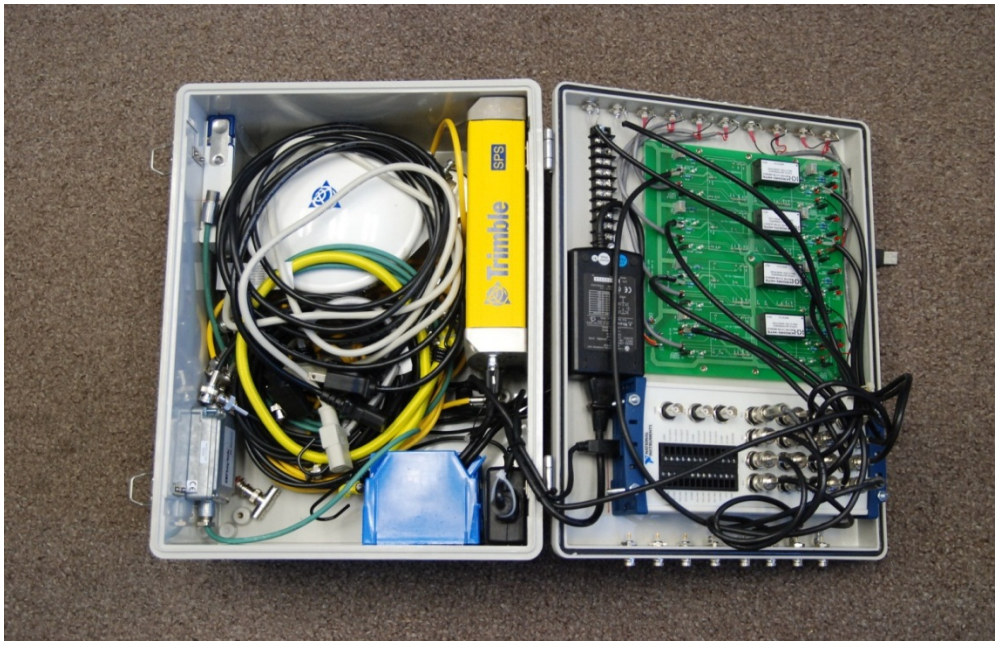

Figure 4.4: Inside the Control box

In March 2011, as shown in Figure 4.5, the complete deflection geophone assembly was mounted on the TPAD and demonstrated at the TxDOT airport facility. Runs were made at different speeds. However it was concluded that the geophone mounting systems were still not ideal. The data collected at 1 mph were good, but substantial sensor noise was encountered with the higher speeds.

Figure 4.5: First time RDD geophones are installed in TPAD at TXDOT terminal of Austin

4.3 Updates to the Data Acquisition Software

The TTI team continued to streamline the data acquisition program developed to collect TPAD data. The main menu buttons for the updated system are shown below in Figure 4.6; all menu functions are described in Table 4.1.

Figure 4.6: Main Menu in Updated TPAD Data Acquisition Program

Table 4.1: Options in RDD Data Collection Software

	Start the data collection and save all the data to disk
	Shows the TPAD system control dialog box for user to input all the information needed for the data acquisition job. Before starting the test by , user needs to input the filename and comments from here.
	For collecting GPR metal plate data. Usually we do the metal plate test after finishing all of the deflection testing.
	For viewing the GPR signal and to check if the GPR system is working correctly. Just for checking purposes. No data is saved.
	For viewing the RDD data acquisition system working status. It has the same interface as the button. But here it is just for view, no data is saved.
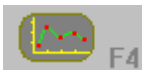	For viewing the RDD sensor's signal in a graphical format, this function is useful for sensor checking purposes. No data is saved.
	For viewing the GPS location over the map showing the current location.
	For setup of the GPS interface with computer. Serial port parameters are set here. After setting these, the GPS satellite information will be shown on the screen.
	Stops the action activated by buttons like , , , , 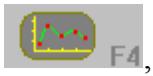 , , .
	For setup of the TPAD camera.

Figures 4.7 and 4.8 show additional setup screens that are activated from the main menu screen.

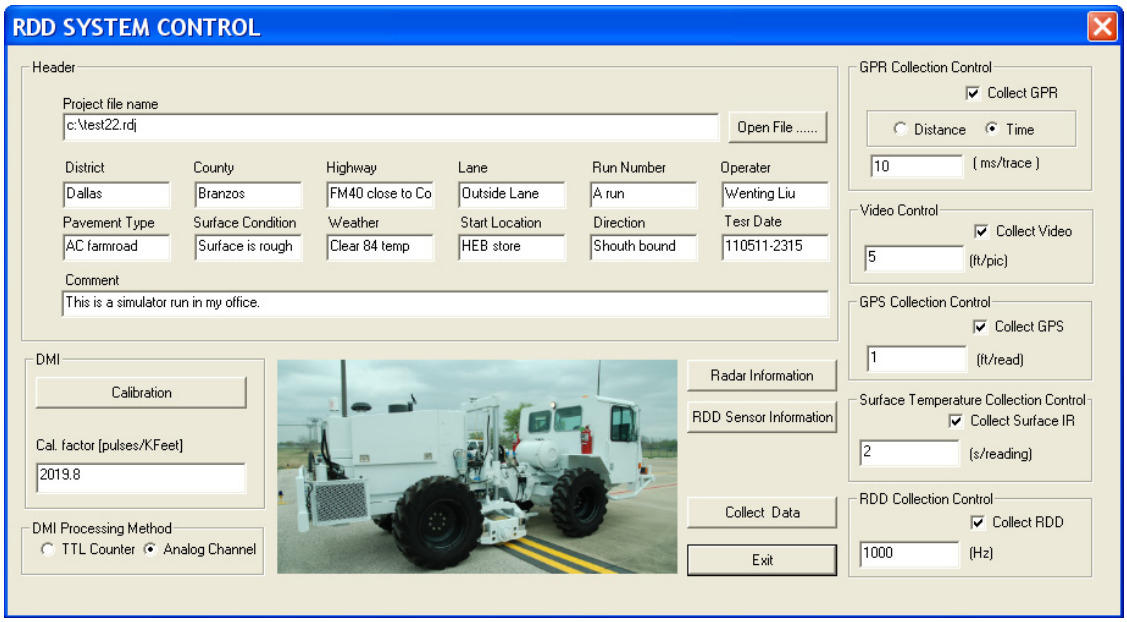

Figure 4.7: Main Input Screen for Controlling Data Collection Rates

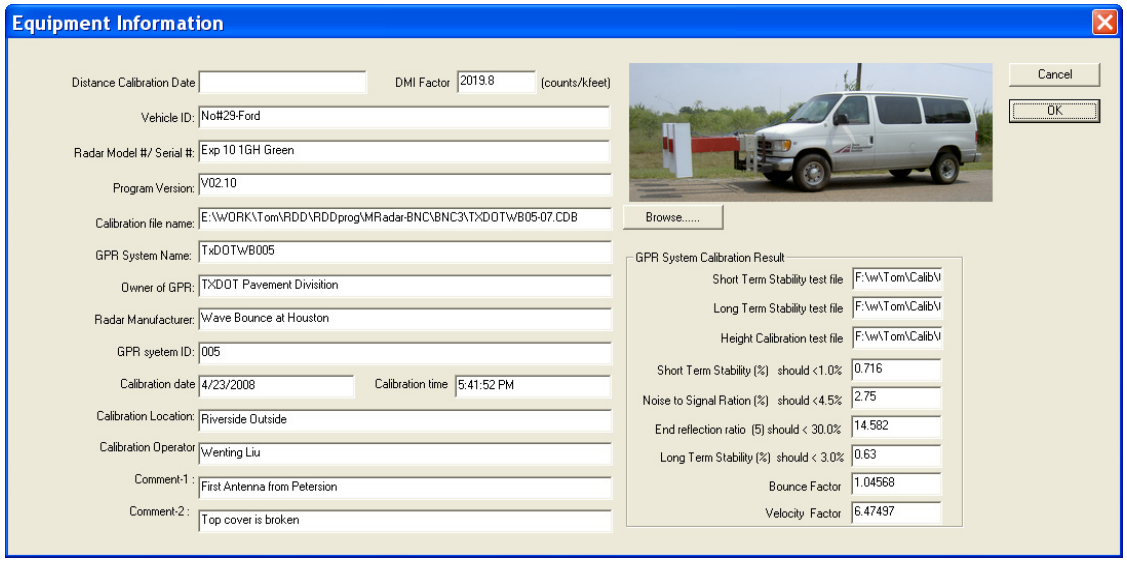

Figure 4.8: Entering Equipment Calibration Information (GPR Calibration Factors)

The RDD sensors setup control menu screen is shown in Figure 4.9; it lets the user select how many geophone data channels to collect and save. The RDD system can change the number, location and configuration of geophones based on what kind of testing the researcher requires; this option will increase the flexibility of the data acquisition system.

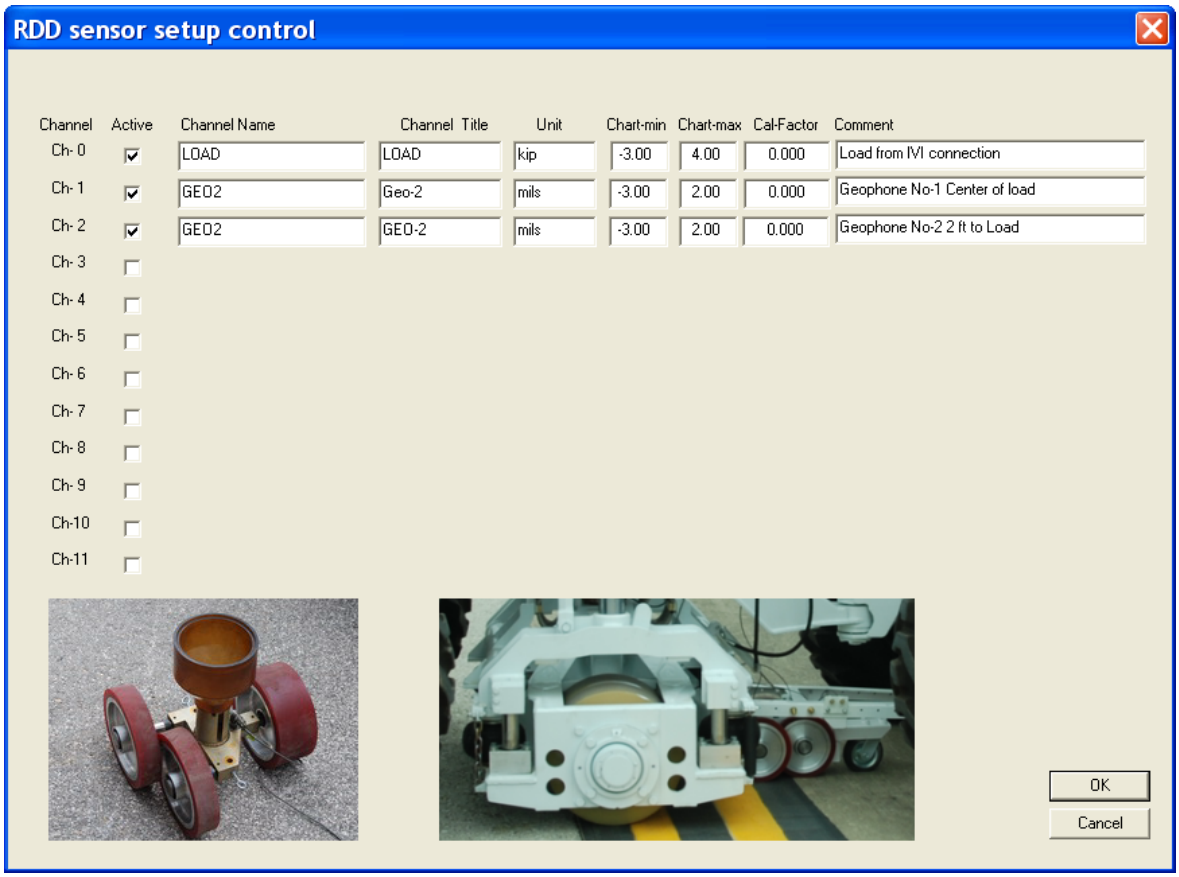

Figure 4.9: Entering Geophone Information in Updated Data Acquisition Software

4.4 RDD Field Data Analysis Software Development

RDD post processing will be a two-step process. It will include;

- Initial processing of the RDD geophones and load data, to view the deflection data and make sure the system is working well and secondly to filter and graphically display the areas of high deflection where additional testing or coring may be required.
- Loading this RDD deflection results file into an updated PAVECHECK-like program for complete integration of all collected field testing data, including GPR/IR/Video etc.

This section demonstrates the screens and typical outputs from the processing of a typical RDD data set. This software was developed in the third year of this project; it has been field tested and it is ready for use in the next round of RDD testing once sensor mounting improvements have been made.

Following are limitations of the current version of the software:

- The software can show the data from only one geophone at a time; the software provides options to select data from any of the available geophones;

- Currently the maximum array size for the load and geophone data is 3200K, which at current sampling rates will be about 1 hour's worth of RDD data; this can be increased in future systems but it is thought adequate at this developmental stage.

The main graphical output functions of this software are listed below:

- Displays of the raw load and geophone raw data (with Distance as the x-axis).
- Shows the load and geophone filtered data (with Distance as the x-axis). The system lets the operator set the band pass filter limits for data processing (for example 28 to 32 Hz).
- Shows both the raw and filtered load and geophone data together on the same plot (with distance as the x-axis)
- Displays the peak location on the raw data for load and geophone data (for calculating the peak-peak loads and deflections)
- Shows the Power Spectrum chart for the load and geophone raw data (in the frequency domain, showing the components at each frequency)
- Displays an RDD Continuous Deflection profile chart. Also outputs the result to an ASCII file for reporting and input into Excel
- Can display the static load chart (to check if the static load is constant)
- Can display the dynamic load chart (to check if the dynamic load is close to the user supplied input value)

This field processing software was fully developed in year 3 of this study. The main interface menu of this software is shown in Figure 4.10:

Figure 4.10: The field RDD Data Processing Software Main Interface (Toolbar Buttons)

Table 4.2 shows the function of each toolbar button:

Table 4.2: Pull Down Menu Options in the Field RDD Processing Software

	Opens the field test file (with the extension name of *.RDD)
	Shows the option dialog box for setting up the analysis parameters
	Shows the raw load data chart with distance as the x-axis
	Shows the raw geophone data chart with distance as the x-axis
	Shows the raw load's data power spectrum chart with the frequency component distribution of the raw load data.
	Shows the raw deflection's data power spectrum chart with the frequency component distribution of the raw deflection data.
	Shows the filtered load data chart with distance as the x-axis
	Shows the filtered geophone data chart with distance as the x-axis
	Shows the filtered and raw load data chart with distance as the x-axis, also shows the peak location
	Shows the filtered and raw geophone data chart with distance as the x-axis, also shows the peak location
	Saves the analysis results to ASCII file format

	For all the raw, filtered and power spectrum data charts, this button shows the previous screen
	For all the raw, filtered and power spectrum data charts, this button shows the next screen
	Shows the final maximum deflection results chart
	Shows the dynamic loading chart
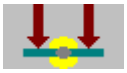	Shows the static loading chart
	Shows the dynamic deflection chart from the filtered data

By clicking the button, the option dialog box (Figure 4.11) is displayed for inputting the setup requirements of the analysis parameters. The most important parameters are the desired filter frequency limits and the sensor calibration factors.

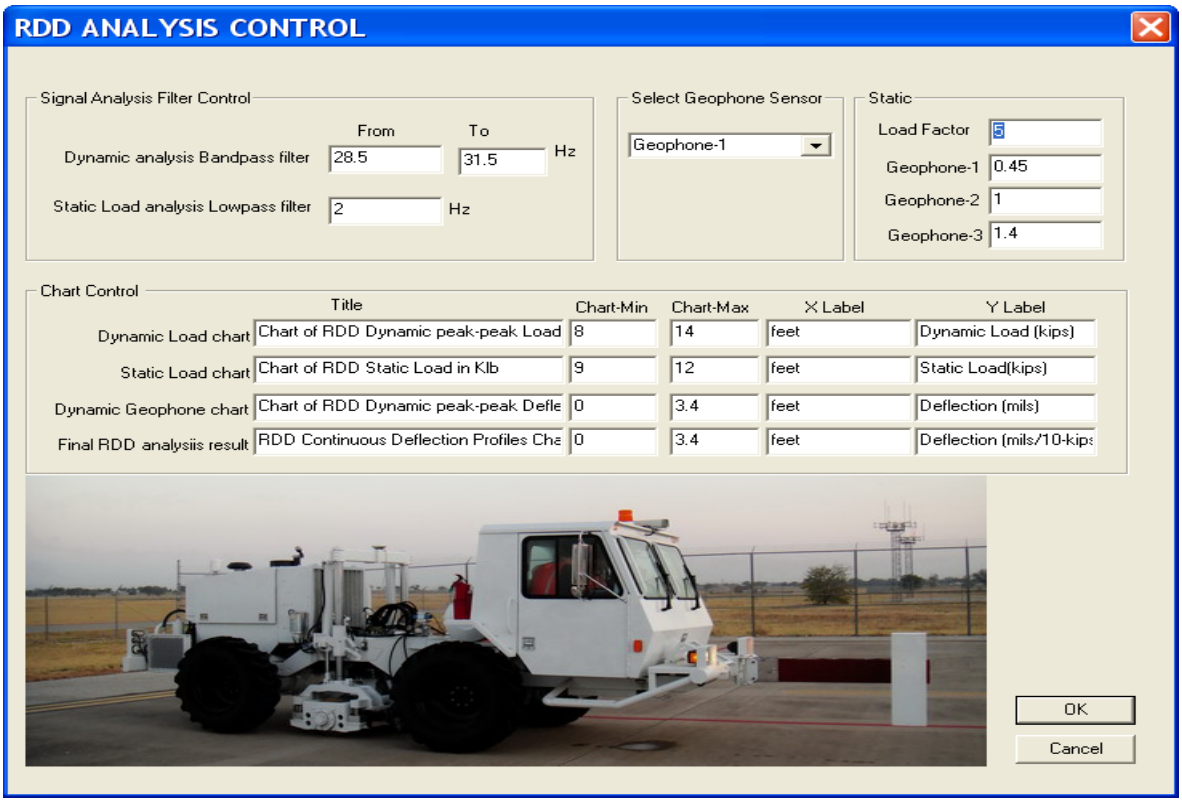

Figure 4.11: Set Up Menu for the Geophone Processing System

Once the parameters required in Figure 4.11 are entered, the data display and processing can proceed.

The user must first select the file to be processed. By then clicking button, the typical raw geophone data is displayed, an example of which is shown in Figure 4.12.

As shown in Figure 4.13 the power spectrum chart of raw data is displayed by clicking the button.

As shown in Figure 4.14 the filtered and raw load data chart is displayed by clicking toolbar button

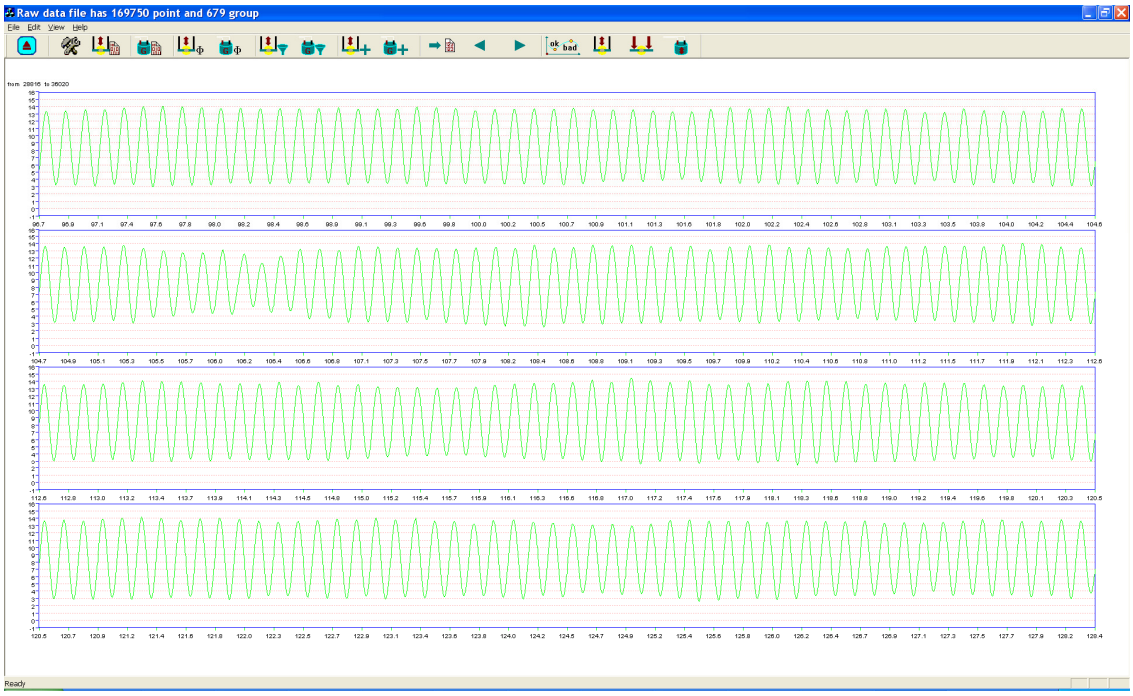

Figure 4.12: Raw Geophone Data

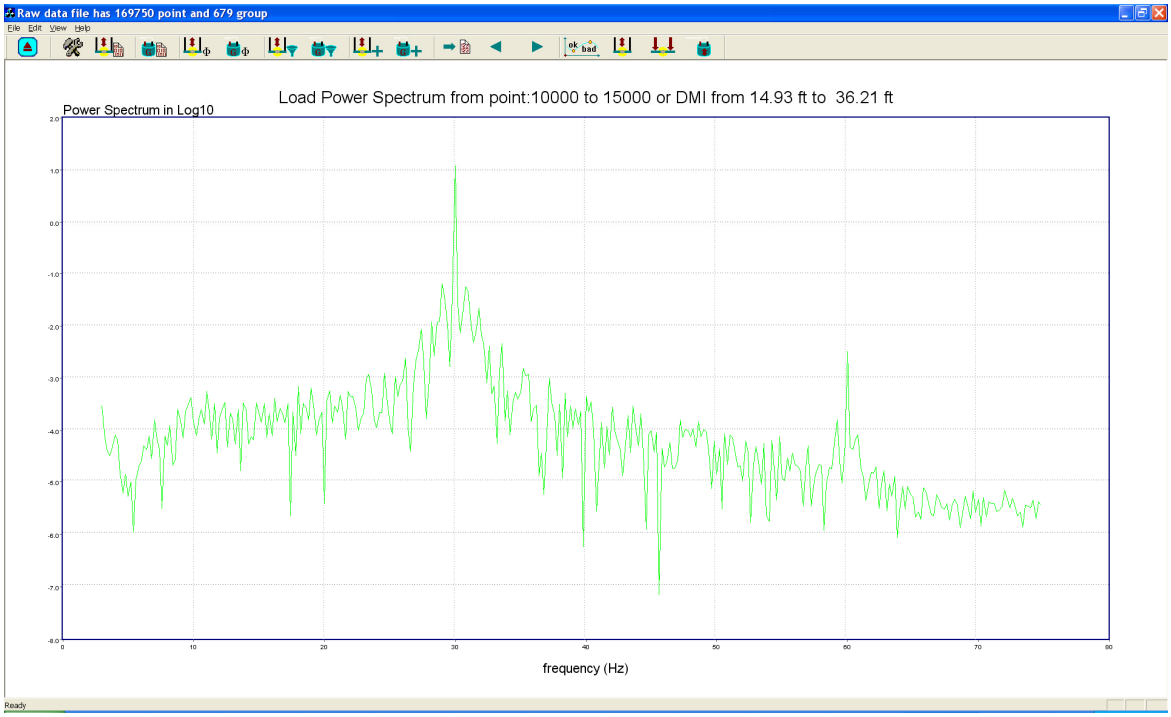

Figure 4.13: Power Density Spectra Data for One of the Data Sets (Peak being at 30 Hz)

Figure 4.14: Display of both Raw and Filtered Geophone Data, with Peaks Defined

By clicking the

toolbar button the final display of pavement deflections is displayed. The data set shown in Figure 4.15 is from the TxDOT FSF in Austin.

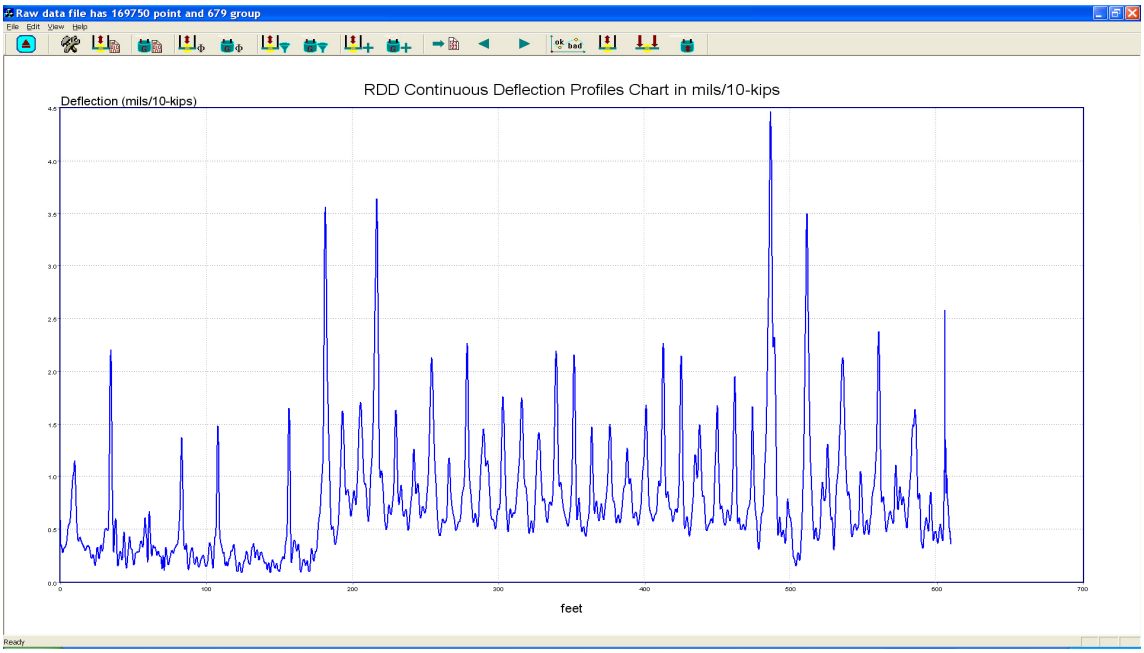

Figure 4.15: Typical Final Deflection Data Set from TxDOT Terminal

As shown in Figure 4.16 and 4.17 the system also provides the option for viewing the dynamic or static RDD load data by clicking the (dynamic) button or (static) buttons.

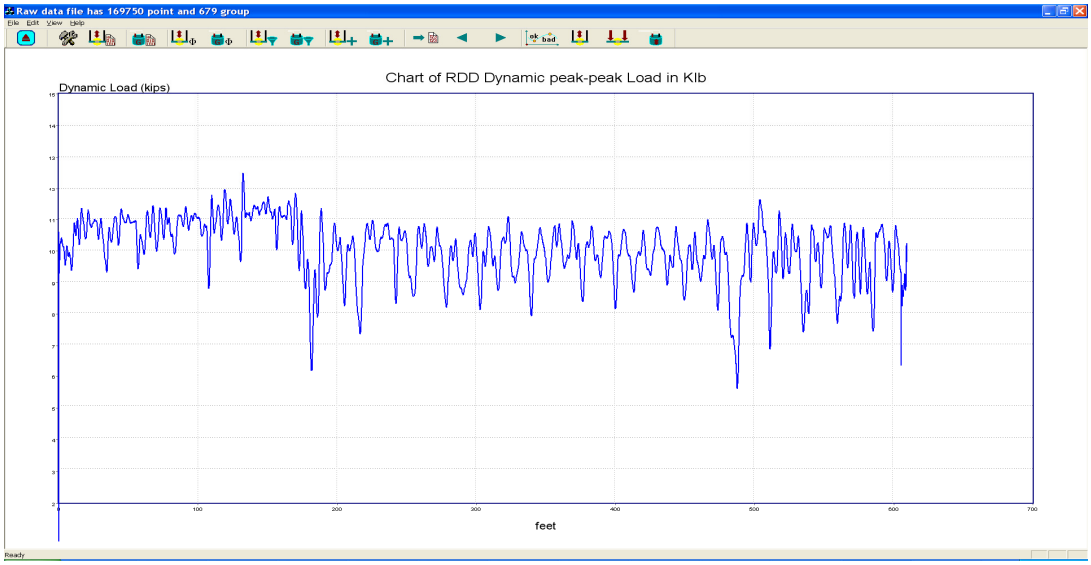

Figure 4.16: Dynamic Load Profile from Test Run

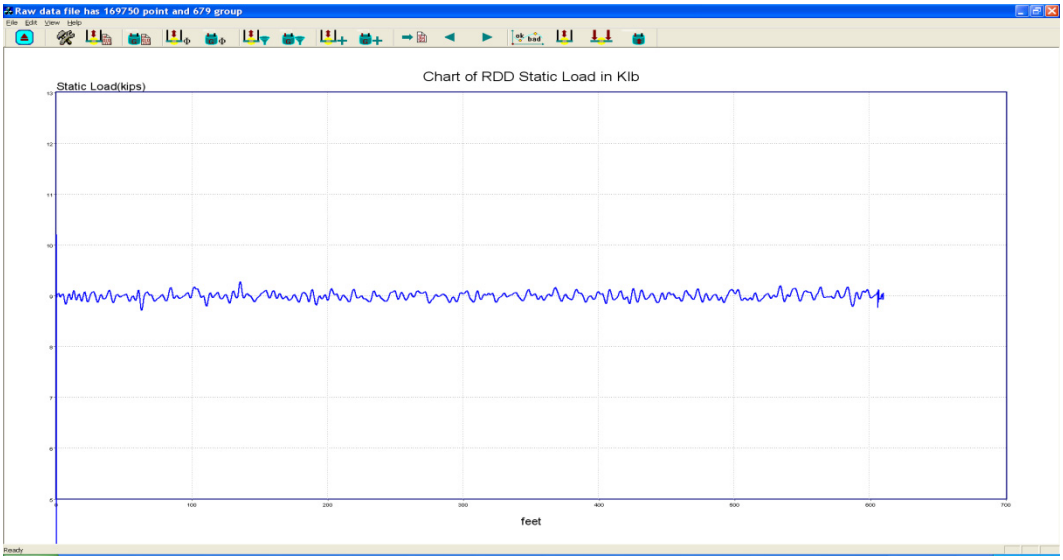

Figure 4.17: Static (Hold-Down) Load Profile for Test Run

Chapter 5. Summary of Year 3 Activities

The activities during Year 3 have been successful and productive. Previously, deliveries of the TPAD mobile platform and the TPAD dedicated hauling equipment (tractor and trailer) to CTR were completed and the initial acceptance testing of the TPAD mobile platform was performed in December 2010. Subsequent testing was continued over this reporting period. Acceptance testing involved evaluating (1) the speed control, (2) the static load control, (3) the dynamic load control, (4) the portable load calibration system, and (5) the DMI.

During acceptance testing, it was found that the speed control of the TPAD was acceptable after improvements were made but the static and dynamic load controls were not acceptable. It was determined that the TPAD computer software needed to be modified to fulfill the specifications. After the software modifications, the load control was re-evaluated. Some improvements and modifications were emplaced but continued improvements were required. The final acceptance testing should occur in spring 2012.

Two CEM designed speed-improved rolling sensors were assembled and installed in the TPAD. They are designated sensors #1 and #2 herein. Sensor #1 is located mid-way between the two loading rollers and sensor #2 is located about 25 in. in front of sensor #1. The initial testing with the rolling sensors was performed at the TxDOT FSF in March 2011.

During the testing with the speed-improved rolling sensors and the first-generation RDD portion of the TPAD, it was shown that sensor #1 can be used up to a testing speed of 3 mph with an acceptable S/N ratio. However, sensor #2 showed lateral oscillations in the direction of travel when crossing joints or cracks at testing speeds of 2 or 3 mph. Modifications were made to the locating mechanism of sensor #2 and its performance was re-evaluated. Some modifications were helpful in better understanding the performance but the modifications were not completely successful. Further activities directed at improving the rolling sensors are planned for fall 2011.

As mentioned in the Year 2 Activity Report, CEM designed speed-improved rolling sensors with four different wheel designs and three different hold-down weights. The performance based on the amount of rolling noise generated with each wheel type was evaluated with an independent towing frame using the PRC accelerated loading pavement test site. It was concluded that larger diameter wheels and heavier hold-down weights showed the best performance; hence, the lowest rolling noise. For more understanding of the rolling sensor performance, additional noise-level measurements with the independent towing frame will be conducted on jointed concrete pavement at the TxDOT FSF in fall 2011.

During the third year of the TxDOT 0-6005 project, the main task of TTI was to install the TTI DAQ system into the TPAD mobile platform and conduct performance checks. During the initial acceptance testing with the TPAD and TTI DAQ system in December 2010, an incompatibility was discovered in the connection of the TPAD control system and the TTI DAQ system. At first, the addition of a second DMI solely for the TTI DAQ system resolved the incompatibility. Later, an improved encoder allowed for signal sharing. In addition to the DAQ system, TTI also developed the software for analysis of the raw data. At that time, the definition of what is meant by the measuring of “raw data” surfaced. As a result, one set of RDD raw data was developed by CTR personnel. This set of data is presented in Appendix B. Improvements to the TTI DAQ system, combined with recording raw data and presenting processed data, will continue in Year 4.

References

Stokoe, K. H., Kallivokas, L. F., Nam, B. H., Carpenter, C. K., Bryant, A. D., Weeks, D. A., Beno, J. H., Scullion, T., and Liu, W. (2010),"Progress during the First Year towards Building the Total Pavement Acceptance Device (TPAD)," CTR Technical Report 0-6005-1, Center for Transportation Research, University of Texas at Austin.

Stokoe, K. H., Kallivokas, L. F., Nam, B. H., Carpenter, C. K., Lee, J. –S., Bryant, A. D., Weeks, D. A., Hayes, R., Scullion, T., and Liu, W. (2011),"Developing a Testing Device for Total Pavements Acceptance-Second-Year Report," CTR Technical Report 0-6005-2, Center for Transportation Research, University of Texas at Austin.

Appendix A: Noise-Level Measurements with Towing Frame at PRC

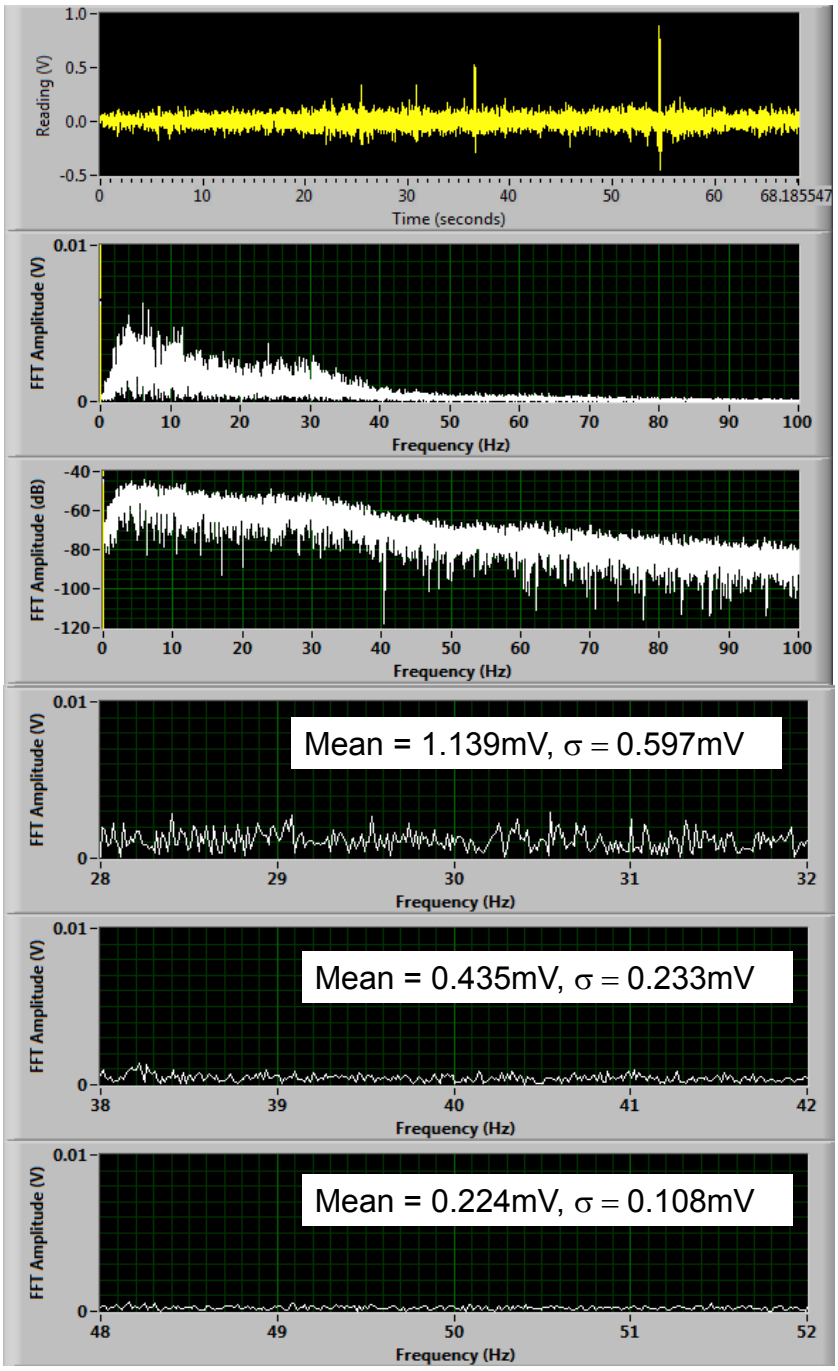

Figure A.1: SA with 20 lb Hold-Down Weight at 1 mph

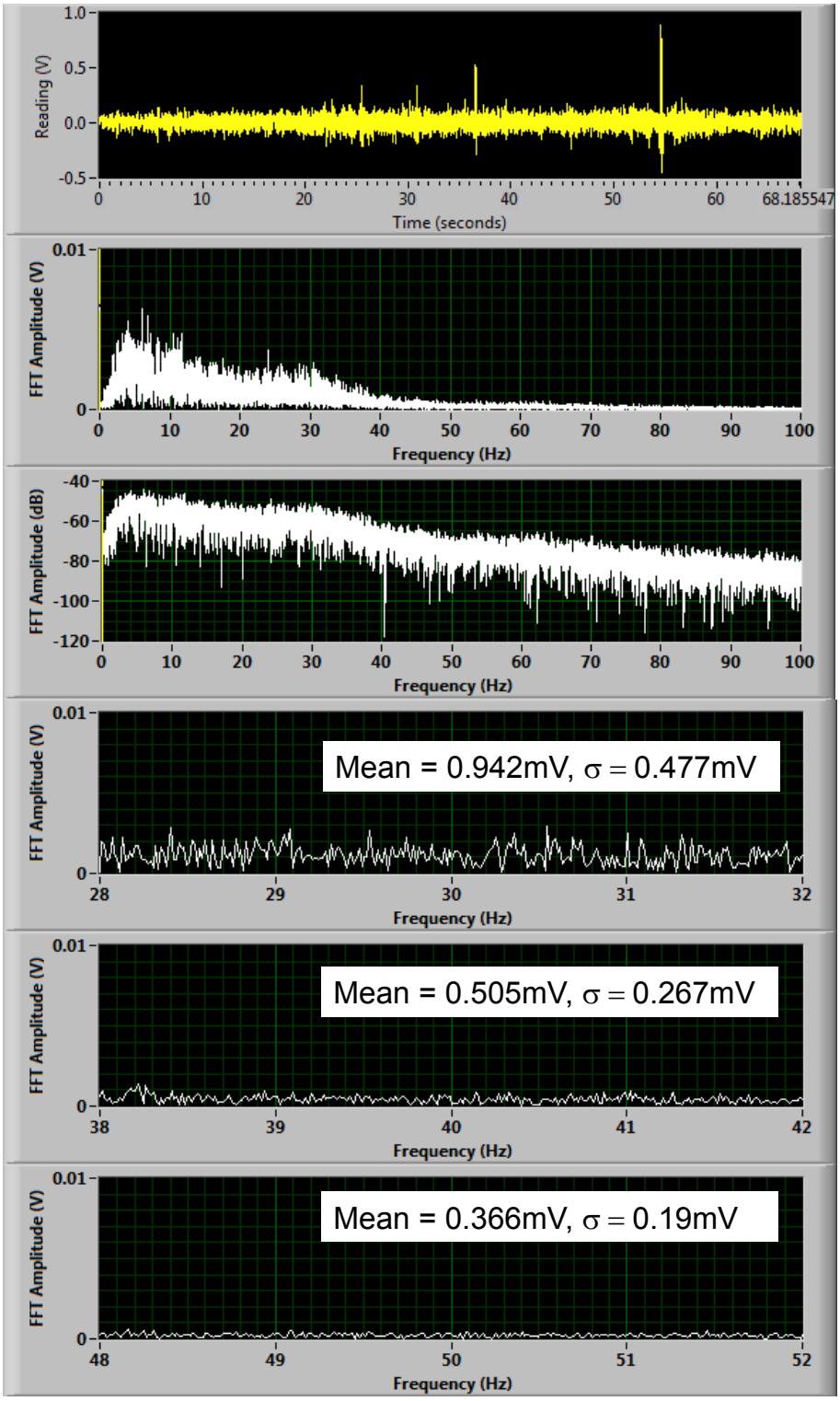

Figure A.2: SA with 40 lb Hold-Down Weight at 1 mph

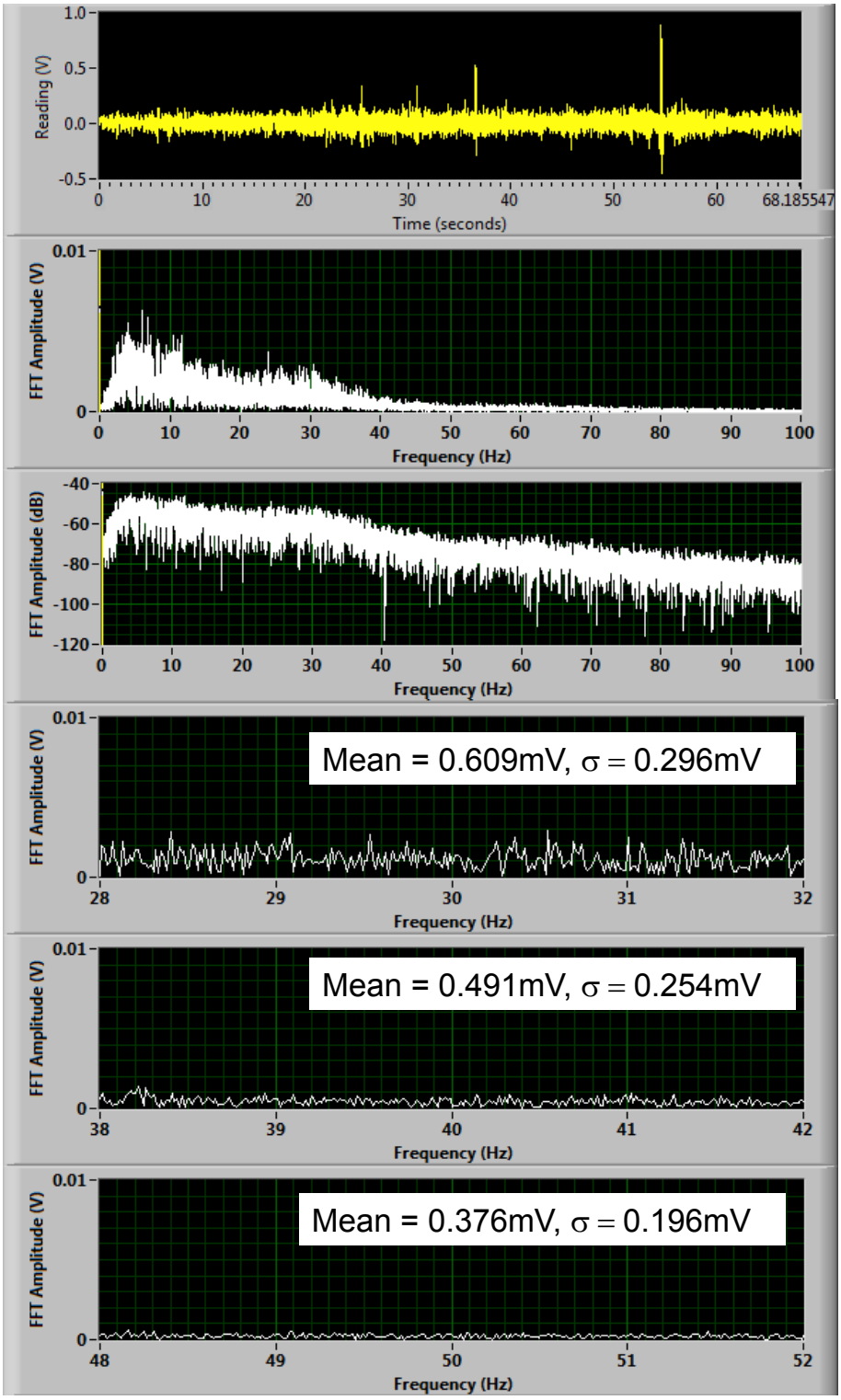

Figure A.3: SA with 90 lb Hold-Down Weight at 1 mph

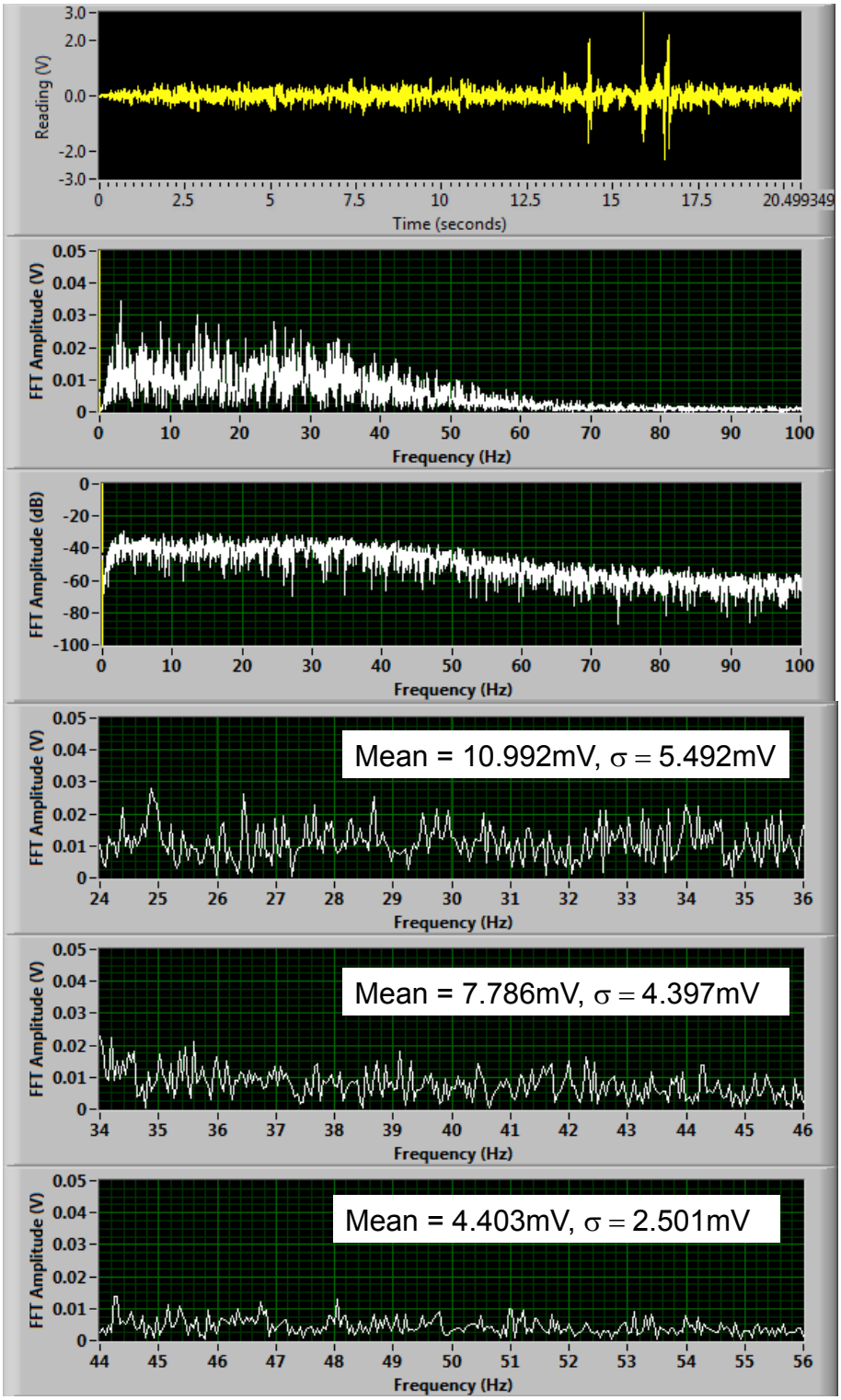

Figure A.4: SA with 20 lb Hold-Down Weight at 3 mph

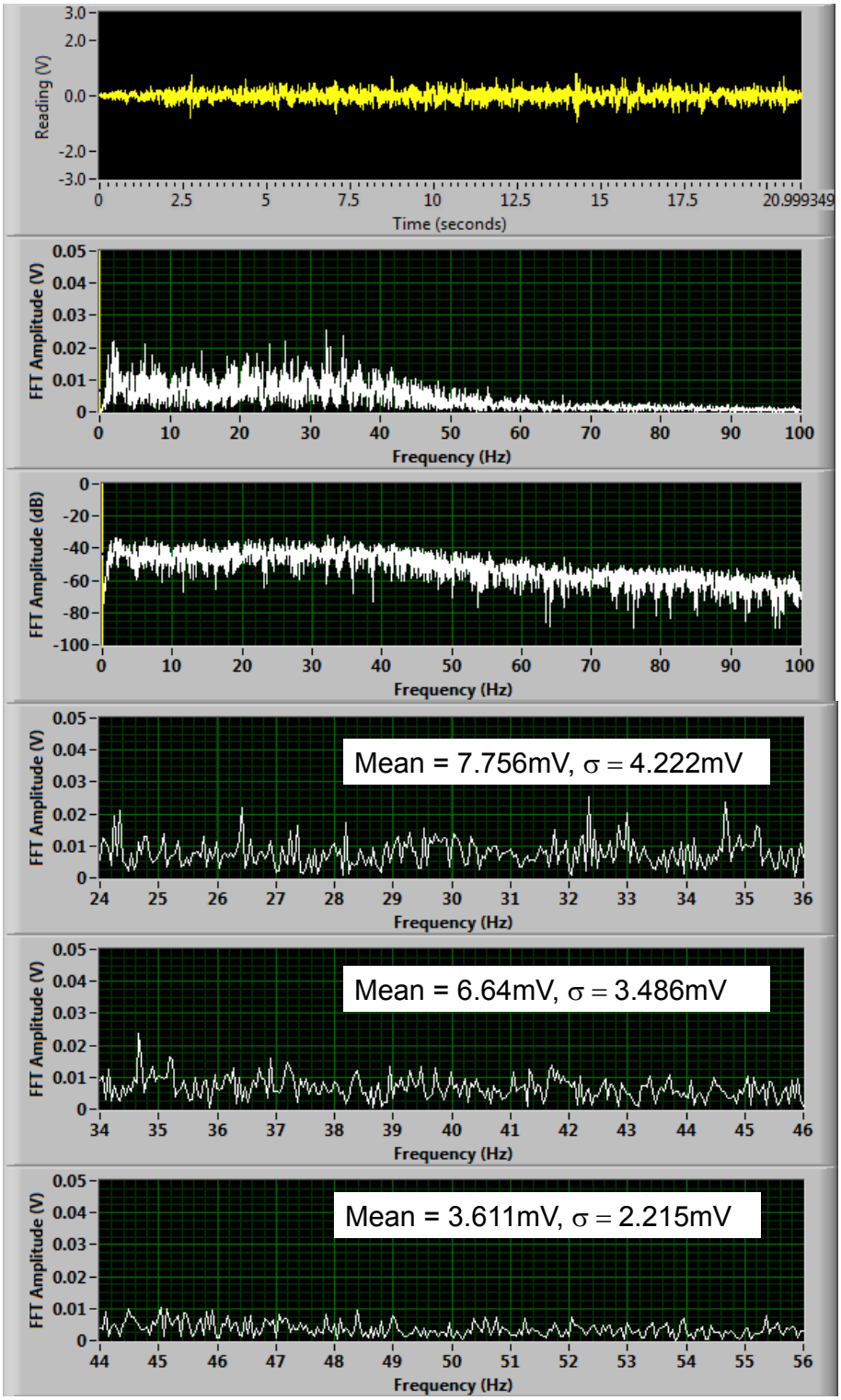

Figure A.5: SA with 40 lb Hold-Down Weight at 3 mph

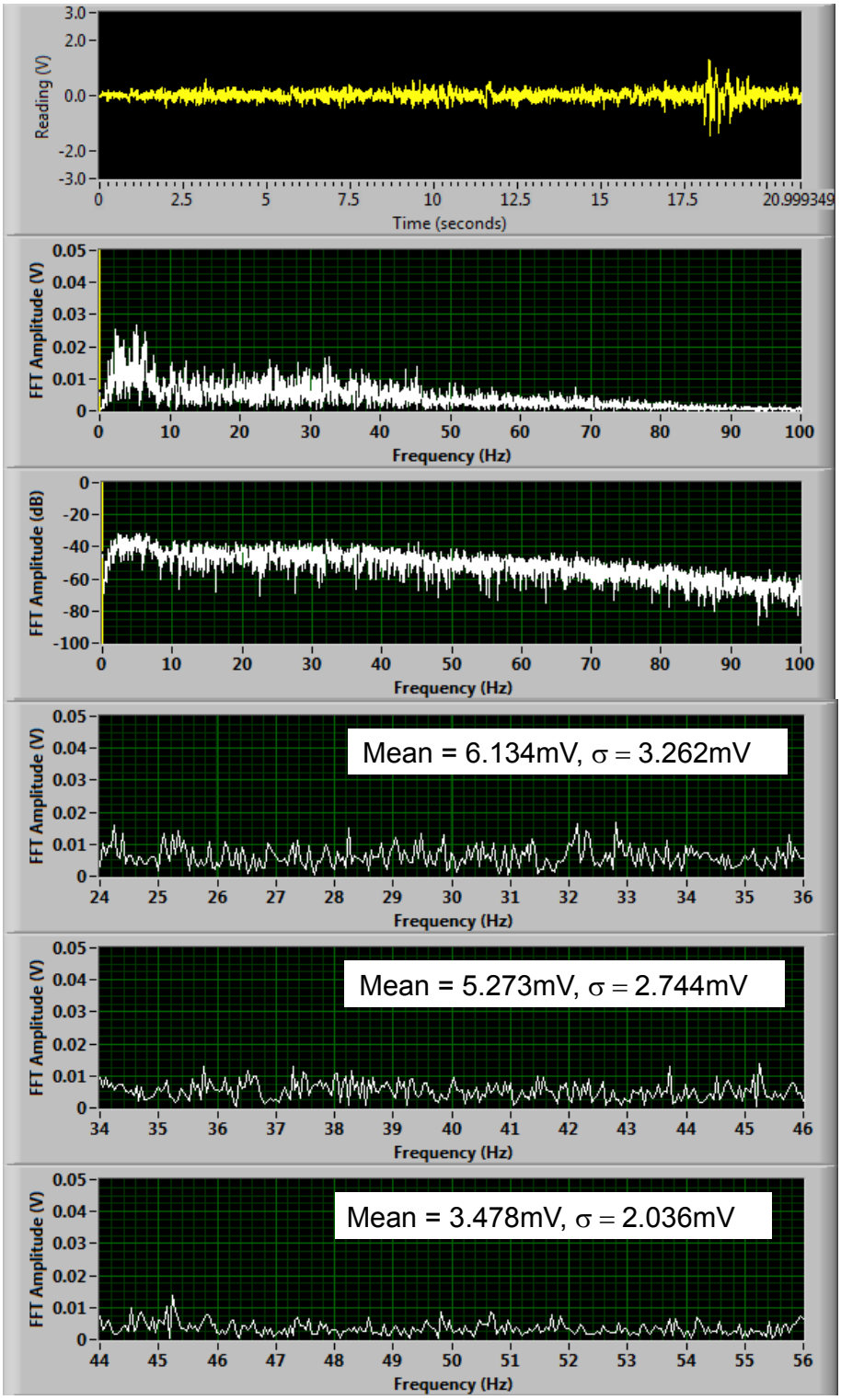

Figure A.6: SA with 90 lb Hold-Down Weight at 3 mph

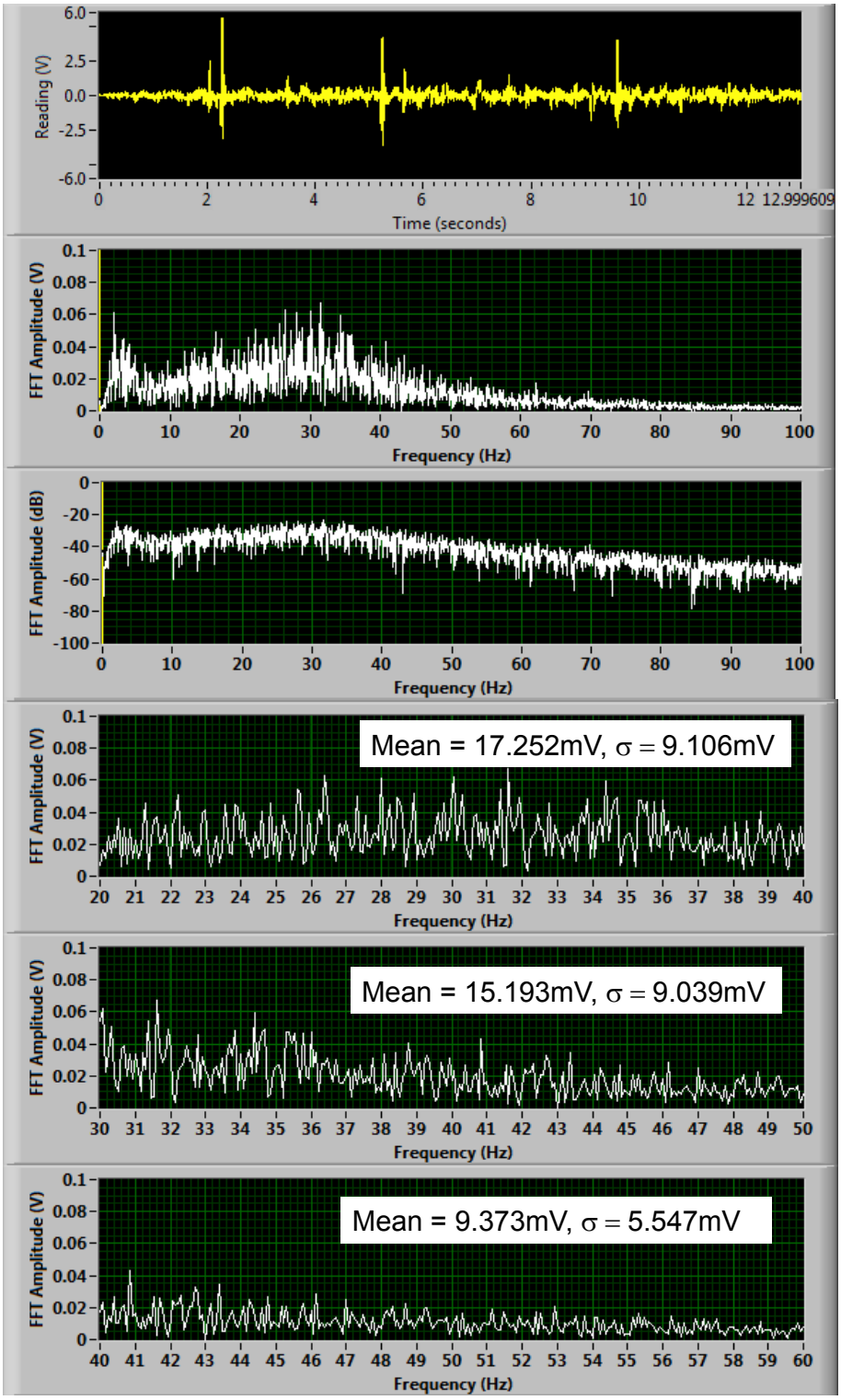

Figure A.7: SA with 20 lb Hold-Down Weight at 5 mph

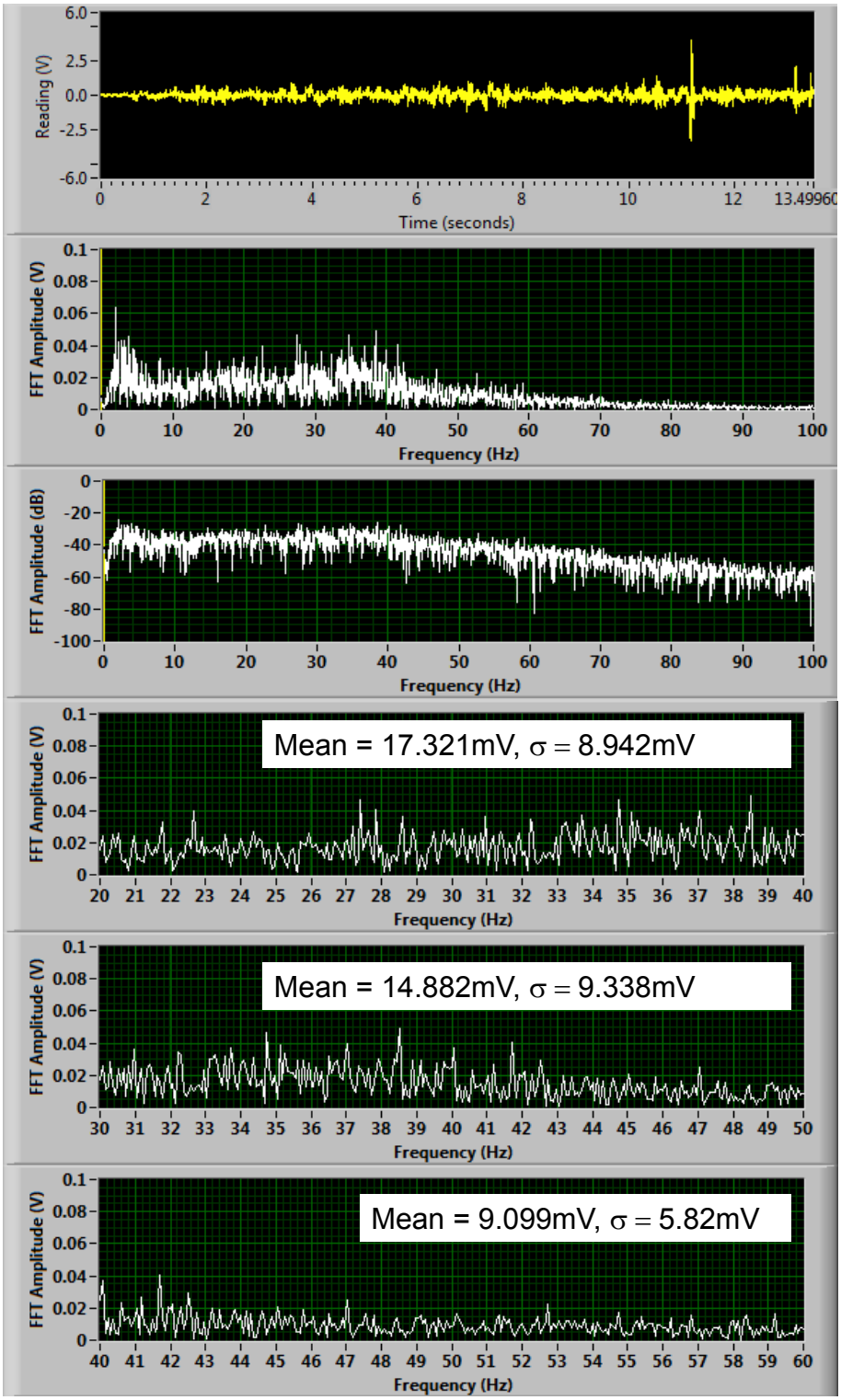

Figure A.8: SA with 40 lb Hold-Down Weight at 5 mph

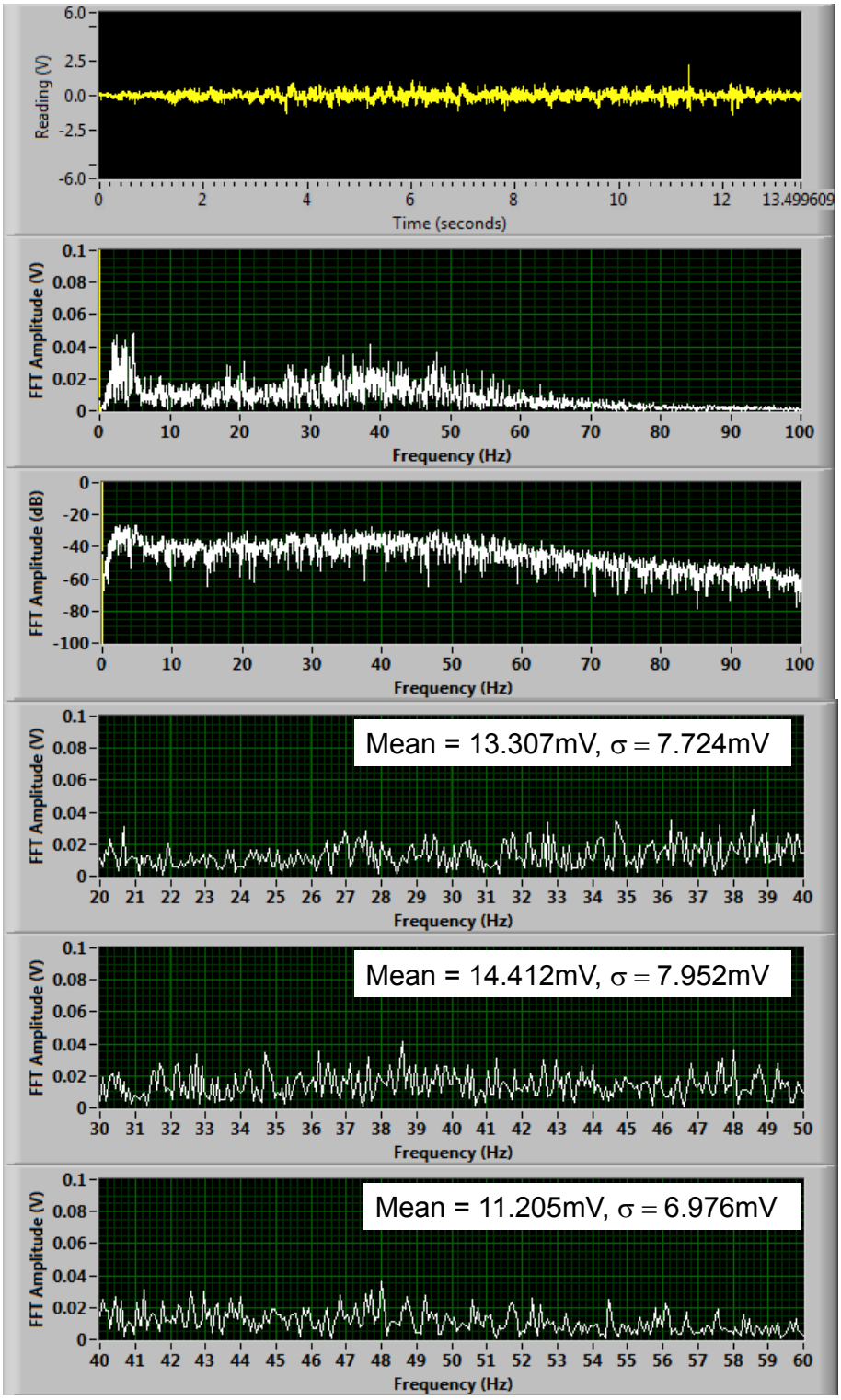

Figure A.9: SA with 90 lb Hold-Down Weight at 5 mph

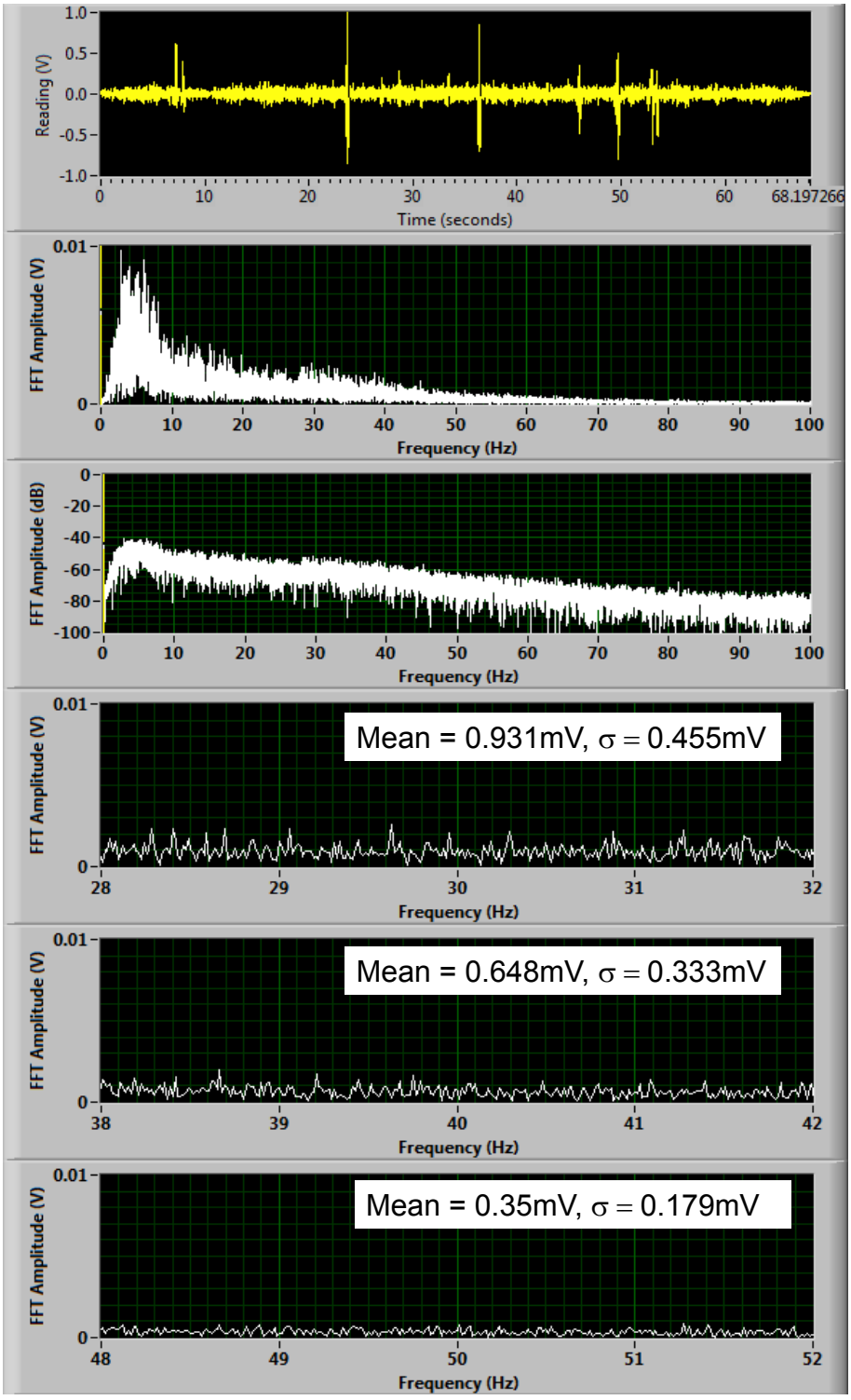

Figure A.10: SB with 20 lb Hold-Down Weight at 1 mph

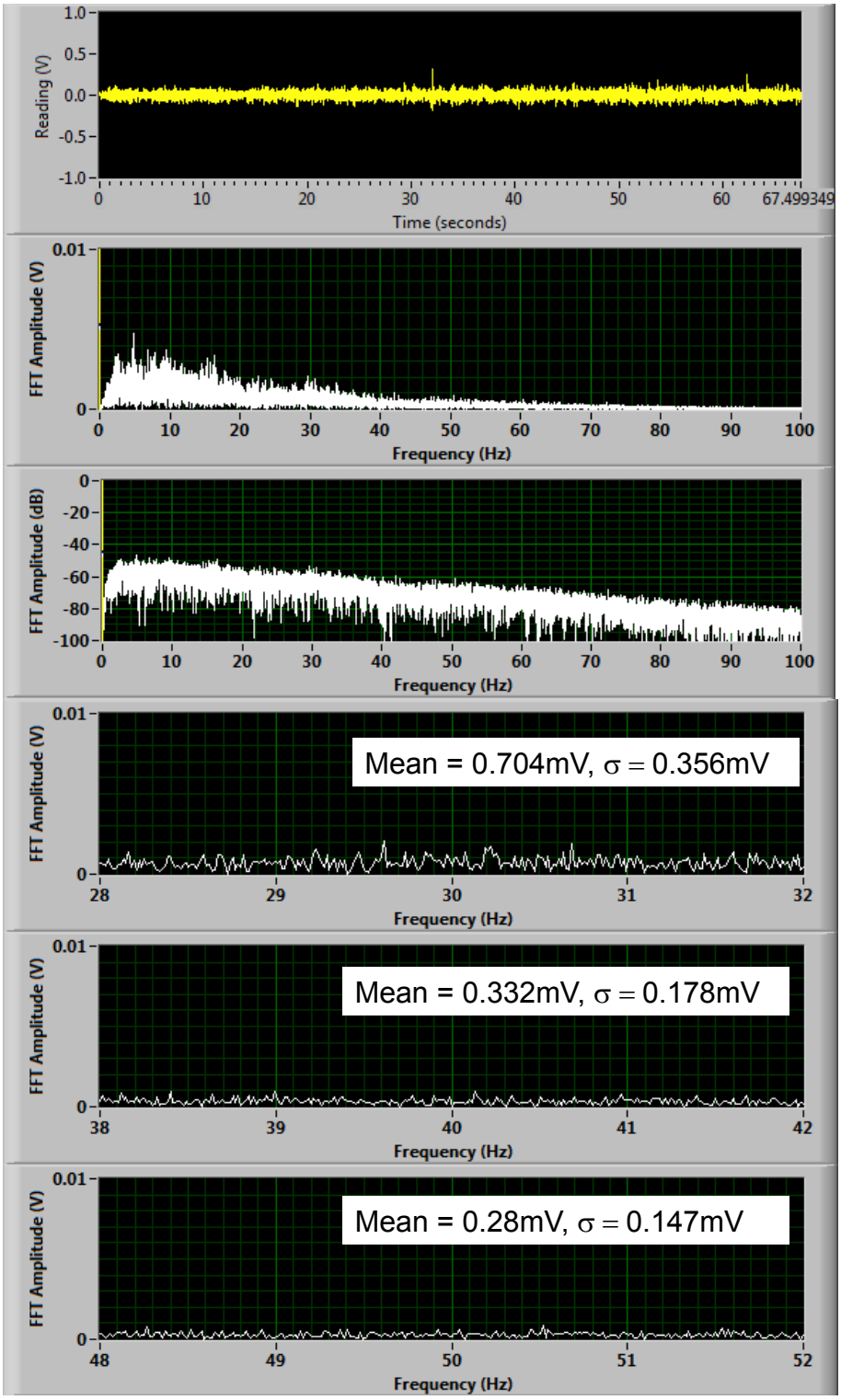

Figure A.11: SB with 40 lb Hold-Down Weight at 1 mph

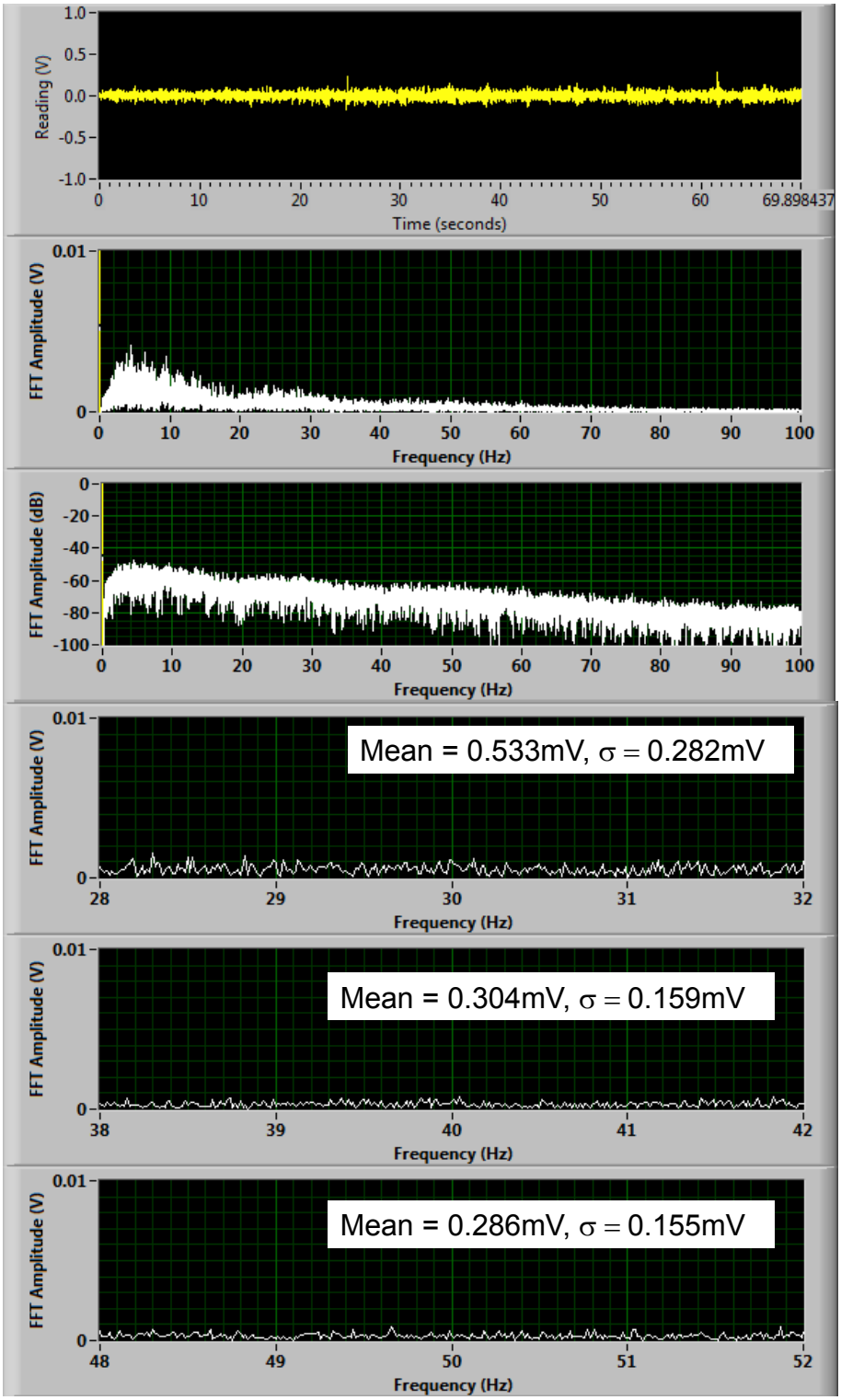

Figure A.12: SB with 90 lb Hold-Down Weight at 1 mph

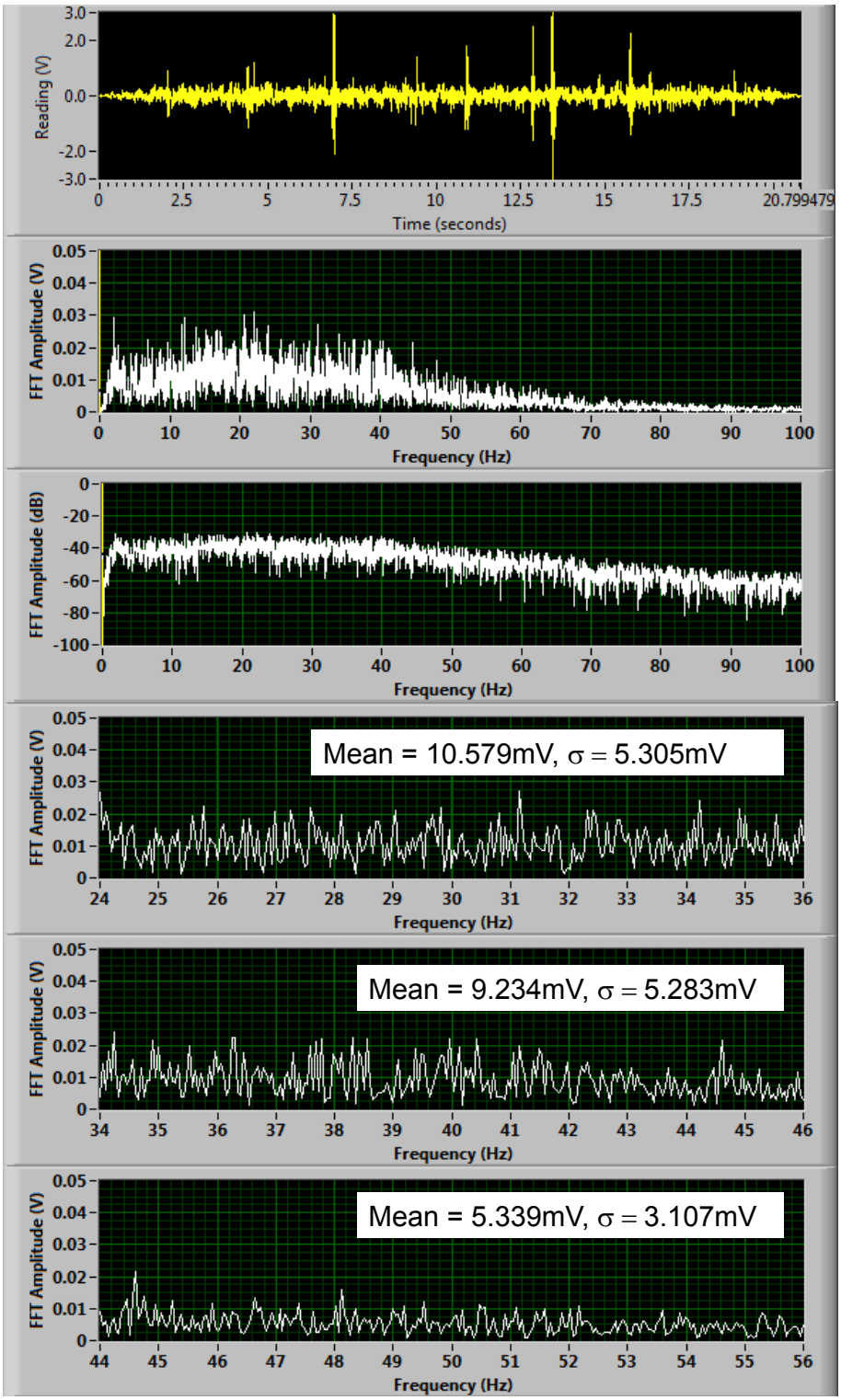

Figure A.13: SB with 20 lb Hold-Down Weight at 3 mph

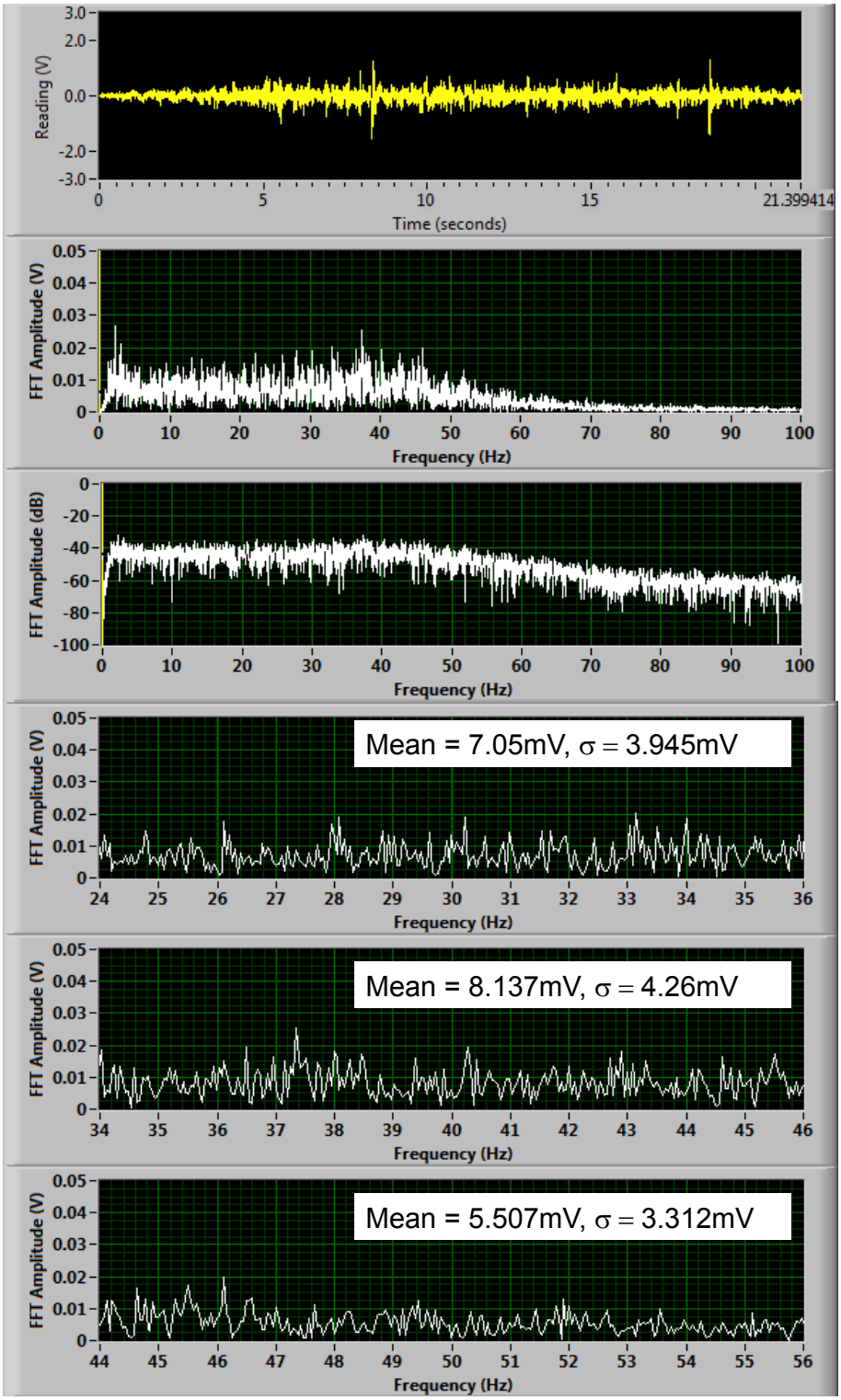

Figure A.14: SB with 40 lb Hold-Down Weight at 3 mph

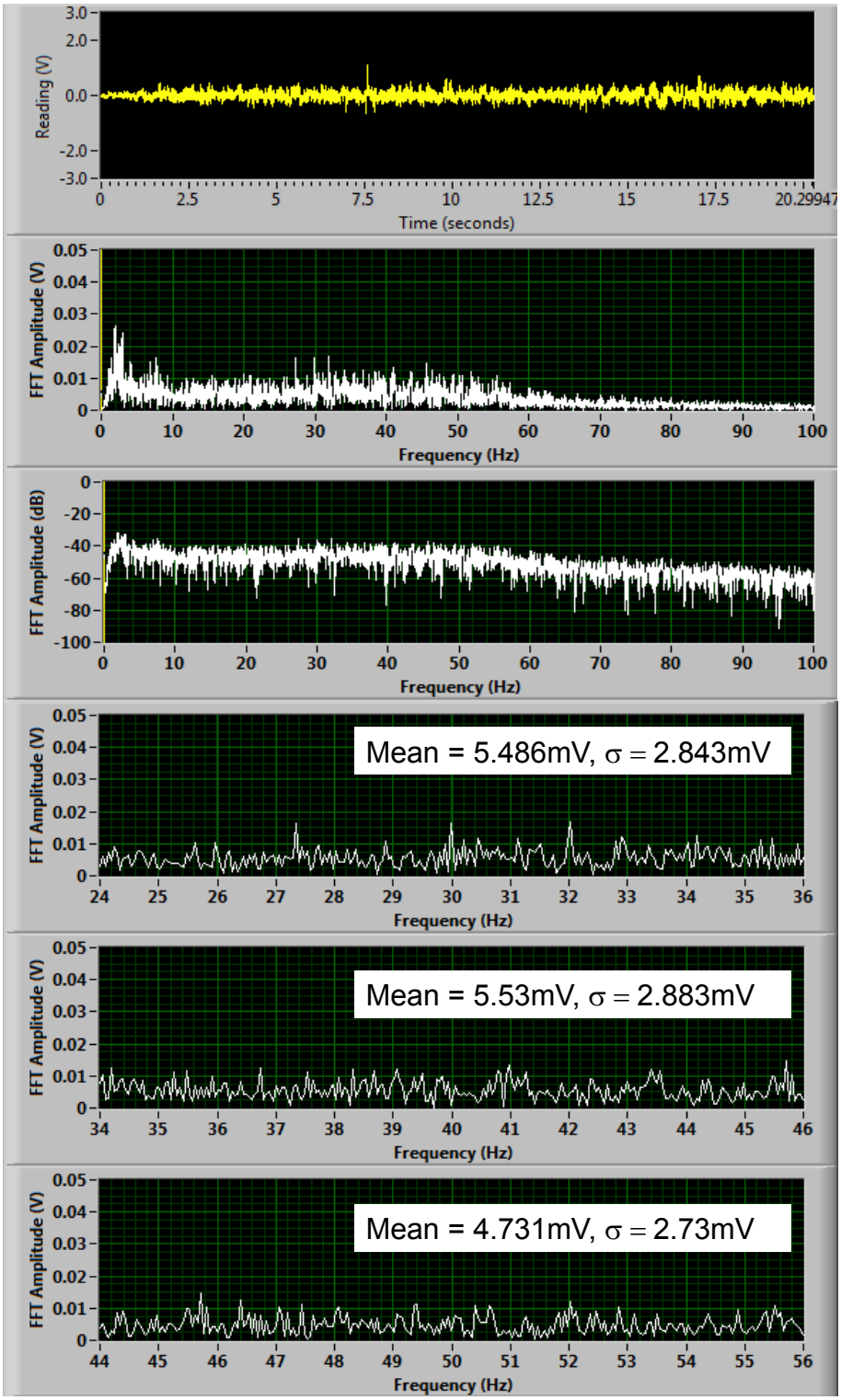

Figure A.15: SB with 90 lb Hold-Down Weight at 3 mph

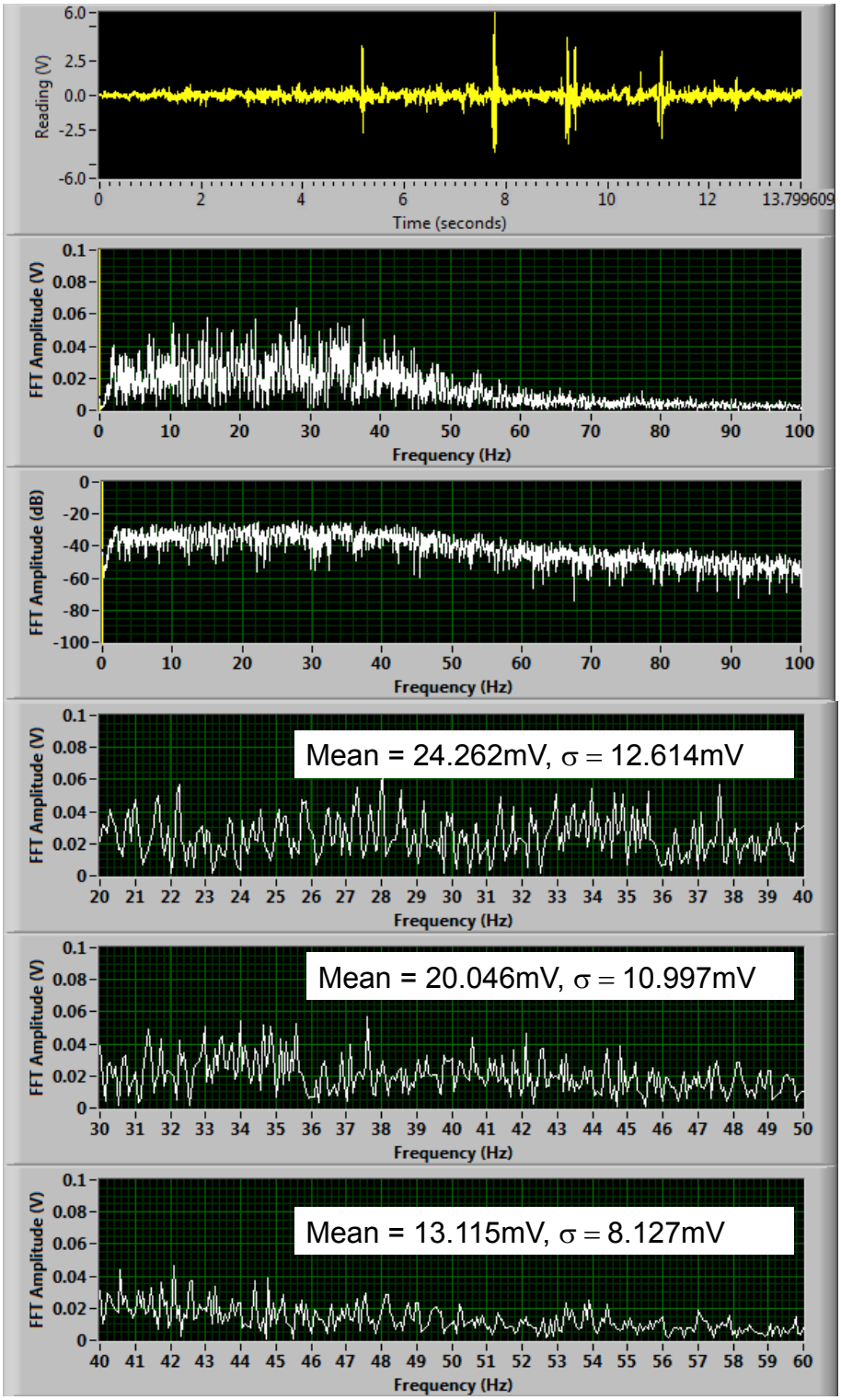

Figure A.16: SB with 20 lb Hold-Down Weight at 5 mph

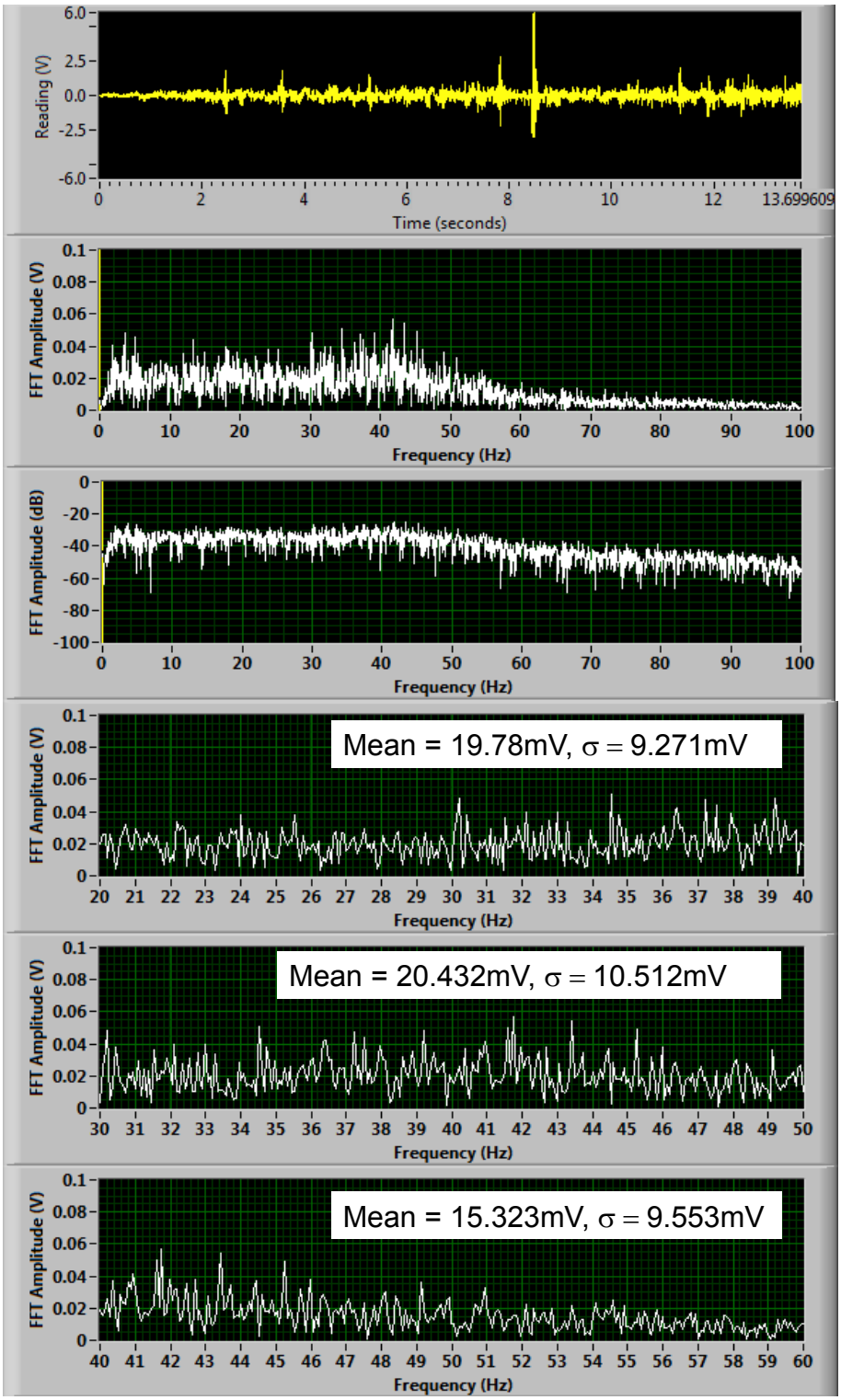

Figure A.17: SB with 40 lb Hold-Down Weight at 5 mph

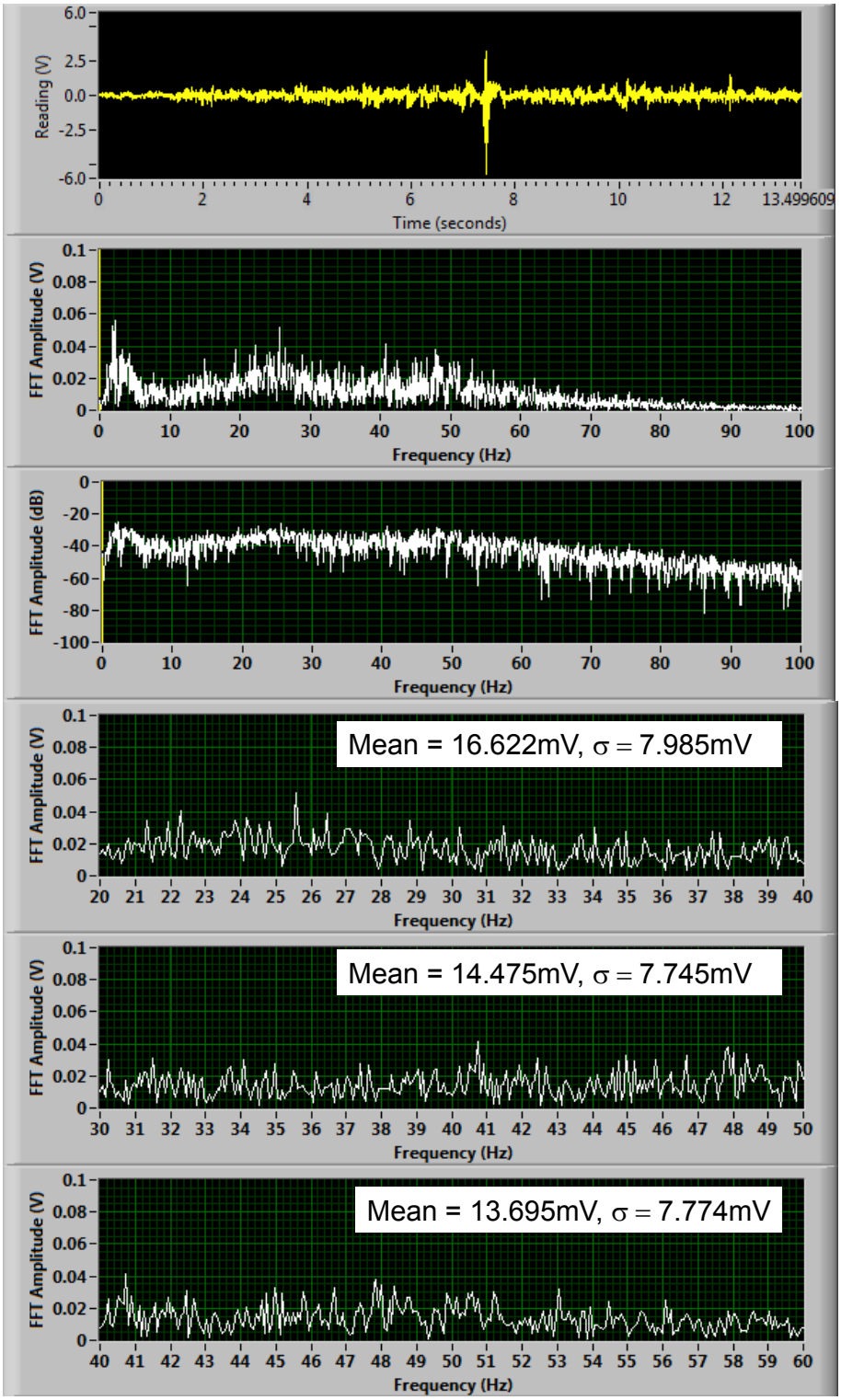

Figure A.18: SB with 90 lb Hold-Down Weight at 5 mph

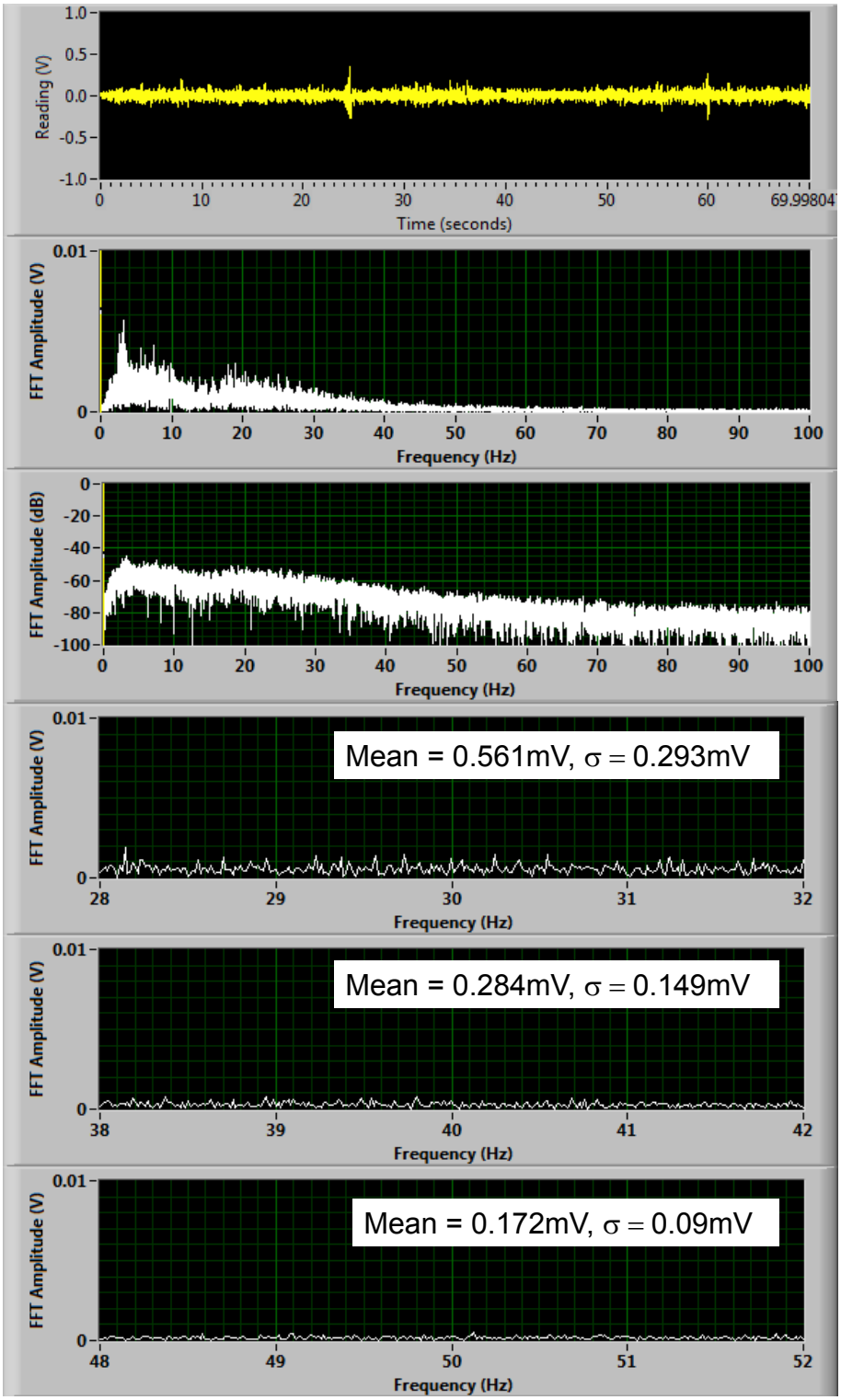

Figure A.19: SC with 20 lb Hold-Down Weight at 1mph

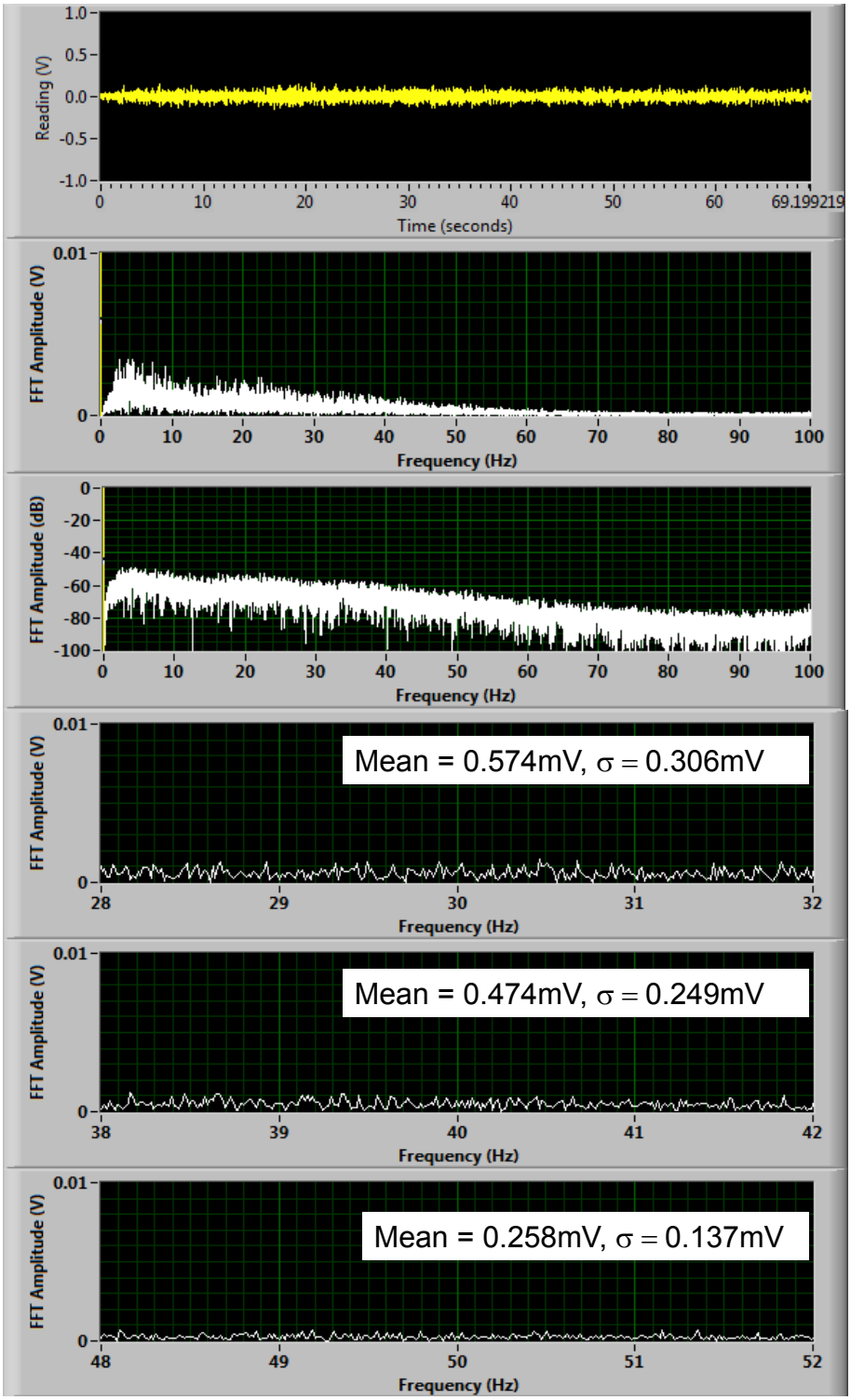

Figure A.20: SC with 40 lb Hold-Down Weight at 1mph

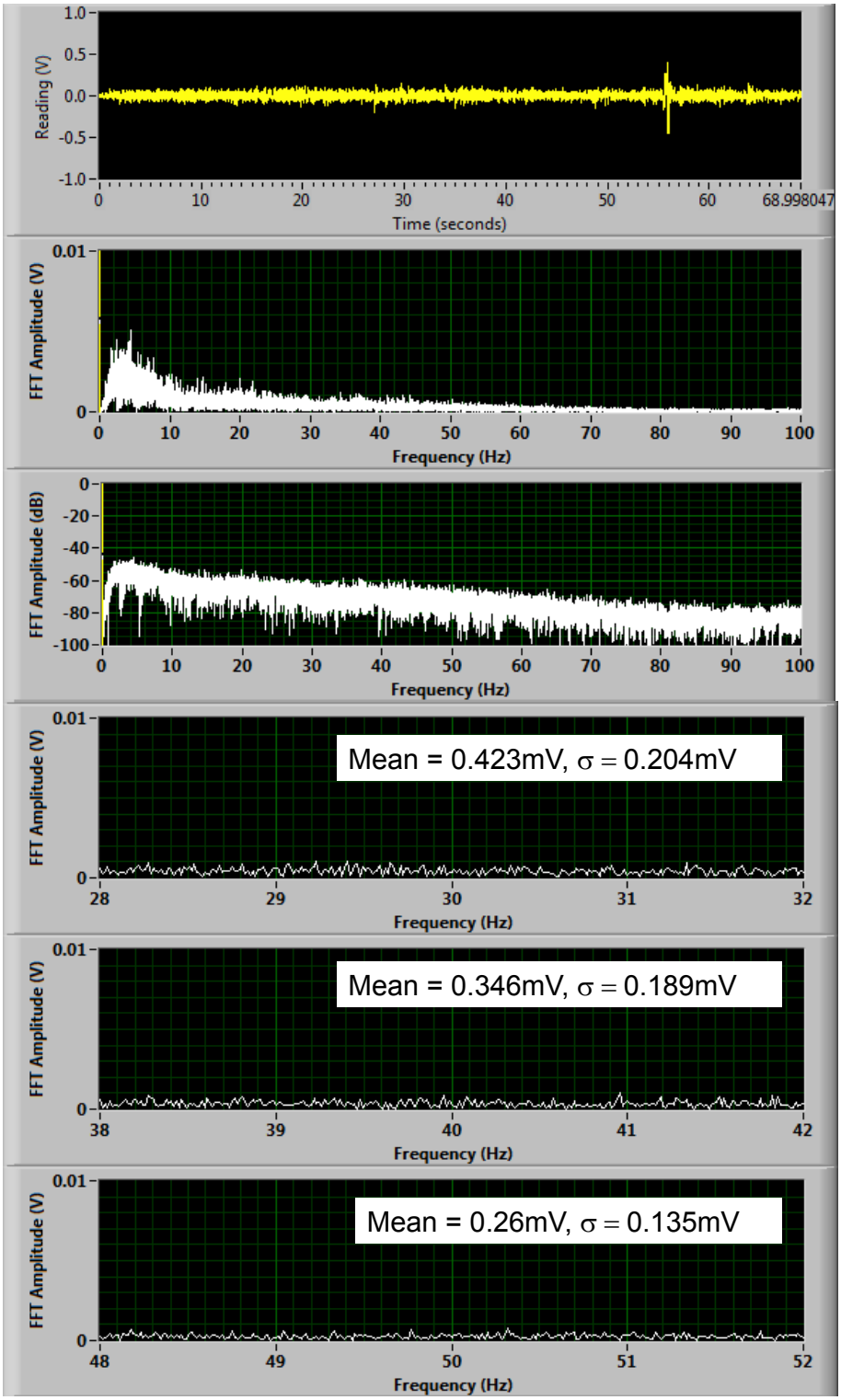

Figure A.21: SC with 90 lb Hold-Down Weight at 1mph

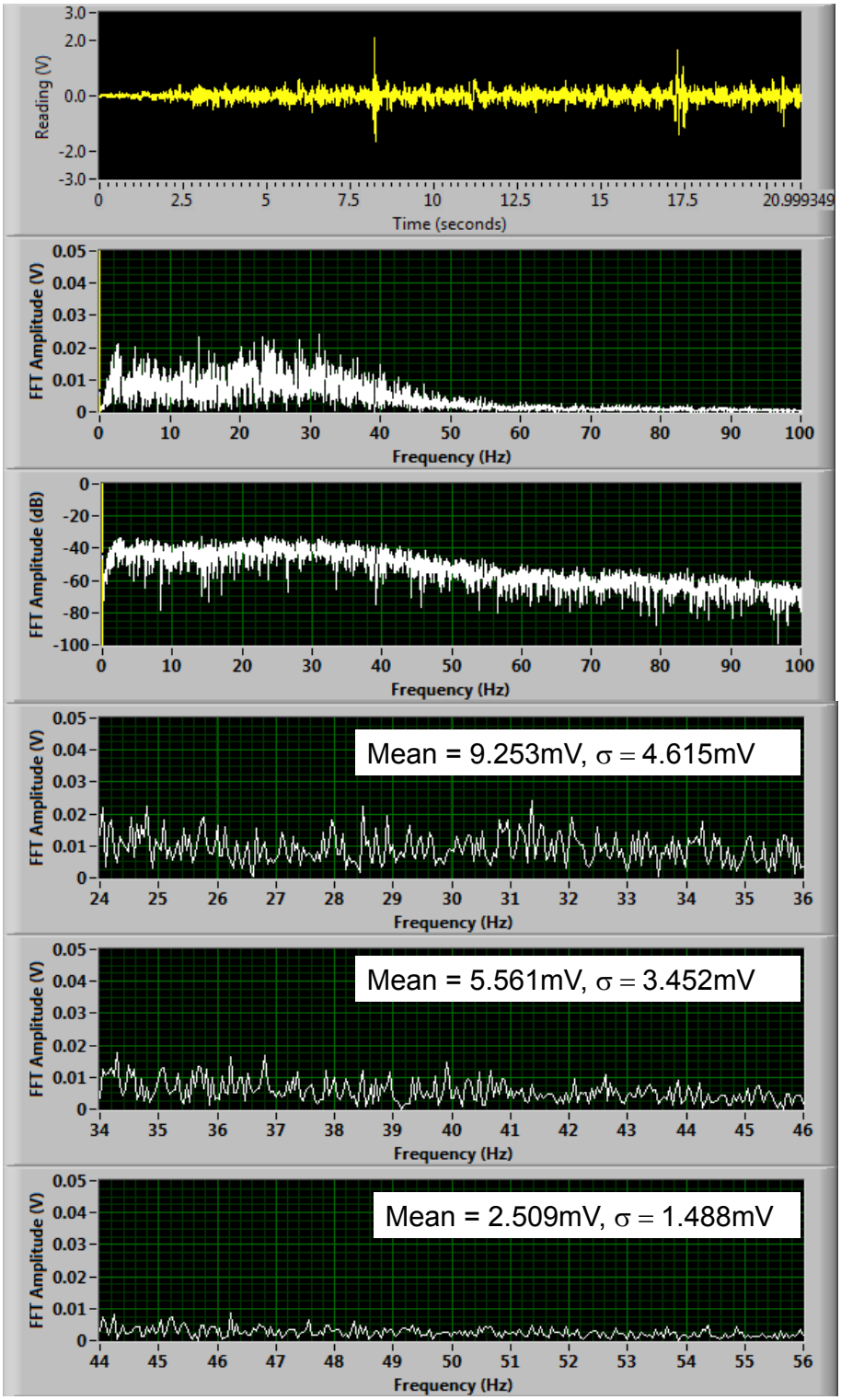

Figure A.22: SC with 20 lb Hold-Down Weight at 3 mph

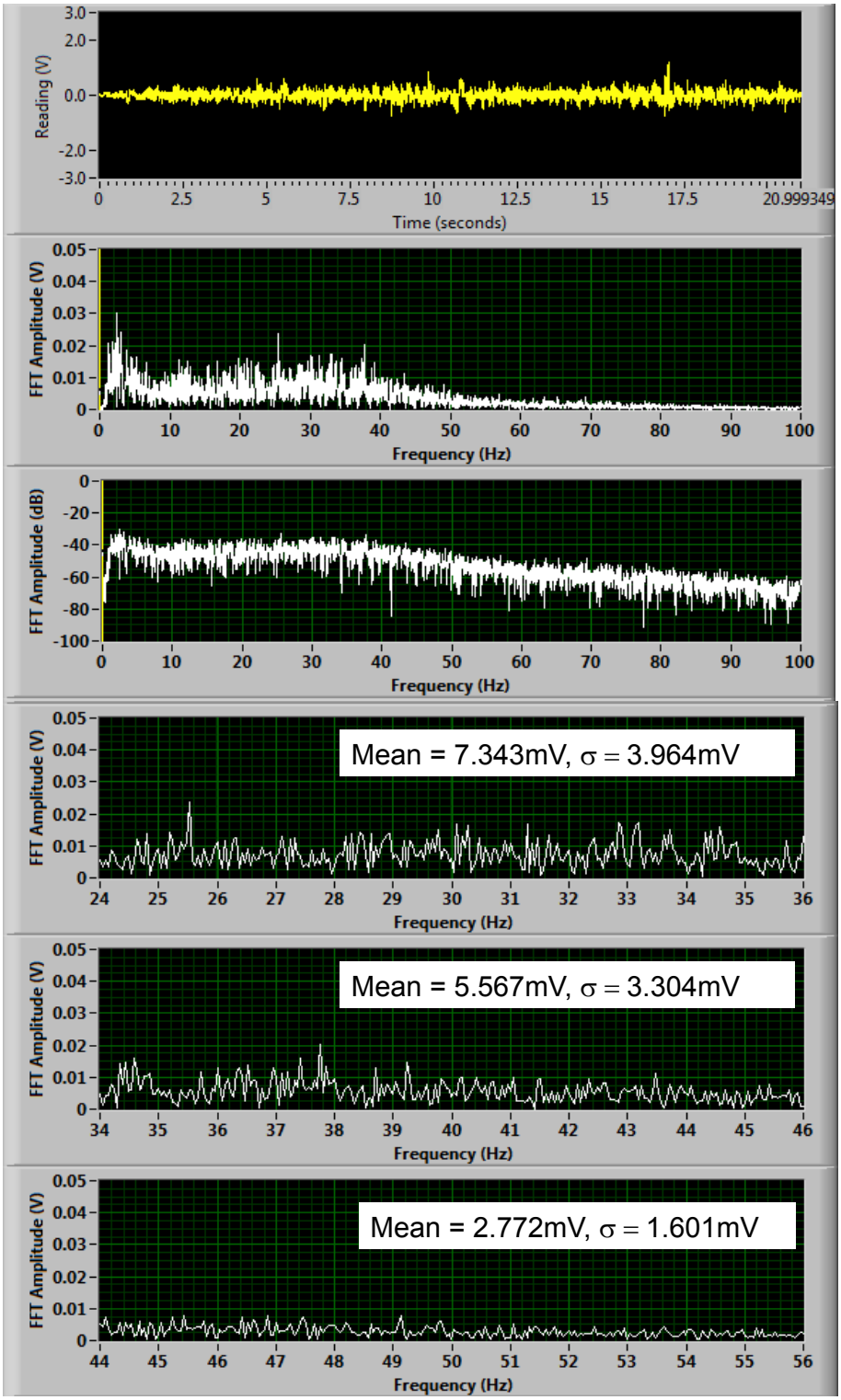

Figure A.23: SC with 40 lb Hold-Down Weight at 3 mph

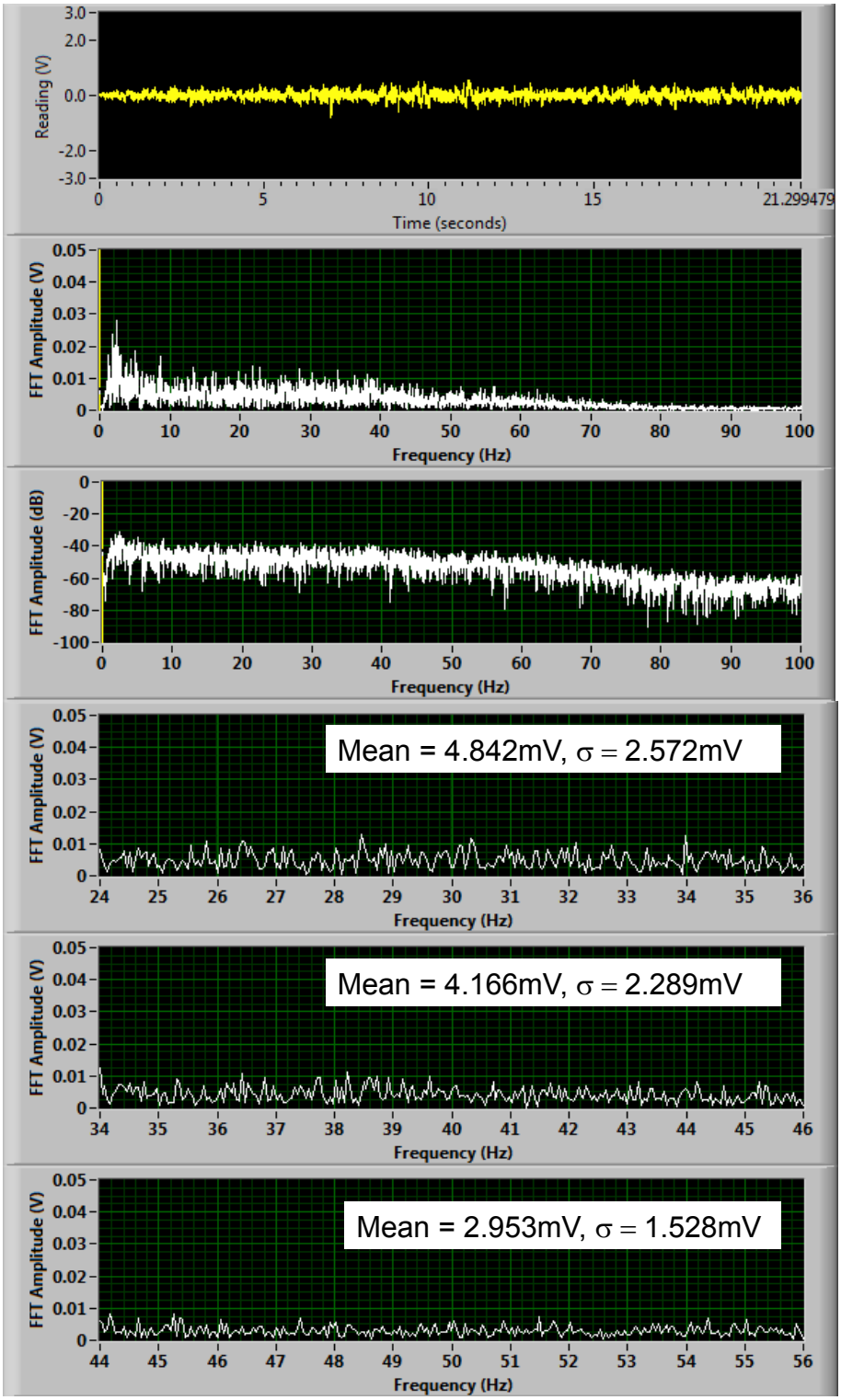

Figure A.24: SC with 90 lb Hold-Down Weight at 3 mph

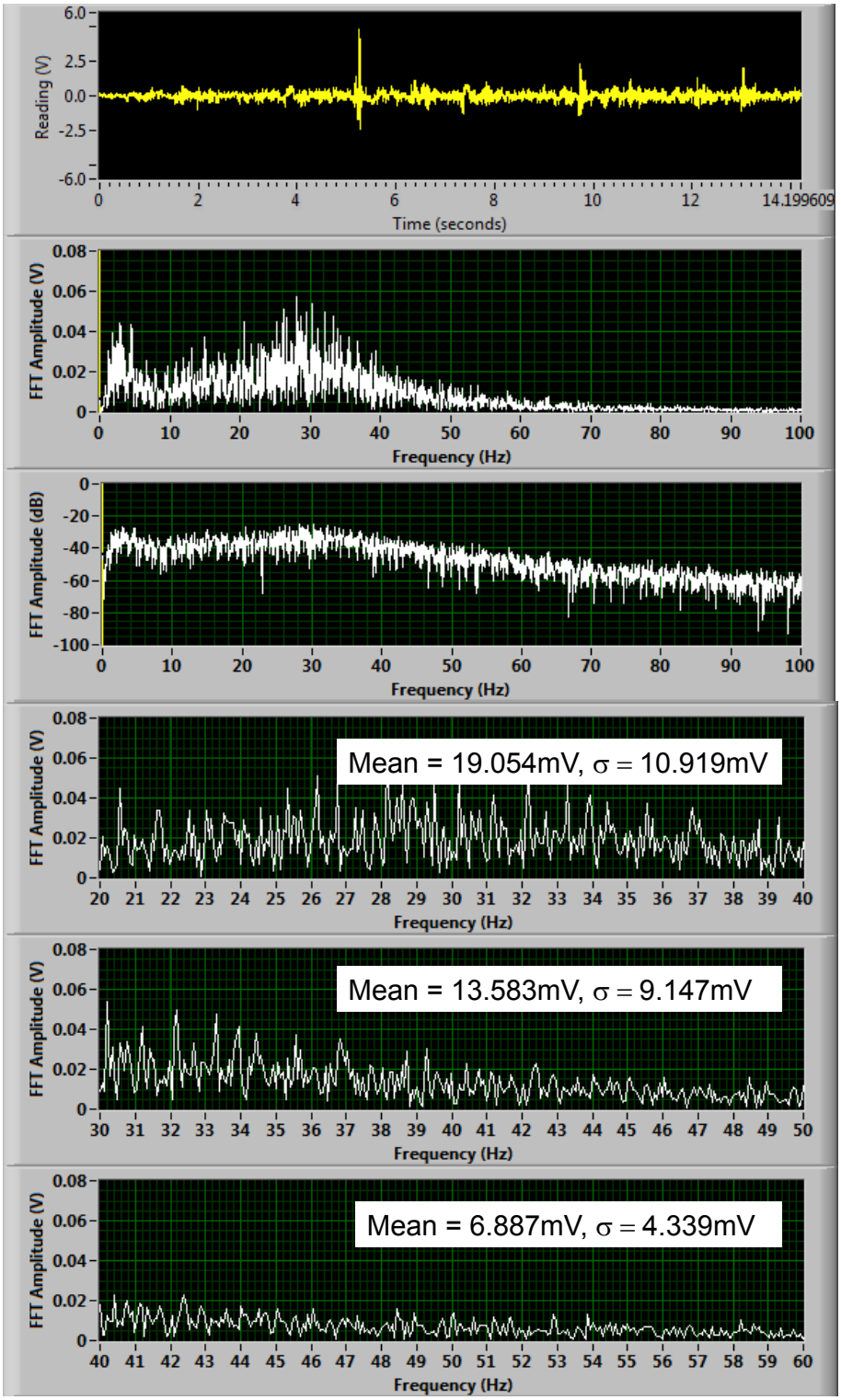

Figure A.25: SC with 20 lb Hold-Down Weight at 5 mph

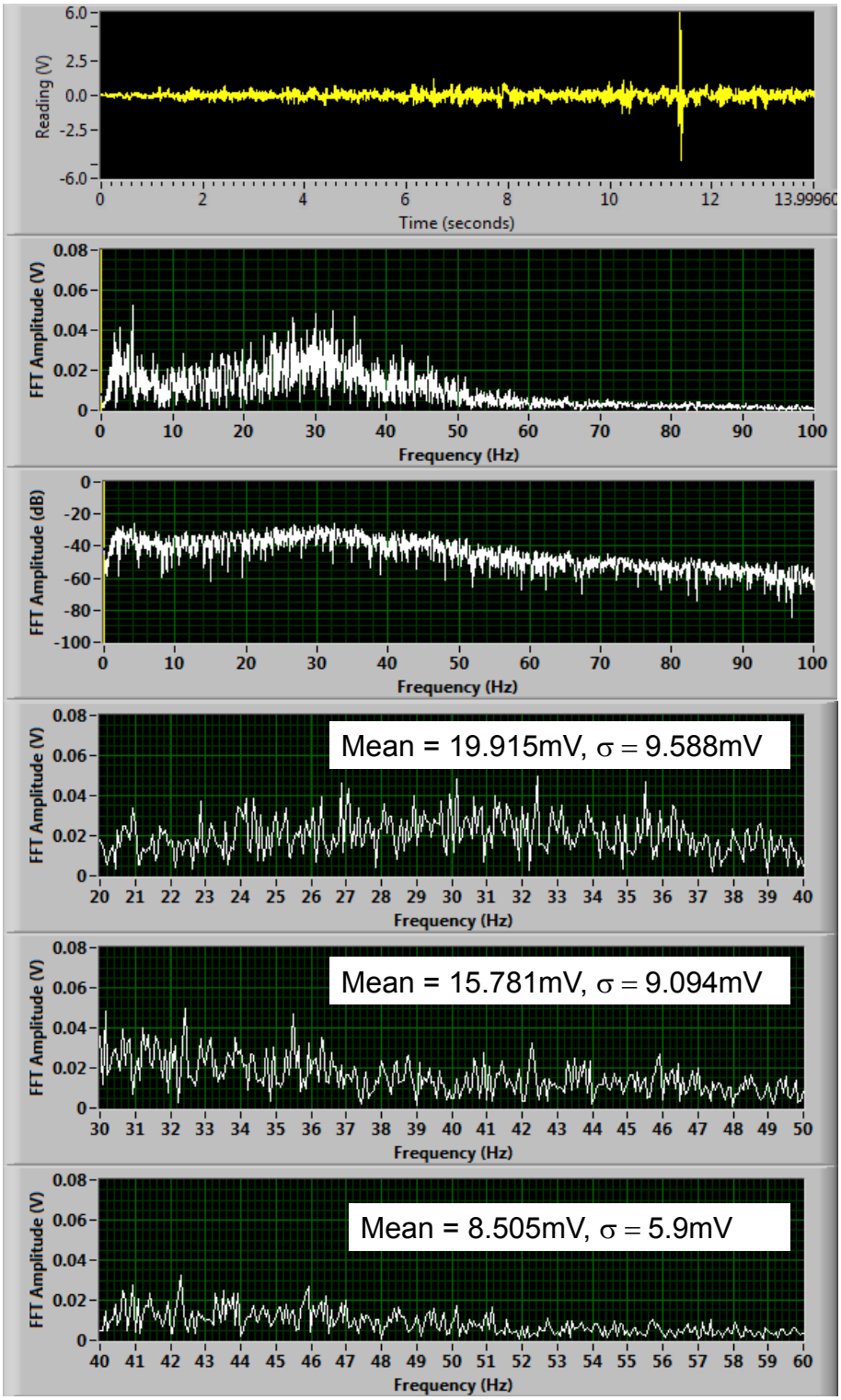

Figure A.26: SC with 40 lb Hold-Down Weight at 5 mph

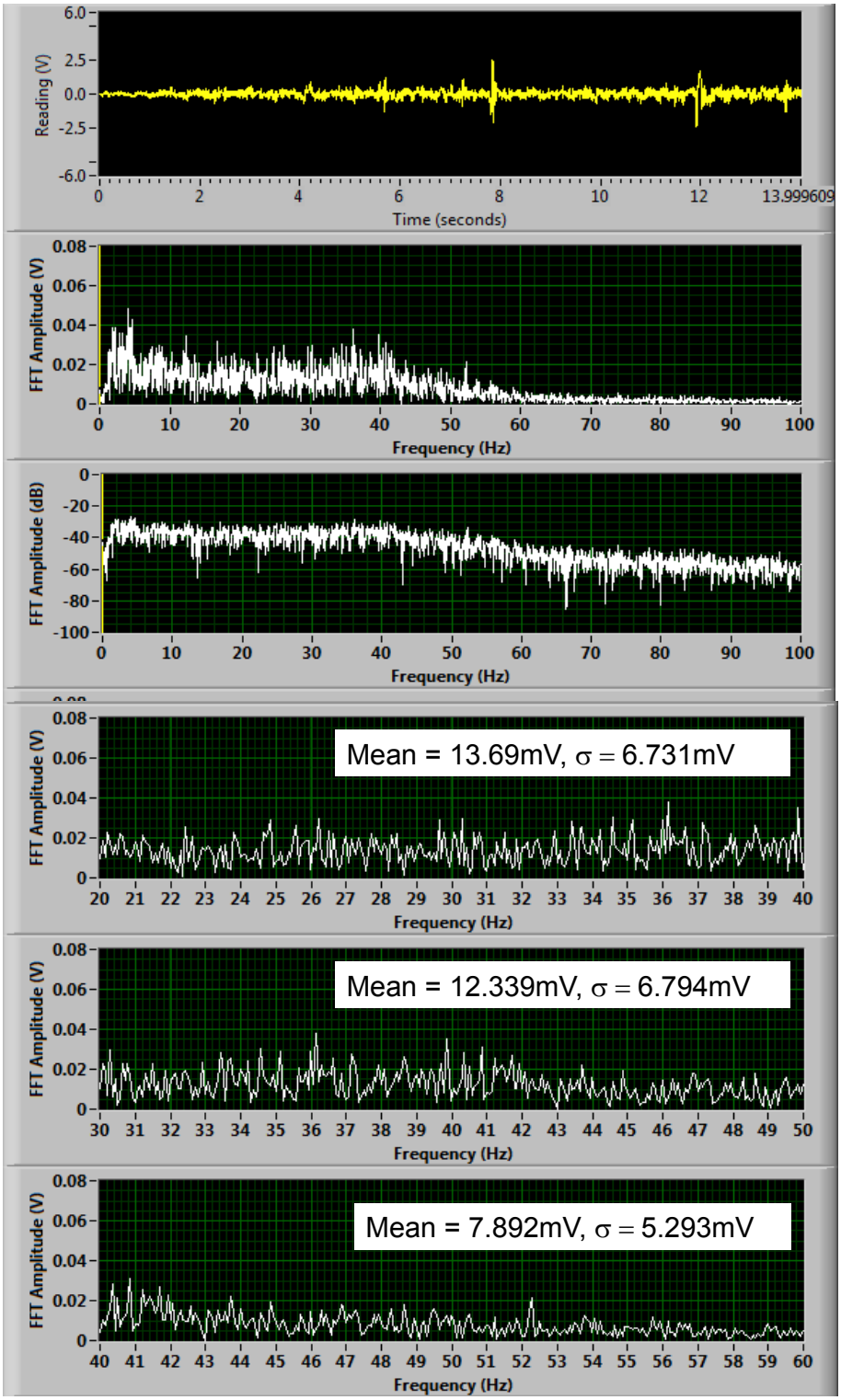

Figure A.27: SC with 90 lb Hold-Down Weight at 5 mph

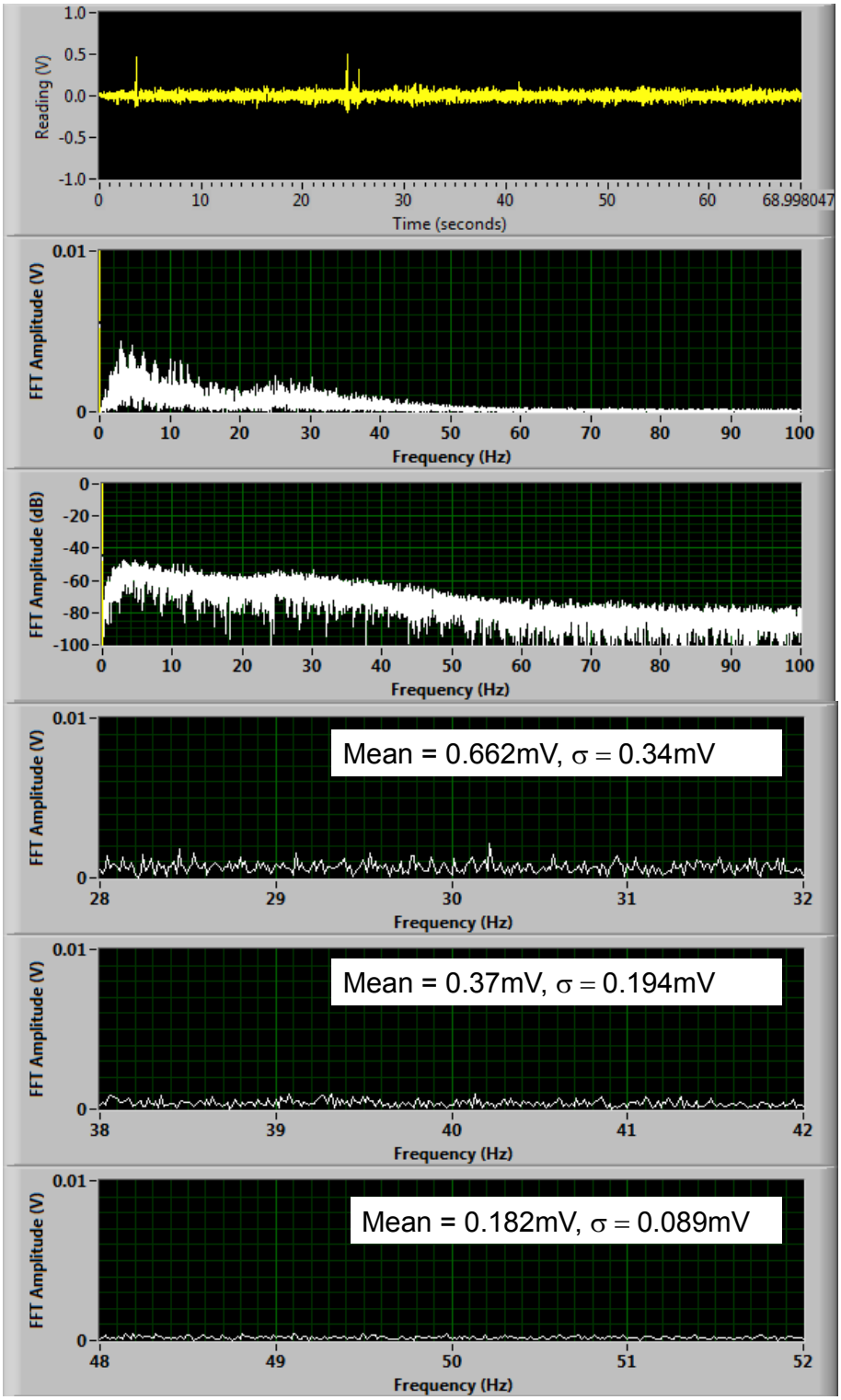

Figure A.28: SD with 20 lb Hold-Down Weight at 1 mph

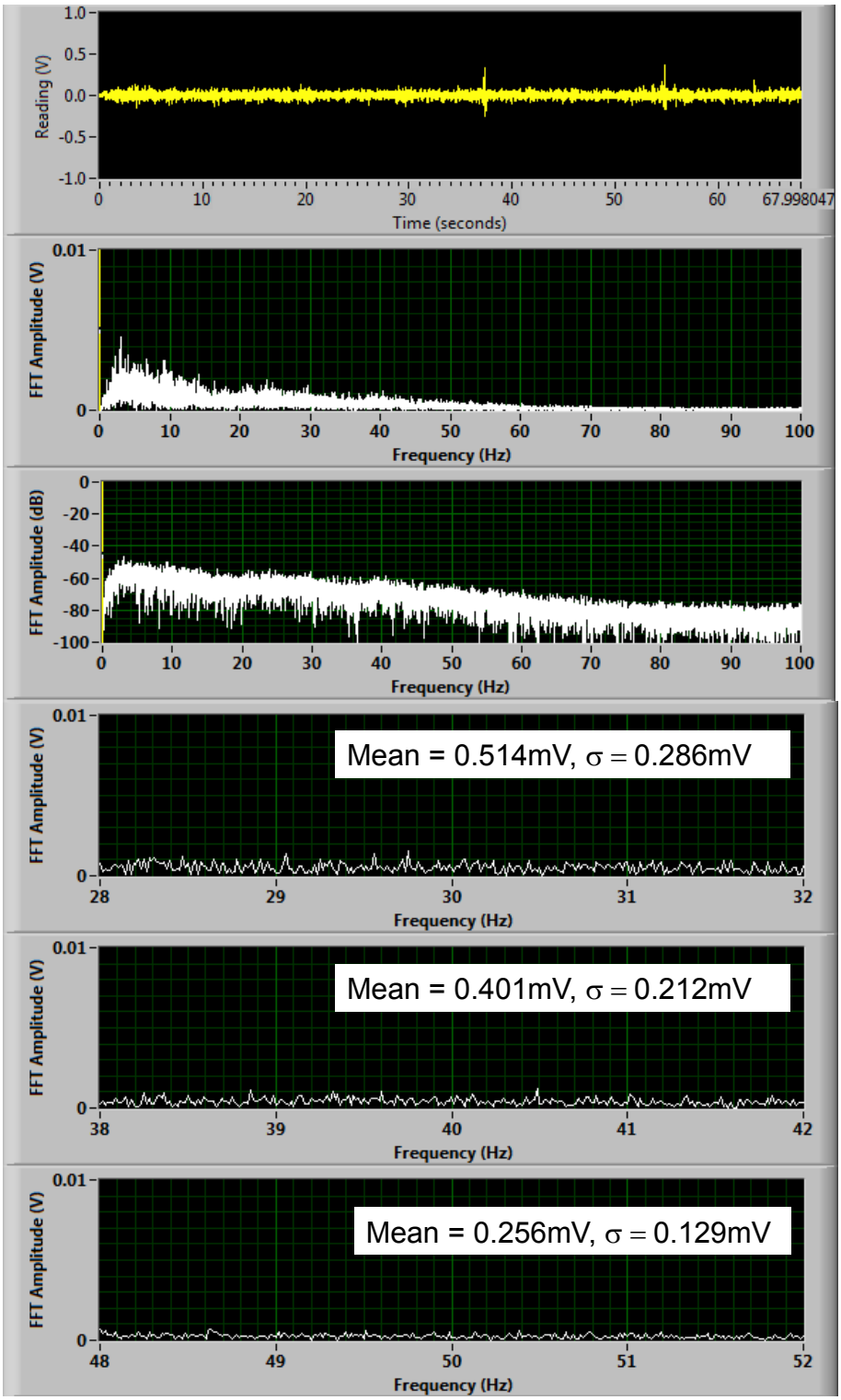

Figure A.29: SD with 40 lb Hold-Down Weight at 1 mph

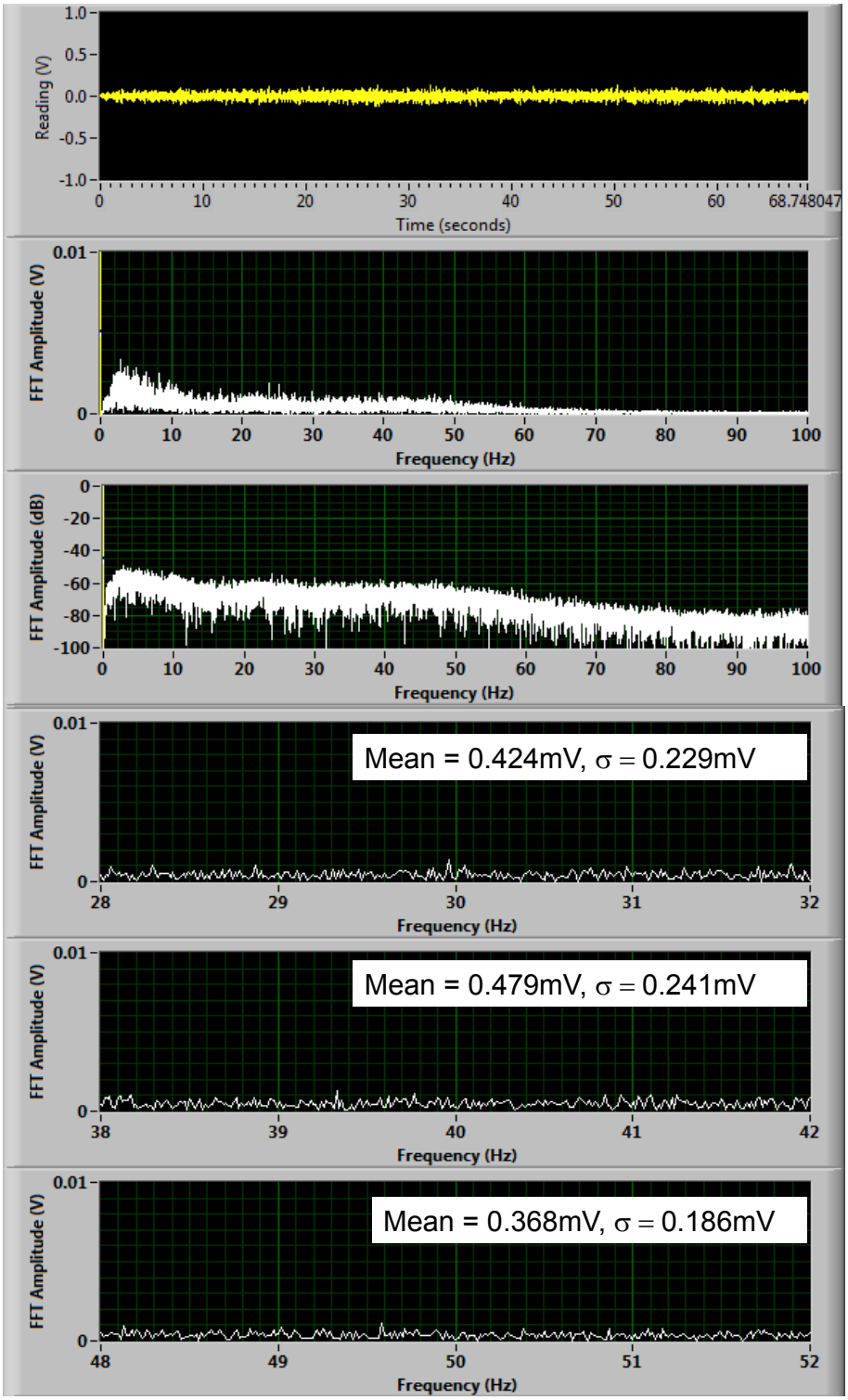

Figure A.30: SD with 90 lb Hold-Down Weight at 1 mph

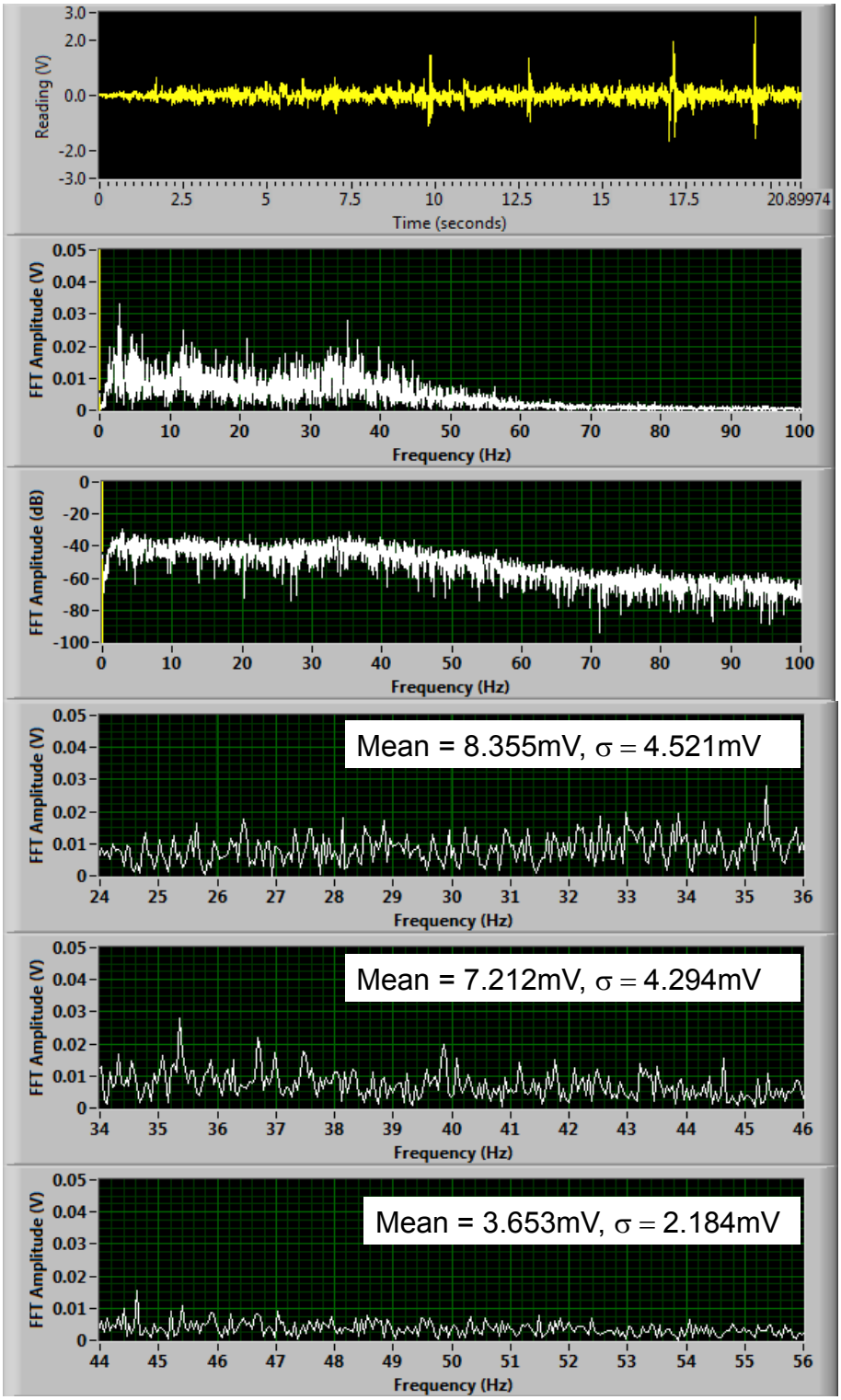

Figure A.31: SD with 20 lb Hold-Down Weight at 3 mph

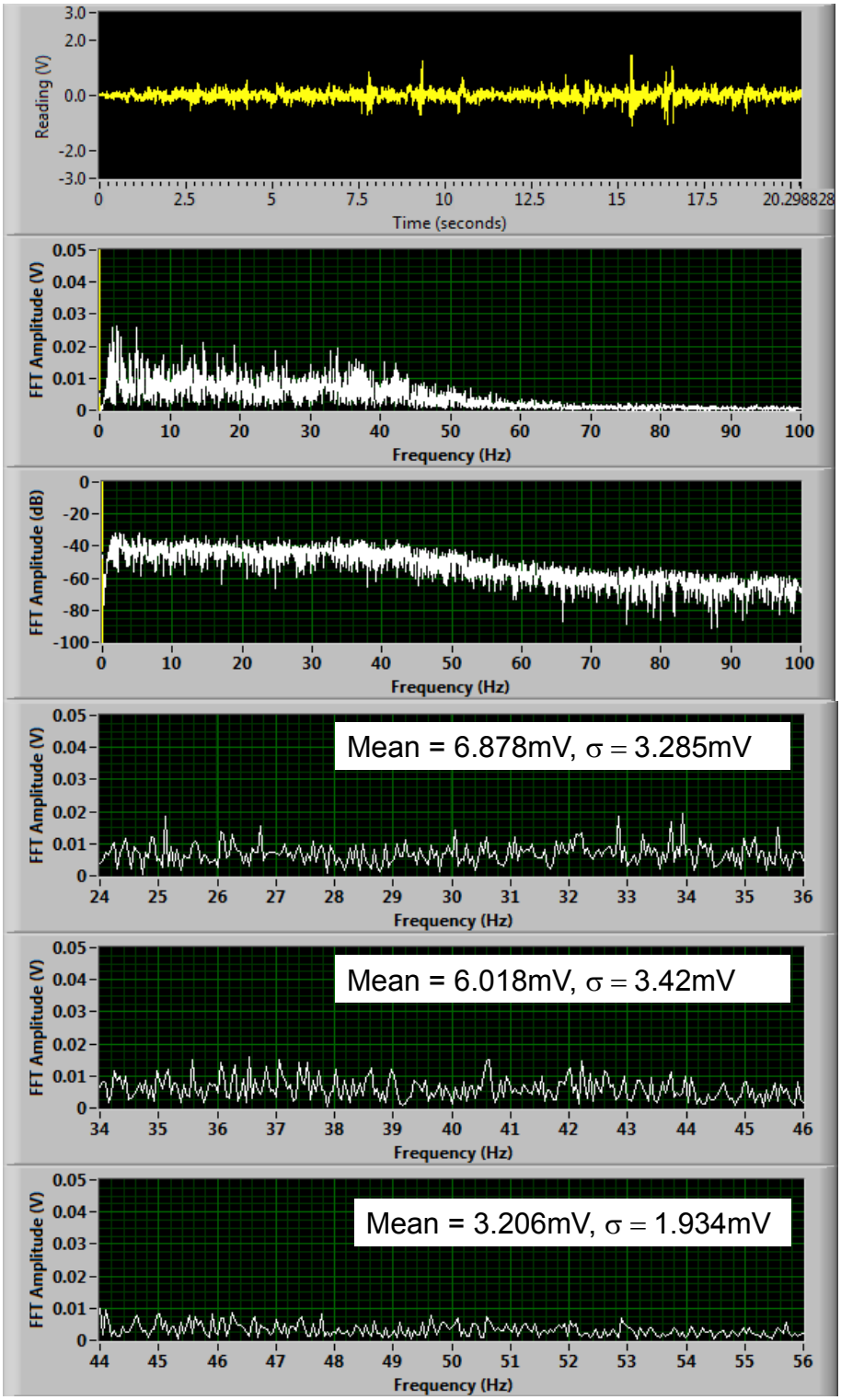

Figure A.32: SD with 40 lb Hold-Down Weight at 3 mph

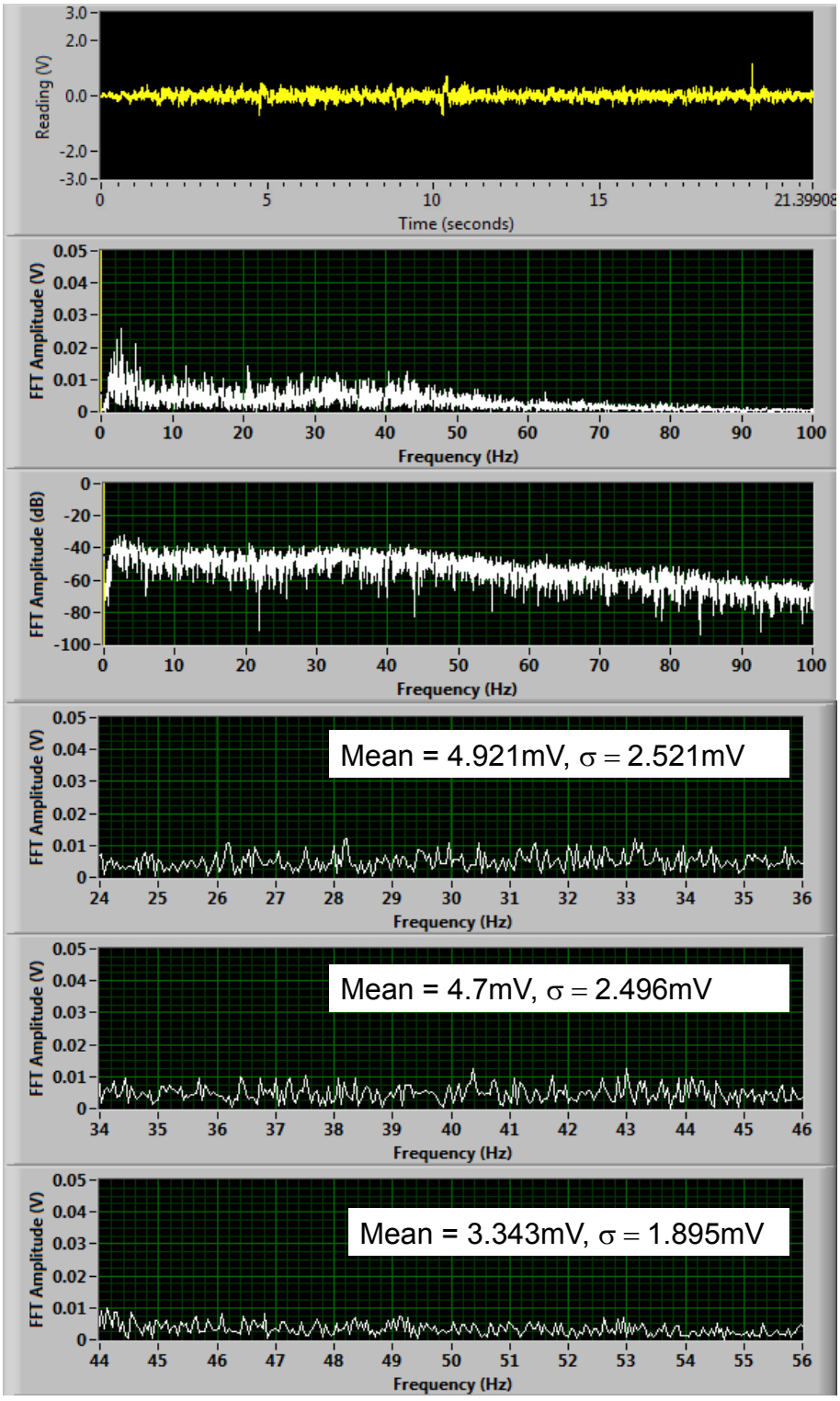

Figure A.33: SD with 90 lb Hold-Down Weight at 3 mph

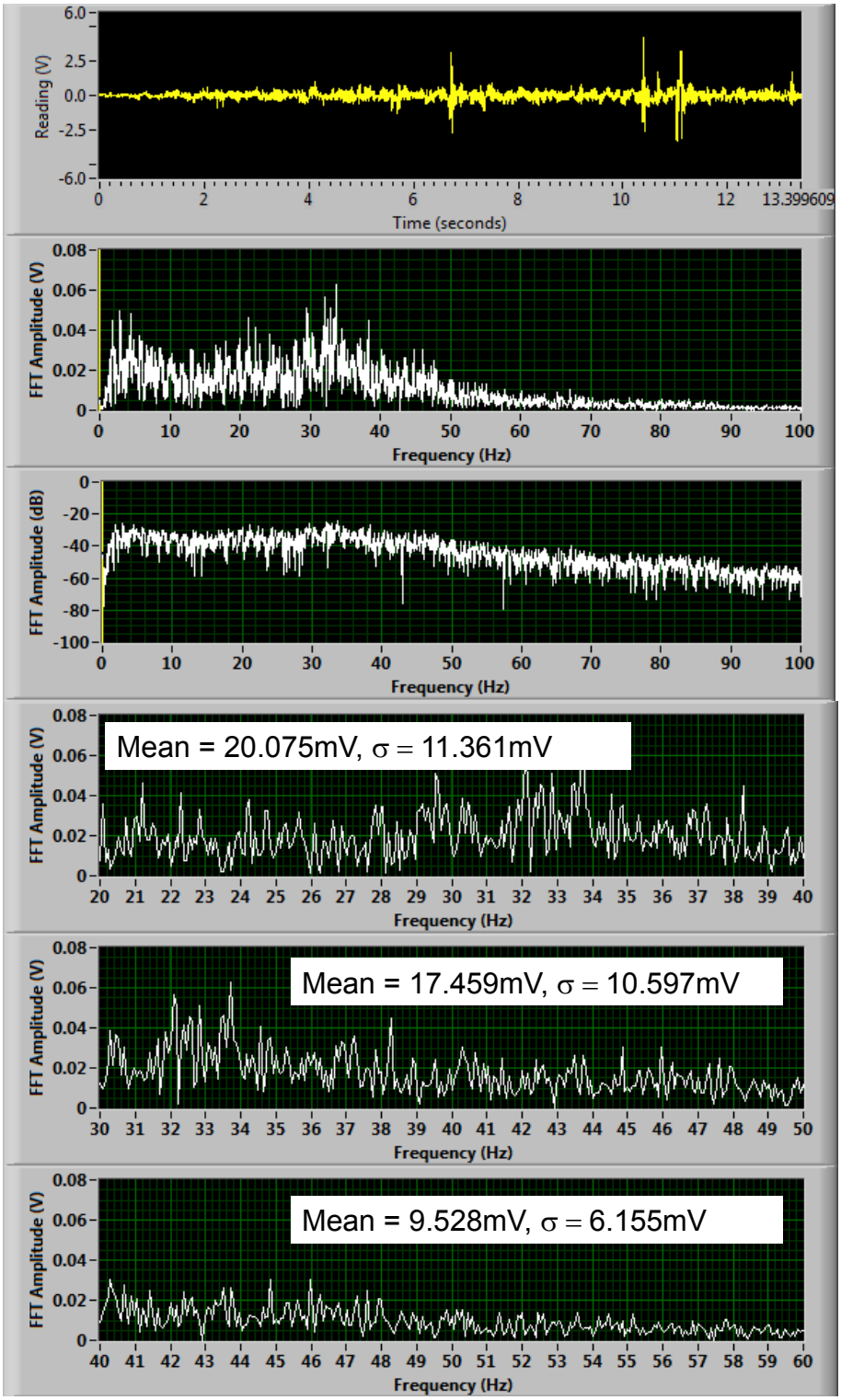

Figure A.34: SD with 20 lb Hold-Down Weight at 5 mph

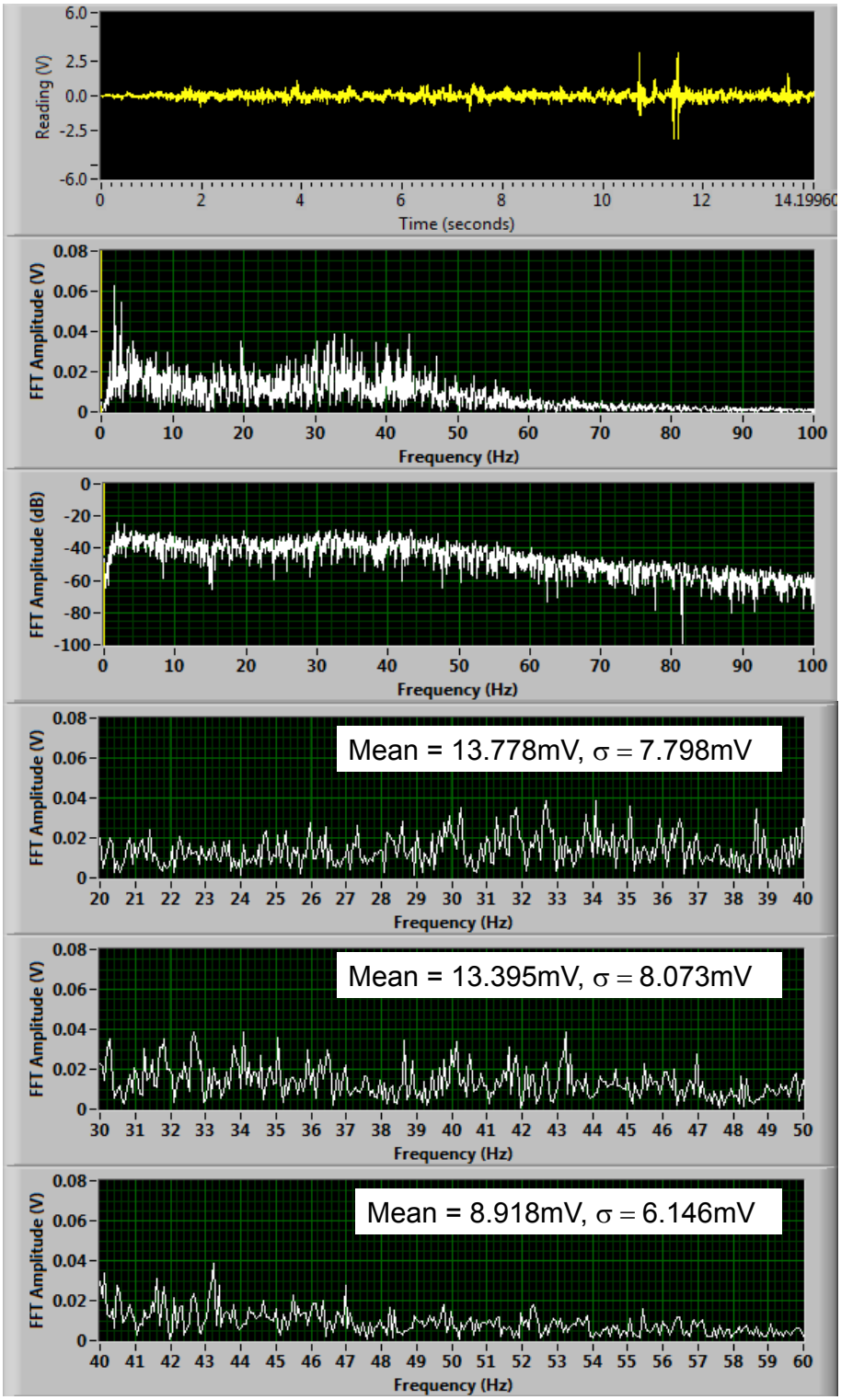

Figure A.35: SD with 40 lb Hold-Down Weight at 5 mph

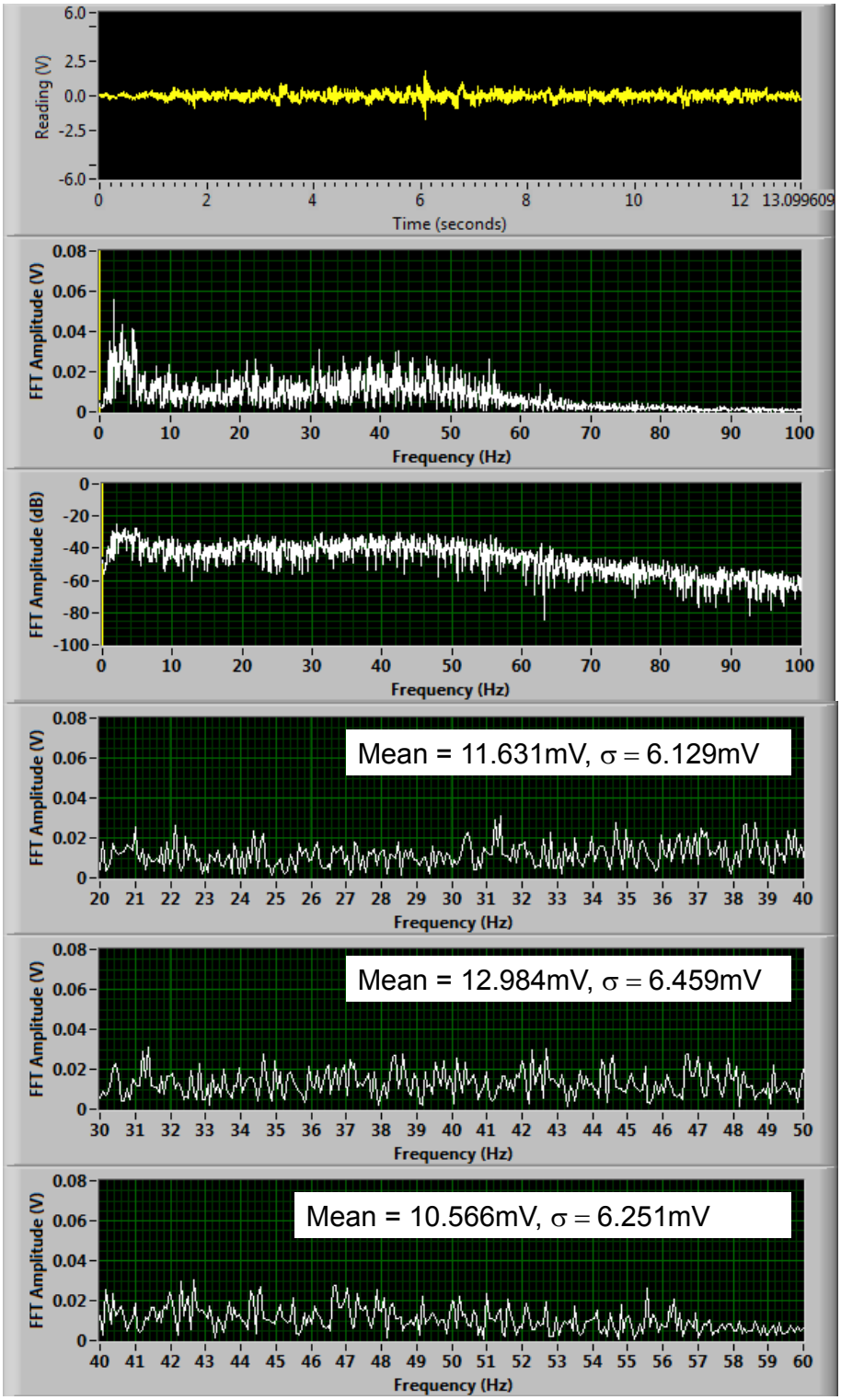

Figure A.36: SD with 90 lb Hold-Down Weight at 5 mph

Appendix B: TPAD Measurements at TxDOT FSF

Data recorded on March 18, 2011

B.1 Introduction

Appendix B consists of five sections that are identical except for the speed at which TPAD testing was conducted. Testing speeds at which raw and processed data were collected during TPAD operations are 0.5, 1, 2, 3, and 4 mph and the data are presented in Sections B.2, B.3, B.4, B.5, and B.6, respectively. Each section contains processed signals, which are typical data reduced to terms of standard civil engineering parameters, such as applied load or deflection used in RDD deflection evaluations, and raw signals, which are recorded data, typically in terms of voltages, during the testing and then processed for the deflection evaluations. The raw and processed data in each section are (1) applied static and dynamic loads, (2) output from rolling sensor #1, and (3) output from the DMI. The raw signals were requested during the project meeting on April 19, 2011 so that they could be reviewed before any processing.

As an example of the contents of each section, Section B.2 is outlined hereafter. The first two figures in Section B.2.1 are processed load signals of applied static and dynamic forces along the total length of the FSF testbed (653 ft). The next three figures in Section B.2.2.1 are raw signals of the combined static and dynamic forces collected over the 653-ft long testbed: (1) first in the time domain, (2) next in the frequency domain with a linear scale, and (3) finally in the frequency domain with a decibel scale. Next, the 653-ft long testbed is divided into two parts based on the surface concrete slab thicknesses: 16-in. thick slabs that form a 200-ft long section and 8- and 10-in. thick slabs that form a 453-ft long section. The signals of each part in the time domain and in the frequency domain with linear and decibel scales are shown in Sections B.2.2.2 and B.2.2.3, respectively.

After the applied force signals, processed and raw signals of the output from rolling sensor #1 are shown. Rolling sensor #1 signals are also shown in the same manner as the force signals. First, a processed signal of the rolling sensor #1 along the total 653-ft long testbed is shown in Section B.2.3. The raw signals over 653-ft long FSF testbed (Section B.2.4.1), on 16-in. thick slabs (Section B.2.4.2) and on 8- and 10-in. thick slabs (Section B.2.4.3) are shown in the time and frequency domains. For the raw signals from rolling sensor #1, Signal-to-Noise Ratio (SNR) is also shown in the frequency domain with a decibel scale in Sections B.2.4.1, B.2.4.2, and B.2.4.3.

Finally, processed and raw signals of the output from DMI are shown. The processed signal of the DMI is shown in Section B.2.5 and the raw signals are shown in Section B.2.6.1, B.2.6.2, and B.2.6.3.

An outline of B.2 through B.6 is presented below in Section B.1.1.

B.1.1. Outline of Sections B.2, B.3, B.4, B.5, and B.6

B.2. TPAD TESTING SPEED at 0.5 MPH
B.2.1. PROCESSED LOAD SIGNALS (Applied Static and Dynamic Forces)
B.2.1.1. Static force (Fstat) along the total distance
B.2.1.2. Peak-to-peak dynamic force (Fdyn) along the total distance
B.2.2. RAW LOAD SIGNAL
B.2.2.1. Complete record for 653-ft long testbed
B.2.2.2. on 16-in. thick slabs
B.2.2.3. on 8- and 10-in. thick slabs
B.2.3 PROCESSED ROLLING SENSOR #1 SIGNAL (DEFLECTION PROFILE)
B.2.4. RAW ROLLING SENSOR #1 SIGNAL
B.2.4.1. Complete record for 653-ft long testbed
B.2.4.2. on 16-in. thick slabs
B.2.4.3. on 8- and 10-in. thick slabs
B.2.5. PROCESSED DMI SIGNAL
B.2.6. RAW DMI SIGNAL
B.2.6.1 Complete record for 653-ft long testbed
B.2.6.2. 5-second interval signal (from 100 to 105 second) on 16-in. thick slabs
B.2.6.3. 5-second interval signal (from 343 to 348 second) on 8- and 10-in. thick slabs

B.3. TPAD TESTING SPEED at 1 MPH
B.3.1. PROCESSED LOAD SIGNALS (Applied Static and Dynamic Forces)
B.3.1.1. Static force (Fstat) along the total distance
B.3.1.2. Peak-to-peak dynamic force (Fdyn) along the total distance
B.3.2. RAW LOAD SIGNAL
B.3.2.1. Complete record for 653-ft long testbed
B.3.2.2. on 16-in. thick slabs
B.3.2.3. on 8- and 10-in. thick slabs
B.3.3 PROCESSED ROLLING SENSOR #1 SIGNAL (DEFLECTION PROFILE)
B.3.4. RAW ROLLING SENSOR #1 SIGNAL
B.3.4.1. Complete record for 653-ft long testbed
B.3.4.2. on 16-in. thick slabs
B.3.4.3. on 8- and 10-in. thick slabs
B.3.5. PROCESSED DMI SIGNAL
B.3.6. RAW DMI SIGNAL
B.3.6.1 Complete record for 653-ft long testbed
B.3.6.2. 5-second interval signal (from 60 to 65 second) on 16-in. thick slabs
B.3.6.3. 5-second interval signal (from 255 to 260 second) on 8- and 10-in. thick slabs

B.4. TPAD TESTING SPEED at 2 MPH
B.4.1. PROCESSED LOAD SIGNALS (Applied Static and Dynamic Forces)
B.4.1.1. Static force (Fstat) along the total distance
B.4.1.2. Peak-to-peak dynamic force (Fdyn) along the total distance
B.4.2. RAW LOAD SIGNAL
B.4.2.1. Complete record for 653-ft long testbed
B.4.2.2. on 16-in. thick slabs
B.4.2.3. on 8- and 10-in. thick slabs
B.4.3 PROCESSED ROLLING SENSOR #1 SIGNAL (DEFLECTION PROFILE)
B.4.4. RAW ROLLING SENSOR #1 SIGNAL
B.4.4.1. Complete record for 653-ft long testbed

B.4.4.2. on 16-in. thick slabs
B.4.4.3. on 8- and 10-in. thick slabs
B.4.5. PROCESSED DMI SIGNAL
B.4.6. RAW DMI SIGNAL
B.4.6.1 Complete record for 653-ft long testbed
B.4.6.2. 2.5-second interval signal (from 20 to 22.5 second) on 16-in. thick slabs
B.4.6.3. 2.5-second interval signal (from 85 to 87.5 second) on 8- and 10-in. thick slabs

B.5. TPAD TESTING SPEED at 3 MPH
B.5.1. PROCESSED LOAD SIGNALS (Applied Static and Dynamic Forces)
B.5.1.1. Static force (Fstat) along the total distance
B.5.1.2. Peak-to-peak dynamic force (Fdyn) along the total distance
B.5.2. RAW LOAD SIGNAL
B.5.2.1. Complete record for 653-ft long testbed
B.5.2.2. on 16-in. thick slabs
B.5.2.3. on 8- and 10-in. thick slabs
B.5.3 PROCESSED ROLLING SENSOR #1 SIGNAL (DEFLECTION PROFILE)
B.5.4. RAW ROLLING SENSOR #1 SIGNAL
B.5.4.1. Complete record for 653-ft long testbed
B.5.4.2. on 16-in. thick slabs
B.5.4.3. on 8- and 10-in. thick slabs
B.5.5. PROCESSED DMI SIGNAL
B.5.6. RAW DMI SIGNAL
B.5.6.1 Complete record for 653-ft long testbed
B.5.6.2. 2-second interval signal (from 20 to 22 second) on 16-in. thick slabs
B.5.6.3. 2-second interval signal (from 70 to 72 second) on 8- and 10-in. thick slabs

B.6. TPAD TESTING SPEED at 4 MPH
B.6.1. PROCESSED LOAD SIGNALS (Applied Static and Dynamic Forces)
B.6.1.1. Static force (Fstat) along the total distance
B.6.1.2. Peak-to-peak dynamic force (Fdyn) along the total distance
B.6.2. RAW LOAD SIGNAL
B.6.2.1. Complete record for 653-ft long testbed
B.6.2.2. on 16-in. thick slabs
B.6.2.3. on 8- and 10-in. thick slabs
B.6.3 PROCESSED ROLLING SENSOR #1 SIGNAL (DEFLECTION PROFILE)
B.6.4. RAW ROLLING SENSOR #1 SIGNAL
B.6.4.1. Complete record for 653-ft long testbed
B.6.4.2. on 16-in. thick slabs
B.6.4.3. on 8- and 10-in. thick slabs
B.6.5. PROCESSED DMI SIGNAL
B.6.6. RAW DMI SIGNAL
B.6.6.1 Complete record for 653-ft long testbed
B.6.6.2. 2-second interval signal (from 18 to 20 second) on 16-in. thick slabs
B.6.6.3. 2-second interval signal (from 126 to 128 second) on 8- and 10-in. thick slabs

B.2. TPAD TESTING SPEED at 0.5 MPH

B.2.1. PROCESSED LOAD SIGNALS (Applied Static and Dynamic Forces)

B.2.1.1. Static force (Fstat) along the total distance

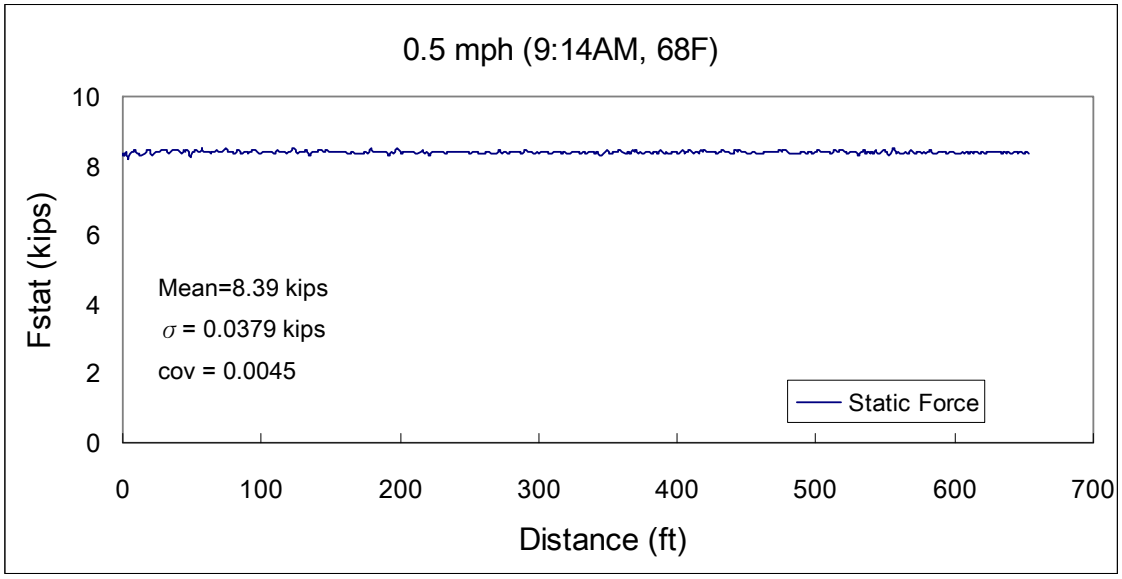

Figure B.1: Processed Static Force Signal with 0.5 mph

B.2.1.2. Peak-to-peak dynamic force (Fdyn) along the total distance

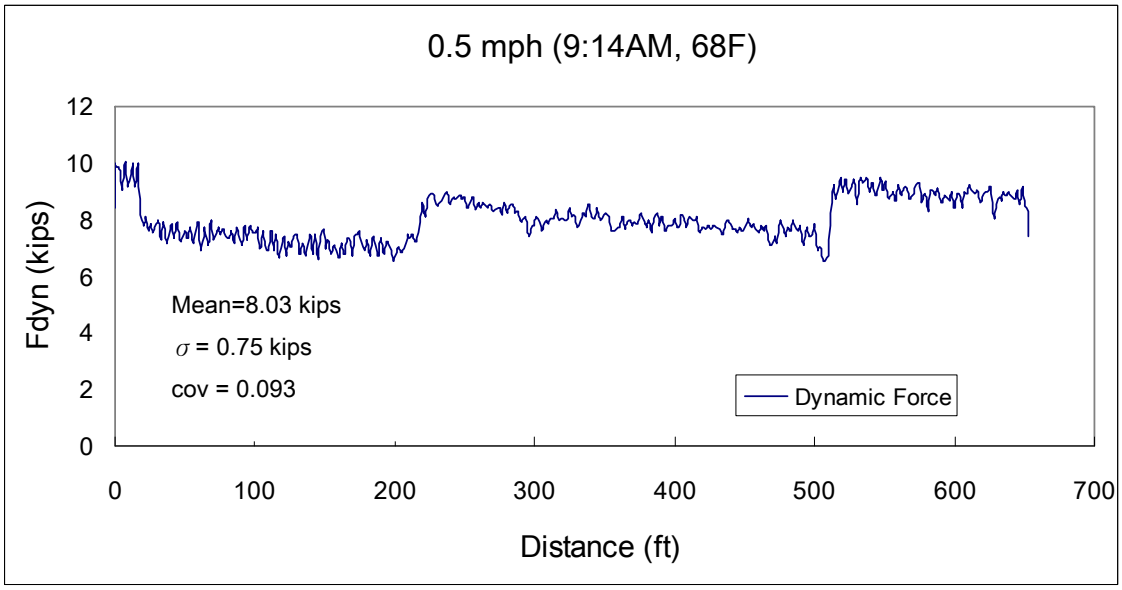

Figure B.2: Processed Peak-to-Peak Dynamic Force Signal with 0.5 mph

B.2.2. RAW LOAD SIGNAL

B.2.2.1. Complete record for 653-ft long testbed

Time domain signal of static and dynamic forces (the number of data point = 456,192)

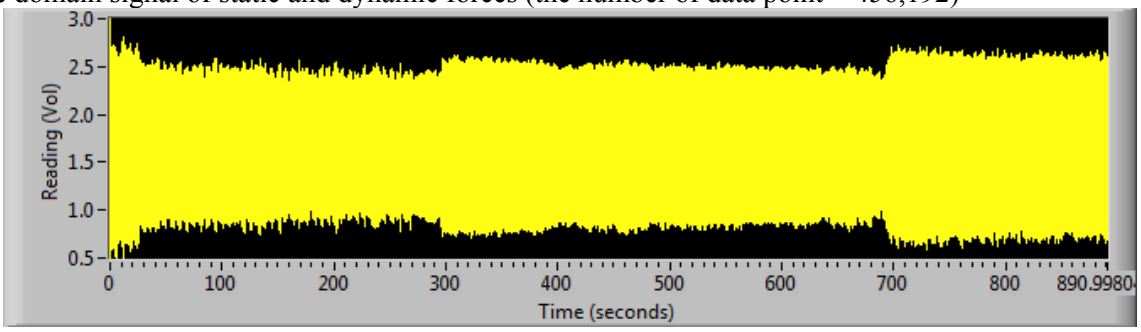

Figure B.3: Time Domain Signal of Raw Data for Combined Static and Dynamic Forces with 0.5 mph along Whole Testbed Length

Frequency domain signal (linear scale)

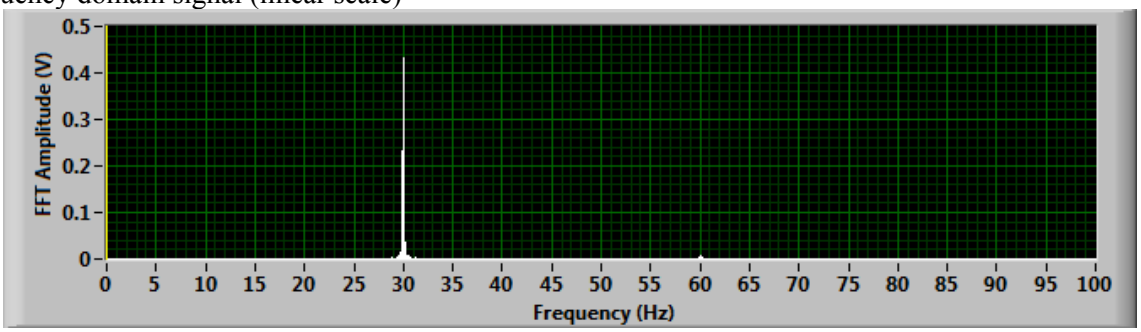

Figure B.4: Frequency Domain Signal (Linear Scale) of Raw Data for Combined Static and Dynamic Forces with 0.5 mph along Whole Testbed Length

Frequency domain signal (dB scale)

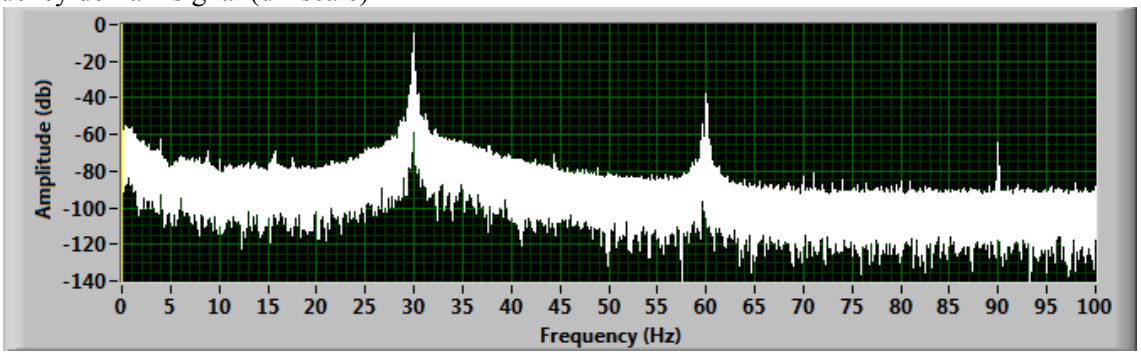

Figure B.5: Frequency Domain Signal (Decibel Scale) of Raw Data for Combined Static and Dynamic Forces with 0.5 mph along Whole Testbed Length

B.2.2.2. on 16-in. thick slabs

Time domain signal of static and dynamic forces (the number of data point = 137,984)

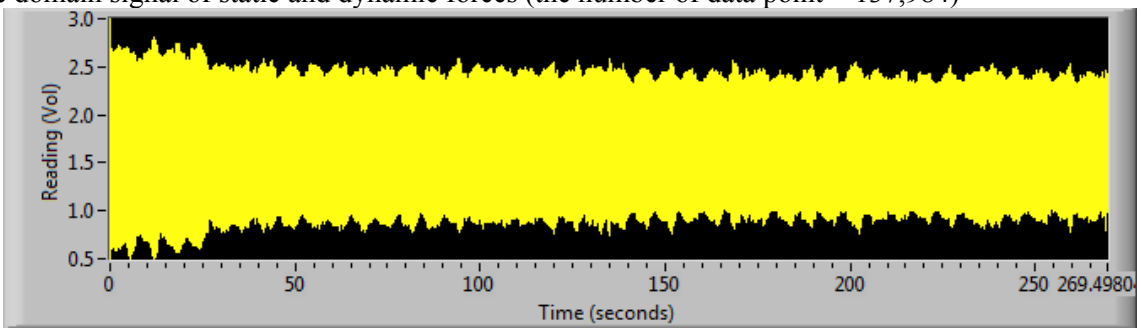

Figure B.6: Time Domain Signal of Raw Data for Combined Static and Dynamic Forces with 0.5 mph along 16-in. Thick Slab Section

Frequency domain signal (linear scale)

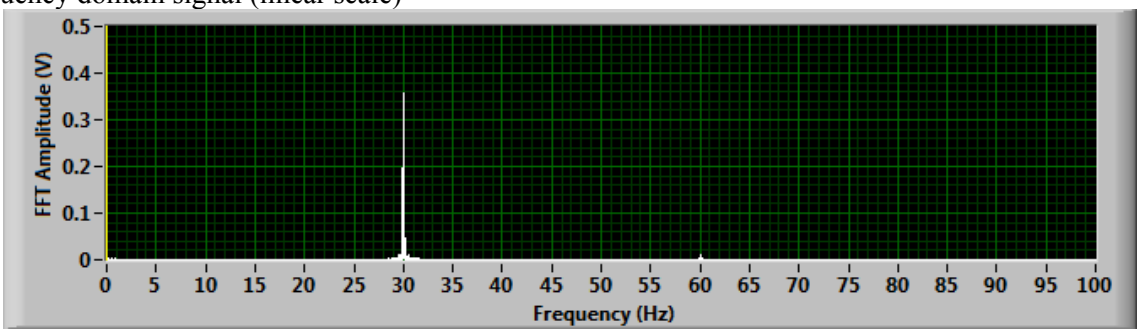

Figure B.7: Frequency Domain Signal (Linear Scale) of Raw Data for Combined Static and Dynamic Forces with 0.5 mph along 16-in. Thick Slab Section

Frequency domain signal (dB scale)

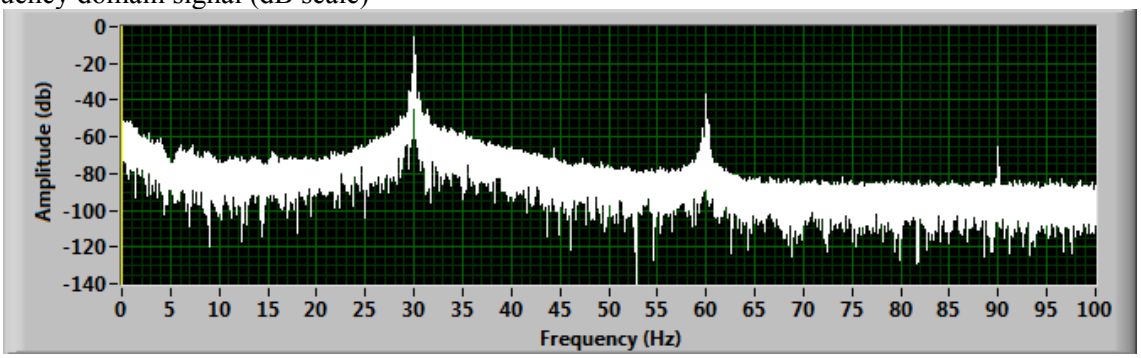

Figure B.8: Frequency Domain Signal (Decibel Scale) of Raw Data for Combined Static and Dynamic Forces with 0.5 mph along 16-in. Thick Slab Section

B.2.2.3. on 8- and 10-in. thick slabs

Time domain signal of static and dynamic forces (the number of data point = 318,208)

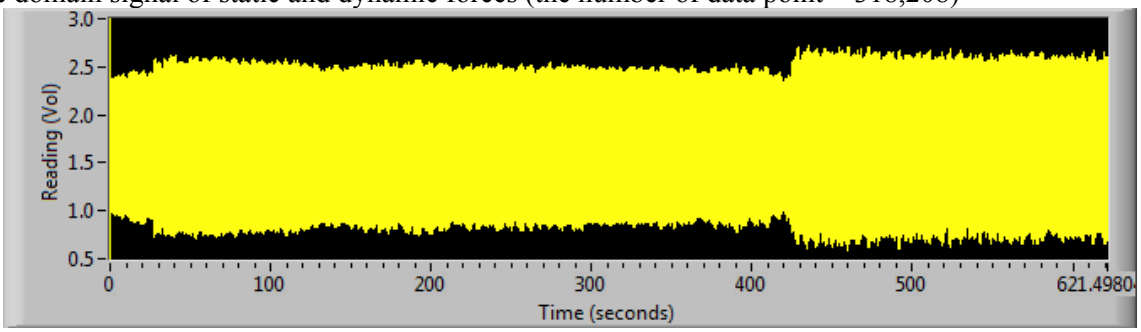

Figure B.9: Time Domain Signal of Raw Data for Combined Static and Dynamic Forces with 0.5 mph along 8- and 10-in. Thick Slab Section

Frequency domain (linear scale)

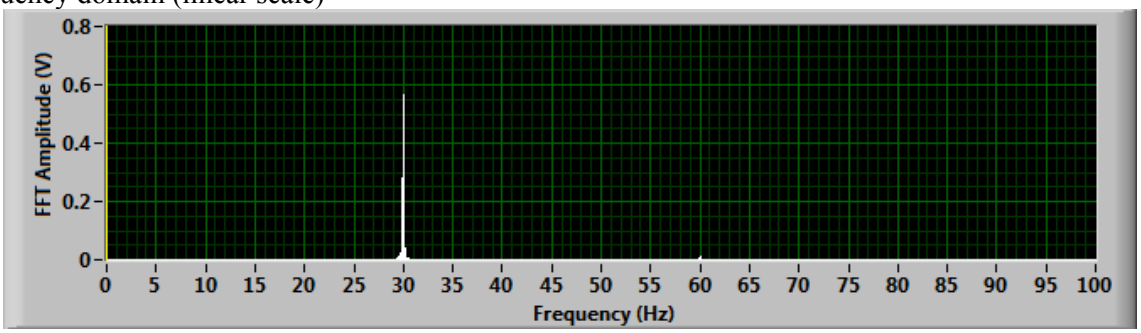

Figure B.10: Frequency Domain Signal (Linear Scale) of Raw Data for Combined Static and Dynamic Forces with 0.5 mph along 8- and 10-in. Thick Slab Section

Frequency domain (dB scale)

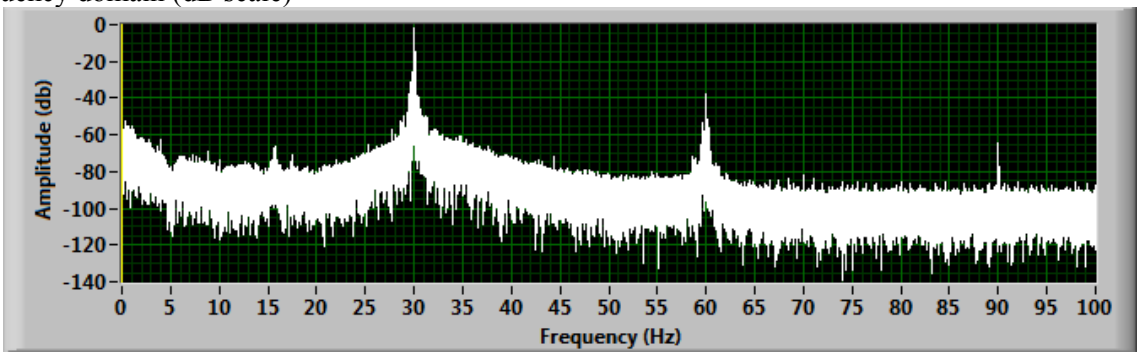

Figure B.11: Frequency Domain Signal (Decibel Scale) of Raw Data for Combined Static and Dynamic Forces with 0.5 mph along 8- and 10-in. Thick Slab Section

B.2.3 PROCESSED ROLLING SENSOR #1 SIGNAL (DEFLECTION PROFILE)

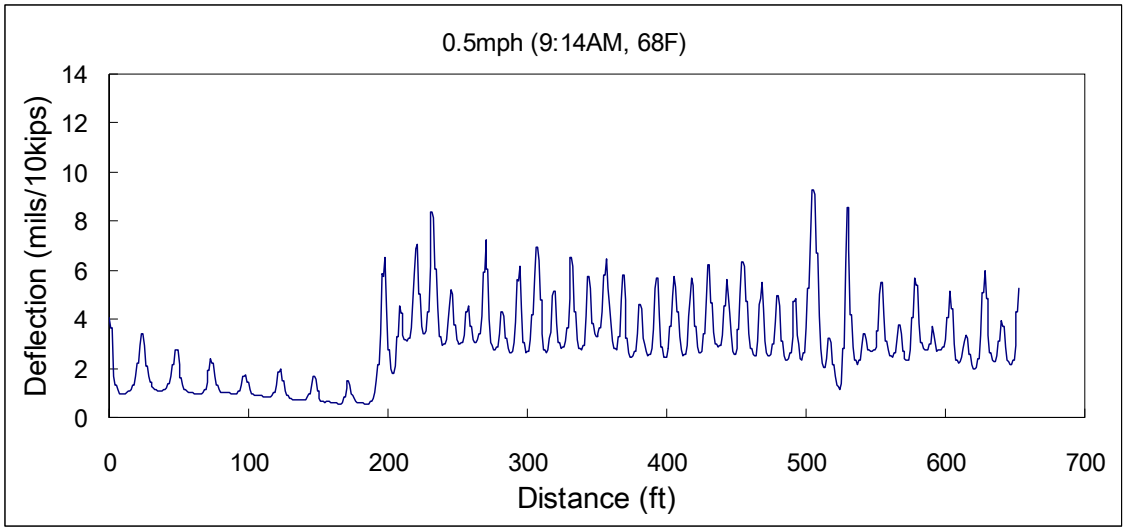

Figure B.12: Processed Rolling Sensor #1 Signal with 0.5 mph

B.2.4. RAW ROLLING SENSOR #1 SIGNAL

B.2.4.1. Complete record for 653-ft long testbed

Time domain signal (the number of data point = 456,192)

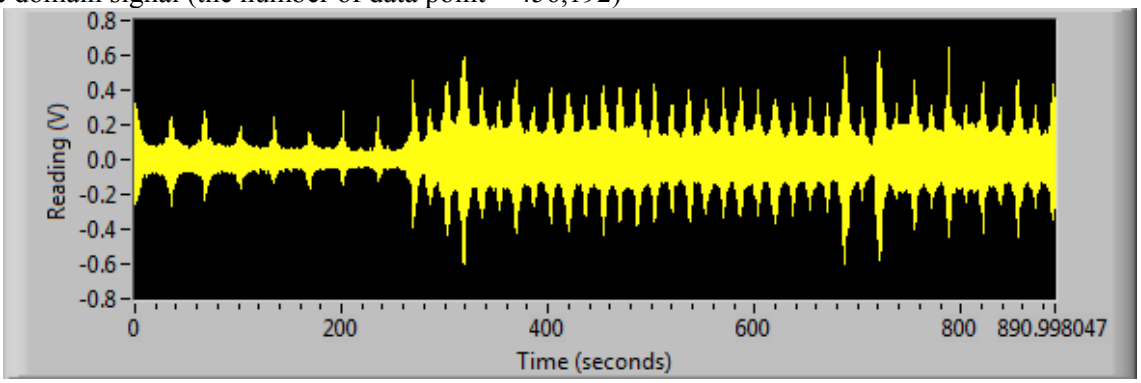

Figure B.13: Time Domain Signal of Raw Data for Rolling Sensor #1 with 0.5 mph along Whole Testbed Length

Frequency domain signal (linear scale)

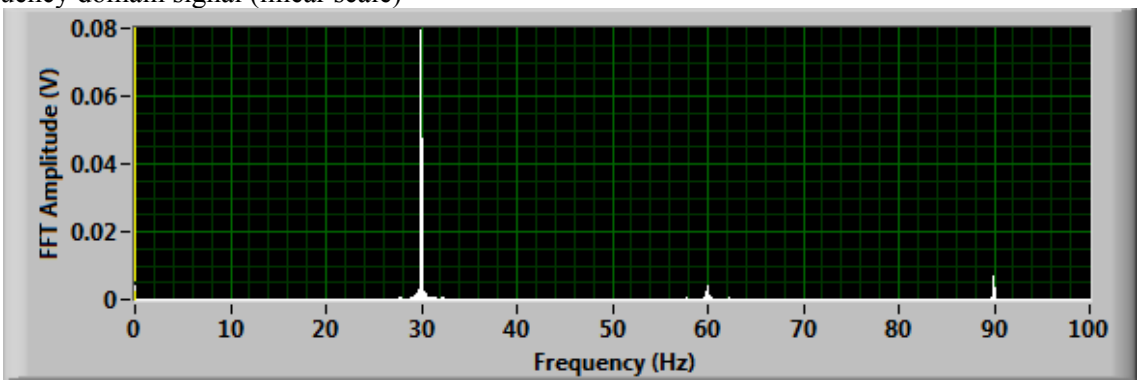

Figure B.14: Frequency Domain Signal (Linear Scale) of Raw Data for Rolling Sensor #1 with 0.5 mph along Whole Testbed Length

Frequency domain signal (dB scale)

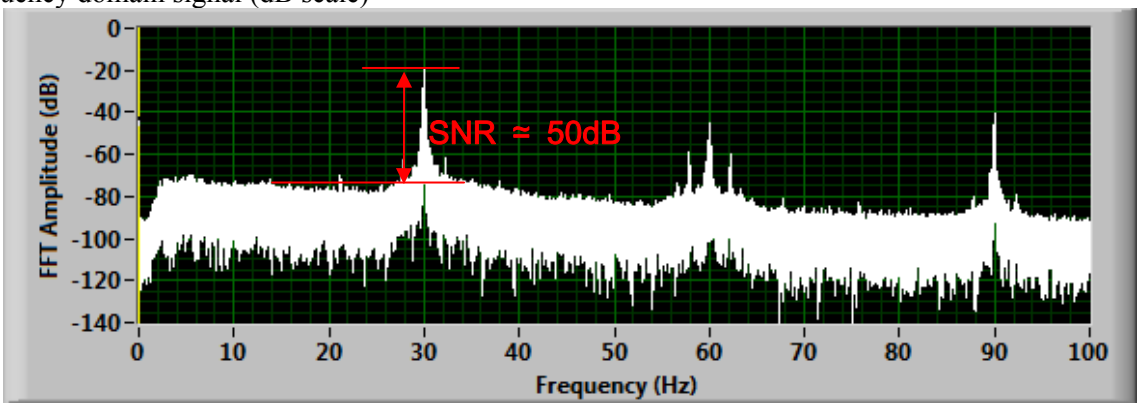

Figure B.15: Frequency Domain Signal (Decibel Scale) of Raw Data for Rolling Sensor #1 with 0.5 mph along Whole Testbed Length

B.2.4.2. on 16-in. thick slabs

Time domain signal (the number of data point = 137,984)

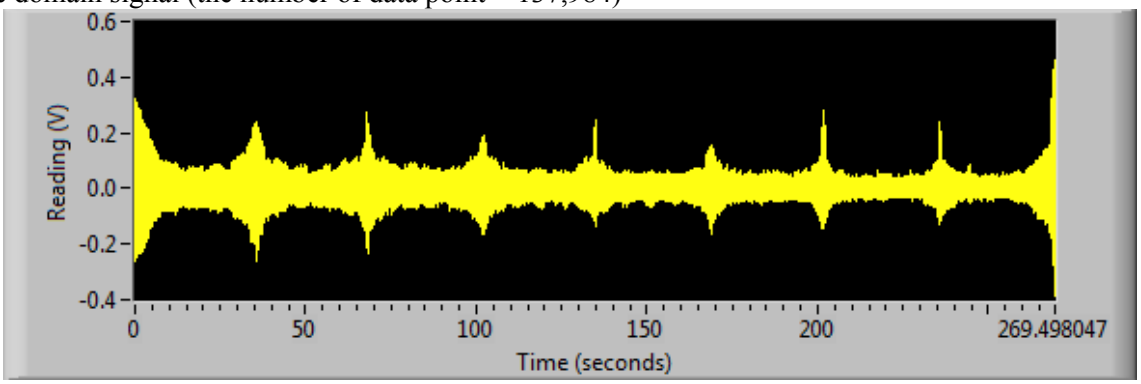

Figure B.16: Time Domain Signal of Raw Data for Rolling Sensor #1 with 0.5 mph along 16-in. Thick Slab Section

Frequency domain signal (linear scale)

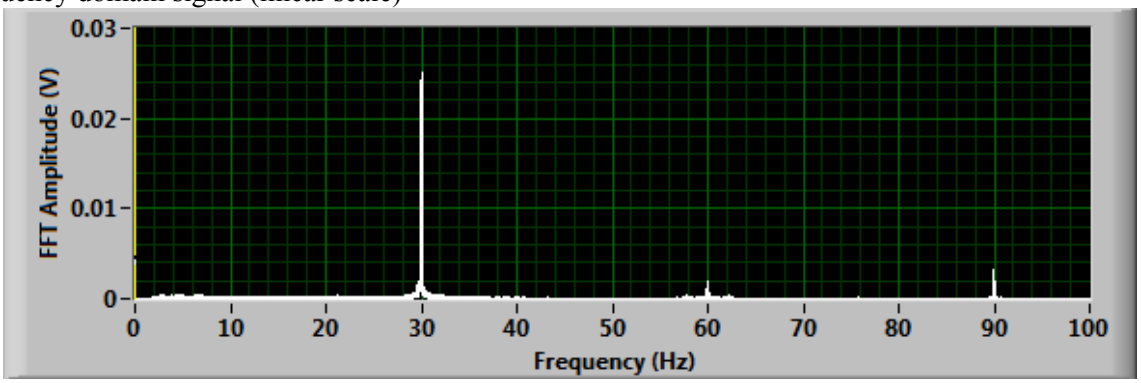

Figure B.17: Frequency Domain Signal (Linear Scale) of Raw Data for Rolling Sensor #1 with 0.5 mph along 16-in. Thick Slab Section

Frequency domain signal (dB scale)

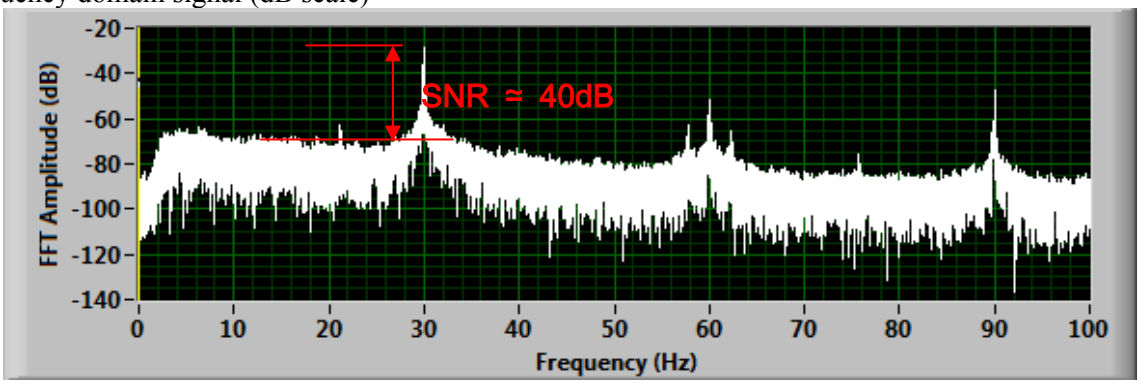

Figure B.18: Frequency Domain Signal (Decibel Scale) of Raw Data for Rolling Sensor #1 with 0.5 mph along 16-in. Thick Slab Section

B.2.4.3. on 8- and 10-in. thick slabs

Time domain signal (the number of data point = 318,208)

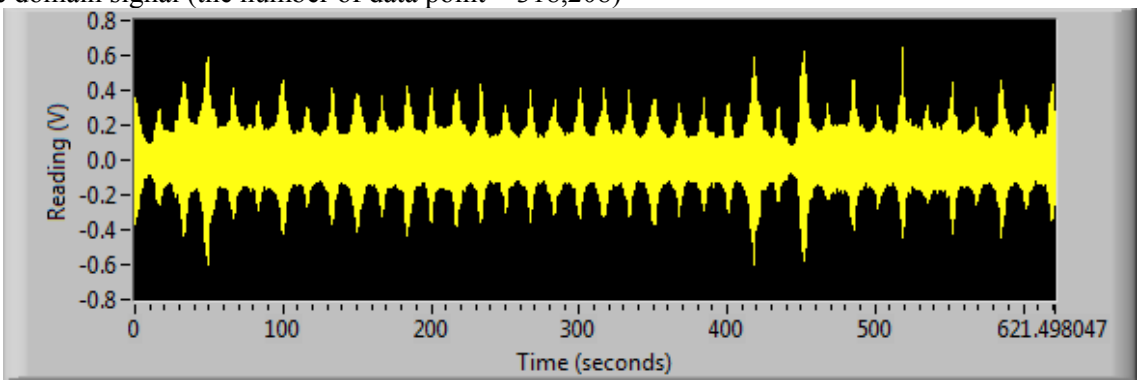

Figure B.19: Time Domain Signal of Raw Data for Rolling Sensor #1 with 0.5 mph along 8- and 10-in. Thick Slab Section

Frequency domain (linear scale)

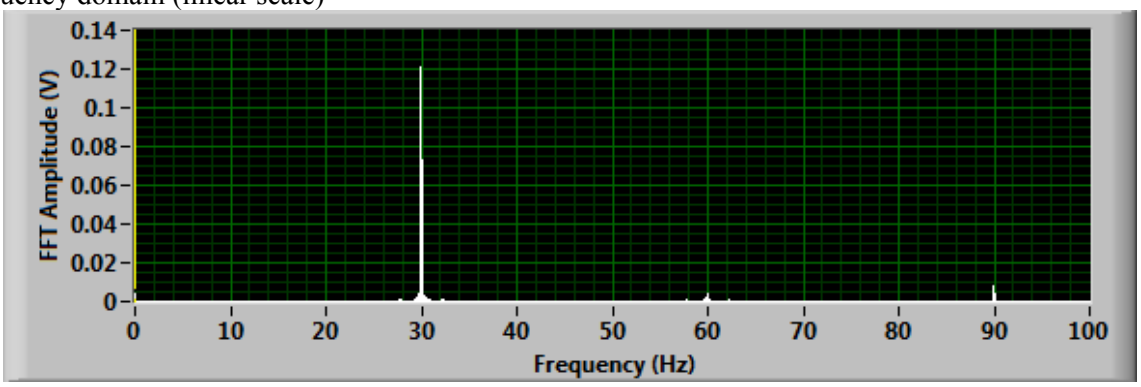

Figure B.20: Frequency Domain Signal (Linear Scale) of Raw Data for Rolling Sensor #1 with 0.5 mph along 8- and 10-in. Thick Slab Section

Frequency domain (dB scale)

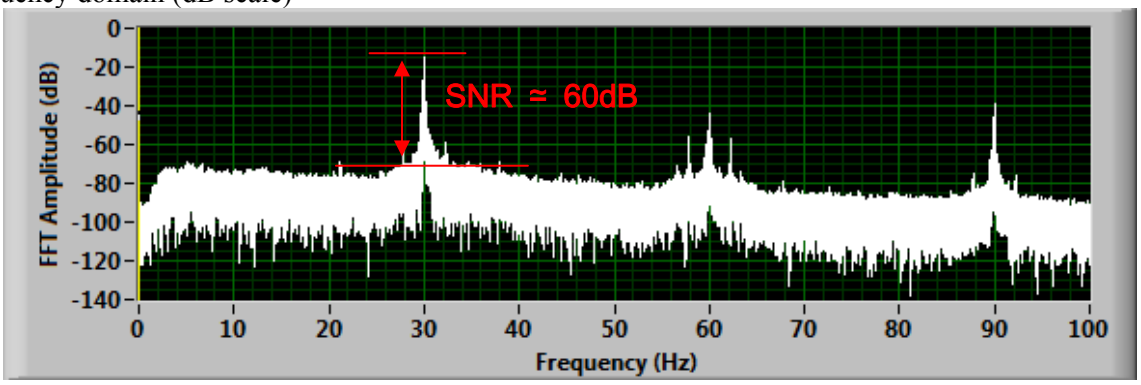

Figure B.21: Frequency Domain Signal (Decibel Scale) of Raw Data for Rolling Sensor #1 with 0.5 mph along 8- and 10-in. Thick Slab Section

B.2.5. PROCESSED DMI SIGNAL

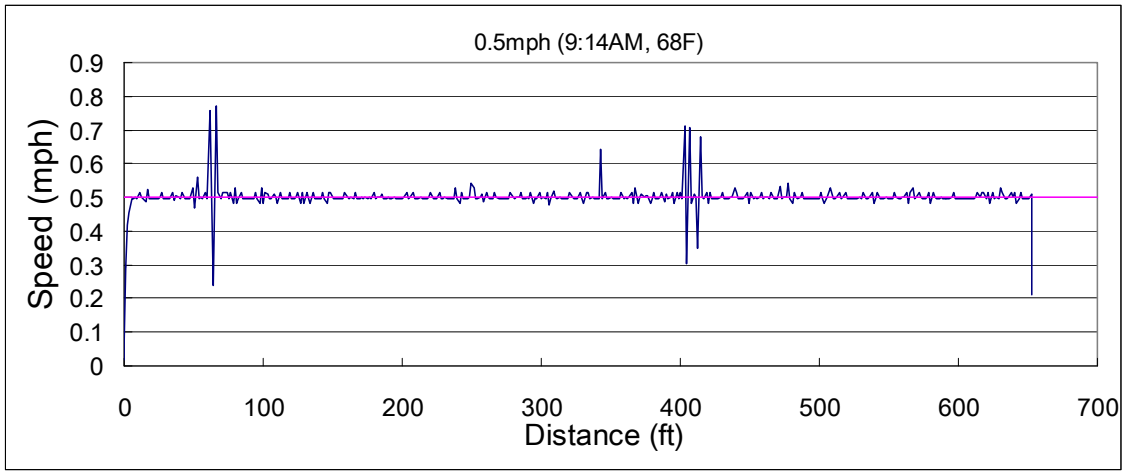

Figure B.22: Processed DMI Signal with 0.5 mph

B.2.6. RAW DMI SIGNAL

B.2.6.1 Complete record for 653-ft long testbed (the number of data point = 456,192)

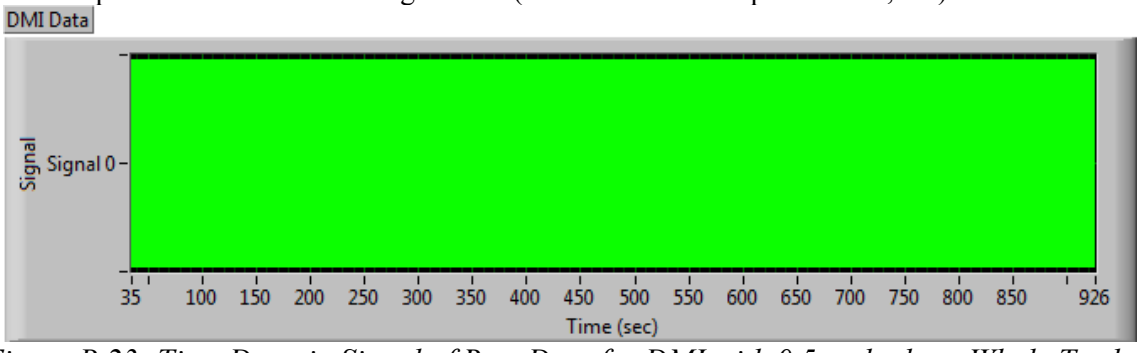

Figure B.23: Time Domain Signal of Raw Data for DMI with 0.5 mph along Whole Testbed Length

B.2.6.2. 5-second interval signal (from 100 to 105 second) on 16-in. thick slabs (the number of data point = 2,560)

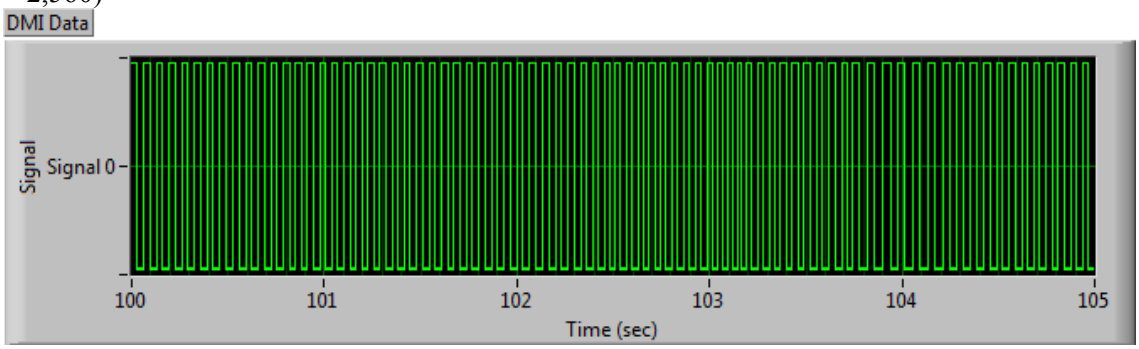

Figure B.24: Time Domain Signal of Raw Data for DMI with 0.5 mph along 16-in. Thick Slab Section

B.2.6.3. 5-second interval signal (from 343 to 348 second) on 8- and 10-in. thick slabs (the number of data point = 2,560)

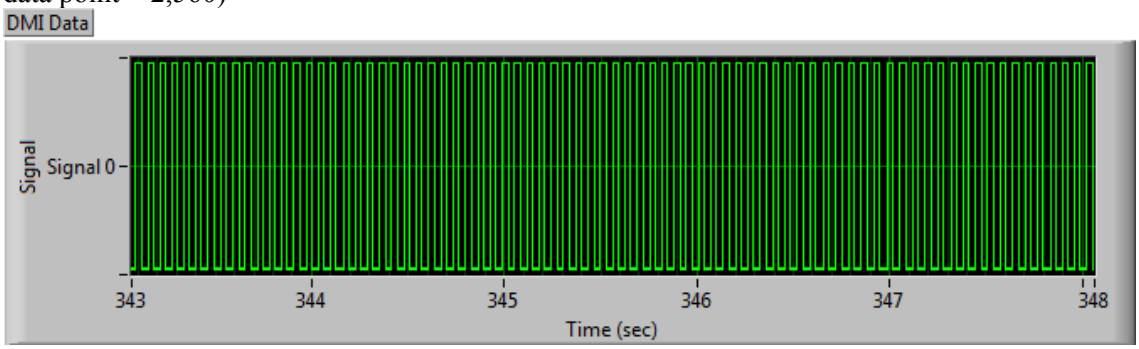

Figure B.25: Time Domain Signal of Raw Data for DMI with 0.5 mph along 8- and 10-in. Thick Slab Section

B.3 TPAD TESTING SPEED AT 1 MPH

B.3.1. PROCESSED LOAD SIGNALS (Applied Static and Dynamic Forces)

B.3.1.1. Static force (Fstat) along the total distance

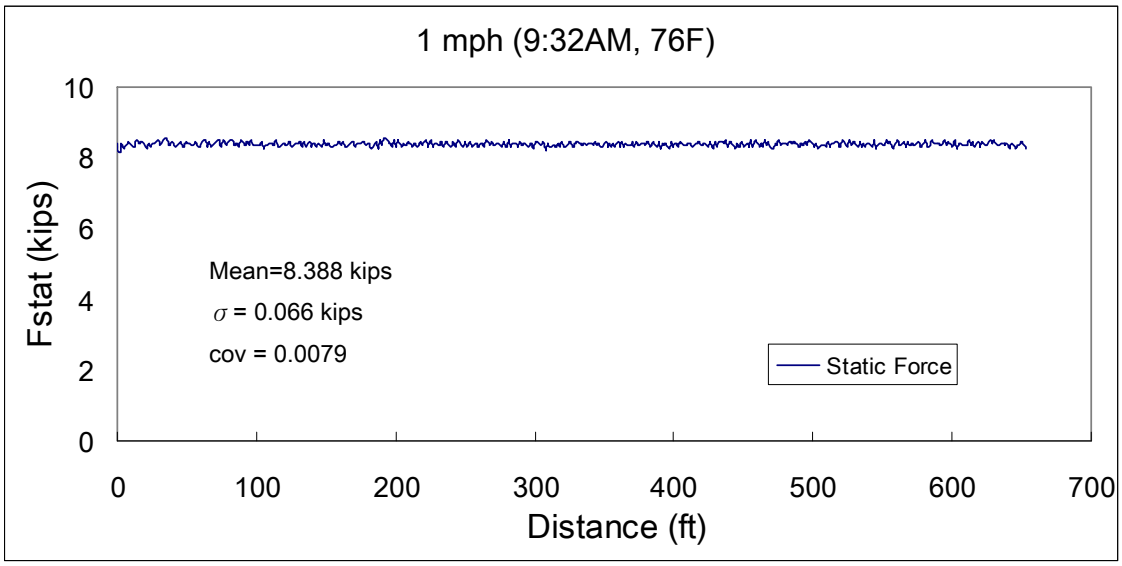

Figure B.26: Processed Static Force Signal with 1.0 mph

B.3.1.2. Peak-to-peak dynamic force (Fdyn) along the total distance

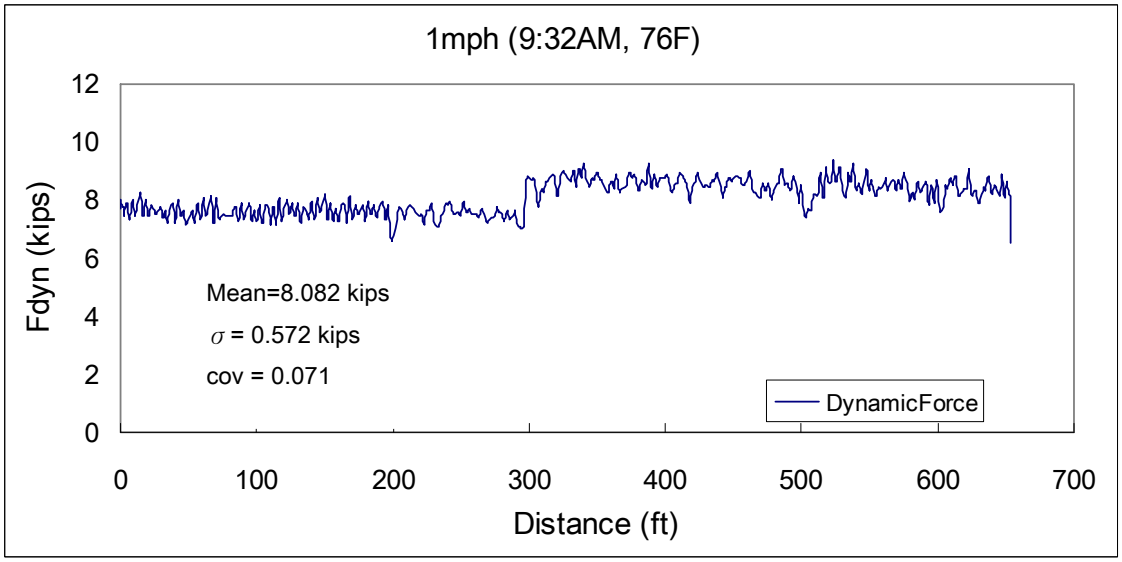

Figure B.27: Processed Peak-to-Peak Dynamic Force Signal with 1.0 mph

B.3.2. RAW LOAD SIGNAL

B.3.2.1. Complete record for 653-ft long testbed

Time domain signal of static and dynamic forces (the number of data point = 229,376)

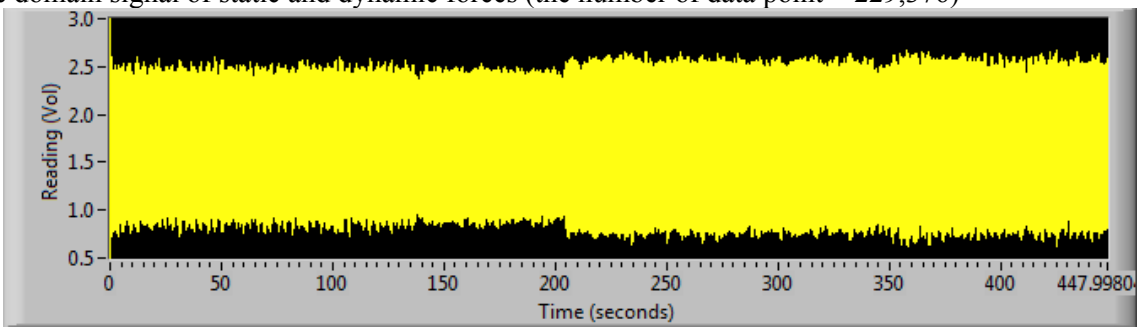

Figure B.28: Time Domain Signal of Raw Data for Combined Static and Dynamic Forces with 1.0 mph on Whole Testbed Length

Frequency domain signal (linear scale)

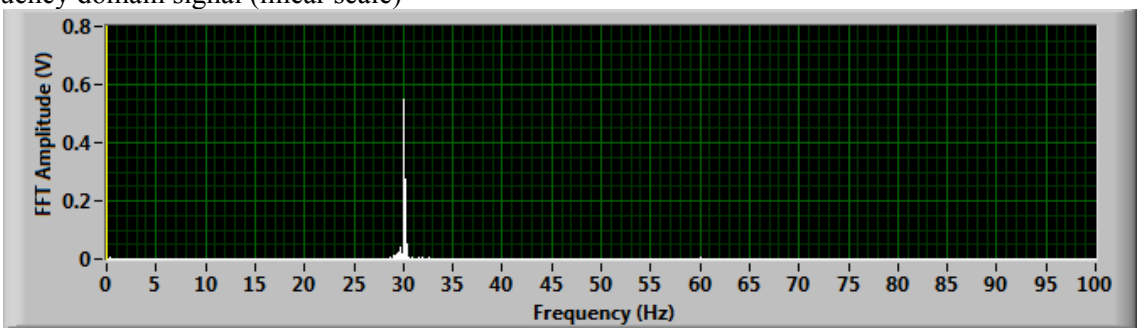

Figure B.29: Frequency Domain Signal (Linear Scale) of Raw Data for Combined Static and Dynamic Forces with 1.0 mph along Whole Testbed Length

Frequency domain signal (dB scale)

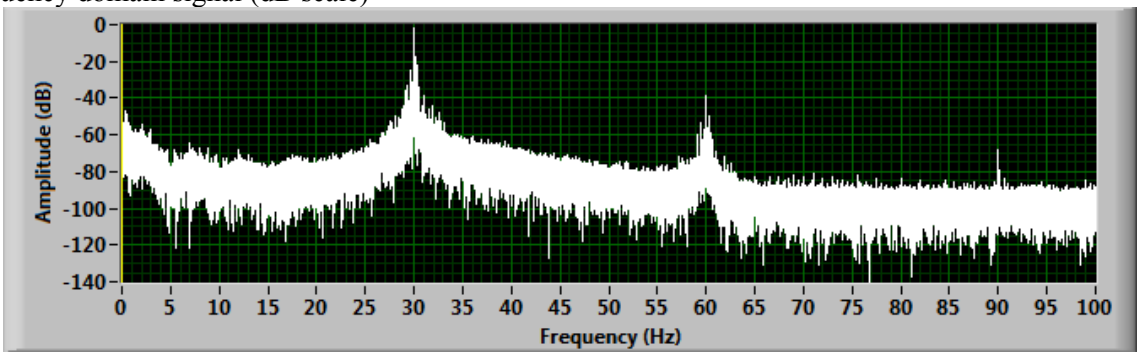

Figure B.30: Frequency Domain Signal (Decibel Scale) of Raw Data for Combined Static and Dynamic Forces with 1.0 mph along Whole Testbed Length

B.3.2.2. on 16-in. thick slabs

Time domain signal of static and dynamic forces (the number of data point = 70,144)

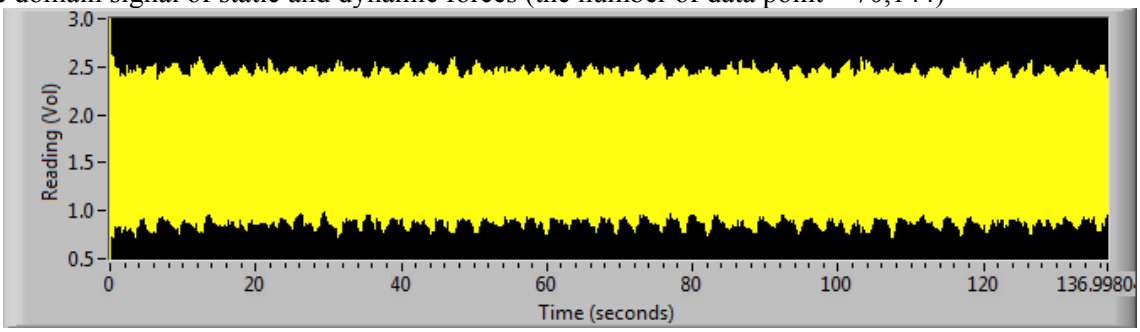

Figure B.31: Time Domain Signal of Raw Data for Combined Static and Dynamic Forces with 1.0 mph along 16-in. Thick Slab Section

Frequency domain signal (linear scale)

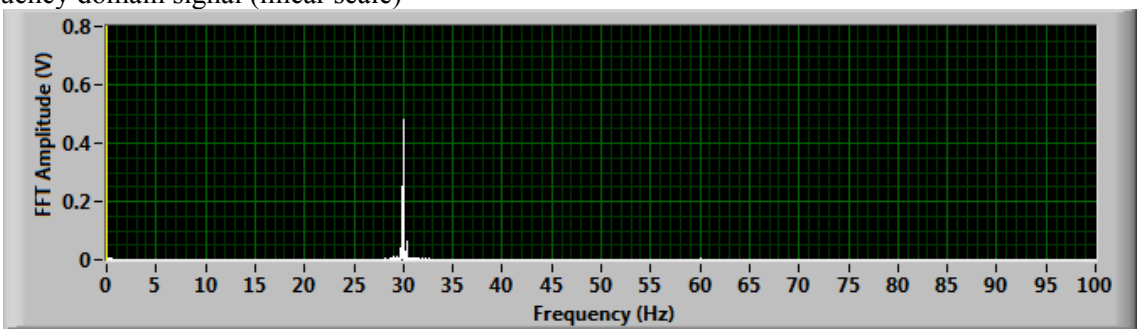

Figure B.32: Frequency Domain Signal (Linear Scale) of Raw Data for Combined Static and Dynamic Forces with 1.0 mph along 16-in. Thick Slab Section

Frequency domain signal (dB scale)

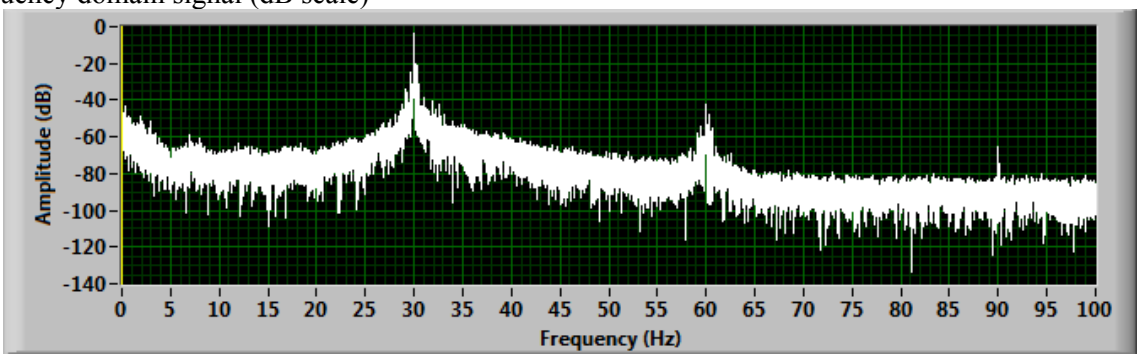

Figure B.33: Frequency Domain Signal (Decibel Scale) of Raw Data for Combined Static and Dynamic Forces with 1.0 mph along 16-in. Thick Slab Section

B.3.2.3. on 8- and 10-in. thick slabs

Time domain signal of static and dynamic forces (the number of data point = 159,232)

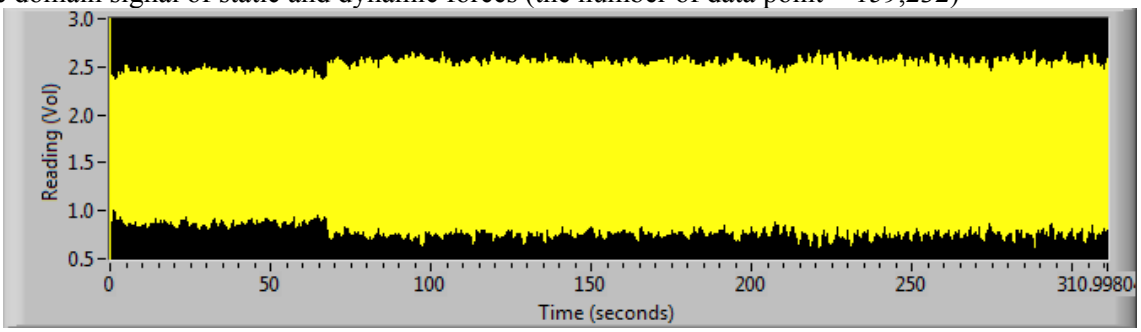

Figure B.34: Time Domain Signal of Raw Data for Combined Static and Dynamic Forces with 1.0 mph along 8- and 10-in. Thick Slab Section

Frequency domain (linear scale)

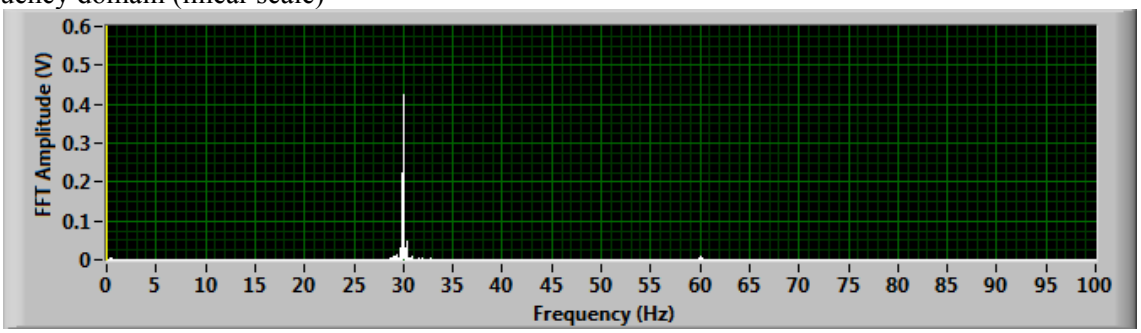

Figure B.35: Frequency Domain Signal (Linear Scale) of Raw Data for Combined Static and Dynamic Forces with 1.0 mph along 8- and 10-in. Thick Slab Section

Frequency domain (dB scale)

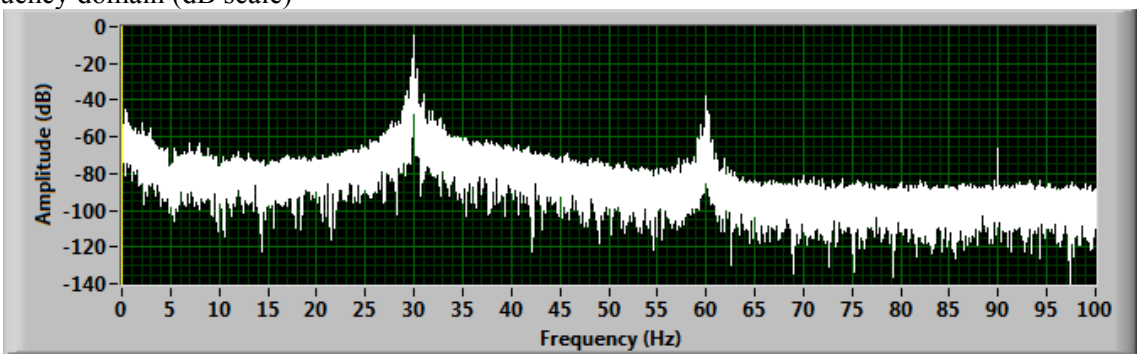

Figure B.36: Frequency Domain Signal (Decibel Scale) of Raw Data for Combined Static and Dynamic Forces with 1.0 mph along 8- and 10-in. Thick Slab Section

B.3.3 PROCESSED ROLLING SENSOR #1 SIGNAL (DEFLECTION PROFILE)

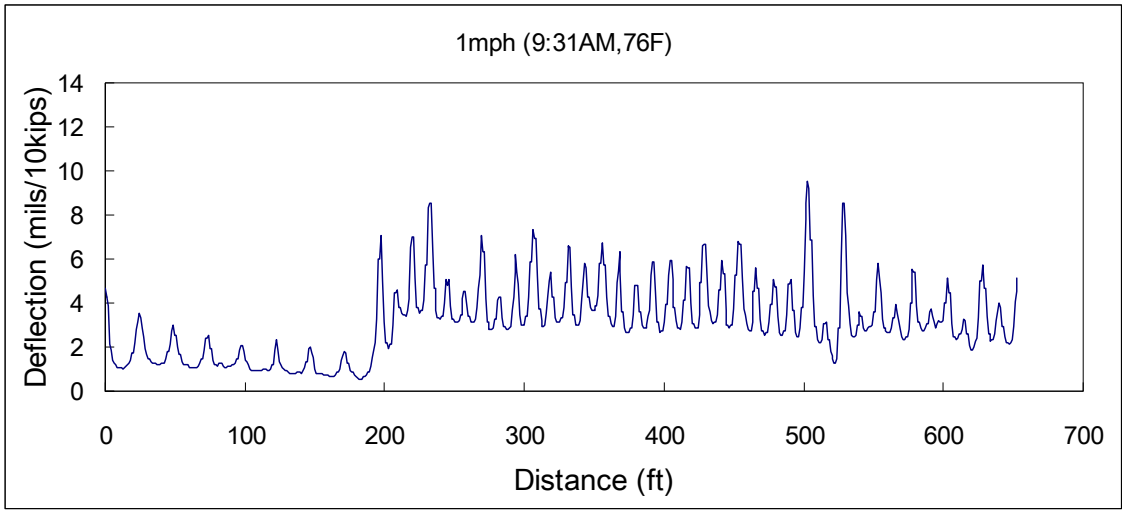

Figure B.37: Processed Rolling Sensor #1 Signal with 1.0 mph

B.3.4. RAW ROLLING SENSOR #1 SIGNAL

B.3.4.1. Complete record for 653-ft long testbed

Time domain signal (the number of data point = 229,376)

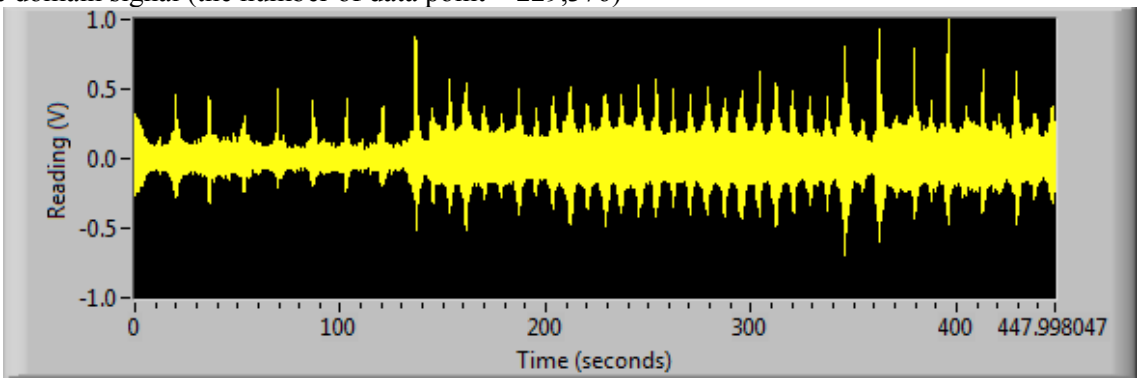

Figure B.38: Time Domain Signal of Raw Data for Rolling Sensor #1 with 1.0 mph along Whole Testbed Length

Frequency domain signal (linear scale)

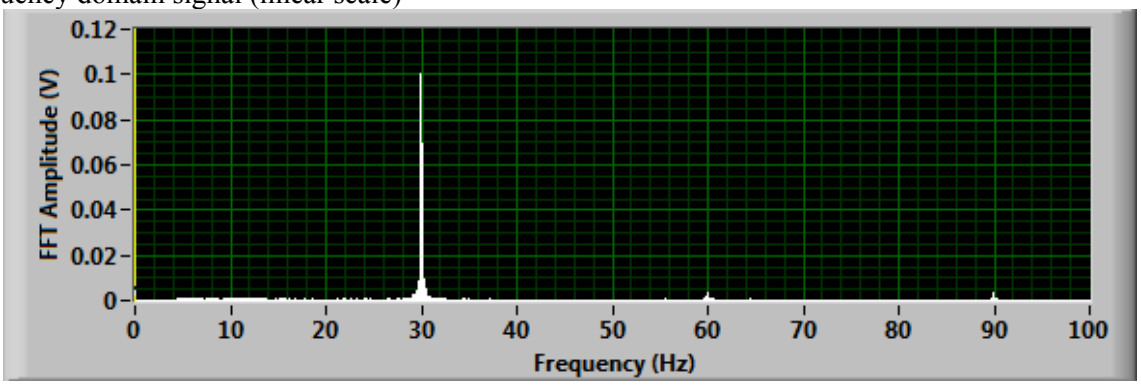

Figure B.39: Frequency Domain Signal (Linear Scale) of Raw Data for Combined Static and Dynamic Forces with 1.0 mph along Whole Testbed Length

Frequency domain signal (dB scale)

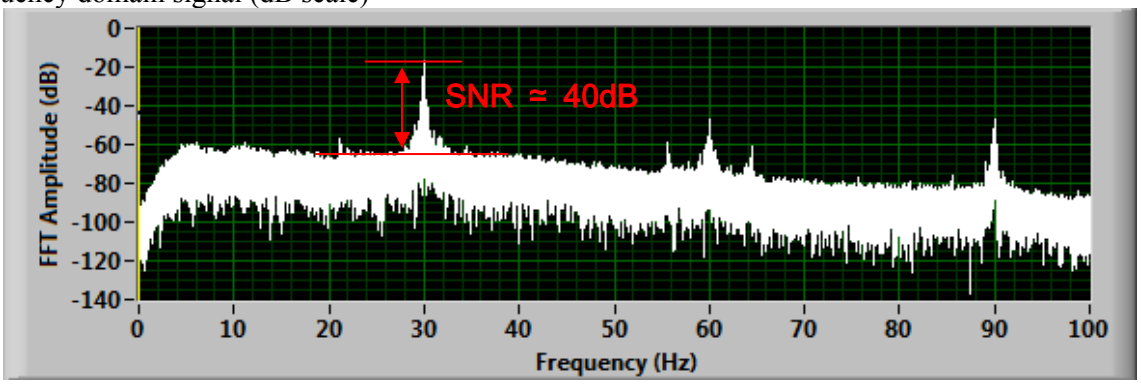

Figure B.40: Frequency Domain Signal (Decibel Scale) of Raw Data for Rolling Sensor #1 with 1.0 mph along Whole Testbed Length

B.3.4.2. on 16-in. thick slabs

Time domain signal (the number of data point = 70,144)

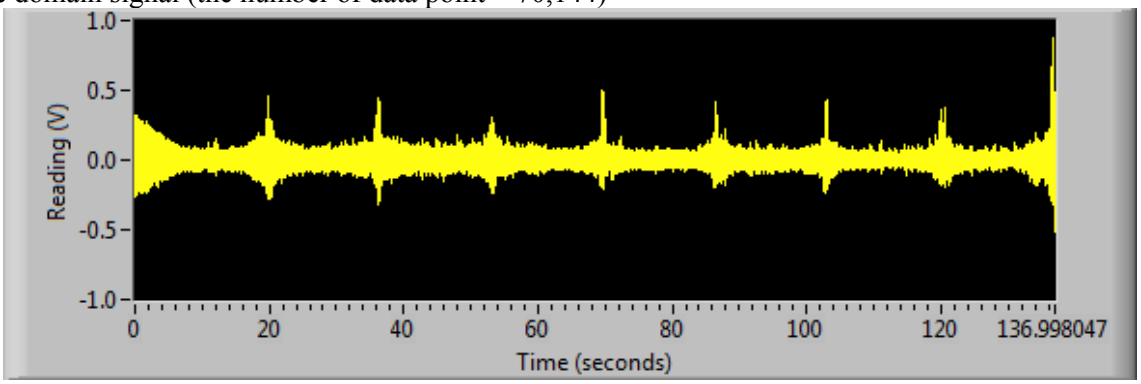

Figure B.41: Time Domain Signal of Raw Data for Rolling Sensor #1 with 1.0 mph along 16-in. Thick Slab Section

Frequency domain signal (linear scale)

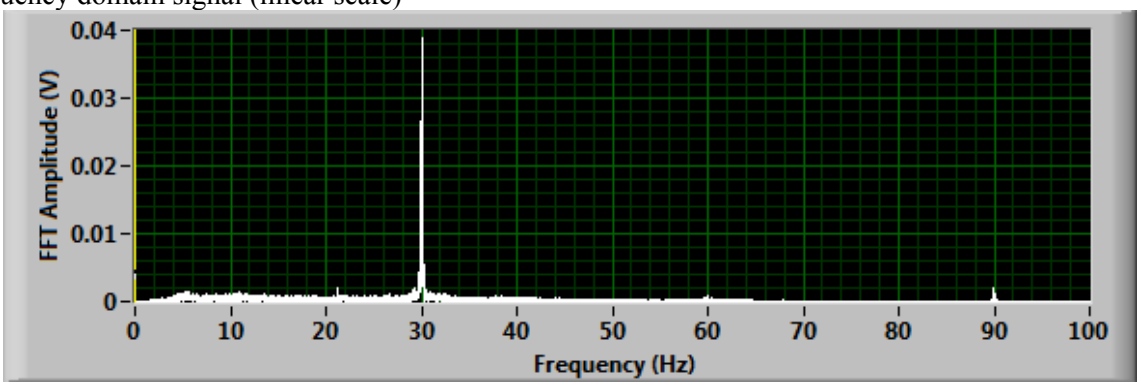

Figure B.42: Frequency Domain Signal (Linear Scale) of Raw Data for Rolling Sensor #1 with 1.0 mph along 16-in. Thick Slab Section

Frequency domain signal (dB scale)

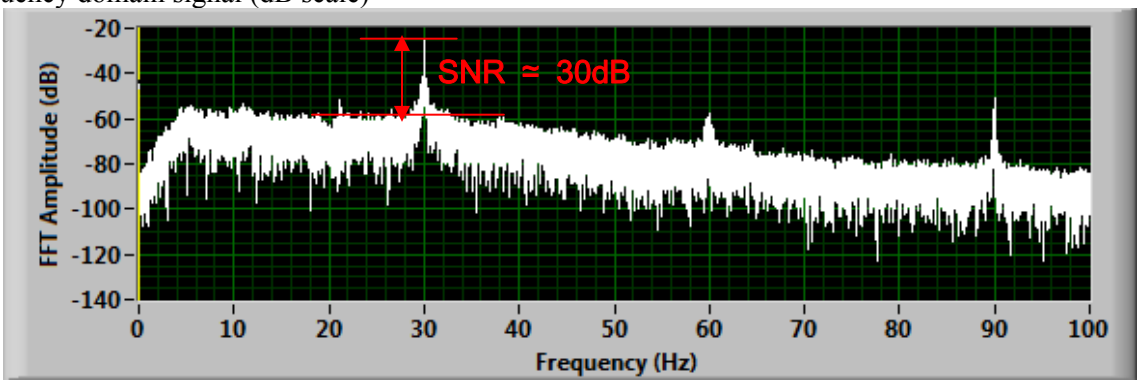

Figure B.43: Frequency Domain Signal (Decibel Scale) of Raw Data for Rolling Sensor #1 with 1.0 mph along 16-in. Thick Slab Section

B.3.4.3. on 8- and 10-in. thick slabs

Time domain signal (the number of data point = 159,232)

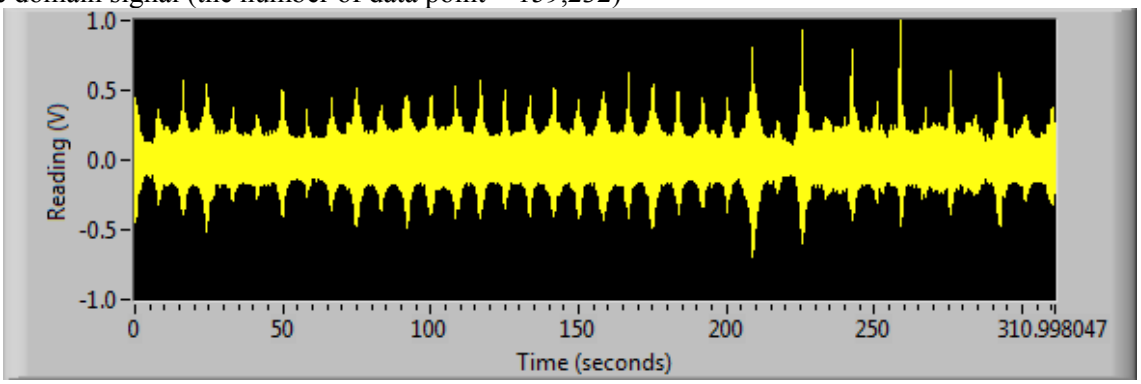

Figure B.44: Time Domain Signal of Raw Data for Rolling Sensor #1 with 1.0 mph along 8- and 10-in. Thick Slab Section

Frequency domain (linear scale)

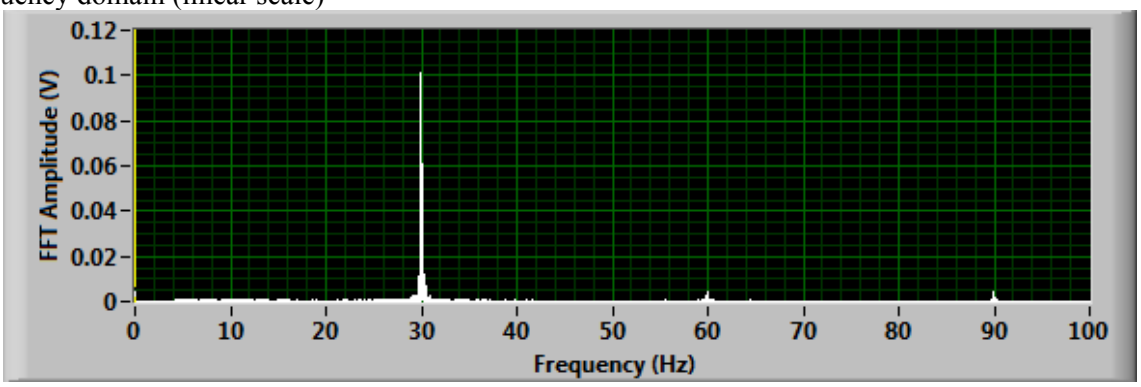

Figure B.45: Frequency Domain Signal (Linear Scale) of Raw Data for Rolling Sensor #1 with 1.0 mph along 8- and 10-in. Thick Slab Section

Frequency domain (dB scale)

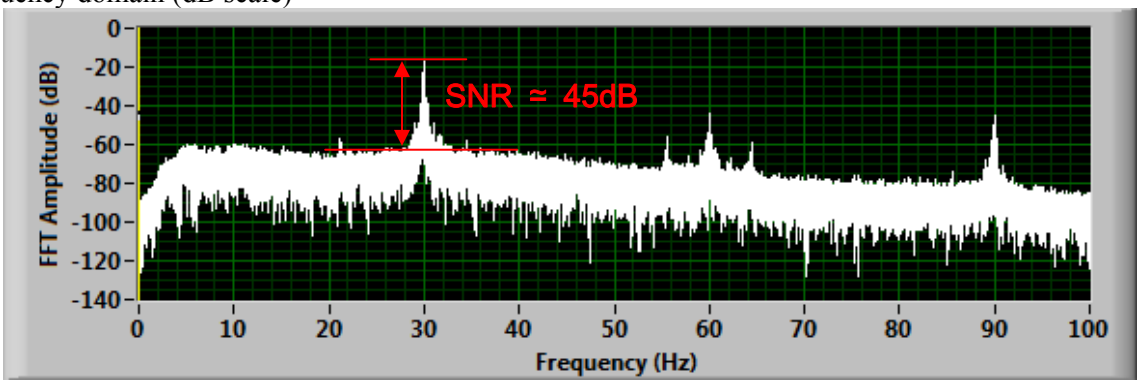

Figure B.46: Frequency Domain Signal (Decibel Scale) of Raw Data for Rolling Sensor #1 with 1.0 mph along 8- and 10-in. Thick Slab Section

B.3.5. PROCESSED DMI SIGNAL

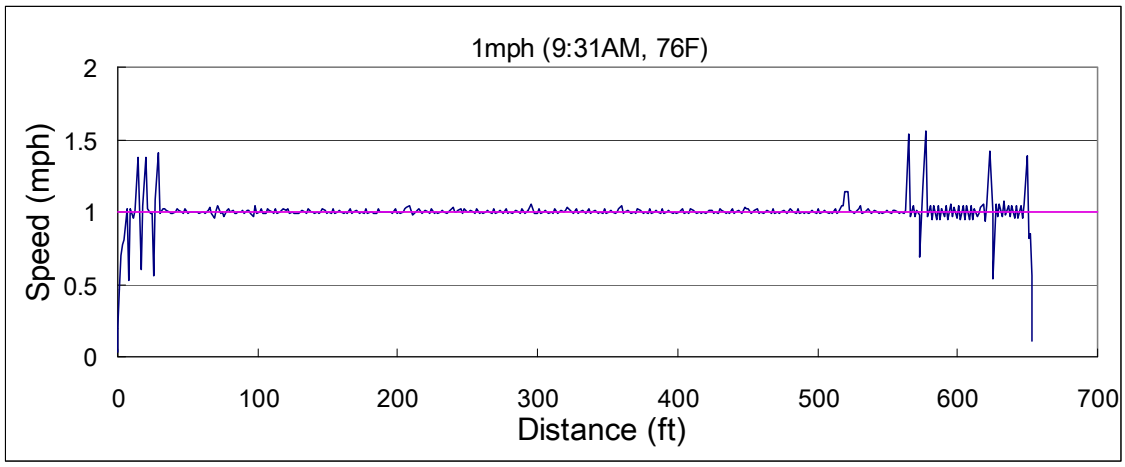

Figure B.47: Processed DMI Signal with 1.0 mph

B.3.6. RAW DMI SIGNAL

B.3.6.1 Complete record for 653-ft long testbed (the number of data point = 229,376)

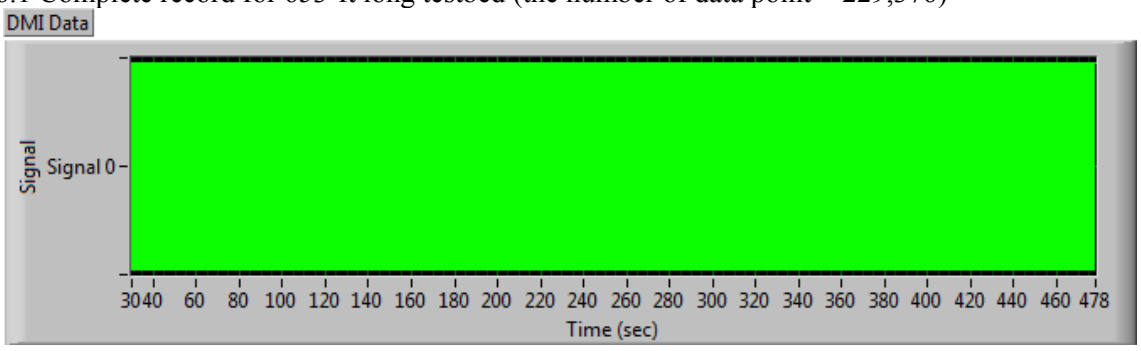

Figure B.48: Time Domain Signal of Raw Data for DMI with 1.0 mph along Whole Testbed Length

B.3.6.2. 5-second interval signal (from 60 to 65 second) on 16-in. thick slabs (the number of data point = 2,560)

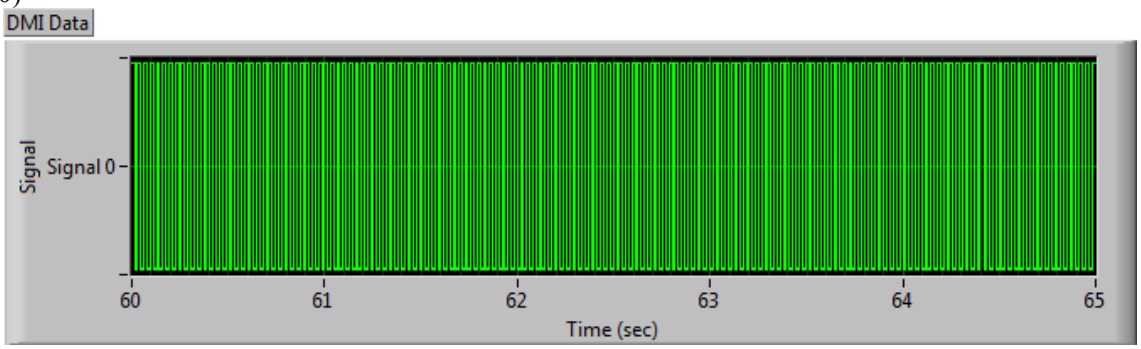

Figure B.49: Time Domain Signal of Raw Data for DMI with 1.0 mph along 16-in. Thick Slab Section

B.3.6.3. 5-second interval signal (from 255 to 260 second) on 8- and 10-in. thick slabs (the number of data point = 2,560)

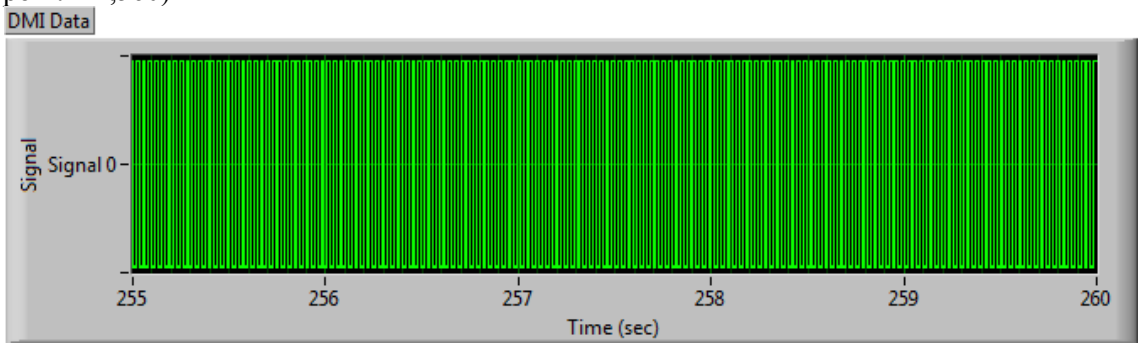

Figure B.50: Time Domain Signal of Raw Data for DMI with 1.0 mph along 8- and 10-in. Thick Slab Section

B.4. TPAD TESTING SPEED at 2 MPH

B.4.1. PROCESSED LOAD SIGNALS (Applied Static and Dynamic Forces)

B.4.1.1. Static force (Fstat) along the total distance

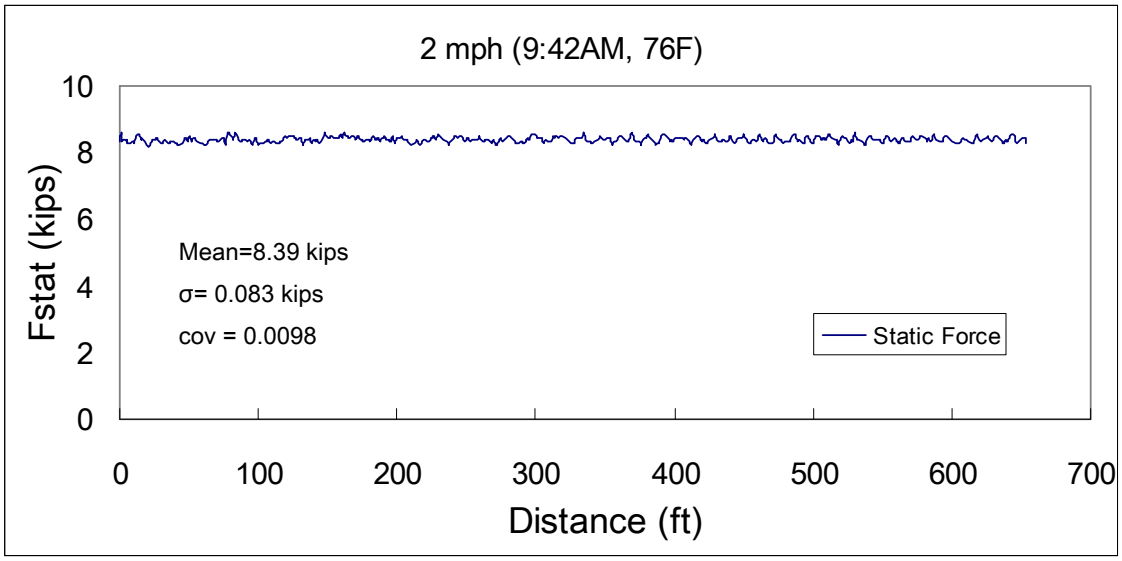

Figure B.51: Processed Static Force Signal with 2.0 mph

B.4.1.2. Peak-to-peak dynamic force (Fdyn) along the total distance

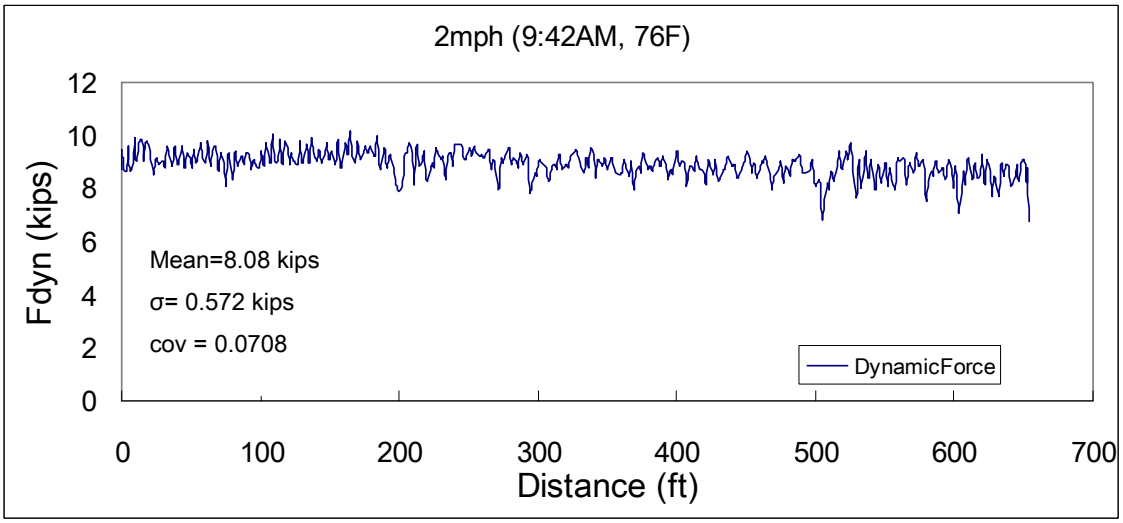

Figure B.52: Processed Pak-to-Peak Dynamic Force Signal with 2.0 mph

B.4.2. RAW LOAD SIGNAL

B.4.2.1. Complete record for 653-ft long testbed

Time domain signal of static and dynamic forces (the number of data point = 229,376)

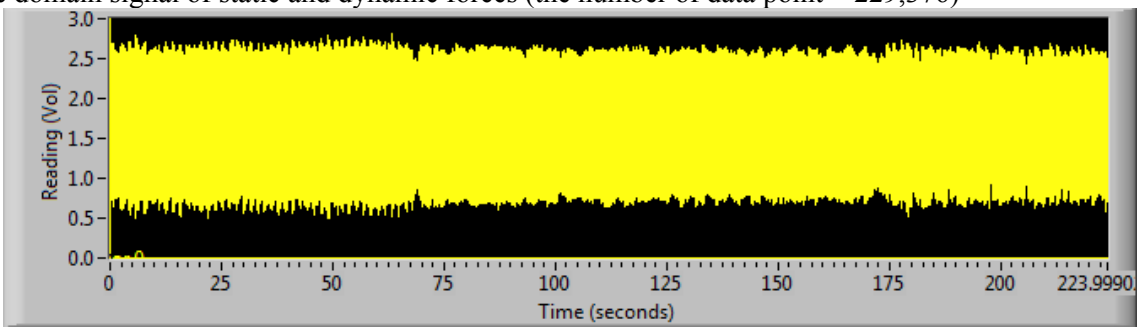

Figure B.53: Time Domain Signal of Raw Data for Combined Static and Dynamic Forces with 2.0 mph on Whole Testbed Length

Frequency domain signal (linear scale)

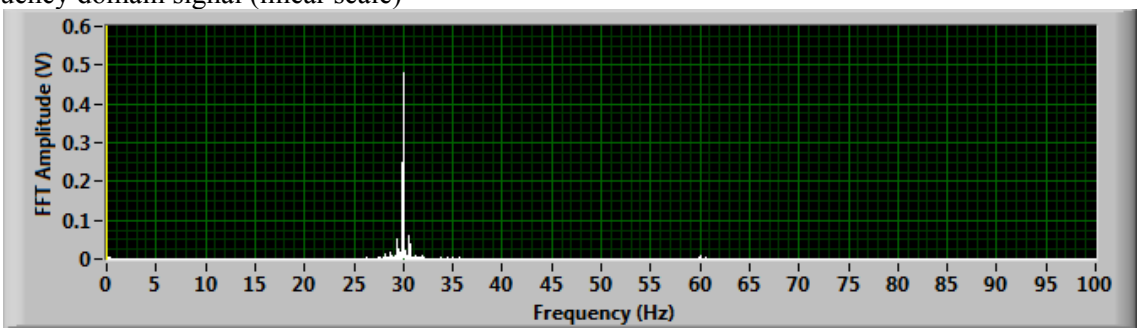

Figure B.54: Frequency Domain Signal (Linear Scale) of Raw Data for Combined Static and Dynamic Forces with 2.0 mph along Whole Testbed Length

Frequency domain signal (dB scale)

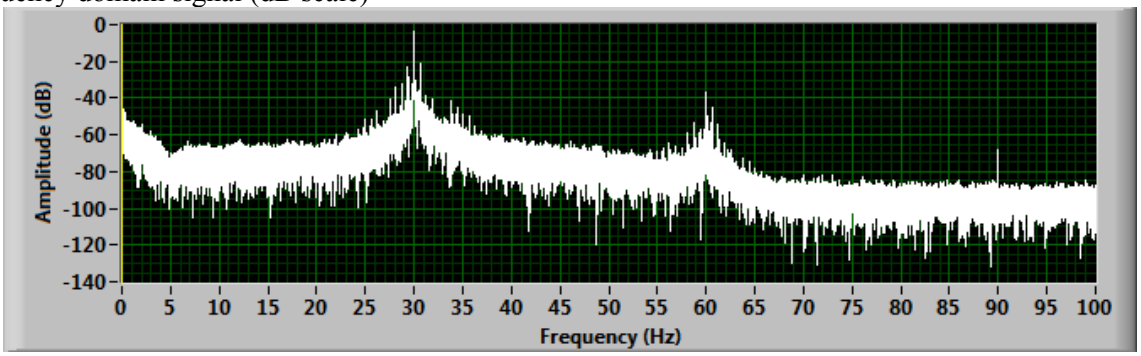

Figure B.55: Frequency Domain Signal (Decibel Scale) of Raw Data for Combined Static and Dynamic Forces with 2.0 mph along Whole Testbed Length

B.4.2.2. on 16-in. thick slabs

Time domain signal of static and dynamic forces (the number of data point = 69,632)

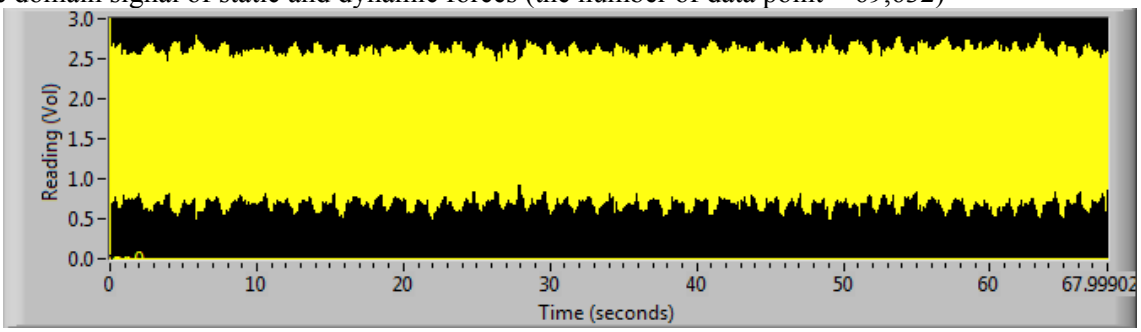

Figure B.56: Time Domain Signal of Raw Data for Combined Static and Dynamic Forces with 2.0 mph along 16-in. Thick Slab Section

Frequency domain signal (linear scale)

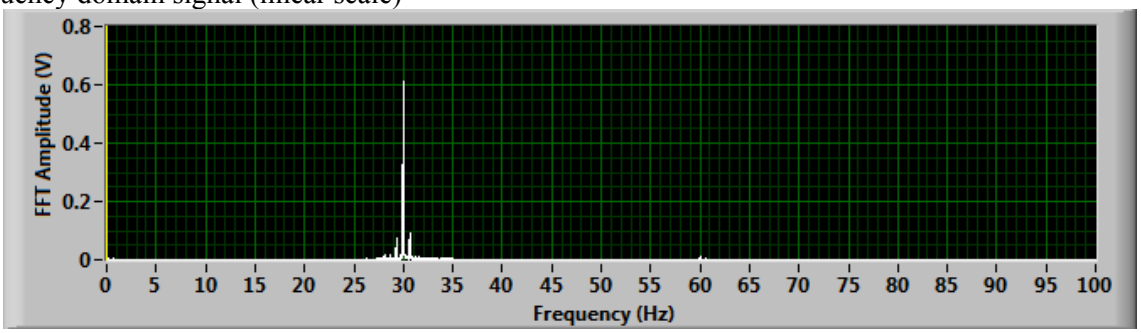

Figure B.57: Frequency Domain Signal (Linear Scale) of Raw Data for Combined Static and Dynamic Forces with 2.0 mph along 16-in. Thick Slab Section

Frequency domain signal (dB scale)

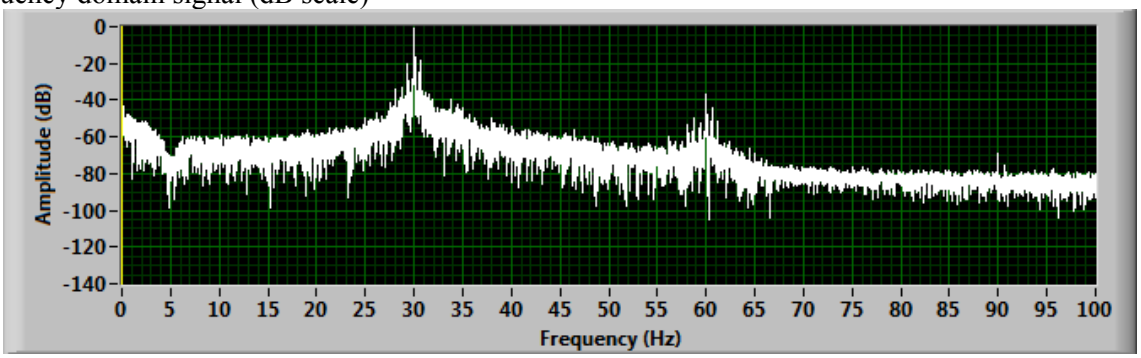

Figure B.58: Frequency Domain Signal (Decibel Scale) of Raw Data for Combined Static and Dynamic Forces with 2.0 mph along 16-in. Thick Slab Section

B.4.2.3. on 8- and 10-in. thick slabs

Time domain signal of static and dynamic forces (the number of data point = 159,744)

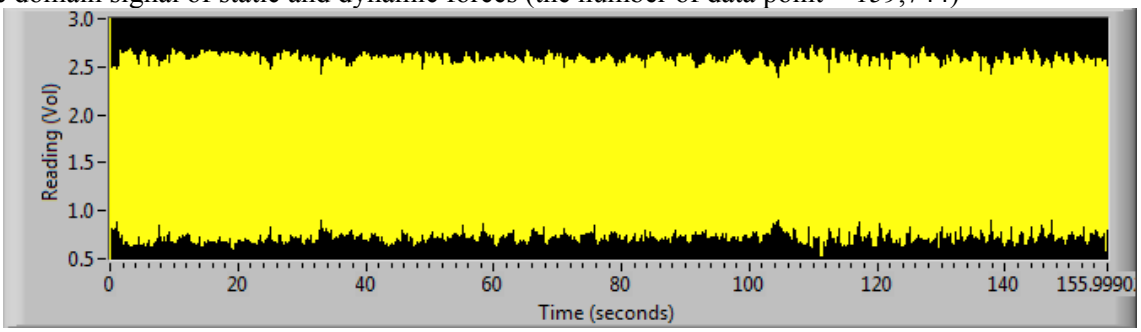

Figure B.59: Time Domain Signal of Raw Data for Combined Static and Dynamic Forces with 2.0 mph along 8- and 10-in. Thick Slab Section

Frequency domain (linear scale)

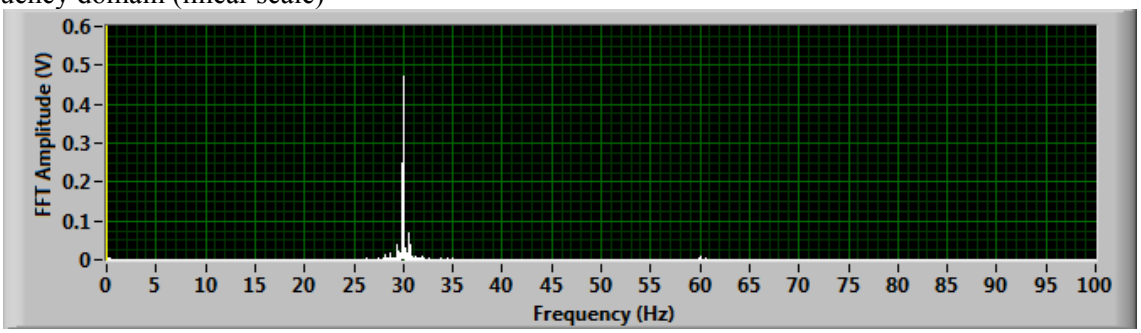

Figure B.60: Frequency Domain Signal (Linear Scale) of Raw Data for Combined Static and Dynamic Forces with 2.0 mph along 8- and 10-in. Thick Slab Section

Frequency domain (dB scale)

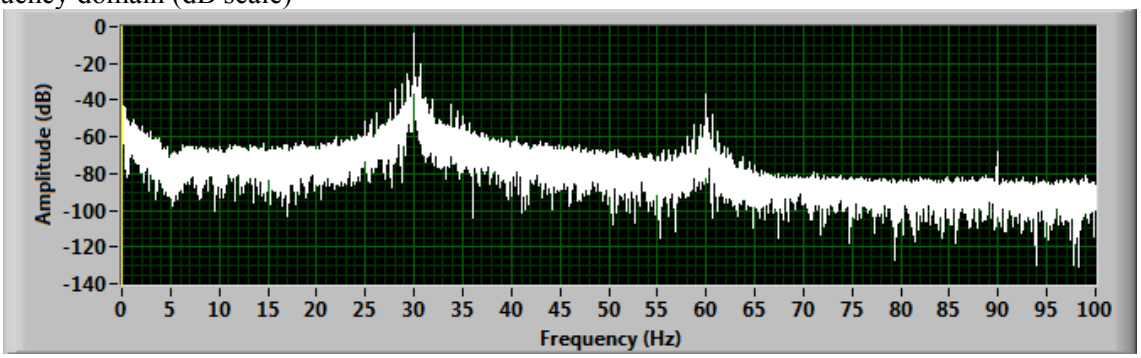

Figure B.61: Frequency Domain Signal (Decibel Scale) of Raw Data for Combined Static and Dynamic Forces with 2.0 mph along 8- and 10-in. Thick Slab Section

B.4.3 PROCESSED ROLLING SENSOR #1 SIGNAL (DEFLECTION PROFILE)

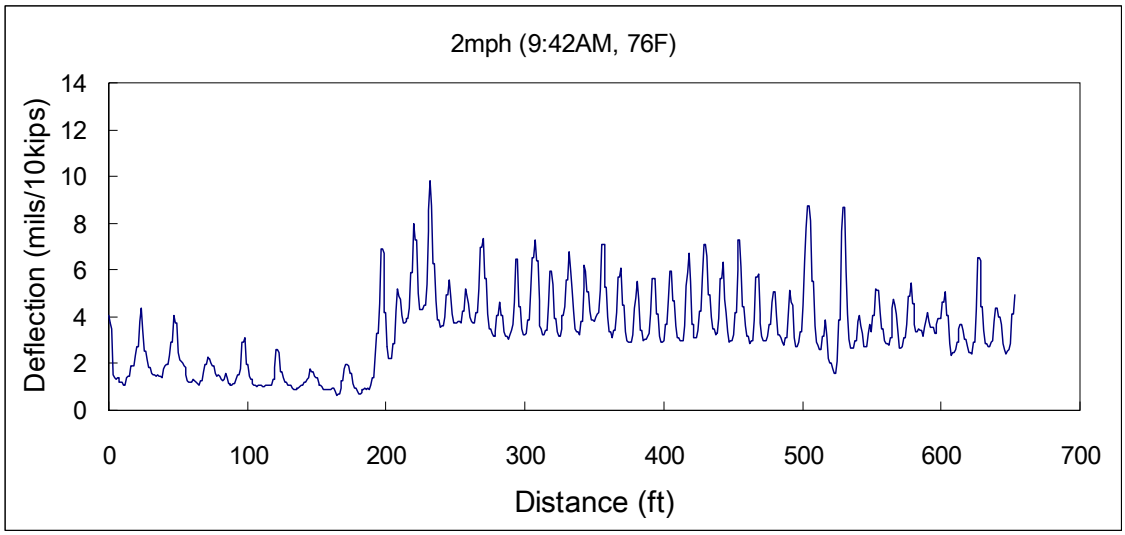

Figure B.62: Processed Rolling Sensor #1 Signal with 2.0 mph

B.4.4. RAW ROLLING SENSOR #1 SIGNAL

B.4.4.1. Complete record for 653-ft long testbed

Time domain signal (the number of data point = 229,376)

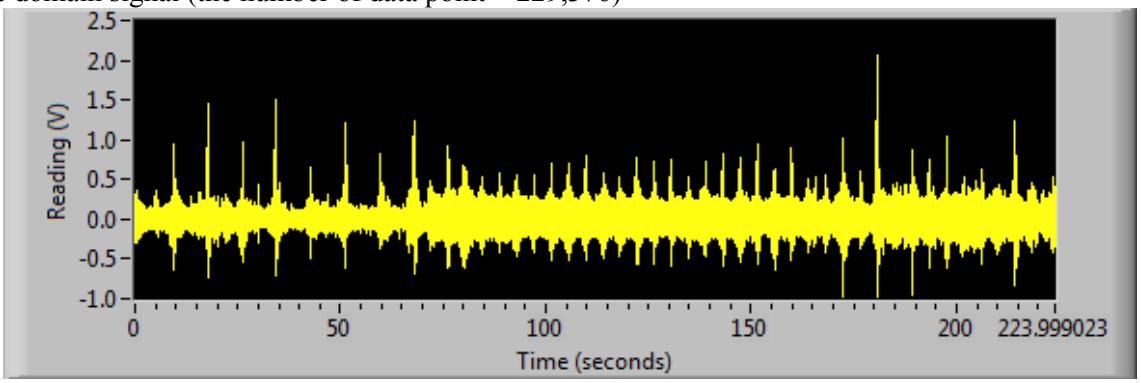

Figure B.63: Time Domain Signal of Raw Data for Rolling Sensor #1 with 2.0 mph along Whole Testbed Length

Frequency domain signal (linear scale)

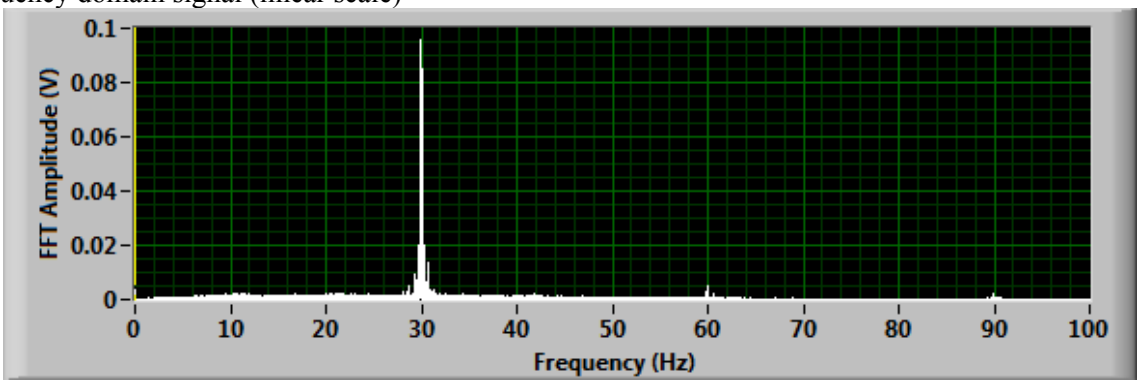

Figure B.64: Frequency Domain Signal (Linear Scale) of Raw Data for Combined Static and Dynamic Forces with 2.0 mph along Whole Testbed Length

Frequency domain signal (dB scale)

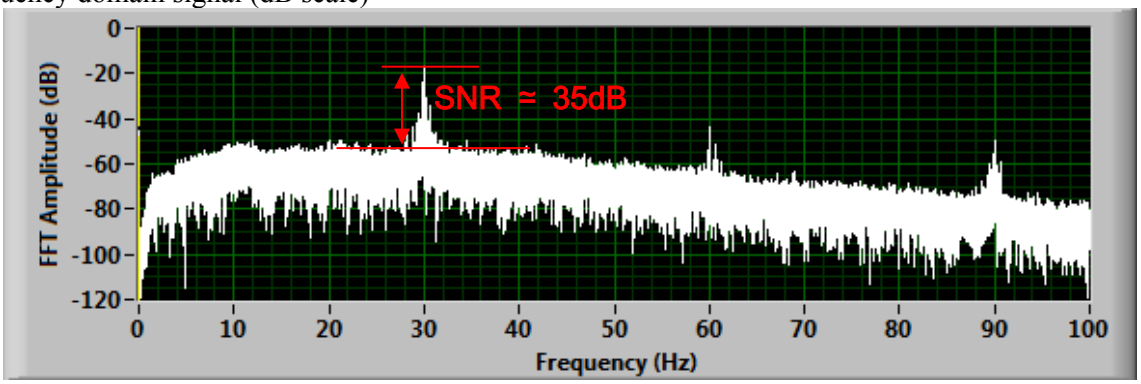

Figure B.65: Frequency Domain Signal (Decibel Scale) of Raw Data for Rolling Sensor #1 with 2.0 mph along Whole Testbed Length

B.4.4.2. on 16-in. thick slabs

Time domain signal (the number of data point = 69,632)

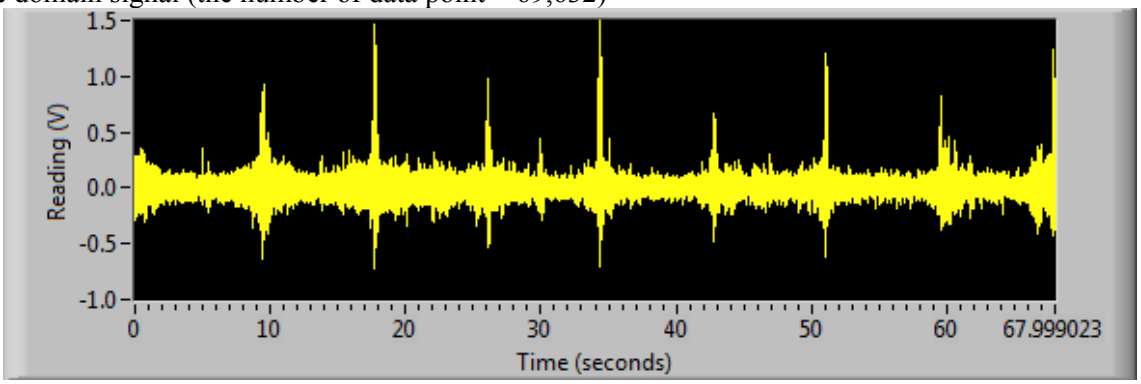

Figure B.66: Time Domain Signal of Raw Data for Rolling Sensor #1 with 2.0 mph along 16-in. Thick Slab Section

Frequency domain signal (linear scale)

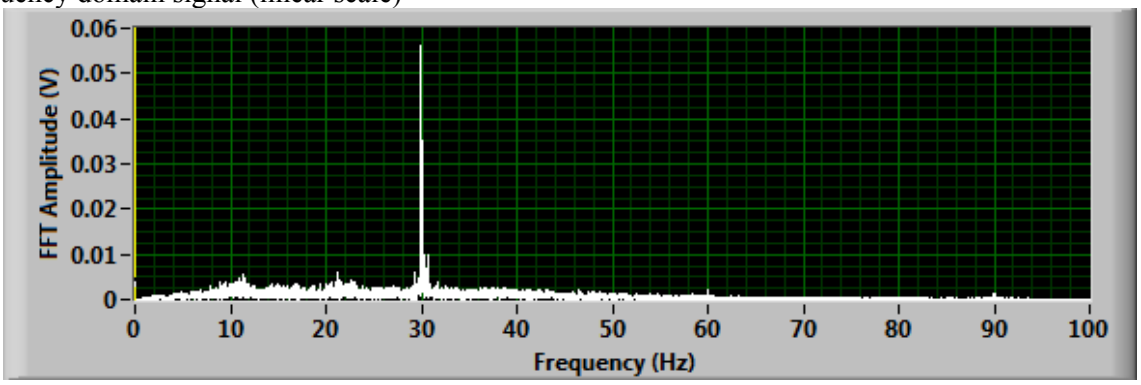

Figure B.67: Frequency Domain Signal (Linear Scale) of Raw Data for Rolling Sensor #1 with 2.0 mph along 16-in. Thick Slab Section

Frequency domain signal (dB scale)

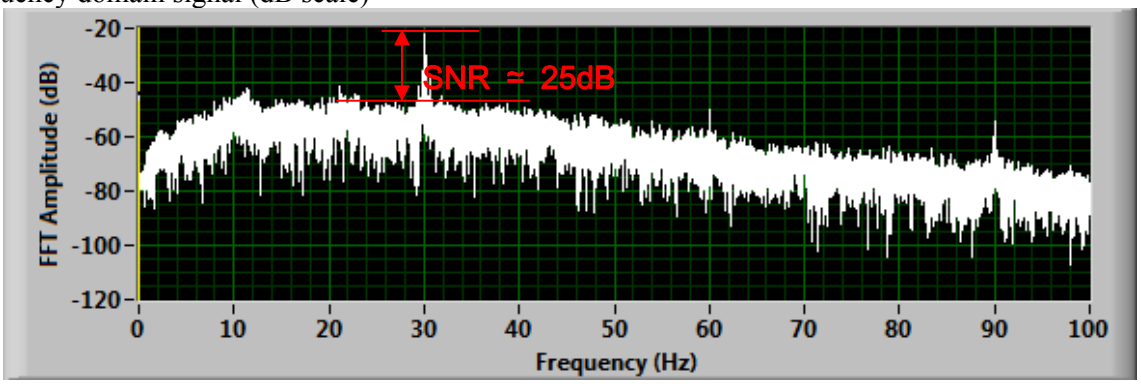

Figure B.68: Frequency Domain Signal (Decibel Scale) of Raw Data for Rolling Sensor #1 with 2.0 mph along 16-in. Thick Slab Section

B.4.4.3. on 8- and 10-in. thick slabs

Time domain signal (the number of data point = 159,744)

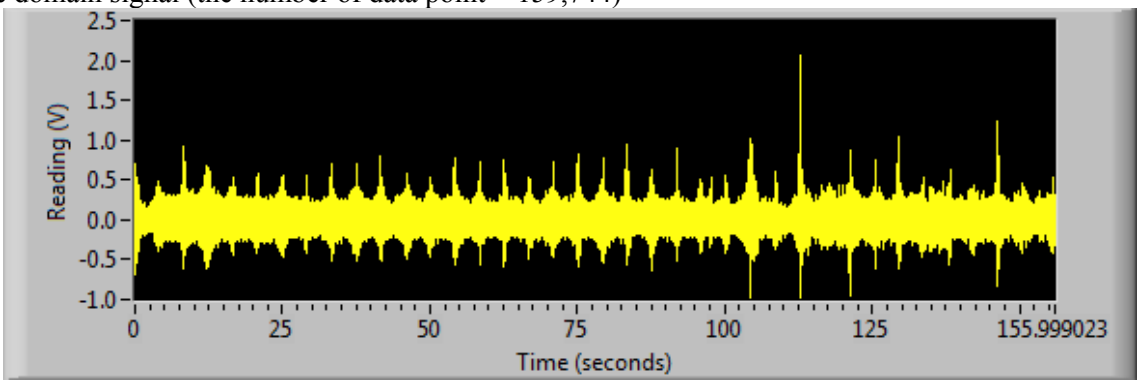

Figure B.69: Time Domain Signal of Raw Data for Rolling Sensor #1 with 2.0 mph along 8- and 10-in. Thick Slab Section

Frequency domain (linear scale)

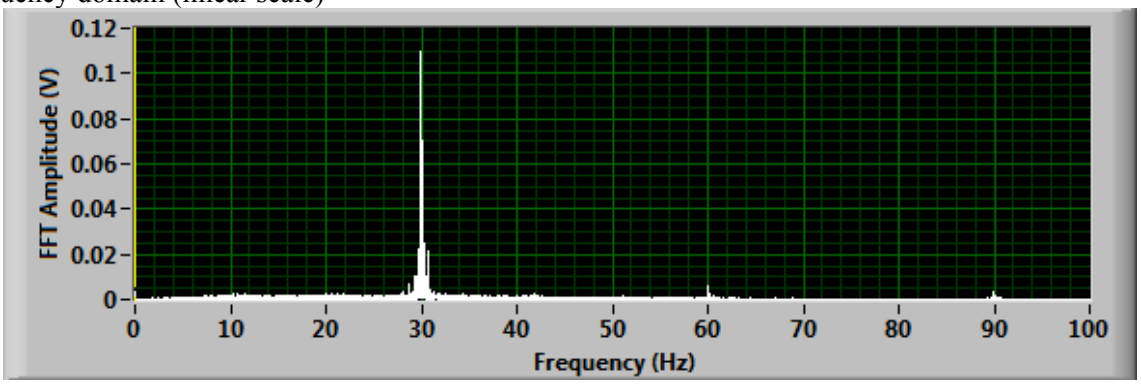

Figure B.70: Frequency Domain Signal (Linear Scale) of Raw Data for Rolling Sensor #1 with 2.0 mph along 8- and 10-in. Thick Slab Section

Frequency domain (dB scale)

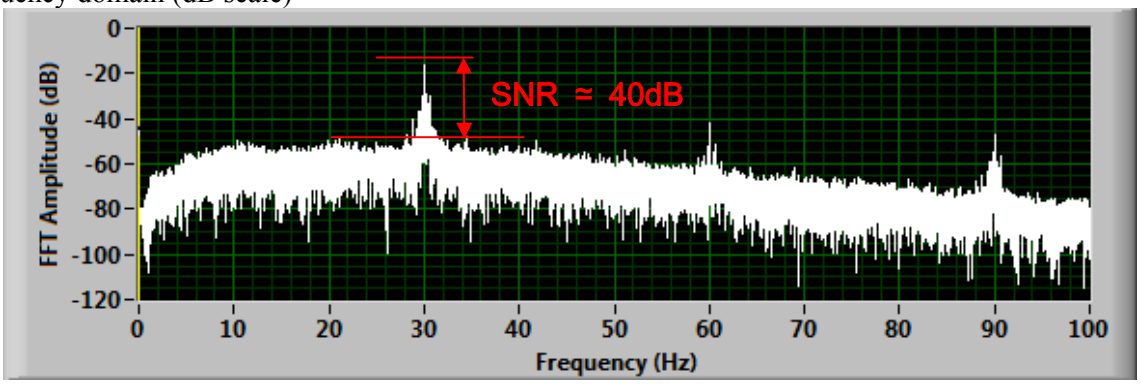

Figure B.71: Frequency Domain Signal (Decibel Scale) of Raw Data for Rolling Sensor #1 with 2.0 mph along 8- and 10-in. Thick Slab Section

B.4.5. PROCESSED DMI SIGNAL

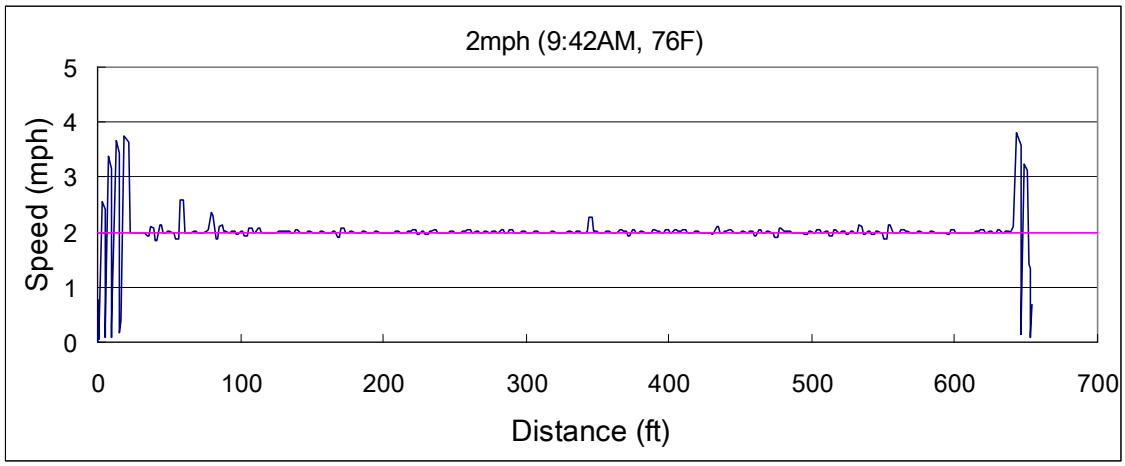

Figure B.72: Processed DMI Signal with 2.0 mph

B.4.6. RAW DMI SIGNAL

B.4.6.1 Complete record for 653-ft long testbed (the number of data point = 229,376)

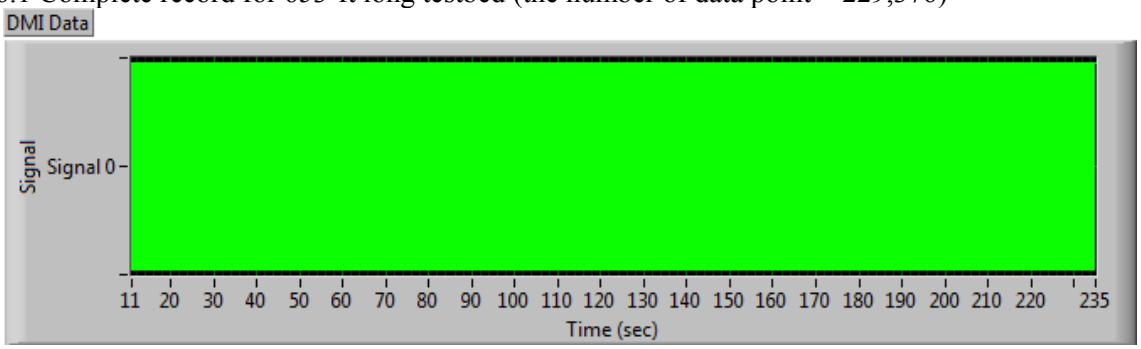

Figure B.73: Time Domain Signal of Raw Data for DMI with 2.0 mph along Whole Testbed Length

3-2-B. 2.5-second interval signal (from 20 to 22.5 second) on 16-in. thick slabs (the number of data point = 2,560)

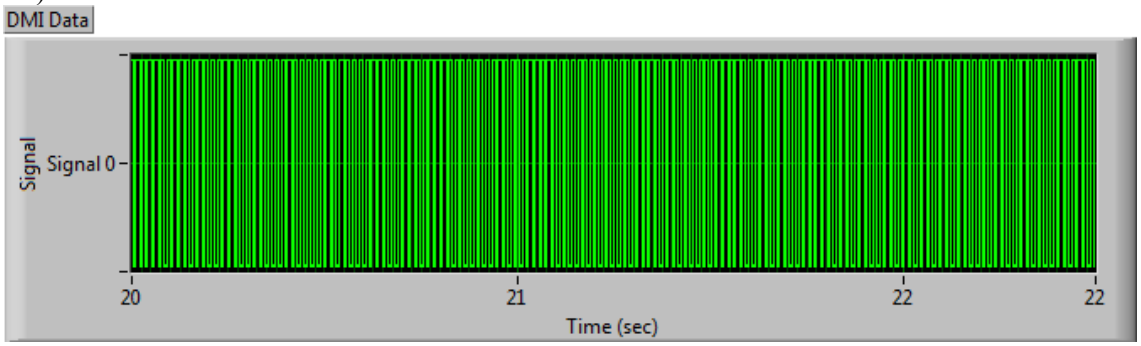

Figure B.74: Time Domain Signal of Raw Data for DMI with 2.0 mph along 16-in. Thick Slab Section

3-2-C. 2.5-second interval signal (from 85 to 87.5 second) on 8- and 10-in. thick slabs (the number of data point = 2,560)

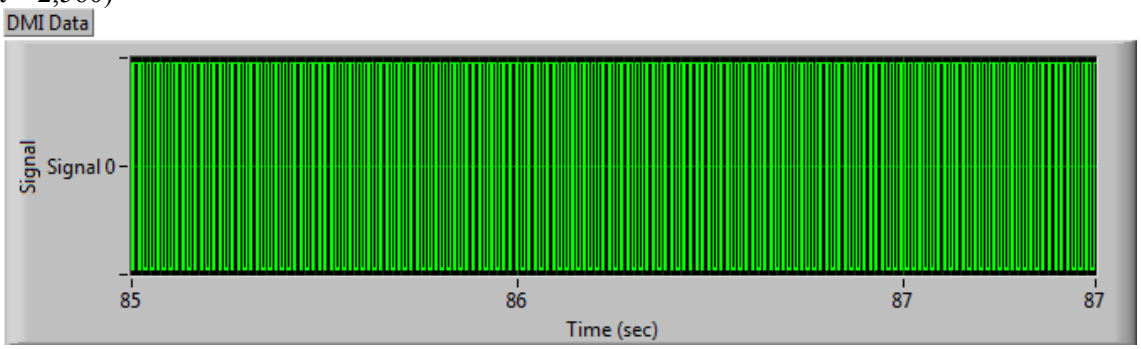

Figure B.75: Time Domain Signal of Raw Data for DMI with 2.0 mph along 8- and 10-in. Thick Slab Section

B.5. TPAD TESTING SPEED at 3 MPH

B.5.1. PROCESSED LOAD SIGNALS (Applied Static and Dynamic Forces)

B.5.1.1. Static force (Fstat) along the total distance

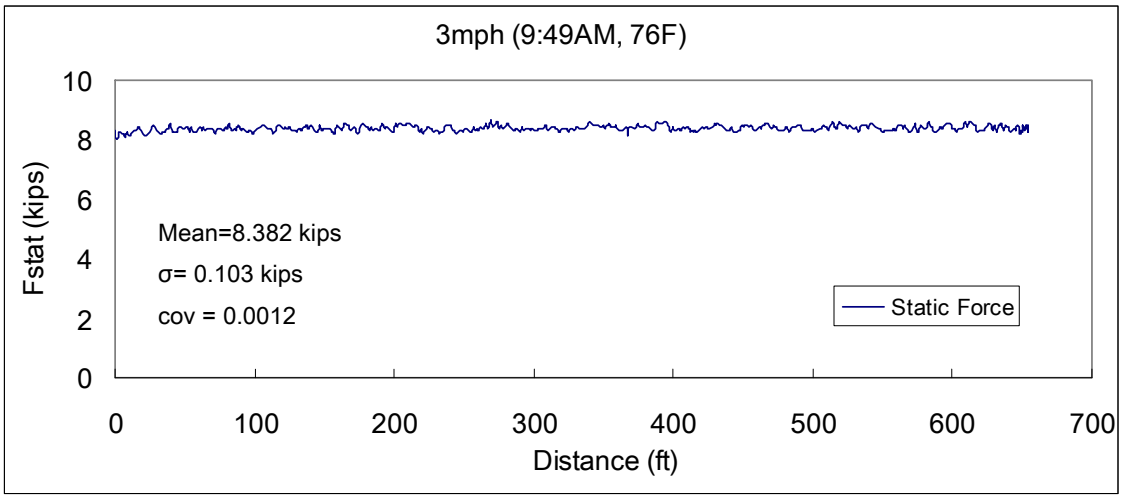

Figure B.76: Processed Static Force Signal with 3.0 mph

B.5.1.2. Peak-to-peak dynamic force (Fdyn) along the total distance

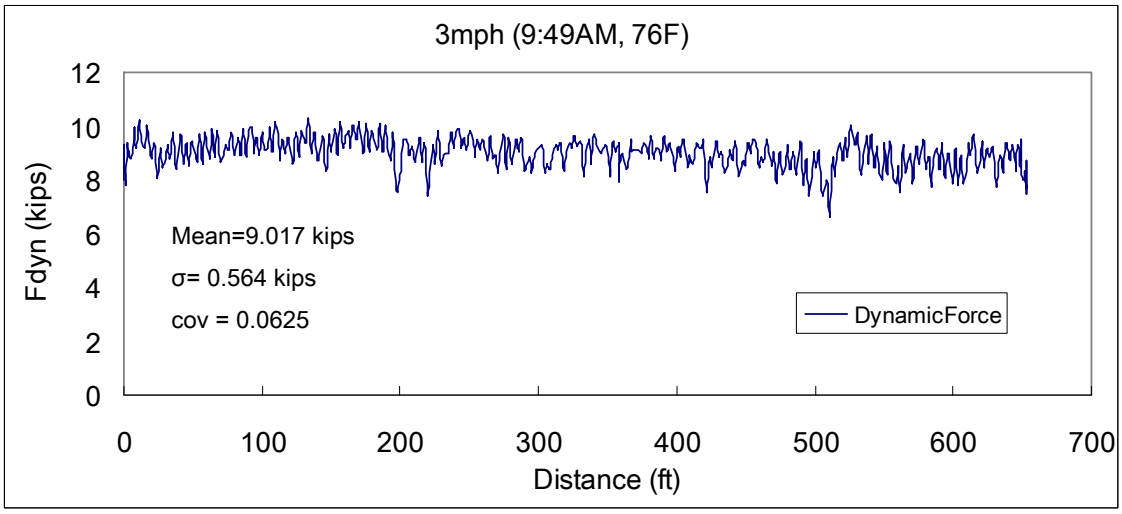

Figure B.77: Processed Pak-to-Peak Dynamic Force Signal with 3.0 mph

B.5.2. RAW LOAD SIGNAL

B.5.2.1. Complete record for 653-ft long testbed

Time domain signal of static and dynamic forces (the number of data point = 230,400)

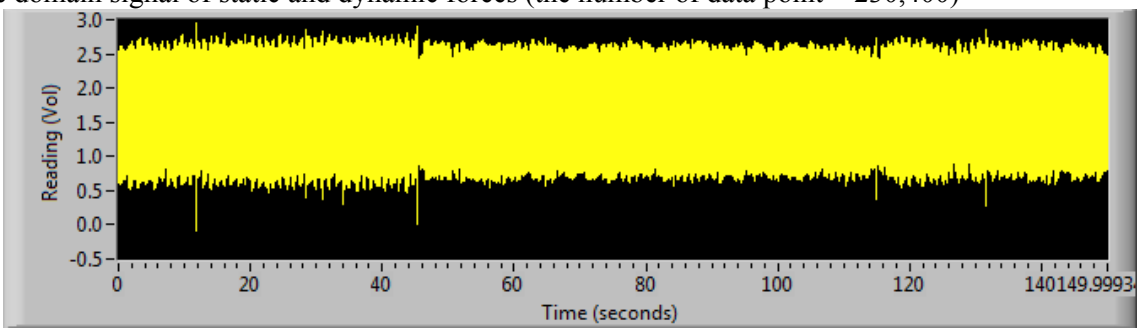

Figure B.78: Time Domain Signal of Raw Data for Combined Static and Dynamic Forces with 3.0 mph on Whole Testbed Length

Frequency domain signal (linear scale)

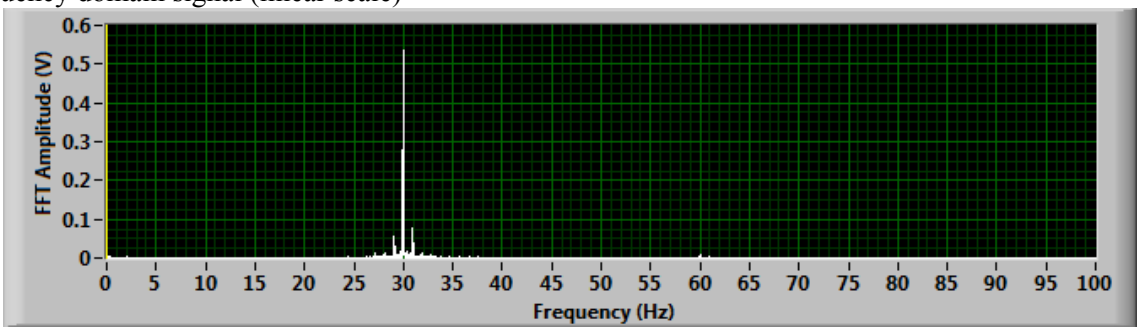

Figure B.79: Frequency Domain Signal (Linear Scale) of Raw Data for Combined Static and Dynamic Forces with 3.0 mph along Whole Testbed Length

Frequency domain signal (dB scale)

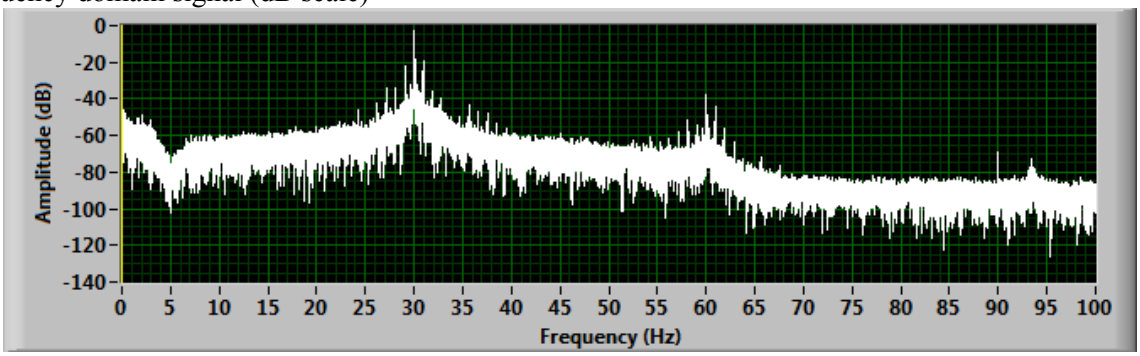

Figure B.80: Frequency Domain Signal (Decibel Scale) of Raw Data for Combined Static and Dynamic Forces with 3.0 mph along Whole Testbed Length

B.5.2.2. on 16-in. thick slabs

Time domain signal of static and dynamic forces (the number of data point = 69,427)

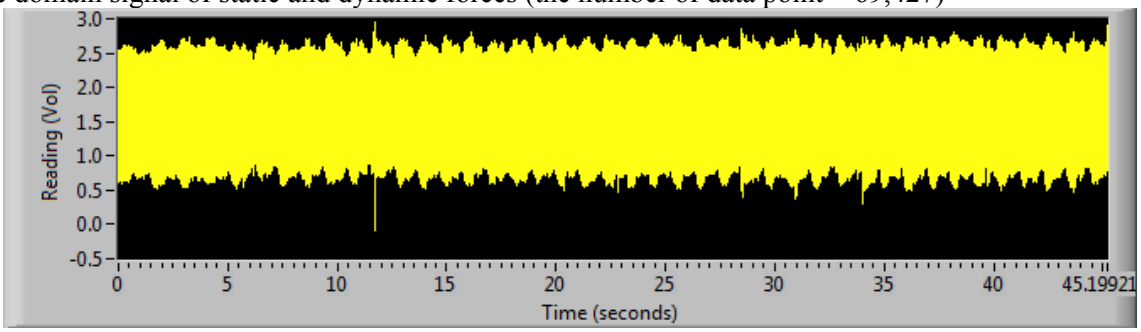

Figure B.81: Time Domain Signal of Raw Data for Combined Static and Dynamic Forces with 3.0 mph along 16-in. Thick Slab Section

Frequency domain signal (linear scale)

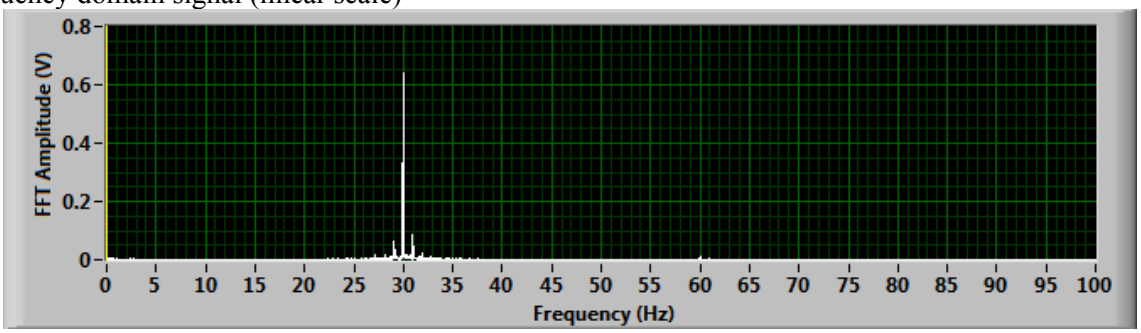

Figure B.82: Frequency Domain Signal (Linear Scale) of Raw Data for Combined Static and Dynamic Forces with 3.0 mph along 16-in. Thick Slab Section

Frequency domain signal (dB scale)

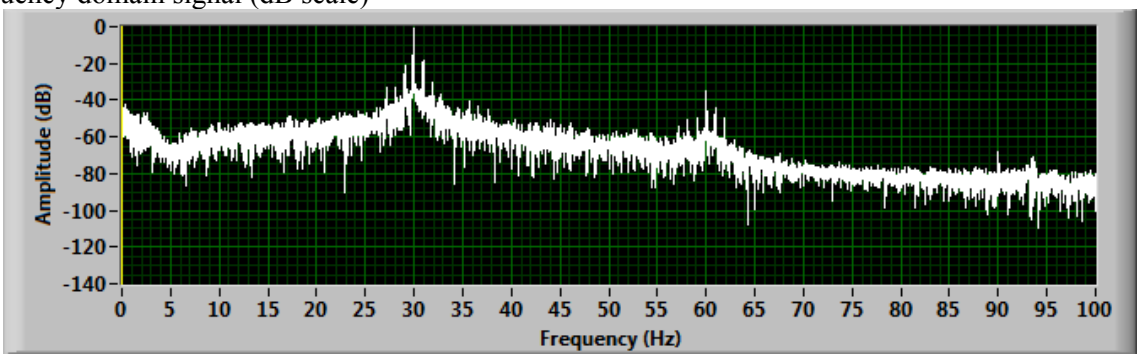

Figure B.83: Frequency Domain Signal (Decibel Scale) of Raw Data for Combined Static and Dynamic Forces with 3.0 mph along 16-in. Thick Slab Section

B.5.2.3. on 8- and 10-in. thick slabs

Time domain signal of static and dynamic forces (the number of data point = 160,973)

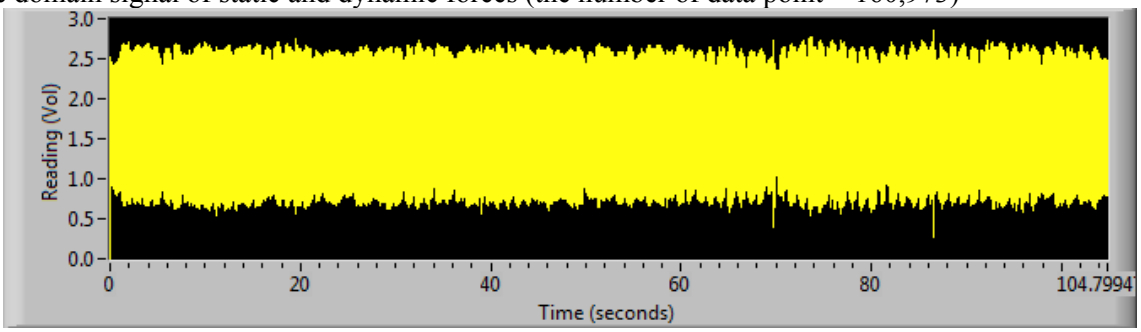

Figure B.84: Time Domain Signal of Raw Data for Combined Static and Dynamic Forces with 3.0 mph along 8- and 10-in. Thick Slab Section

Frequency domain (linear scale)

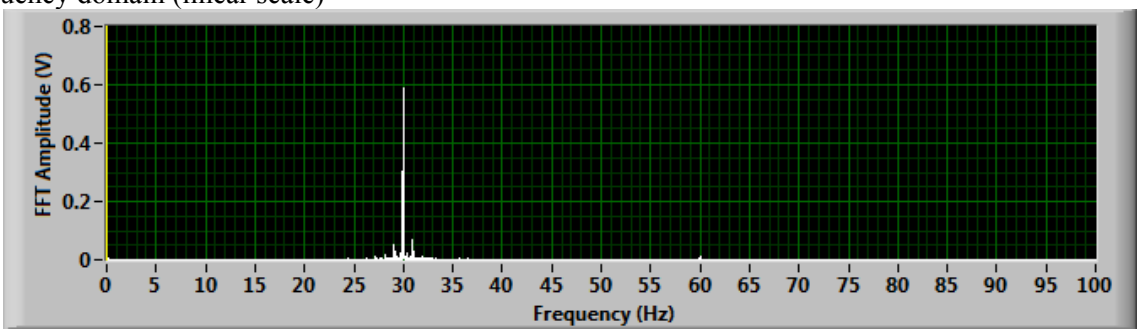

Figure B.85: Frequency Domain Signal (Linear Scale) of Raw Data for Combined Static and Dynamic Forces with 3.0 mph along 8- and 10-in. Thick Slab Section

Frequency domain (dB scale)

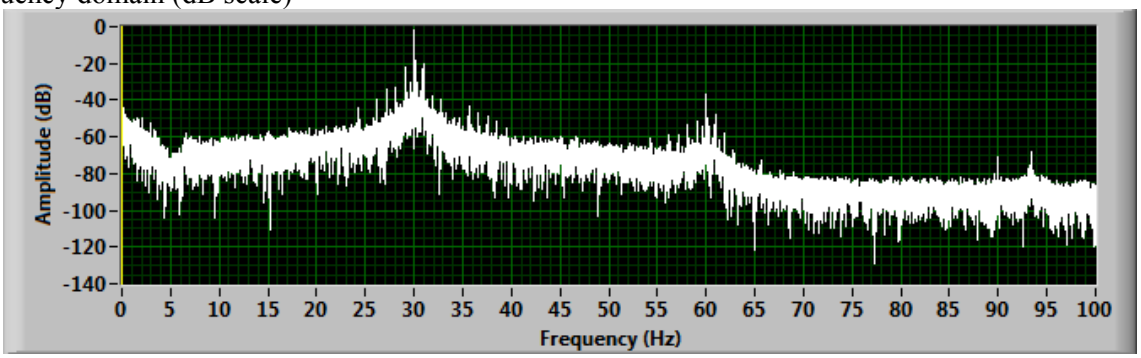

Figure B.86: Frequency Domain Signal (Decibel Scale) of Raw Data for Combined Static and Dynamic Forces with 3.0 mph along 8- and 10-in. Thick Slab Section

B.5.3 PROCESSED ROLLING SENSOR #1 SIGNAL (DEFLECTION PROFILE)

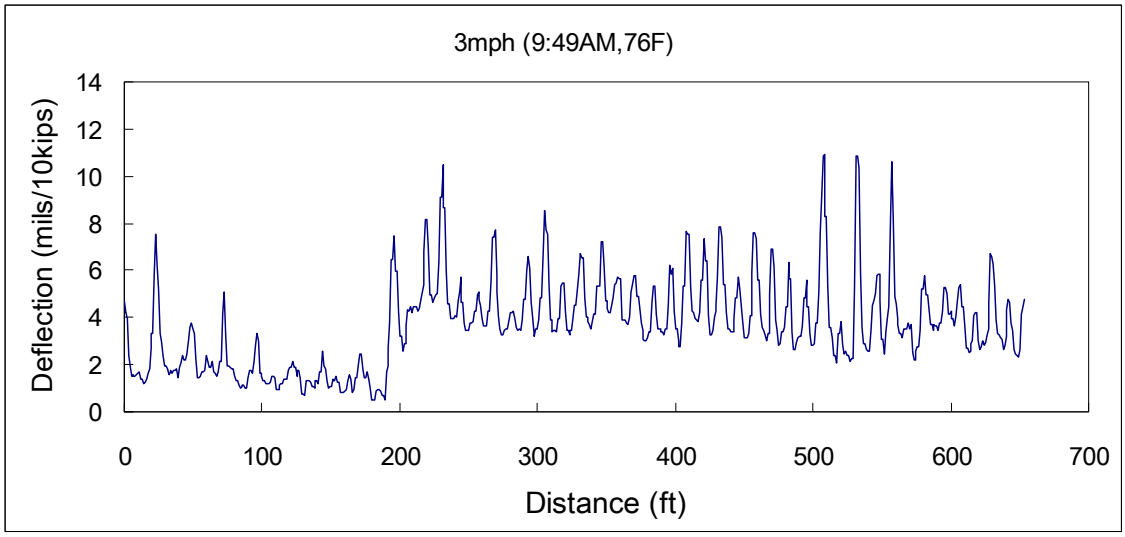

Figure B.87: Processed Rolling Sensor #1 Signal with 3.0 mph

B.5.4. RAW ROLLING SENSOR #1 SIGNAL

B.5.4.1. Complete record for 653-ft long testbed

Time domain signal (the number of data point = 230,400)

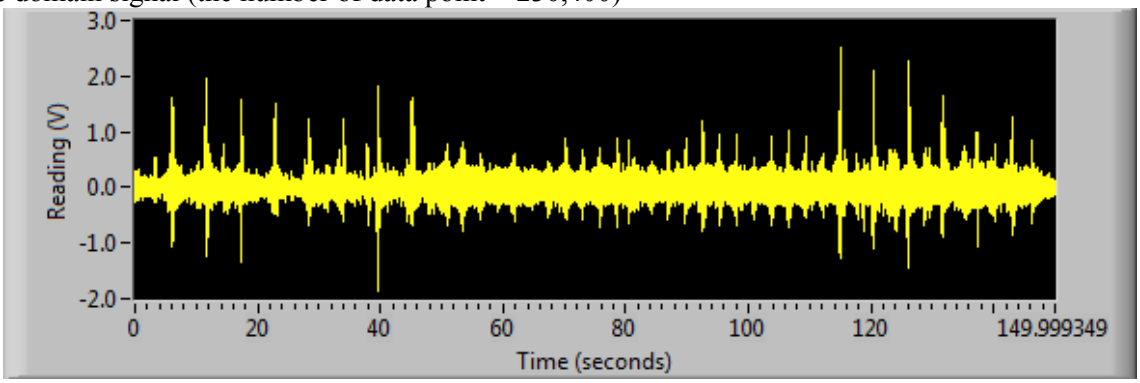

Figure B.88: Time Domain Signal of Raw Data for Rolling Sensor #1 with 3.0 mph along Whole Testbed Length

Frequency domain signal (linear scale)

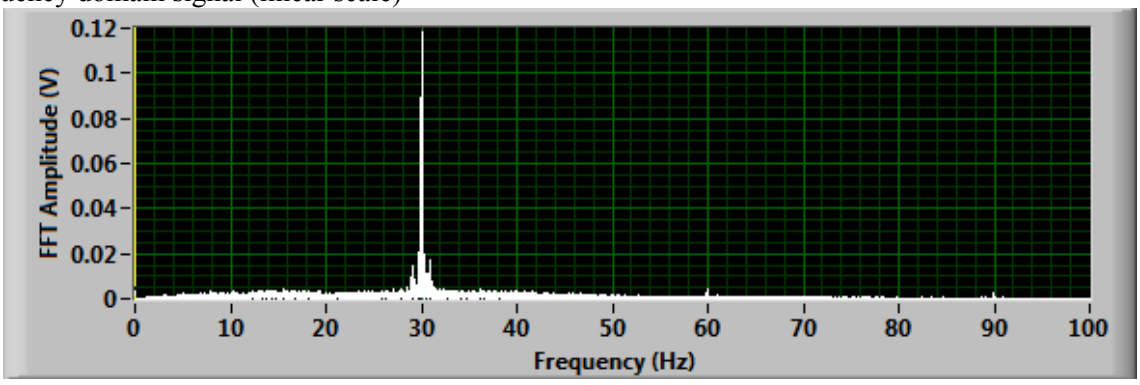

Figure B.89: Frequency Domain Signal (Linear Scale) of Raw Data for Combined Static and Dynamic Forces with 3.0 mph along Whole Testbed Length

Frequency domain signal (dB scale)

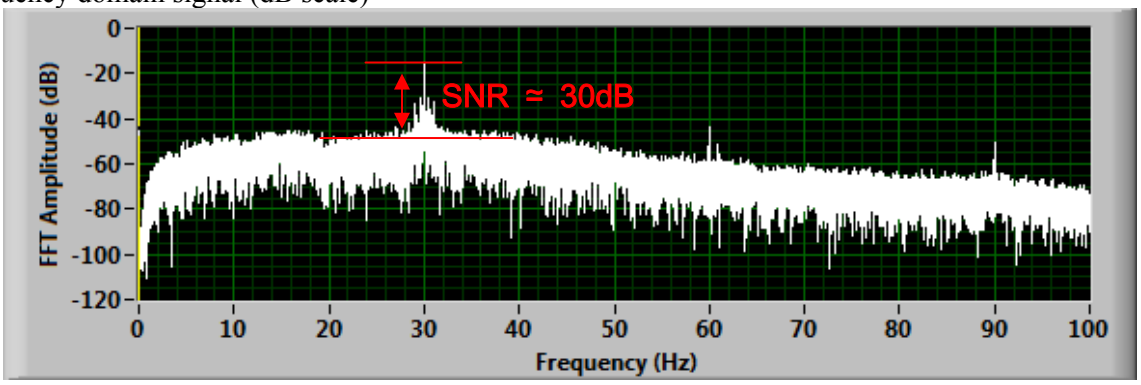

Figure B.90: Frequency Domain Signal (Decibel Scale) of Raw Data for Rolling Sensor #1 with 3.0 mph along Whole Testbed Length

B.5.4.2. on 16-in. thick slabs

Time domain signal (the number of data point = 69,427)

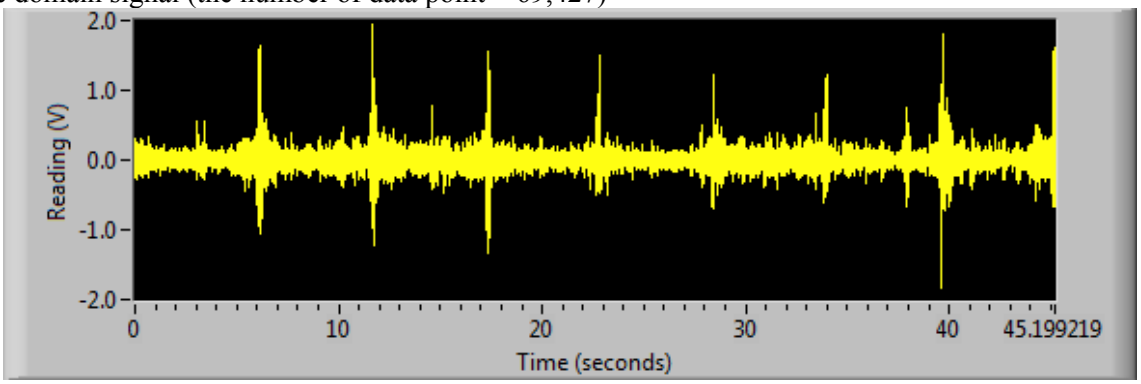

Figure B.91: Time Domain Signal of Raw Data for Rolling Sensor #1 with 3.0 mph along 16-in. Thick Slab Section

Frequency domain signal (linear scale)

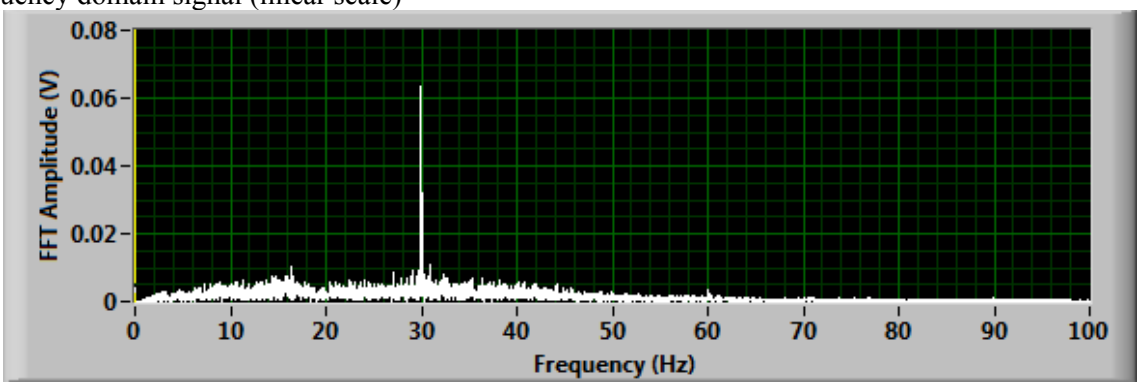

Figure B.92: Frequency Domain Signal (Linear Scale) of Raw Data for Rolling Sensor #1 with 3.0 mph along 16-in. Thick Slab Section

Frequency domain signal (dB scale)

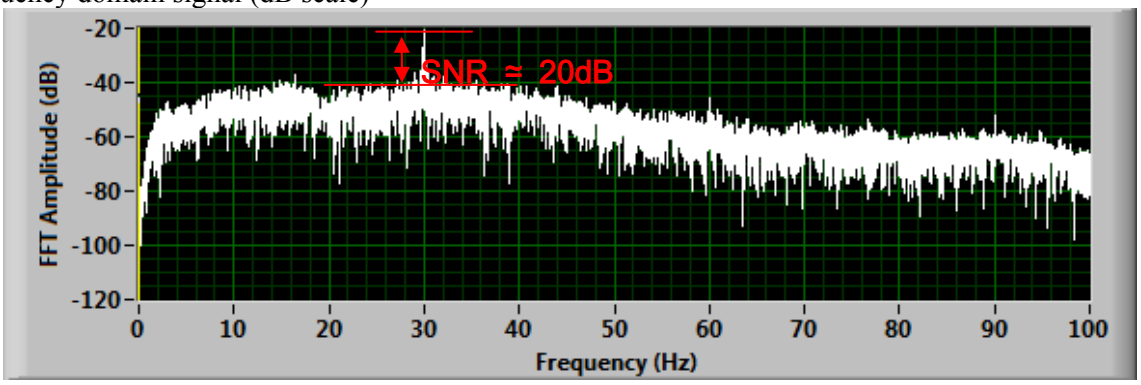

Figure B.93: Frequency Domain Signal (Decibel Scale) of Raw Data for Rolling Sensor #1 with 3.0 mph along 16-in. Thick Slab Section

B.5.4.3. on 8- and 10-in. thick slabs

Time domain signal (the number of data point = 160,973)

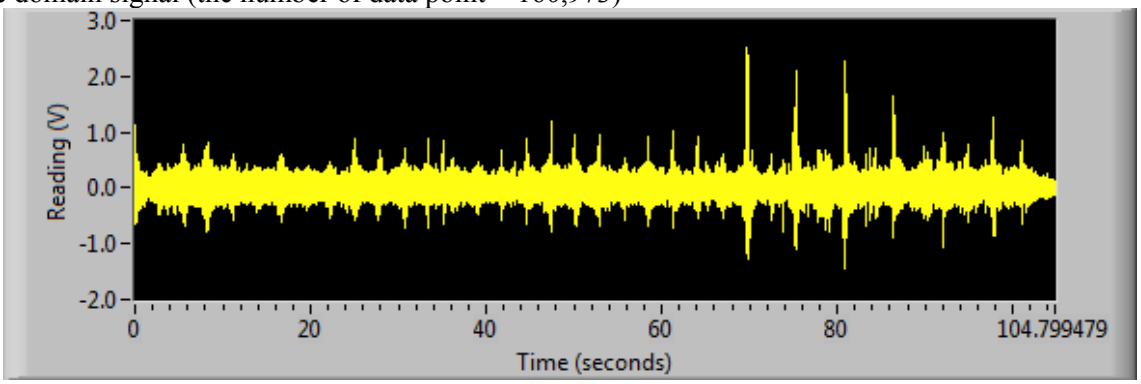

Figure B.94: Time Domain Signal of Raw Data for Rolling Sensor #1 with 3.0 mph along 8- and 10-in. Thick Slab Section

Frequency domain (linear scale)

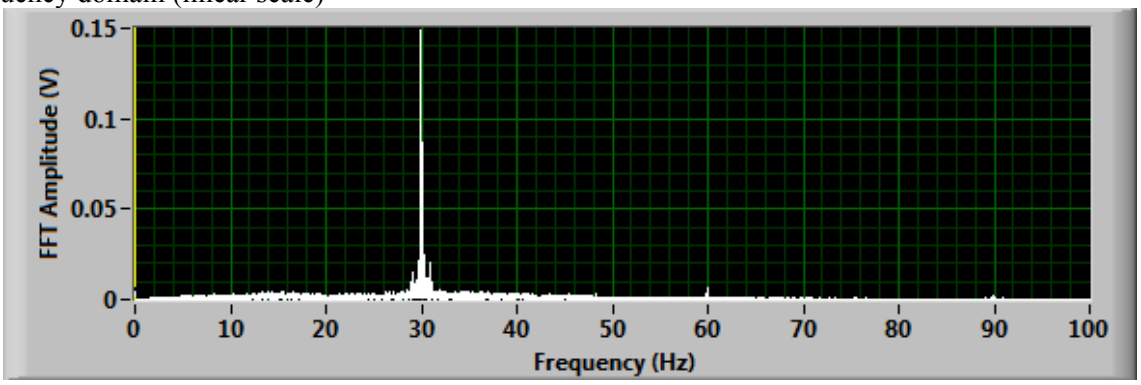

Figure B.95: Frequency Domain Signal (Linear Scale) of Raw Data for Rolling Sensor #1 with 3.0 mph along 8- and 10-in. Thick Slab Section

Frequency domain (dB scale)

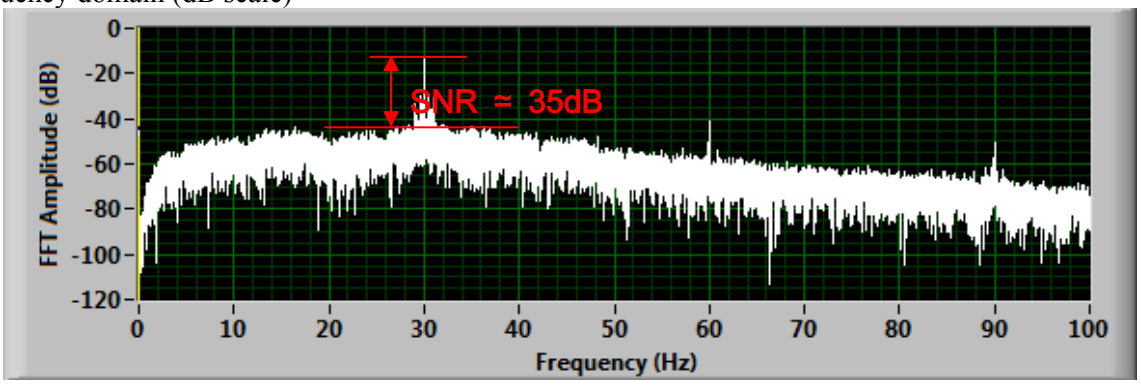

Figure B.96: Frequency Domain Signal (Decibel Scale) of Raw Data for Rolling Sensor #1 with 3.0 mph along 8- and 10-in. Thick Slab Section

B.5.5. PROCESSED DMI SIGNAL

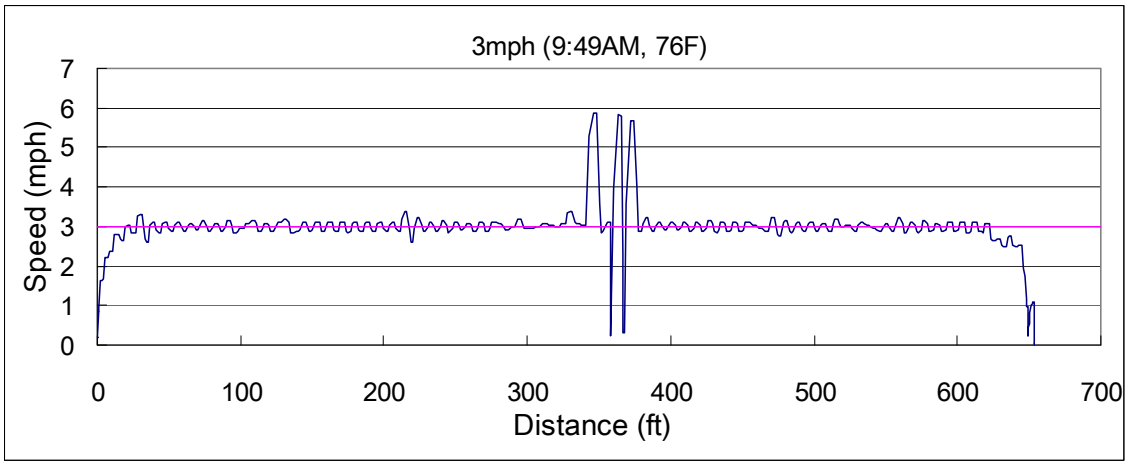

Figure B.97: Processed DMI Signal with 3.0 mph

B.5.6. RAW DMI SIGNAL

B.5.6.1 Complete record for 653-ft long testbed (the number of data point = 230,400)

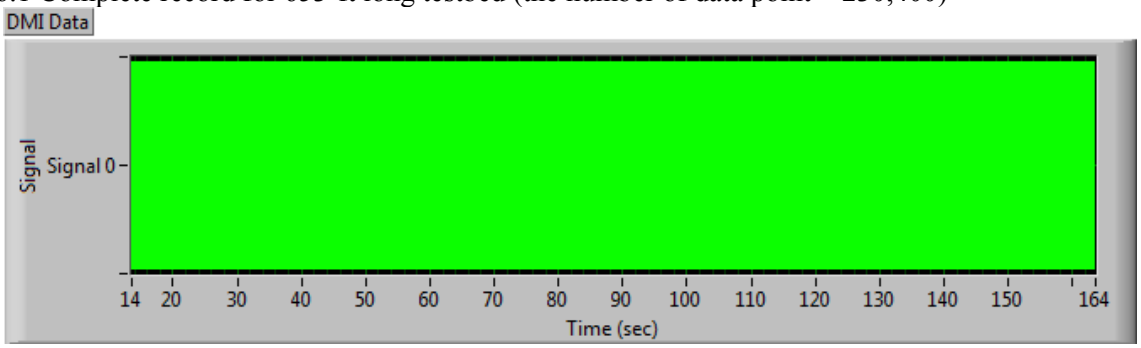

Figure B.98: Time Domain Signal of Raw Data for DMI with 3.0 mph along Whole Testbed Length

B.5.6.2. 2-second interval signal (from 20 to 22 second) on 16-in. thick slabs (the number of data point = 3,072)

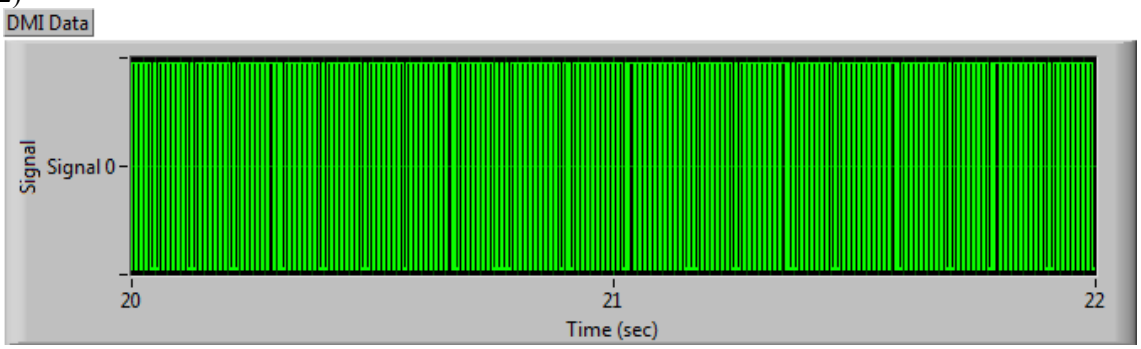

Figure B.99: Time Domain Signal of Raw Data for DMI with 3.0 mph along 16-in. Thick Slab Section

B.5.6.3. 2-second interval signal (from 70 to 72 second) on 8- and 10-in. thick slabs (the number of data point = 3,072)

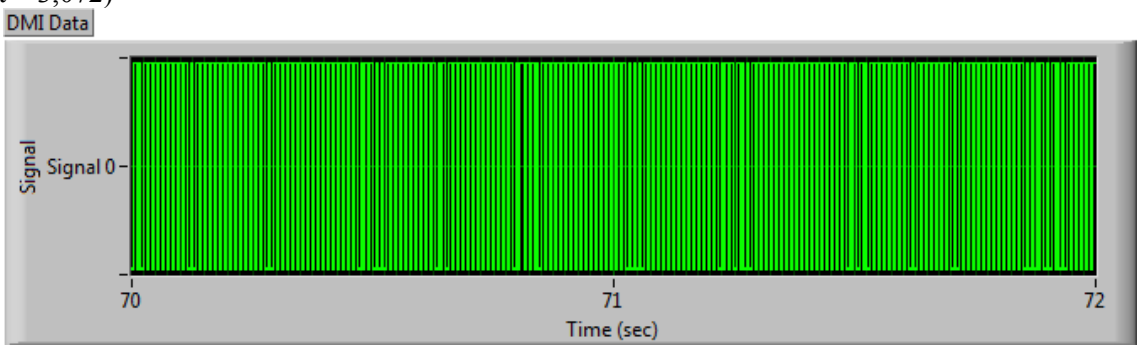

Figure B.100: Time Domain Signal of Raw Data for DMI with 3.0 mph along 8- and 10-in. Thick Slab Section

B.6. TPAD TESTING SPEED at 4 MPH

B.6.1. PROCESSED LOAD SIGNALS (Applied Static and Dynamic Forces)

B.6.1.1. Static force (Fstat) along the total distance

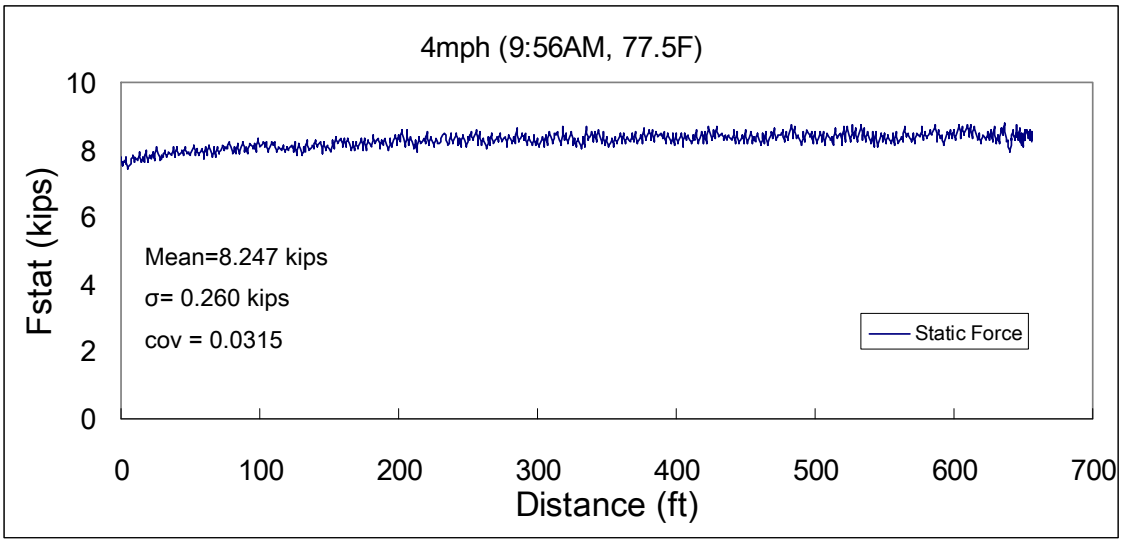

Figure B.101: Processed Static Force Signal with 4.0 mph

B.6.1.2. Peak-to-peak dynamic force (Fdyn) along the total distance

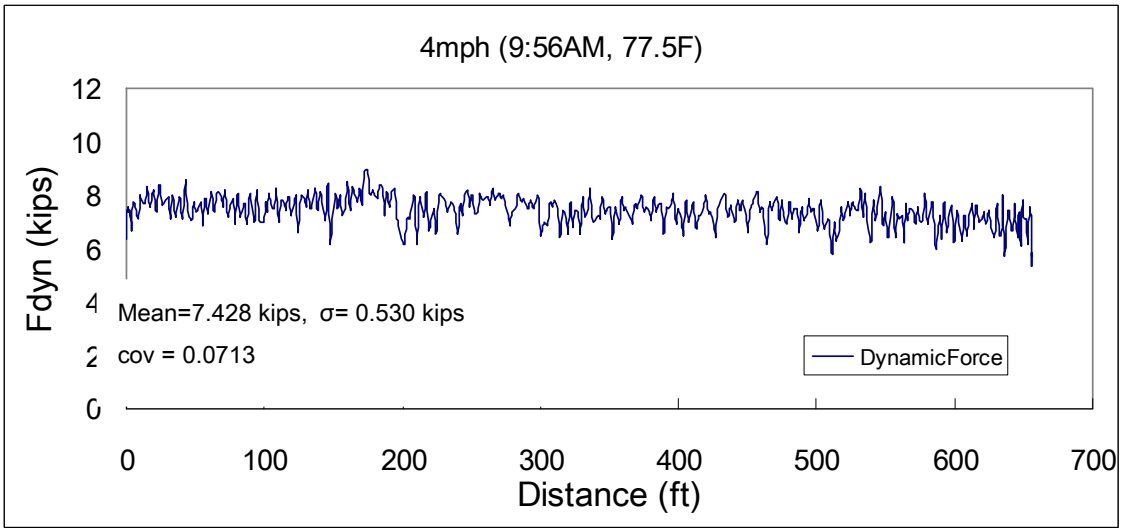

Figure B.102: Processed Pak-to-Peak Dynamic Force Signal with 4.0 mph

B.6.2. RAW LOAD SIGNAL

B.6.2.1. Complete record for 653-ft long testbed

Time domain signal of static and dynamic forces (the number of data point = 229,376)

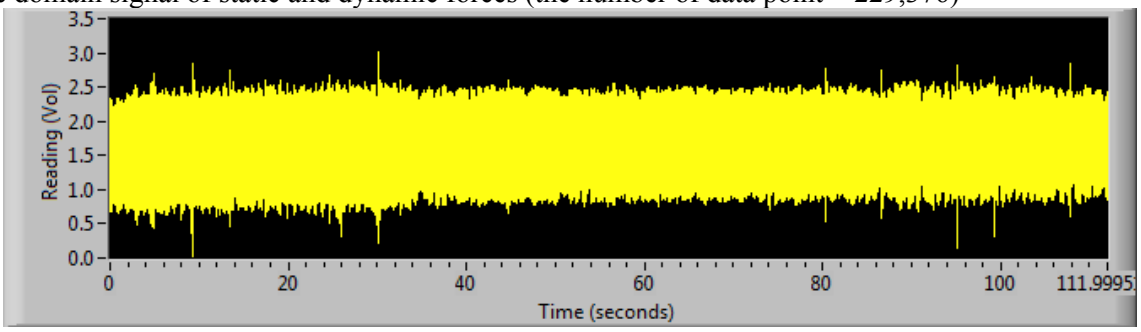

Figure B.103: Time Domain Signal of Raw Data for Combined Static and Dynamic Forces with 4.0 mph on Whole Testbed Length

Frequency domain signal (linear scale)

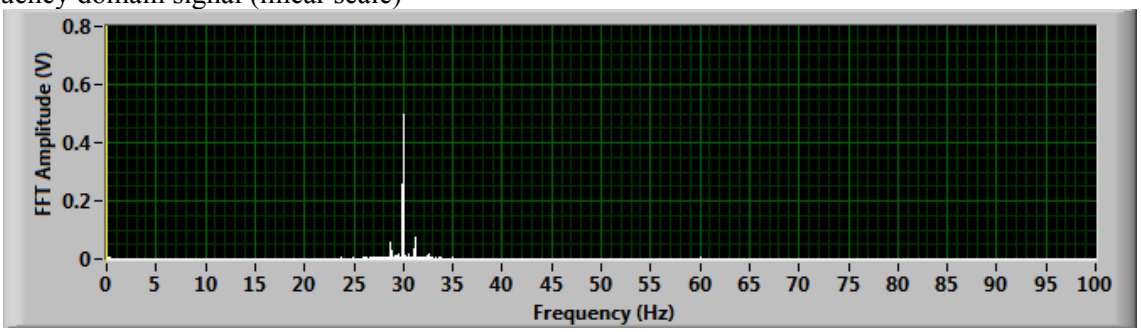

Figure B.104: Frequency Domain Signal (Linear Scale) of Raw Data for Combined Static and Dynamic Forces with 4.0 mph along Whole Testbed Length

Frequency domain signal (dB scale)

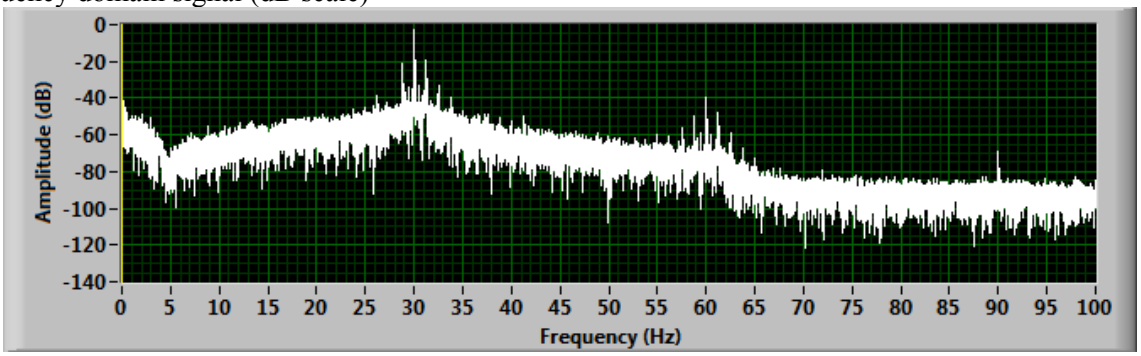

Figure B.105: Frequency Domain Signal (Decibel Scale) of Raw Data for Combined Static and Dynamic Forces with 4.0 mph along Whole Testbed Length

B.6.2.2. on 16-in. thick slabs

Time domain signal of static and dynamic forces (the number of data point = 71,270)

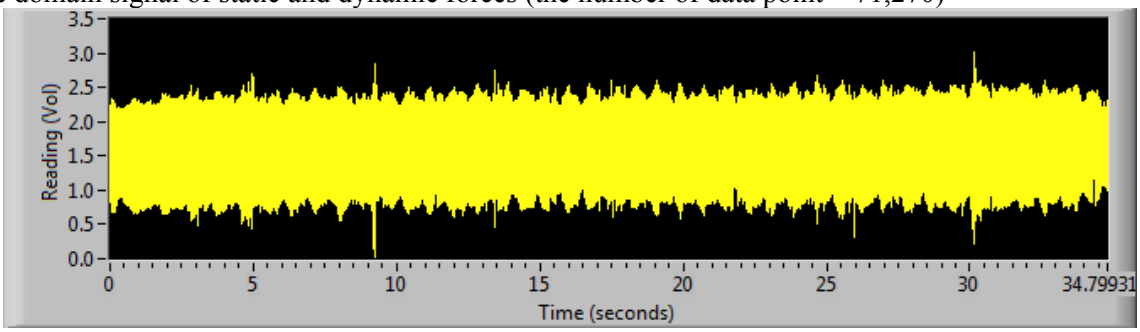

Figure B.106: Time Domain Signal of Raw Data for Combined Static and Dynamic Forces with 4.0 mph along 16-in. Thick Slab Section

Frequency domain signal (linear scale)

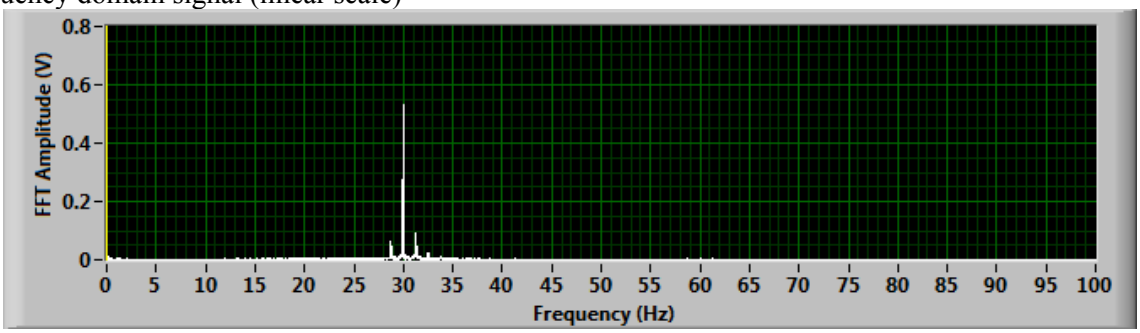

Figure B.107: Frequency Domain Signal (Linear Scale) of Raw Data for Combined Static and Dynamic Forces with 4.0 mph along 16-in. Thick Slab Section

Frequency domain signal (dB scale)

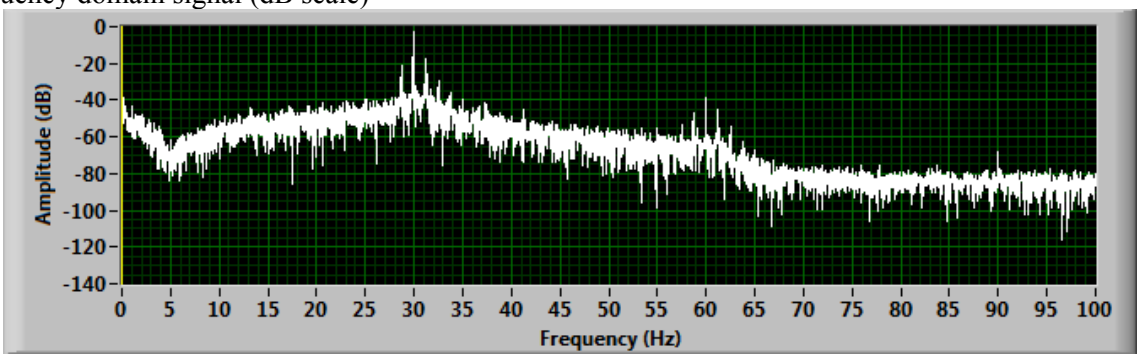

Figure B.108: Frequency Domain Signal (Decibel Scale) of Raw Data for Combined Static and Dynamic Forces with 4.0 mph along 16-in. Thick Slab Section

B.6.2.3. on 8- and 10-in. thick slabs

Time domain signal of static and dynamic forces (the number of data point = 158,106)

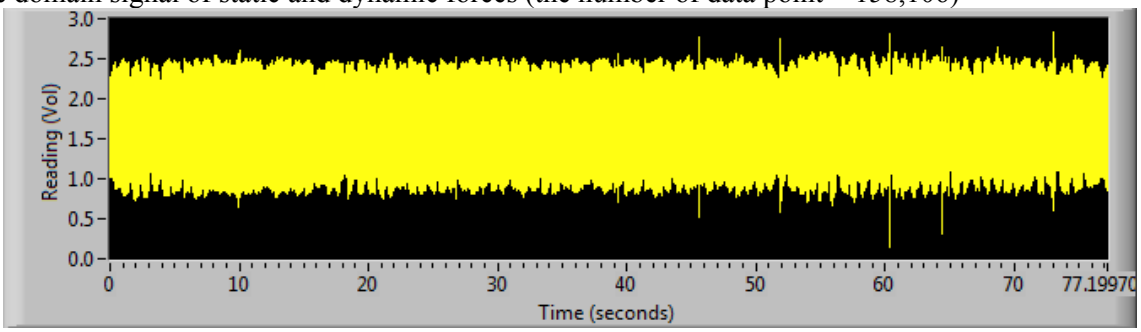

Figure B.109: Time Domain Signal of Raw Data for Combined Static and Dynamic Forces with 4.0 mph along 8- and 10-in. Thick Slab Section

Frequency domain (linear scale)

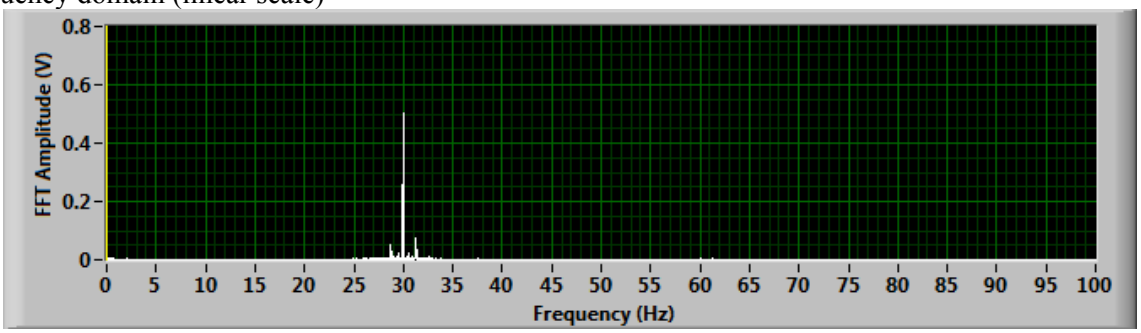

Figure B.110: Frequency Domain Signal (Linear Scale) of Raw Data for Combined Static and Dynamic Forces with 4.0 mph along 8- and 10-in. Thick Slab Section

Frequency domain (dB scale)

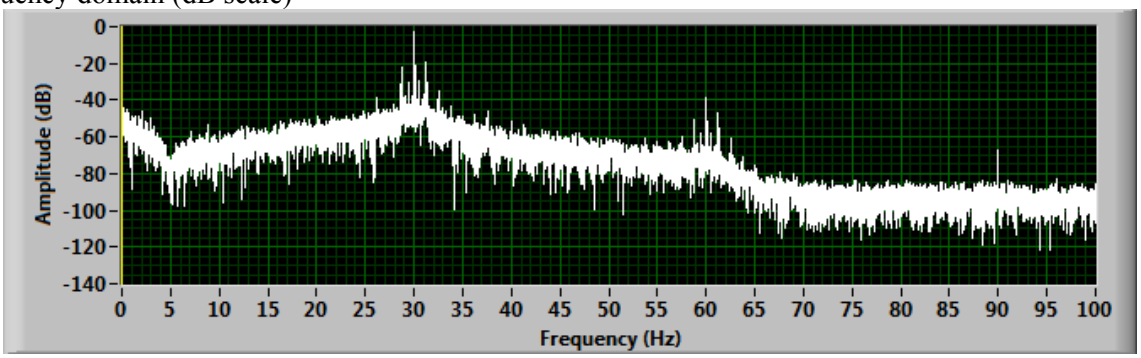

Figure B.111: Frequency Domain Signal (Decibel Scale) of Raw Data for Combined Static and Dynamic Forces with 4.0 mph along 8- and 10-in. Thick Slab Section

B.6.3 PROCESSED ROLLING SENSOR #1 SIGNAL (DEFLECTION PROFILE)

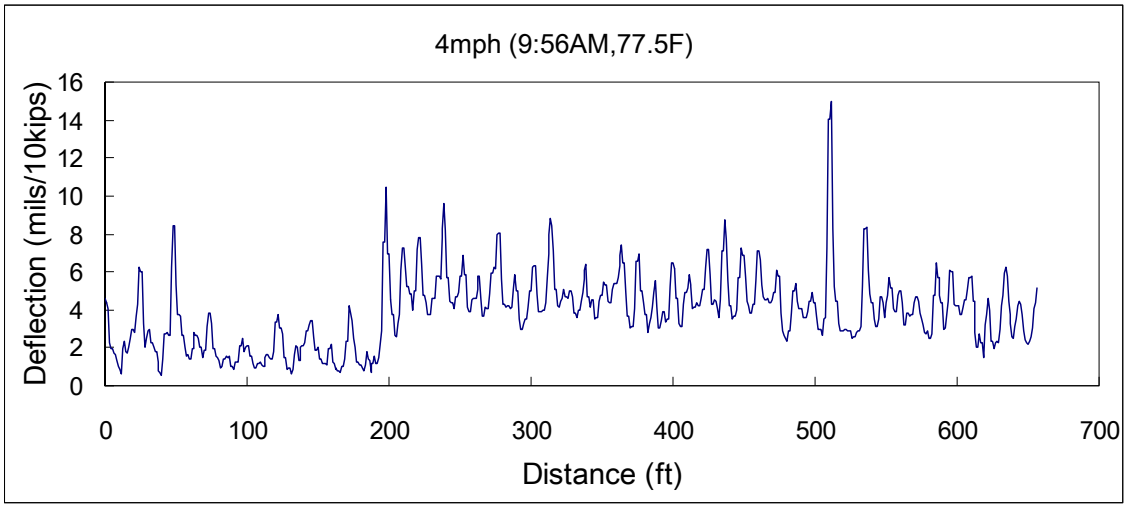

Figure B.112: Processed Rolling Sensor #1 Signal with 4.0 mph

B.6.4. RAW ROLLING SENSOR #1 SIGNAL

B.6.4.1. Complete record for 653-ft long testbed

Time domain signal (the number of data point = 229,376)

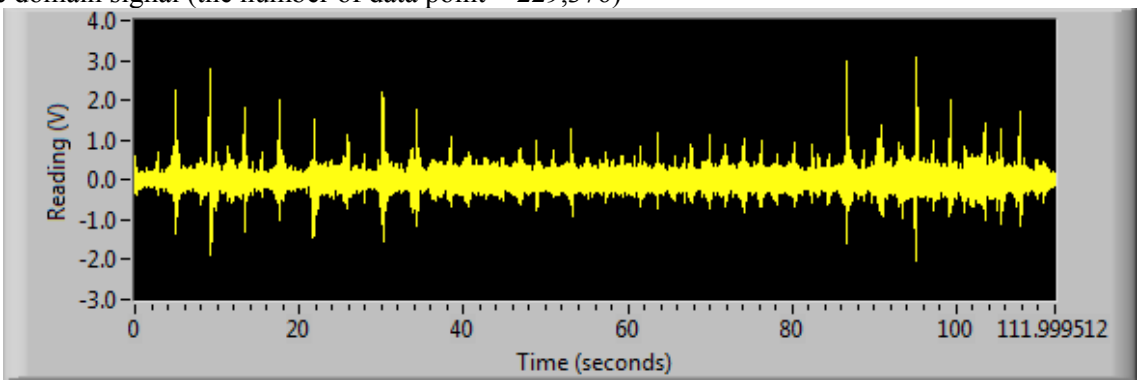

Figure B.113: Time Domain Signal of Raw Data for Rolling Sensor #1 with 4.0 mph along Whole Testbed Length

Frequency domain signal (linear scale)

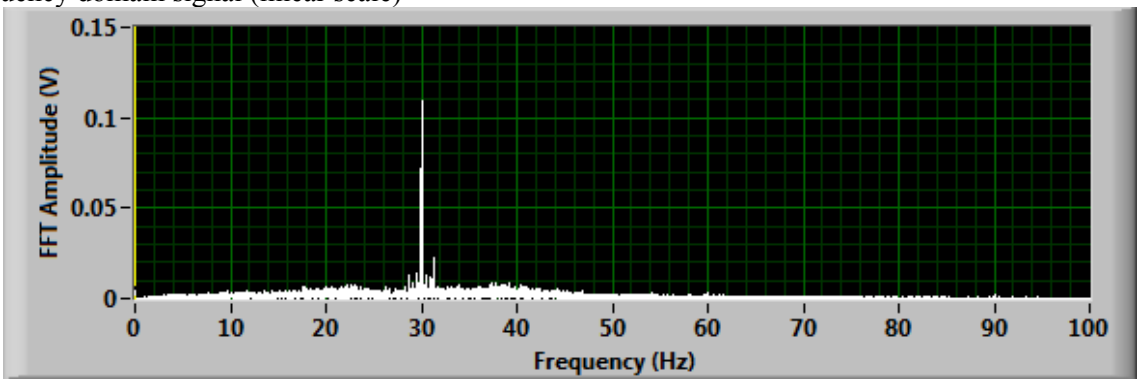

Figure B.114: Frequency Domain Signal (Linear Scale) of Raw Data for Combined Static and Dynamic Forces with 4.0 mph along Whole Testbed Length

Frequency domain signal (dB scale)

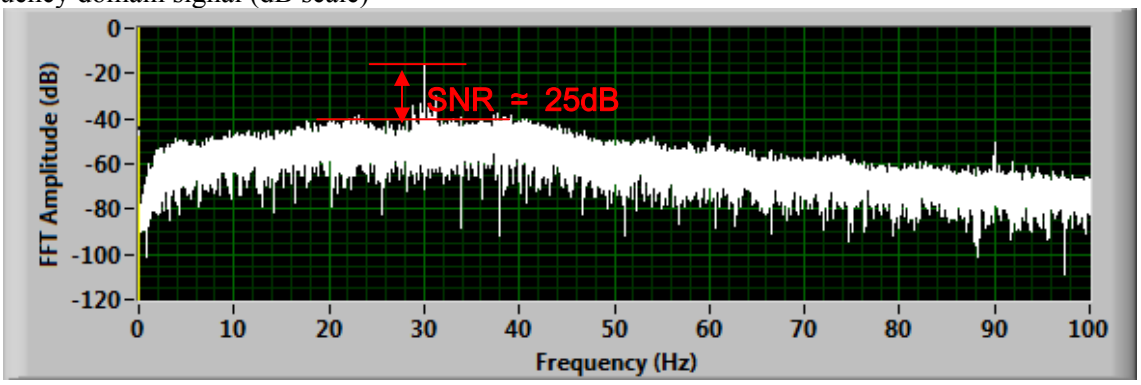

Figure B.115: Frequency Domain Signal (Decibel Scale) of Raw Data for Rolling Sensor #1 with 4.0 mph along Whole Testbed Length

B.6.4.2. on 16-in. thick slabs

Time domain signal (the number of data point = 71,270)

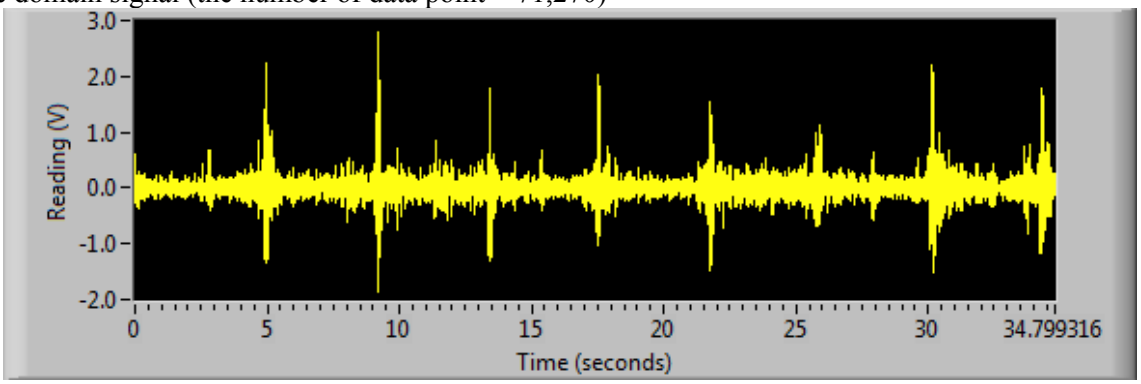

Figure B.116: Time Domain Signal of Raw Data for Rolling Sensor #1 with 4.0 mph along 16-in. Thick Slab Section

Frequency domain signal (linear scale)

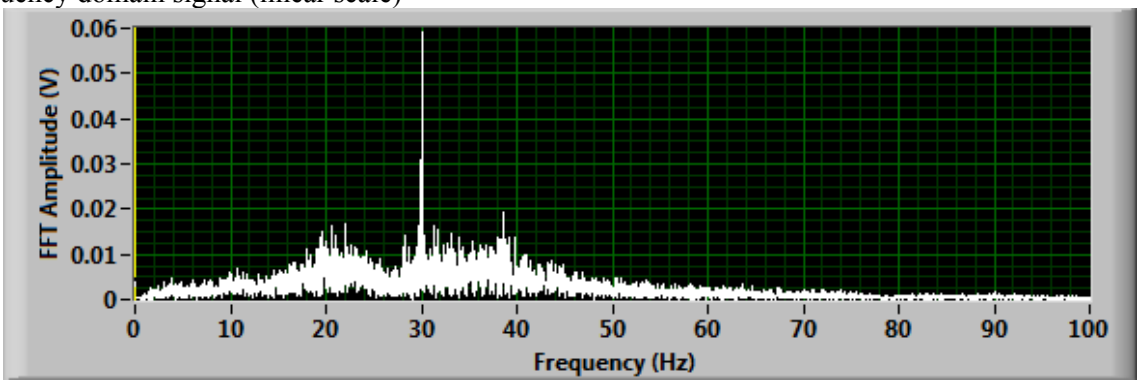

Figure B.117: Frequency Domain Signal (Linear Scale) of Raw Data for Rolling Sensor #1 with 4.0 mph along 16-in. Thick Slab Section

Frequency domain signal (dB scale)

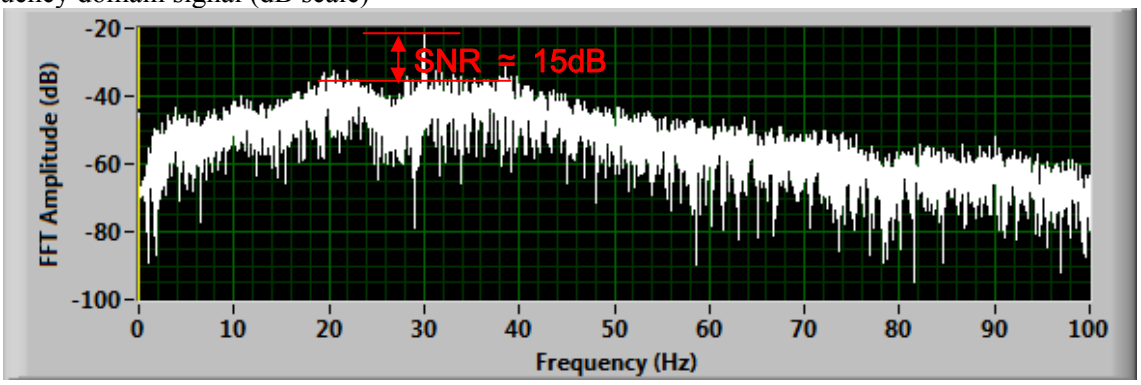

Figure B.118: Frequency Domain Signal (Decibel Scale) of Raw Data for Rolling Sensor #1 with 4.0 mph along 16-in. Thick Slab Section

B.6.4.3. on 8- and 10-in. thick slabs

Time domain signal (the number of data point = 158,106)

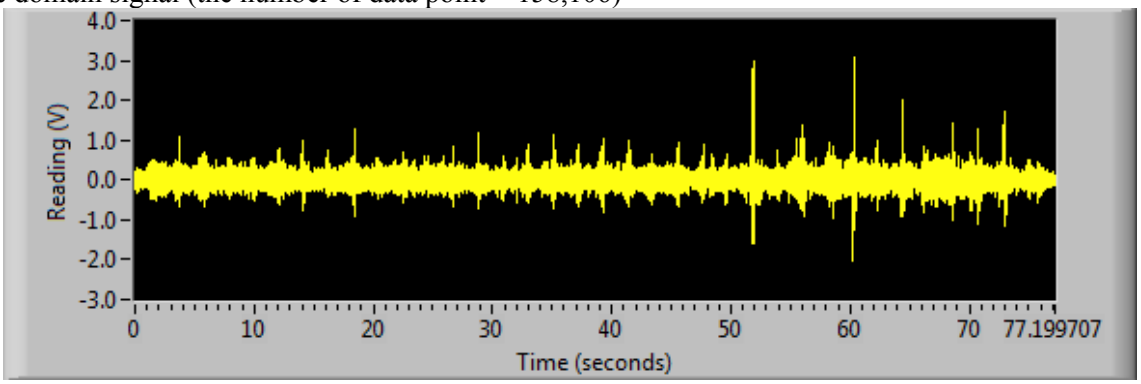

Figure B.119: Time Domain Signal of Raw Data for Rolling Sensor #1 with 4.0 mph along 8- and 10-in. Thick Slab Section

Frequency domain (linear scale)

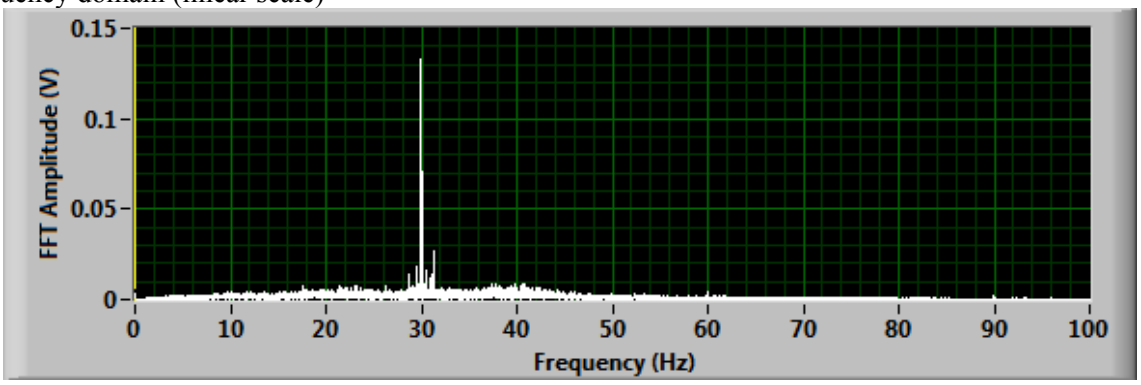

Figure B.120: Frequency Domain Signal (Linear Scale) of Raw Data for Rolling Sensor #1 with 4.0 mph along 8- and 10-in. Thick Slab Section

Frequency domain (dB scale)

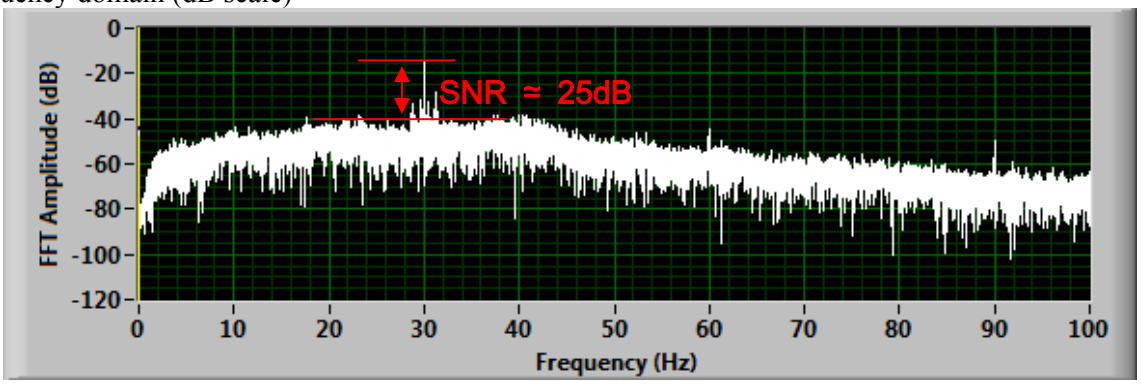

Figure B.121: Frequency Domain Signal (Decibel Scale) of Raw Data for Rolling Sensor #1 with 4.0 mph along 8- and 10-in. Thick Slab Section

B.6.5. PROCESSED DMI SIGNAL

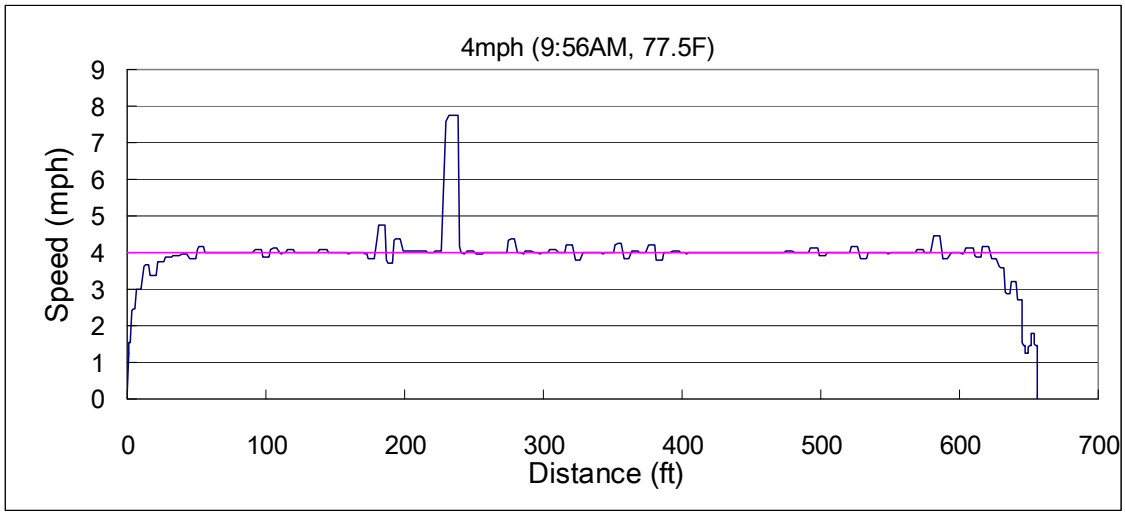

Figure B.122: Processed DMI Signal with 4.0 mph

B.6.6. RAW DMI SIGNAL

B.6.6.1 Complete record for 653-ft long testbed (the number of data point = 229,376)

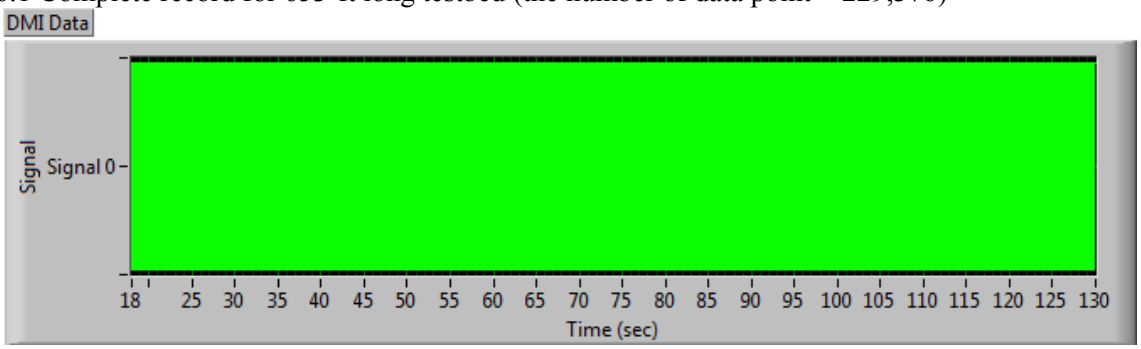

Figure B.123: Time Domain Signal of Raw Data for DMI with 4.0 mph along Whole Testbed Length

B.6.6.2. 2-second interval signal (from 18 to 20 second) on 16-in. thick slabs (the number of data point = 4,096)

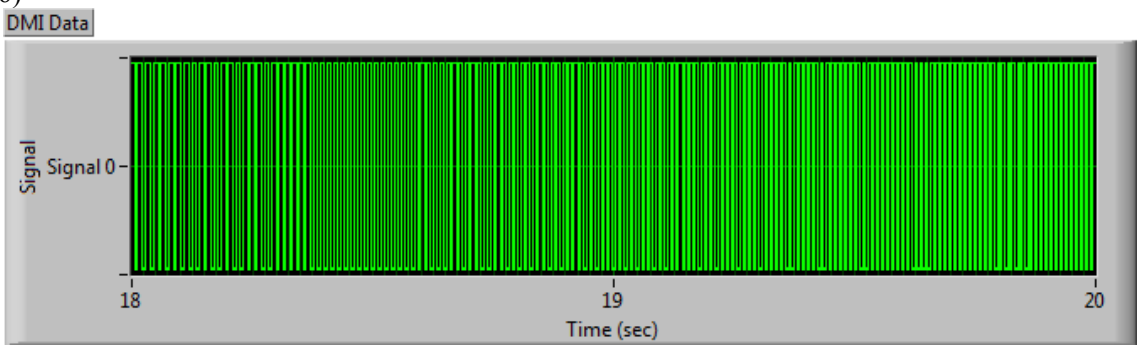

Figure B.124: Time Domain Signal of Raw Data for DMI with 4.0 mph along 16-in. Thick Slab Section

B.6.6.3. 2-second interval signal (from 126 to 128 second) on 8- and 10-in. thick slabs (the number of data point = 4,096)

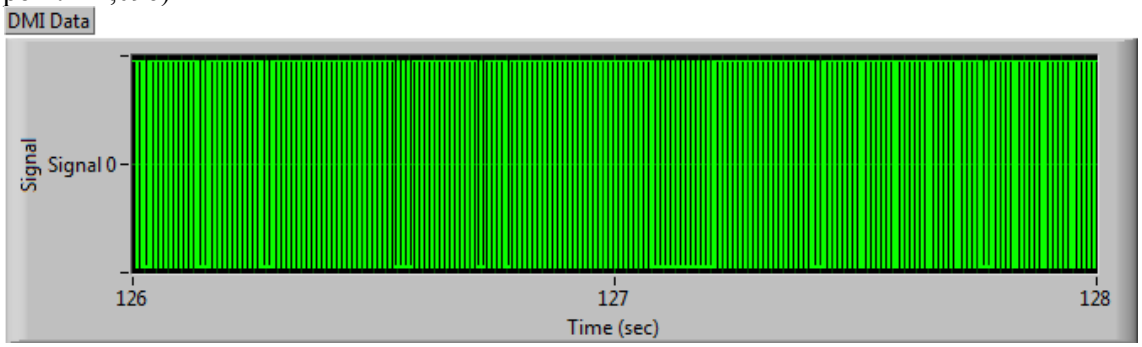

Figure B.125: Time Domain Signal of Raw Data for DMI with 4.0 mph along 8- and 10-in. Thick Slab Section